A Bayesian Network framework for probabilistic identification of model parameters from normal and accelerated tests : application to chloride ingress into conrete

Thanh Binh Tran

l'université nantes angers le mans
PÔLE DE RECHERCHE ET D'ENSEIGNEMENT SUPÉRIEUR

UNIVERSITÉ DE NANTES

Thèse de Doctorat

Thanh Binh TRAN

Mémoire présenté en vue de l'obtention du
grade de Docteur de l'Université de Nantes
sous le label de L'Université Nantes Angers Le Mans

École doctorale : Sciences Pour l'Ingénieur, Géosciences, Architecture

Discipline : Sciences de l'Ingénieur
Spécialité : Génie Civil
Unité de recherche : Institut de recherche en Génie Civil et Mécanique

Soutenue le 27 octobre 2015
Thèse N° :

A Bayesian Network framework for probabilistic identification of model parameters from normal and accelerated tests : application to chloride ingress into conrete

JURY

Rapporteurs :	**M. Joan Ramon CASAS**, Professeur, Université Polytechnique de Catalogne **M. Frédéric DUPRAT**, Professeur, INSA de Toulouse
Examinateurs :	**M. Franck SCHOEFS**, Professeur, Université de Nantes **M. David BIGAUD**, Professeur, Université d'Angers **M. Emilio BASTIDAS ARTEAGA**, Maître de Conférences, Université de Nantes . **M. Bruno CAPRA**, Docteur, Société OXAND. **M. Thomas DE LARRARD**, Maître de Conférences, INSA de Toulouse **Mme. Stéphanie BONNET**, Maître de Conférences, Université de Nantes
Directeur de Thèse :	**M. Franck SCHOEFS**, Professeur, Université de Nantes
Co-directeur de Thèse : Co-encadrant :	**M. Emilio BASTIDAS ARTEAGA**, Maître de Conférences, Université de Nantes **Mme. Stéphanie BONNET**, Maître de Conférences, Université de Nantes

Thesis

A Bayesian Network framework for probabilistic identification of model parameters from normal and accelerated tests: application to chloride ingress into concrete

Thanh-Binh TRAN

Acknowledgements

First of all, I would like to express my special gratitude to Professor Franck SCHOEFS for giving me an opportunity to become your PhD student. During the time we worked together, you always encourage my research and it makes me feel more confident. I would like to express my special appreciation and thanks to Associate professor Emilio BASTIDAS-ARTEAGA. I can never forget some difficult periods during my PhD, when I am almost stuck, pessimistic, he always encourage and lead me to optimistic thinking. Sometimes, I think that he is not only my teacher, he is also my friend. I would especial like to thank Associate professor Stéphanie BONNET who help me a lot in the experimental part of my thesis and give me a lot of advices to complete my thesis.

I am very grateful to all committee members: professor Joan Ramon CASAS, professor Frédéric DUPRAT, professor David BIGAUD, Dr Bruno CAPRA and Dr Thomas DE LARRARD for your acceptance as a scientific reviewer for my PhD. I believe that your knowledge and insights would be valuable for improving greatly my work.

I would also like to appreciate the assistance of all my colleague in the laboratory GeM. The time I worked with you in the laboratory GeM will be an unforgettable memory in my life.

A special thanks to my famify. Words cannot express how grateful I am to my parents and my little brother. You make me feel that I will be never lonely in this world. At the end I would like to express my appreciation to my beloved wife Tra My who always beside my, love me and support me to pursuit my dream.

Summary

Chloride ingress into concrete is one of the major causes leading to the degradation of reinforced concrete (RC) structures. RC structures are often designed for a service life from 50 to 100 years. Under chloride attack important damages are generated after 10 to 20 years. Consequently, they should be periodically inspected and repaired to ensure an optimal level of serviceability and safety during its lifecycle. Reliability assessment of structures subjected to chloride-induced corrosion is performed to predict the safety level and avoid unexpected damage consequences. Relevant material and environmental parameters for reliability analysis could be determined from inspection data. In natural conditions, chloride ingress involves a large number of uncertainties related to material properties and exposure conditions. These uncertainties are also affected by temporal and spatial variability of associated deterioration process and their characterisation requires larger amount of inspection data. However, due to the slow process of chloride ingress and the difficulties for implementing the inspection techniques, it is difficult to obtain sufficient inspection data to characterise the mid- and long-term behaviour of this phenomenon. The main objective of this thesis is to develop a framework based on Bayesian Network updating for improving the identification of uncertainties related to material and environmental model parameters in case of limited amount of measurements in time and space. The identification process is based on results coming from in-lab normal and accelerated tests that simulate tidal conditions. Based on these data, several procedures are proposed to: (1) identify input random variables from normal or natural tests; (2) determine an equivalent exposure time (and a scale factor) for accelerated tests; and (3) characterise time-dependent parameters combining information from normal and accelerated tests. The identified parameters are after used to evaluate their impact on the assessment of the probability of corrosion initiation. The results indicate that the proposed framework could be a useful tool to identify model parameters even from limited data.

Keywords: chloride ingress, parameter identification, Bayesian Network, uncertainty, accelerated test, corrosion.

Résumé

La pénétration des chlorures dans le béton est l'une des causes principales de dégradation des ouvrages en béton armé. La durée de vie de l'ouvrage en béton armé est normalement de 50 à 100 ans. Sous l'attaque des chlorures des dégradations importantes auront lieu après 10 à 20 ans. Par conséquent, ces ouvrages devraient être périodiquement inspectés et réparés afin d'assurer des niveaux optimaux de capacité de service et de sécurité pendant leur durée de vie. L'évaluation de la fiabilité de structures soumises à la corrosion induite par chloration sert à prédire le niveau de sécurité et à éviter des conséquences de dégradation inattendues. Des paramètres matériels et environnementaux pertinents peuvent être déterminés à partir des données d'inspection. En conditions naturelles, la pénétration des chlorures implique un grand nombre d'incertitudes liées aux propriétés des matériaux et les conditions d'exposition. Ces incertitudes sont également influencées par la variabilité temporelle et spatiale des processus de dégradation associés et sa caractérisation nécessite un nombre important des données d'inspection. Toutefois, en raison de la cinétique longue des mécanismes de pénétration de chlorures et des difficultés pour mettre en place des techniques d'inspection, il est difficile d'obtenir des données d'inspection suffisantes pour caractériser le comportement à moyen et à long-terme de ce phénomène. L'objectif principal de cette thèse est de développer une méthodologie basée sur la mise à jour du réseau bayésien pour améliorer l'identification des incertitudes liées aux paramètres matériels et environnementaux des modèles en cas de quantité limitée de mesures dans le temps et l'espace. Le processus d'identification est appuyé sur des résultats provenant de tests normaux et accélérées effectués en laboratoire qui simulent les conditions de marée. Sur la base de ces données, plusieurs procédures sont proposées pour: (1) identifier des variables aléatoires d'entrée à partir de tests normaux ou naturels; (2) déterminer un temps équivalent d'exposition (et un facteur d'échelle) pour les tests accélérés; et (3) caractériser les paramètres en dépendants du temps en combinant des informations obtenues à partir d'essais normaux et accélérés. Les paramètres identifiés sont après utilisés pour évaluer leur impact sur l'évaluation de la probabilité d'amorçage de la corrosion. Les résultats indiquent que le cadre proposé peut être un outil utile pour identifier les paramètres du modèle, même à partir d'une base de données limitée.

Mot clés: Pénétration des chlorures, identification des paramètres, réseaux bayésiens, incertitude, test accéléré, corrosion.

Contents

Introduction

Introduction about corrosion in RC structures due to chloride attack

Reinforced concrete (RC) has been recognised as a very durable material in a large range of severe environments: marine, industrial, alpine and radioactive conditions, etc. For all of concrete structures located in marine environments or in contact with de-icing salts, the surrounded environment is even more severe because outside chloride ions interact with material to generate rebar corrosion. Over decades, chloride agents are frequently considered as the main cause of deterioration of various types of RC structures: bridges, wharves, off-shore platforms, marine structures pipelines etc. In fact, current design standards have already taken into consideration the mechanical loadings and other deterioration process in serviceability of structures at design stage. Therefore, most RC structures exposed good long-term service life with high reliability level. However, there is still a large number of structures lost their integrity when they are subjected to chloride ingress due to the lack of knowledge about this phenomenon. In these cases, structure's protective properties may be lost and allow the appearance of corrosion even if structures were well designed and constructed.

RC structures are often designed for a service life from 50 to 100 years. Under chloride attack, loading capacity of structures are affected through: reduction of reinforcement cross-section, loss of bond between steel and concrete, concrete cracking and concrete delamination (Lounis and Amleh 2003). Damages increase gradually with structure's age if no maintenance action is taken and important damages could appear after 10-20 years of exposure (Kumar Mehta 2004; Poupard et al. 2006). Statistical data from Federal Highway Administration (FHWA) revealed that among approximately 600,000 bridges in the US, about 24% (146,633 bridges) are considered structurally deficient or functionally obsolete (Ebrahim Abbas et al. 2014) partly due to chloride attack. Planning a maintenance strategies to minimise impact of corrosion therefore becomes an essential task. In fact,

the collapse of structures due to corrosion rarely happens suddenly excepting for structures with inadequate inspections. The collapse of Silver Bridge in Ohio (US) in the year 1967 was due to the lack of an inspection technique that was not capable of detecting the tiny cracks (Wikipedia 2009). After this event, the nationwide inspection procedures had been undertaken. Nevertheless, in the year 1983, the Mianus River Bridge in Connecticut (US) suffered a suddenly collapse (Wikipedia 2012). The main cause of this disaster was found in corrosion from water build-up due to inadequate drainage. The lack of inspection resources in the state of Connecticut was also cited as important reason. Recently, inadequate inspections were blamed for causing failure of a building-Algo Centre Mall in Elliot Lake, Ontario, Canada in the year 2012 (McDonald 2013). The indicators for corrosion in the steel frame were missed from inspection. Therefore, no warning comment had been made about dangerous states of structure leading to a sudden collapse. There are also many cases of structural failures due to improper corrosion management.

Nowadays, different solutions have been developed to delay and prevent corrosion initiation, however the related costs remain significant. Data from a study carried out by the FHWA indicated that the total annual estimated direct cost of corrosion in the US is about $276 billion, being approximately 3.1% of the nation's Gros Domestic Product (GDP) (Koch et al. 2002). Interestingly, the indirect cost also takes conservatively the same proportion in total national budget as direct cost, being 6.2% in total. A half of direct cost ($137.9 billion) belongs to industry sectors which are divided in different categories (Figure I). It is worth noticing that infrastructure and transportation sectors received $52.3 billion, being equal to 37.9% of total budget of 5 sectors. Similar durability problems and extensive costs due to corrosion have also been reported in Australia, Europe and the Middle East (Daly 2000; Holland 1990; Lee 1990; Moore and Emerton 2010; Rasheeduzzafar et al. 1992). These statistical data highlights the economic issues associated to corrosion and raises the need for developing maintenance strategies that balance between effectiveness, accuracy and cost.

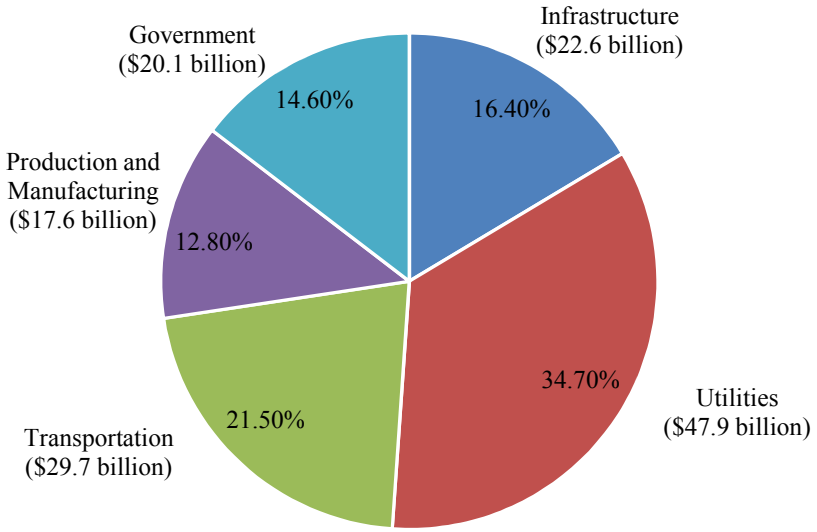

Figure I: Cost of corrosion in industry categories

Challenges in planning inspection and maintenance strategies

Management of deteriorating structures under chloride attack consists of two mainly stages: inspection and repair or replace. Inspection data provides valuable information about damage state of RC structure under chloride attack. Based on these data, appropriate repair actions should be undertaken at appropriated stages of deterioration. Frequently, parameters taking into consideration the characterisation of material durability or environmental exposure could be estimated from inspection measurements. These parameters combined with chloride ingress models are useful for the following applications: to update service life prediction models (Samarakoon and Sælensminde 2015), optimise inspection campaigns (Bastidas-Arteaga and Schoefs 2012; Bastidas-Arteaga et al. 2010a) and update the expected future maintenance cost (Vu and Stewart 2000). However, the results of the above mentioned applications are influenced by two main difficulties: (1) a high level of uncertainty in the chloride ingress process and (2) the limitation of inspection data. Concerning the first difficulty, Saassouh and Lounis (2012) proposed that these uncertainty may come from following sources: model parameters, physical model, statistical uncertainty and uncertainty in measurement. Uncertainties due to model parameters have a considerable variability and seems to be very sensitive meanwhile the other uncertainties could be pre-estimated based on selected models or methods of measurement. For the second difficulties, chloride ingress is a very slow process that require considerable exposure time to reach an important amount of chloride in RC structures. Accordingly, inspections are often taken at several-year intervals, e.g., Bastidas-Arteaga and Schoefs (2012) suggested that optimal inspection intervals should be 8-13 years. Therefore, it is required a significant time for collecting sufficient and representative data from inspection campaigns. Moreover, despite a large number of effective inspection techniques has been developed, they still expose some limitations. Inspection techniques often consists of destructive and non-destructive methods. Non-destructive techniques are less

expensive but theirs results are highly affected by environmental conditions and human errors. Destructive or semi-destructive techniques could provide more accurate inspection results, however, they are more expensive and time-consuming. In other words, larger inspection intervals and difficulties of inspection techniques leaded to the lack of inspection data.

To deal with the above mentioned difficulties, inspectors/engineers have to face with following questions:

1. How to construct a model integrating all uncertainties for identification of model parameters from inspection data?
2. How to improve/optimise the identification when inspection data is limited?
3. How to characterise the mid- and long-term behaviour of construction or repair material

Concerning the first question, one way to express the real complexity of chloride ingress is to develop stochastic models based on models with a physical sense and statistics for a probabilistic analysis. Bayesian Network (BN) is an efficient tool for such a problem which allows incorporating inspection data to update statistical information of parameters to identify. To propose a general framework, it is required sufficient information. Therefore, simulated data could be more appropriate to perform analysis because real data is always limited. For the second question, it is necessary to analyse the influence of different inspection data and BN configuration on parameter estimation. Using all information from inspection data might not ensure a best estimation. Therefore, the answers for this question lie in using selectively inspection data and improved BN configuration to reduce identification errors. To deal with the third question, the penetration of chloride ions into concrete could be speeded up under laboratory conditions. Then, chloride profiles obtained from an accelerated test after short exposure time will equivalent to those observed under larger exposure time in normal conditions. Data from accelerated test could be used to characterise mid- or long-term material behaviour if a scale factor of time between natural and accelerated conditions is identified.

Scope and objectives

Within this context, the present study concentrates mainly on the following issues:

- Developing a framework based on BN for parameter identification from inspection data
- Improving the identification of model parameters when inspection data is limited
- Characterisation the mid- and long-term material durability from accelerated tests

The specific objectives of this study are:

1. To carry out a literature review on: (i) available models used to describe chloride ingress, (ii) different approaches for uncertainty modelling and (iii) methods for parameter identification. On the basis of this literature survey, proposing a framework based on BN to identify model parameters from inspection data.
2. To apply the BN theory to identify chloride ingress model parameters and to suggest some numerical aspects that should be consistent to enhance the identification process.

3. To define appropriate BN configuration which minimise identification errors for each model parameters and to analyse the effects of combining inspection data obtained at different times.

4. To propose an approach to determine a scale factor from experimental data from accelerated tests and to propose a methodology for characterising the age factor.

5. To improve the assessment of the probability of corrosion initiation with parameters identified from limited data and various materials, environmental conditions and accelerated tests.

Thesis organisation

This thesis consists of four chapters. The first chapter carries out a literature view on chloride-induced deterioration processes, different chloride ingress models and various approaches for uncertainty modelling and parameter identification. The discussions analyse the advantages and disadvantages of each method to justify the selection of the BN approach considered for further research in this study.

Based on the BN approach selected in chapter one, chapter 2 describes the adaptation of selected method to chloride ingress. Some numerical aspects are discussed to improve and enhance the estimation of model parameters. There are also examples in this chapter to illustrate the algorithms used for each numerical issue.

In chapter 3, the identification of model parameters using BN updating with inspection data is discussed. Firstly, based on natural data, the influences of number inspection points in depth and inspection times on the identification of each parameter are investigated. These results provide a general framework for the identification of parameters from inspection data. This framework is then developed to determine scale factor in accelerated test from both normal and accelerated data. This chapter also studies the time-variant effect of the chloride diffusion coefficient by considering a more complex chloride ingress model that introduces the age factor. An approach for characterising the age factor from normal and accelerated data is also proposed in this chapter.

Finally, chapter 4 proposes strategies to improve the assessment of probability of corrosion initiation from identified parameters when inspection data is limited, various analysis cases corresponding to different material quality and environmental conditions are investigated to determine a configuration minimising identification errors for each case.

Résumé étendu en français

Aujourd'hui, les ions chlorure sont souvent considérés comme la cause principale de la détérioration de divers types de structures en béton armé : ponts, quais, structures marines, pipelines, ... Les structures en béton armé sont souvent conçues pour une durée de vie de 50 à 100 ans. Sous l'attaque d'ions chlorure, leur capacité portante est affectée par : la réduction de section d'acier effectif, la perte d'adhérence entre l'acier et le béton et la fissuration du béton et l'éclatement du béton (Lounis and Amleh 2003). Des endommagements importants peuvent apparaître après 10-20 ans d'exploitation et augmentent progressivement avec l'âge de la structure si aucune action de maintenance n'est effectuée (Kumar Mehta 2004; Poupard et al. 2006). Aujourd'hui, plusieurs solutions ont été développées pour retarder voire même empêcher l'amorçage de la corrosion, mais les coûts de mise en œuvre sont souvent élevés. Par exemple, Koch et al., (2002) ont estimé que les coûts annuels dus à corrosion des ponts routiers aux États-Unis étaient d'environ 8,3$ milliards (US dollars), dont 4,5$ milliards dépensés dans l'entretien et 3,8$ milliards pour le remplacement de ces structures.

La maintenance des structures détériorées par les chlorures comporte généralement deux étapes principales: l'inspection et la réparation de la structure. Les données d'inspection fournissent des informations précieuses sur l'état d'endommagement de la structure soumise à l'attaque des chlorures. A partir de ces données, des actions appropriées doivent être mises en œuvre afin de réparer les dégradations subies par la structure. Les mesures des inspections servent aussi à estimer les paramètres des modèles de dégradation qui caractérisent la performance des matériaux (vis-à-vis leur durabilité) et l'exposition à l'environnement. Cette étude se concentre sur l'identification des paramètres pour des modèles de pénétration d'ions chlorure dans le béton. L'identification de ces paramètres à partir des données d'inspection est utile pour : (1) la mise à jour des modèles de prédiction de la durée de vie (Samarakoon and Sælensminde 2015), (2) l'optimisation des intervalles d'inspection (Bastidas-Arteaga and Schoefs 2012; Bastidas-Arteaga et al. 2010a), et (3) la mise à jour des coûts de maintenance prévus (Vu and Stewart 2000). Toutefois, les résultats des applications mentionnées ci-dessus sont influencés par deux difficultés majeures qui sont : (1) un niveau élevé d'incertitude dans le

processus de pénétration des chlorures et (2) la limitation des données d'inspection. Ces difficultés posent les questions pratiques suivantes :

1. Comment intégrer les incertitudes du problème dans la procédure l'identification des paramètres du modèle à partir des données d'inspection ?
2. Comment améliorer / optimiser l'identification lorsque les données d'inspection sont limitées ?
3. Comment améliorer la prédiction du phénomène de transfert ionique à moyen et à long terme pour des matériaux d'origine et de réparation ?

Dans ce contexte, les objectifs de cette thèse portent sur:

- L'application de la théorie des Réseaux Bayésiens (RB) afin d'identifier les paramètres d'entrée des modèles de transfert des chlorures et la recommandation d'aspects numériques à prendre en compte pour améliorer la procédure d'identification.
- La définition de la configuration des RBs qui minimise les erreurs d'identification pour chaque paramètre du modèle et l'analyse du bénéfice de la combinaison des données d'inspection obtenues à des échéances différentes.
- La proposition d'une approche servant à déterminer un facteur d'échelle (pour des données expérimentales issues des essais accélérés) et d'une méthodologie pour caractériser le facteur de vieillissement.
- L'amélioration de l'évaluation de la probabilité d'initiation de la corrosion avec des paramètres identifiés à partir de données limitées.

Modélisation de la pénétration de chlorures en utilisant réseaux bayésiens (RB)

Réseaux Bayésiens

Cette section présente des aspects théoriques de base sur les réseaux bayésiens. Les RBs sont des modèles probabilistes composés de nœuds qui représentent des variables aléatoires. Ils sont connectés par des liens pour illustrer les dépendances probabilistes. Les RBs peuvent être vus comme un outil efficace pour faciliter la représentation la dépendance entre les variables aléatoires par structures graphiques sous la forme de graphes acycliques dirigés (GAD). S'il existe une relation de cause à effet entre les variables (nœuds), il y aura un lien directionnel, menant de la variable de cause (nœud parent) à la variable d'effet (nœud enfant). Chaque variable dans le GAD est liée à une densité de probabilité (DP) qui dépend des relations de cause à effet avec les autres variables. La Figure 1 montre un RB simple composé de trois nœuds X_1, X_2 et X_3 correspondant à trois variables aléatoires avec un nœud parent (X_1) et deux nœuds enfants (X_2 et X_3). Les nœuds enfants ont des distributions de probabilité

conditionnelles qui dépendent de la relation avec les nœuds parents qui ont des distributions de probabilité marginales. Pour un ensemble de m variables aléatoires $\mathbf{X}= [X_1, X_2, \ldots, X_m]$, $P(\mathbf{X})$ représente la fonction de masse de probabilité conjointe (FMP) du RB. Pour chaque nœud, son FMP appartient conditionnellement à ses parents et à la FMP conjointe du RB. Par exemple pour le RB présenté en Figure 1, elle est calculée en fonction d'un produit de probabilités conditionnelles:

$$P(X_1, X_2, X_3) = P(X_1)P(X_2 \mid X_1)P(X_3 \mid X_1) \tag{1}$$

où $P(X_i \mid X_j)$ désigne la probabilité conditionnelle de X_i sachant X_j.

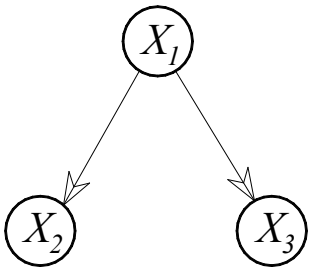

Figure 1: Exemple d'un réseau bayésien simple.

Le RB permet d'introduire des nouvelles informations (évidences) dans certains nœuds pour mettre à jour les probabilités dans le réseau. Par exemple, si nous avons des évidences à introduire au nœud X_2 $(X_2 = o)$, cette information peut se propager à travers le réseau et la FMP conjointe des deux autres nœuds peut être recalculée :

$$P(X_1, X_3 \mid o) = \frac{P(X_1, o, X_3)}{P(o)} = \frac{P(X_1)P(o \mid X_1)P(X_3 \mid X_1)}{\sum_{X_1} P(X_1)P(o \mid X_1)} \tag{2}$$

Les RBs seront utilisés dans cette étude pour l'identification de paramètres avec des évidences issues des campagnes d'inspection (nœuds enfants ou sorties du RB).

Modélisation de la pénétration des ions chlorure

Les deux modèles simplifiés de pénétration des ions chlorure utilisés dans la thèse sont présentés dans cette section. Dans le béton saturé, l'équation de diffusion de Fick est généralement utilisée pour estimer la diffusion unidirectionnelle des chlorures (Tuutti 1982) :

$$\frac{\partial C_{f_c}}{\partial t} = D_c \frac{\partial^2 C_{f_c}}{\partial x^2} \tag{3}$$

où C_{fc} (kg/m^3) est la concentration en chlorures libres, t (s) est le temps et D_c (m/s^2) est le coefficient effectif de diffusion des chlorures. En supposant que le béton est un matériau homogène et isotrope avec les conditions initiales suivantes : (i) la concentration est égale à zéro à l'instant t = 0 et (ii) la

concentration de chlorures en surface, C_s, est constante, la concentration en chlorures libres à la profondeur x et l'instant t dans un milieu semi-infini est donnée par :

$$C(x,t) = C_s\left[1 - erf\left(\frac{x}{2\sqrt{D_c t}}\right)\right] \tag{4}$$

où erf(.) est la fonction d'erreur. Malgré certaines hypothèses simplificatrices, le modèle à fonction d'erreur est largement utilisé en pratique en raison de leur expression mathématique relativement simple. Il traite le coefficient de diffusion des chlorures comme constant dans le temps et l'espace. Cette simplification ne tient pas compte des effets retardateurs sur le processus de diffusion résultant par exemple de la fixation des chlorures à la pâte du ciment et des évolutions de la structure poreuse du béton avec le temps. Ce modèle est utilisé dans cette thèse dans un premier temps pour illustrer quelques aspects numériques et pratiques dans le but de minimiser l'erreur d'identification.

Dans un modèle plus avancé, le coefficient de diffusion des chlorures est dépendant du temps suivant une loi de type (Luping and Gulikers 2007) :

$$D(t) = D_0\left(\frac{t}{t_0^{'}}\right)^{-n_D} \tag{5}$$

où D_0 est le coefficient de diffusion de chlorure mesuré au moment $t_0^{'}$ et n_D est le facteur de vieillissement. Cette thèse utilise le modèle proposé par Nilsson and Carcasses (2004) qui décrit la diffusion ionique en fonction du temps :

$$C(x,t) = C_s\left[1 - erf\left(\frac{x}{2\sqrt{\frac{D_0}{1-n_D}\left[\left(1+\frac{t_{ex}^{'}}{t}\right)^{1-n_D} - \left(\frac{t_{ex}^{'}}{t}\right)^{1-n_D}\right]\left(\frac{t_0^{'}}{t}\right)^{n_D} t}}\right)\right] \tag{6}$$

où $t_{ex}^{'}$ est l'âge du béton au début de l'exposition. Ce modèle est utilisé pour estimer un facteur d'échelle servant à intégrer des résultats des essais accélérés dans le processus d'identification.

Configuration du RB pour la modélisation de la pénétration des ions chlorure

Dans les modèles de pénétration des chlorures, la teneur en chlorures $C\left(x_i,t_j\right)$ à la profondeur x_i et à l'instant t_j peut être décrite comme une fonction générale des paramètres associés :

$$C\left(x_i,t_j\right)=f\left(C_s,D,n_D,...\right) \tag{7}$$

Le nombre de paramètres intervenant dans le second membre de l'équation (7) dépend du modèle $f(.)$ choisi pour décrire la pénétration des chlorures. Le RB représentant le modèle de pénétration des chlorures le plus simple (Eq.(4)) est décrit en Figure 2. Les deux paramètres du modèle (C_s et D) sont définis comme deux nœuds parents (variables aléatoires à identifier). La teneur en chlorure $C\left(x_i,t_j\right)$ à la profondeur x_i et à l'instant t_j dépend des paramètres du modèle et est modélisée comme nœud enfant. Il y a n nœuds enfants $C\left(x_i,t_j\right)$ représentant les mesures discrètes de la concentration en chlorures dans le temps et l'espace (par exemple : un profil en ions chlorure à l'instant t_j). Le nombre de nœuds enfants est calculé comme :

$$n = n_x n_t \tag{8}$$

où n_x est le nombre total de points en profondeur à chaque inspection et n_t est le nombre total de d'inspections.

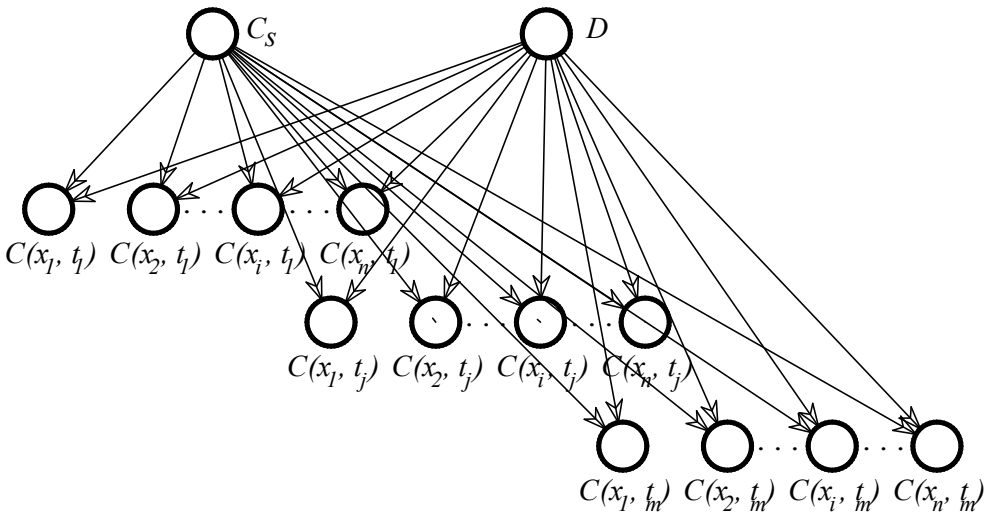

Figure 2: Configuration générale du RB pour la modélisation du transfert de chlorures

L'application du théorème de Bayes au modèle du transfert des chlorures est détaillée dans le chapitre 2. On s'intéresse particulièrement aux distributions a posteriori de nœuds parents car elles

fournissent des informations statistiques utiles pour l'identification des paramètres du modèle : moyenne, écart-type et loi de distribution.

Le processus d'identification porte tout database sur une grande quantité de données expérimentales (profils de chlorures) pour estimer les modèles probabilistes de reférence des paramètres et par conséquent pour tester et de comparer différentes configurations de RBs. Cependant, une telle base de données est très difficile à obtenir en pratique. Ces données sont généralement obtenues à partir de tests expérimentaux semi-destructifs qui sont coûteux et chronophages. Par conséquent, afin de fournir des recommandations générales sur des configurations améliorées des RBs, nous considérons des évidences numériques (profils de chlorures) générées par simulations de Monte Carlo. Ces profils de chlorures numériques sont obtenus à partir des modèles probabilistes théoriques des variables aléatoires d'entrée (variables aléatoires à identifier). Les valeurs théoriques sont présentées dans la section 3.2. Ainsi, la performance de chaque configuration du RB est évaluée en termes de l'erreur d'identification du paramètre Z:

$$Error(Z) = \frac{\left| Z_{identified} - Z_{theory} \right|}{Z_{theory}} \times 100\% \tag{9}$$

où Z est le paramètre à identifier (moyenne ou écart-type de C_s ou D), $Z_{identified}$ est la valeur identifiée (par exemple la moyenne identifié de la distribution a posteriori de D) et Z_{theory} est la valeur théorique utilisée pour générer les profils de chlorures numériques (moyenne théorique de D).

Identification des paramètres en utilisant les données des essais « non-accélérés »

Cette section examine l'influence de la configuration du RB sur l'erreur d'identification par rapport aux paramètres théoriques. Les configurations des RBs se composent d'un ou de plusieurs nœuds enfants correspondant à un ou plusieurs points d'inspection en profondeur et à un instant donné n_t=1.

Identification à partir des mesures prises d'un point en profondeur

Dans cette partie, on s'intéresse à l'identification des moyennes et écart-types de C_s et de D à partir des évidences obtenues en un point de mesure à une profondeur n_x=1 et à un temps n_t=1 donnés (Figure 3). La Figure 4 montre les erreurs dans l'identification de la moyenne et de l'écart type de C_s et de D. Pour C_s, les données issues des profils de chlorures proches de la surface fournissent des informations encore très utiles pour l'identification de C_s, alors que les informations relatives aux parties les plus profondes augmentent l'erreur.

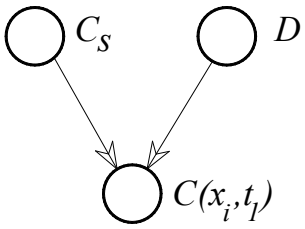

Figure 3: Configuration du RB utilisant un point d'inspection en profondeur.

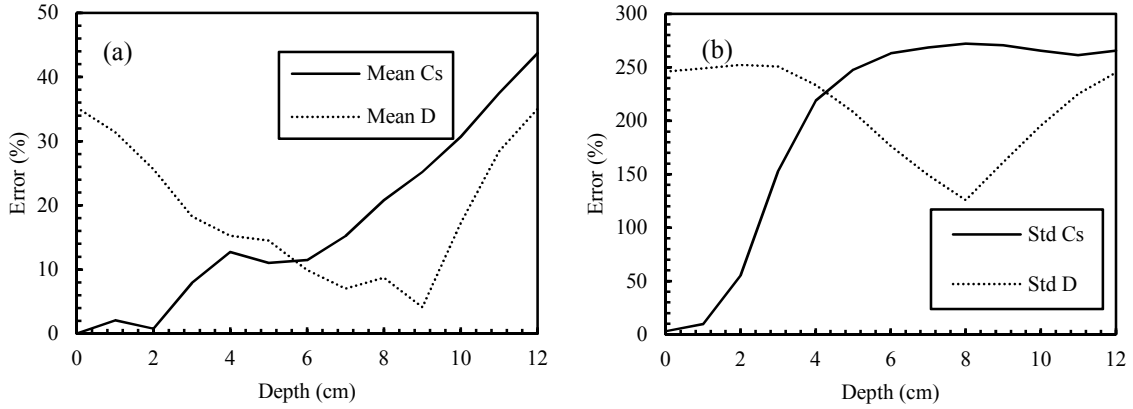

Figure 4: Erreur d'identification en considérant un point de mesure en profondeur: (a) Moyenne – (b) écart-type

On observe également sur la Figure 4a que la teneur en chlorures dans les zones profondes est plus utile pour l'identification du coefficient de diffusion. Cependant, en des points très profonds, où les teneurs en chlorure tendent vers zéro, l'erreur augmente. Les erreurs dans l'identification de l'écart-type suivent une tendance similaire, mais leurs valeurs sont très éloignées des valeurs théoriques. Par conséquent, on peut conclure qu'il est très difficile d'effectuer une bonne identification de D en utilisant des données expérimentales obtenues à partir d'un seul point d'inspection en profondeur.

Identification à partir de plusieurs points d'inspection

Dans cette section, l'identification avec des RBs utilise les données sur la profondeur totale d'inspection. La profondeur totale d'inspection (12cm) est divisée en plusieurs points de contrôle avec le même pas de discrétisation Δx (Figure 5). Le pas de discrétisation ne doit pas être inférieur à 0,3 cm qui correspond à la précision de l'équipement semi-destructif (machine de broyage) utilisé pour déterminer les profils de chlorure. Le RB possède aussi un nombre de nœuds enfant (n_x) égal au nombre de mesures en profondeurs. Par exemple, si Δx = 2 cm, la configuration du RB se compose de 2 nœuds parents et de 7 nœuds enfants comme décrit sur la Figure 5.

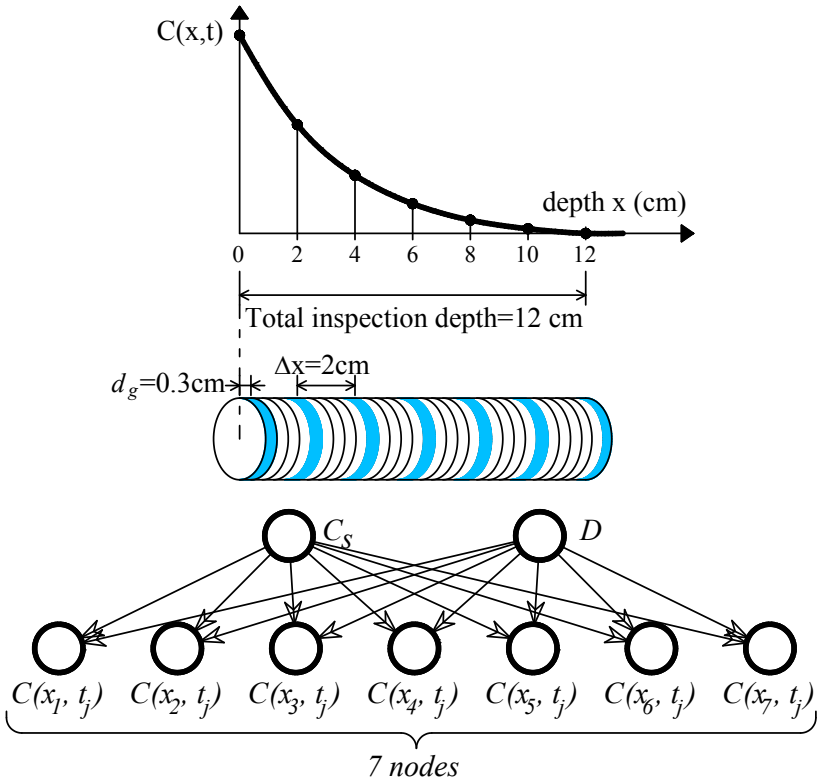

Figure 5: Configuration du RB avec plusieurs points d'inspection en profondeur et Δx=2 cm

Discrétisation avec les mêmes bornes pour tous les nœuds enfants

La Figure 6 présente l'erreur dans l'identification en utilisant plusieurs points d'inspection en profondeur et en considérant les mêmes bornes dans la discrétisation des nœuds enfants. Ces résultats ont été obtenus en discrétisant tous nœuds enfants en 15 états. Pour toutes les configurations des RBs étudiées, on constate qu'il n'y a aucun changement remarquable dans l'identification de la moyenne de C_s (Figure 6a) : les erreurs sont proches de 5%. Cependant, l'augmentation des points d'inspection (utilisation des faibles valeurs de Δx) génère plus d'erreurs dans l'évaluation de l'écart-type de C_s. Au contraire, l'écart entre les valeurs identifiées et théoriques de D se réduit de manière significative quand la longueur de discrétisation Δx diminue. Par conséquent, nous pouvons conclure que des mesures en chlorures prises sur l'intégralité de la profondeur d'inspection fournissent des informations plus appropriées pour l'identification de D.

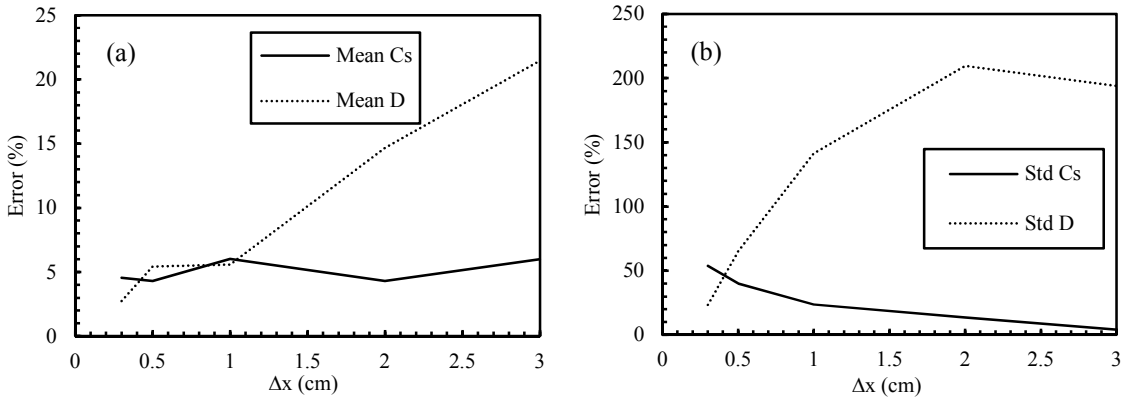

Figure 6: Erreur d'identification calculée avec des données issues de l'intégralité de la profondeur d'inspection : (a) Moyenne – (b) écart-type

Discrétisation avec des bornes différentes pour tous les nœuds enfants

La section précédente a indiqué qu'une discrétisation plus fine en espace minimise les erreurs d'identification de *D*. Cette section explore la piste de l'utilisation de bornes différentes pour les nœuds enfants dans le but d'améliorer les résultats de l'identification. L'utilisation de bornes différentes pour chaque nœud enfant peut s'avérer utile pour bénéficier des informations issues des points les plus profonds où la teneur en chlorure est faible. Le choix des valeurs pour les bornes est défini par les valeurs minimales et maximales de la concentration en chlorure à une profondeur *x* obtenue à partir des données utilisées a priori pour créer les tableaux de probabilités conditionnelles (TPC) (Section 2.4.4).

La Figure 7 compare les erreurs d'identification commises avec et sans l'utilisation des bornes différentes pour les nœuds enfants. Trois cas son représentés : (1) 15 états avec les mêmes bornes, (2) 200 états avec les mêmes bornes et (3) 15 états avec des bornes différentes. Il est clair que la prise en compte d'un grand nombre d'états (200 états avec les mêmes bornes) et/ou des bornes différentes (15 états) diminue considérablement les erreurs d'identification. Cette discrétisation améliorée pourrait être très utile en pratique lorsque le nombre de points de mesure est limité ou lorsque la teneur en chlorure à l'intérieur du béton est faible.

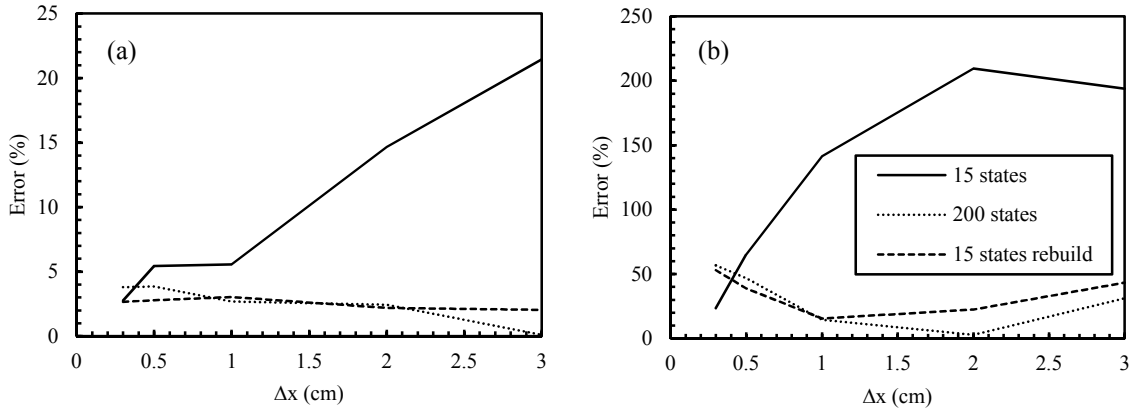

Figure 7 : Erreur d'identification de *D* pour trois discrétisations des nœuds enfants: (a) Moyenne – (b) écart-type

Identification des paramètres avec des données provenant des tests accélérés

Essais de vieillissement du béton

Les essais de vieillissement ont été réalisés dans le cadre du projet MAREO (MAintenance et REparation d'Ouvrages littoraux et fluviaux en béton : Optimisation par analyse de risque) dans la période 2008-2012. Ils cherchent à caractériser les performances (vis-à-vis de la durabilité) des matériaux de réparation (mortiers et bétons) en zone de marnage en effectuant des tests non-accélérés et accélérés. Dans ces essais, des dalles de béton sont placées dans une cuve remplie avec de l'eau synthétique salée. La salinité de la solution est proche de la salinité moyenne de l'Atlantique Nord afin de garantir une simulation de la pénétration des chlorures similaire aux conditions naturelles. L'exposition des dalles assure une diffusion unidimensionnelle des chlorures. Des cycles de marée (hauts et bas) sont simulés en faisant varier le niveau de l'eau toutes les 12 heures. Pour les tests accélérés, des ventilateurs sont utilisés pour accélérer le séchage des échantillons pendant le cycle de marée basse. Le séchage accélère la pénétration des chlorures à cause d'une augmentation de la capacité d'absorption capillaire du béton (Hong 1998). Les tests non-accélérés sont soumis aux mêmes cycles de marée sans séchage. Les tests sont automatiquement pilotés par un programme Labview®. Les réservoirs sont placés à l'intérieur d'un bâtiment et trois paramètres environnementaux (température ambiante, salinité de l'eau et humidité relative) sont enregistrés.

Caractérisation du facteur de vieillissement et détermination du temps équivalent

Cette section propose une approche pour déterminer un facteur de vieillissement n_D et un temps équivalent des tests accélérés t_{eq}. La combinaison des données issues des tests non-accélérés et accélérées peuvent mener à une évaluation plus précise du facteur de vieillissement et donc à une meilleure estimation du temps d'initiation de la corrosion. Pour la même échéance, les profils de chlorures pour les essais accélérés donnent des teneurs en chlorures plus importants par rapport aux essais non-accélérés. Par conséquent, l'intégration des données issues des essais accélérés nécessite la détermination d'un temps d'exposition équivalent. Ce temps représente le temps nécessaire pour un échantillon soumis à une exposition normale (sans séchage) pour atteindre un niveau de chlorures issu d'un essai accéléré. Dans ce but nous avons proposé la configuration du RB présenté en Figure 8.

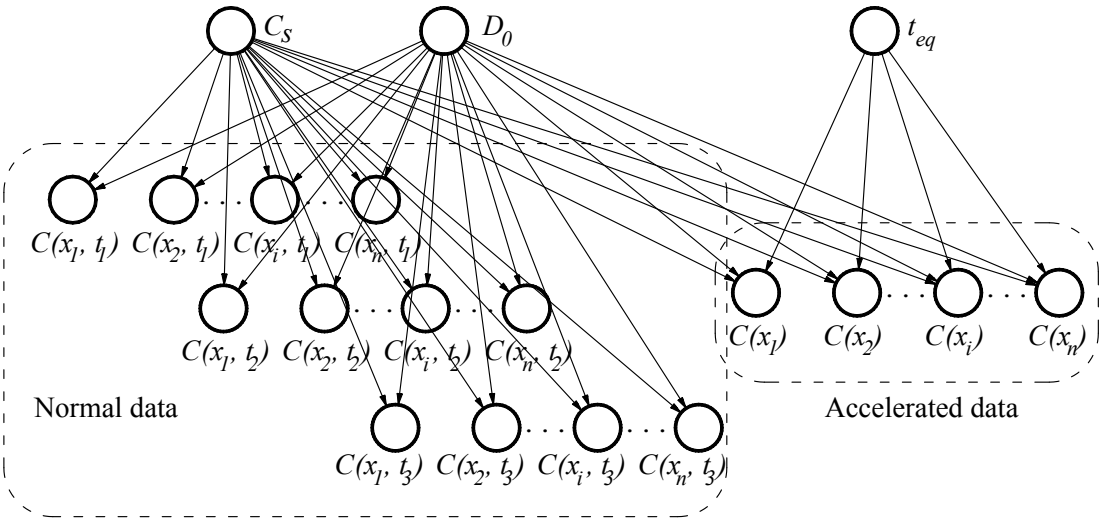

Figure 8: Configuration du RB combinant des données non-accélérées et accélérées pour l'identification de t_{eq}

La méthodologie pour caractériser le facteur de vieillissement peut être décrite par l'organigramme présenté en Figure 9. La phase I de cette procédure consiste à réaliser un fittage pour déterminer l'ensemble des valeurs de C_s et D pour chaque profil expérimental de chlorures. Les profils de chlorure servent à calculer les évidences utilisées pour la mise à jour du RB. Les valeurs moyennes de D à des échéances différentes pour trois essais normaux (T1, T2 et T3) sont utilisées pour estimer une première valeur du facteur de vieillissement en fittant des courbes expérimentales à partir de l'équation (5). Ce facteur de vieillissement (valeur déterministe) est introduit dans le RB pour déterminer les temps d'exposition équivalents pour les essais accélérés dans l'étape suivante.

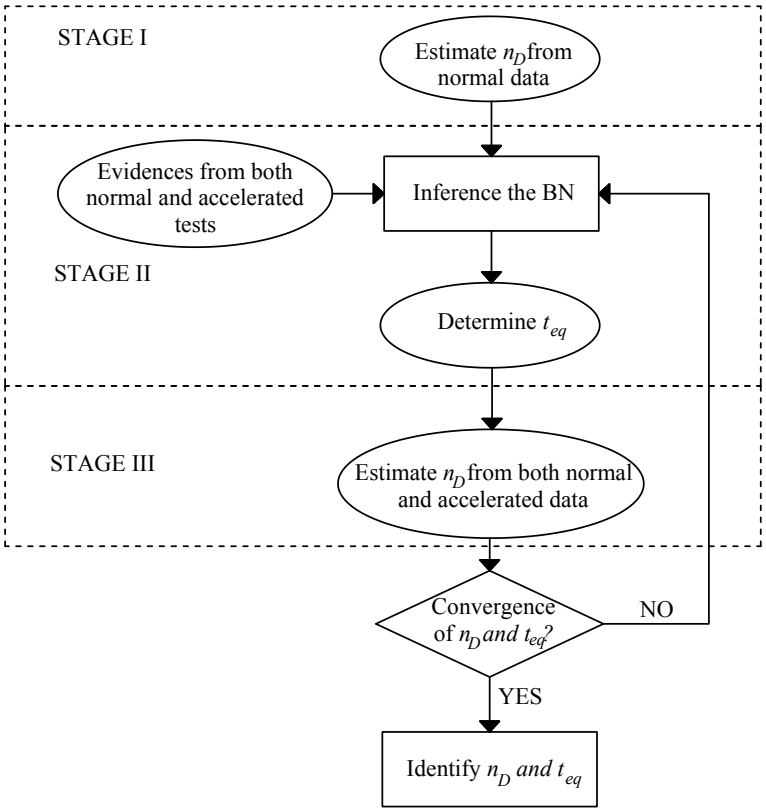

Figure 9: Organigramme d'identification du facteur de vieillissement et des temps d'exposition équivalents

La phase II de cette procédure vise à déterminer les temps d'exposition équivalents (t_{eq}) avec les données issues des tests normaux et accélérés (Figure 8). Les données accélérées ont été obtenues pour 3 durées d'exposition différentes (T4, T5 et T6). Cette phase se termine lorsque les temps d'exposition équivalents T4, T5 et T6 sont déterminés.

Les temps équivalents identifiées dans l'étape II sont essentiels pour la ré-estimation du facteur de vieillissement dans la phase III. Ils permettent de ré-estimer le facteur de vieillissement en intégrant des nouvelles valeurs de D obtenues aux durées T4, T5 et T6 avec celles obtenues à partir des essais non-accélérés (T1, T2 et T3). Le réajustement du modèle avec ces nouvelles informations est présenté en Figure 10. On observe que l'introduction des nouvelles données issues des essais accélérés donne des informations complémentaires sur l'évolution à moyen ou à long terme du coefficient de diffusion des chlorures en fonction du temps. Dans ce cas, le coefficient peut être surestimé si l'on utilise seulement les données de tests non-accélérés. La nouvelle valeur du facteur de vieillissement obtenue après ce nouveau fittage sera insérée dans le RB pour une nouvelle itération. Les étapes II et III sont répétées jusqu'à convergence dans l'estimation des paramètres.

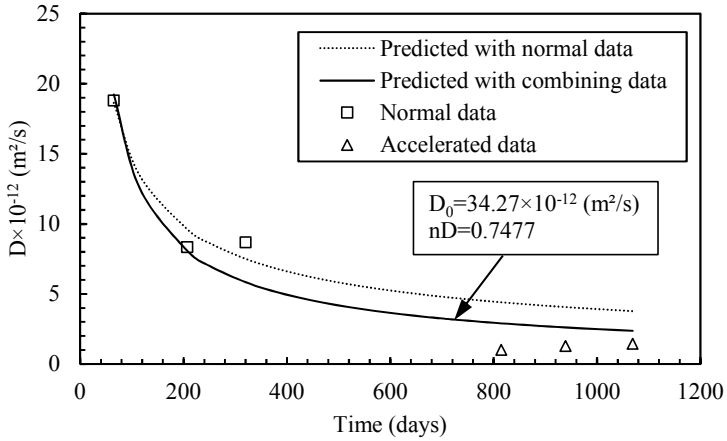

Figure 10: Ré-estimation du facteur de vieillissement en effectuant un fittage des données avec des tests non-accélérés et accélérés à l'itération 1.

Le Tableau 1 présenté l'évolution des paramètres après quelques itérations. La procédure pour identifier le facteur de vieillissement dans cette étude s'arrête après 4 itérations lorsque la valeur de n_D atteint une valeur quasi-constante (à 1‰ près) n_D = 0,74. Les temps équivalents T4, T5 et T6 voient également leur valeur converger au bout de 4 itérations. Après chaque itération, la moyenne et l'écart-type des paramètres C_s et D_0 sont aussi recalculés; il est constaté que leur valeur converge également (Tableau 1). Ainsi, on peut conclure que cette approche est efficace pour la caractérisation du facteur de vieillissement, malgré des données expérimentales limitées.

Tableau 1: Évolution des paramètres du modèle pendant la procédure itérative

Paramétrés	Mise à jour avec des données normales	Itération 1	Itération 2	Itération 3	Itération 4
Moyenne C_s [kg/m^3]	0.6048	0.5912	0.5712	0.5719	0.5719
Écart-type C_s [kg/m^3]	0.0999	0.0975	0.0920	0.0923	0.0923
Moyenne D ×10^{-12}[m²/s]	12.4	12.1	16.3	16.2	16.2
Écart-type D ×10^{-12} [m²/s]	4.91	4.80	5.09	5.09	5.10
n_D	0.5700	0.5700	0.7477	0.7398	0.7401
T4 [jours]	–	815	899	893	893
T5 [jours]	–	939	1036	1035	1035
T6 [jours]	–	1069	1253	1245	1245

Probabilité d'initiation de la corrosion lorsque les données d'inspection sont limitées

Cette section examine l'influence de la qualité des paramètres probabilistes identifiés à partir du RB sur l'évaluation de la probabilité d'initiation de la corrosion en béton armé qui est l'estimateur recherché lorsque l'on inspecte une structure dégradée. La probabilité d'initiation de la corrosion est calculée en considérant que la concentration critique en chlorures suit une loi uniforme: $C_{th} = U\left(\mu = 1kg/m^3; \sigma = 0.29kg/m^3\right)$ et une épaisseur du béton d'enrobage de $c = 6$ cm. La mise à jour du RB pour chacun des paramètres donne des histogrammes a posteriori des variables aléatoires à identifier. Ces histogrammes sont directement utilisés dans un algorithme de Monte Carlo pour éviter les hypothèses sur des lois distributions analytiques.

La Figure 11a indique que les paramètres d'entrée identifiés à partir d'un point en profondeur ne fournissent pas des prédictions suffisamment acceptables par rapport aux valeurs théoriques. En revanche, la Figure 11b montre que la considération des données sur la totalité de la profondeur améliore considérablement la prédiction de la probabilité d'initiation de la corrosion. Elle montre également que, lorsque Δx est petit, les résultats de l'identification sont plus proches des valeurs théoriques.

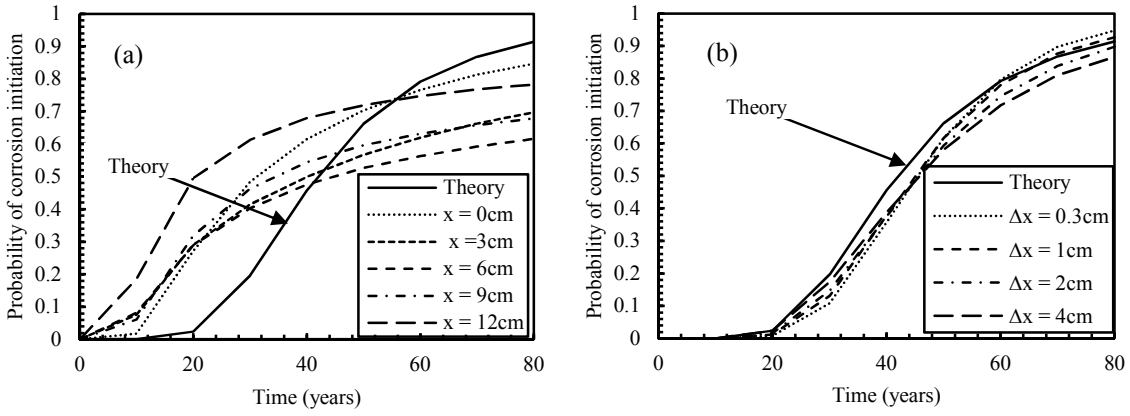

Figure 11 - Probabilité d'initiation de corrosion avec les données obtenues: (a) à partir d'un point d'observation de profondeur unique - (b) de la profondeur totale d'inspection

Les résultats présentés précédemment utilisent un nombre de simulations très large pour la génération des évidences. Cependant, en pratique le nombre de profils que l'on peut obtenir lors d'une campagne d'inspection reste limité. La Figure 12a montre la probabilité d'initiation de la corrosion

lorsque il y a uniquement 15 profils disponibles. On note que les écarts sont très importants en comparaison avec la Figure 11b. Afin d'améliorer l'identification dans le cas d'un faible nombre de mesures, nous allons utiliser les résultats de l'identification de C_s obtenus avec un point d'inspection ($x \approx 0$) comme des données a priori pour l'identification de D avec l'ensemble de mesures sur la profondeur. D'après la Figure 12b, on observe que cette identification en deux étapes donne des estimations de la probabilité de défaillance plus proches des valeurs théoriques. L'écart augmente lorsque le temps est supérieur au temps d'inspection (t=10ans) mais il pourrait se réduire en considérant un deuxième temps d'inspection.

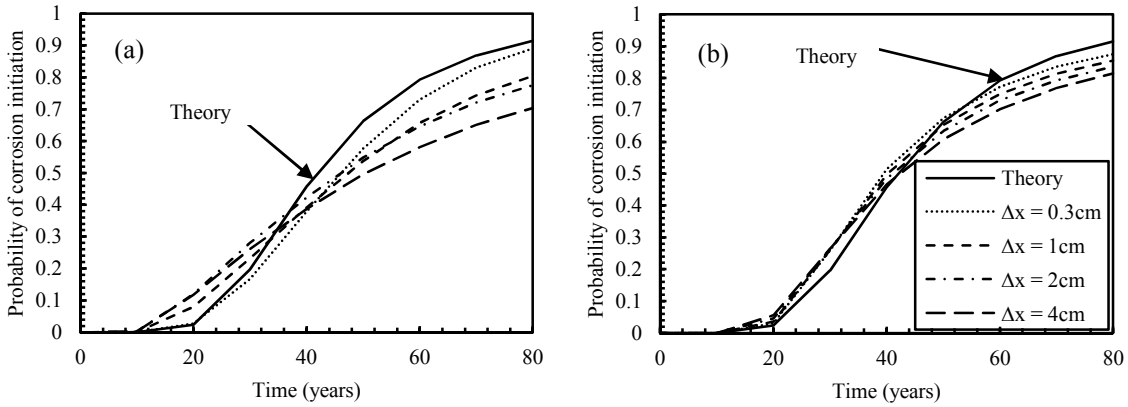

Figure 12: Probabilité d'initiation de la corrosion avec des données limitées: (a) avant amélioration - (b) après amélioration

Conclusions et perspectives

La pénétration des chlorures est l'une des principales causes de la corrosion des structures en béton armé. L'identification probabiliste des paramètres des modèles de chloration est donc cruciale pour améliorer la prédiction du temps d'initiation de la corrosion. Cette étude a mis en évidence qu'un RB fournit une possibilité d'identifier des variables aléatoires à partir des données d'inspection récoltées lors de tests non-accélérés et/ou accélérés. Les résultats ont montré qu'il existait des configurations optimales des RBs pour l'identification de chaque paramètre (C_s ou D). Pour C_s, une inspection avec un point de mesure proche de la surface et au début de l'exposition réduit les erreurs d'identification. Concernant D, l'identification doit utiliser des données issues de la profondeur totale d'inspection. La performance (vis-à-vis la durabilité) à moyen ou long-terme des matériaux peut être évaluée à partir des données accélérés. Nous avons donc proposé une méthodologie pour intégrer les résultats des essais accélérés dans la procédure d'identification des paramètres des modèles. Les résultats obtenus montrent que l'approche proposée est un outil puissant pour un tel problème

d'identification en fonction du temps. Une stratégie visant à améliorer l'évaluation de la probabilité d'amorçage de la corrosion est aussi proposée. Dans cette stratégie, des résultats des deux configurations des RBs sont combinés pour réduire les erreurs d'identification. Les résultats révèlent que cette stratégie est utile même si les données d'inspection sont limitées.

Suite à cette étude, plusieurs aspects pourront être développés dans des travaux futurs :

- La considération de l'erreur du modèle à partir des données expérimentales.
- L'extension de la méthode pour l'identification des champs aléatoires.
- L'application de la procédure développée pour l'identification des paramètres de modèle d'autres types de dégradations : carbonatation, biodégradation, etc.

La considération des coûts d'inspection pour recommander des configurations visant à minimiser l'erreur d'identification et le coût au même temps.

Chapter 1
Literature review

1.1. Introduction

Nowadays, Reinforced concrete (RC) is a widely used construction material for various types of structures: bridges, offshore platforms, quays, buildings, sewer networks, tunnels, pipelines, etc. In general, RC is a very durable material capable of withstand a large range of severe environments including marine, industrial and alpine conditions. Despite the fact that the majority of these structures shows good long-term performance and high durability, there is still a large number of failures of concrete structures as a result of premature reinforcement corrosion. Bhide (1999) reported that about 173,000 bridges in the United States are structurally deficient or functionally obsolete due in part to corrosion. With regards to economic aspects, Virmani (2002) reports that the annual direct cost of corrosion highway bridges in US was about $8.3 billion, where $4.5 billion was spent on maintenance and $3.8 billion was used to replace structurally deficient bridges over a time window of 10 years. There are similar results from Australia, Europe and the Middle East.

One of the main factors leading to corrosion in reinforcing bar is chloride ingress into the concrete. In regions with a marine environment and warm climatic conditions, the corrosion process may be significantly accelerated. From a scientific point of view, chloride-induced corrosion in RC structures is a complex process. It is characterised by several factors related to concrete properties (water/cement ratio, porosity, strength, etc.), environmental conditions (temperature, humidity, level of chloride concentration, etc.) and loading conditions (Bastidas-Arteaga et al. 2010b; El Hassan et al. 2010). In the literature, both probabilistic and deterministic approaches have been proposed. However, due to the large number of uncertainties, using deterministic approaches for modelling this deterioration issue can lead to inaccurate and inadequate assessments. As an alternative, statistic and/or probabilistic methods could bring rational predictions of the lifetime of structures (Bastidas-Arteaga et al. 2011; El Hassan et al. 2010; Nogueira and Leonel 2013; Samarakoon and Sælensminde 2015). Parameters in these models can be estimated from data obtained by laboratory tests and/or periodic inspection or

monitoring of structures. An appropriate model with a comprehensive method for parameter estimation can provide very useful information for scheduling proactive maintenance in RC structures (Gjorv 2009) .

Within this context, the main objectives of this chapter are:

- to describe the deterioration process of RC concrete subjected to chloride penetration;
- to introduce various models for describing chloride ingress into concrete;
- to present several methods for uncertainty modelling and parameter estimations and, based on this review, to select appropriate approach for probabilistic modelling of chloride ingress and for parameter identification.

The deterioration process of RC structures under chloride attack is presented in section 1.2. Section 1.3 describes several chloride ingress models. Different methods for parameter estimation are introduced in section 1.4. Section 1.5 and 1.6 present reliability assessment of chloride ingress model and different metamodels approaches for uncertainty modelling.

1.2. Deterioration process due to chloride-induced corrosion

The conditions which lead to corrosion of steel in RC structures are becoming well understood. Nevertheless, many existing RC structures show significant corrosion, often when comparatively new, leading to the need for expensive repair. In most cases either the structures were not durable enough or the appropriate maintenance had been neglected. Corrosion of the reinforcement embedded in concrete causes most of the failures of concrete structures. This process reduces structural capacity of structures or of structural members affecting the structural safety.

Chloride ions can come from several sources. They can be already present in concrete after casting or they can diffuse in from the outside. Pre-existing chloride in concrete can be due to (Broomfield 2006):

- deliberate addition of chloride set accelerators (calcium chloride $CaCl_2$ was widely used until the mid-1970s);
- use of seawater in the mix; and
- contaminated aggregates.

Chloride can ingress into concrete due to:

- sea salt spray and direct seawater wetting;
- use of de-icing salts during winter seasons; and
- use of chemicals (structures used for salt storage, brine tanks, aquaria, etc).

Most of studies on corrosion focus on the chloride ingress into concrete from external sources because this is the major problem in most parts of the world either due to marine salt spray or use of de-icing salts. However, the proportion to corrosion due to pre-existing chloride in concrete must not

be neglected especially when they are part of the problem. This often happens in marine conditions where the seawater contaminates the original concrete mix and then diffuses into the hardened concrete.

The service life of RC structures can be divided into two distinct phases (Figure 1.1).

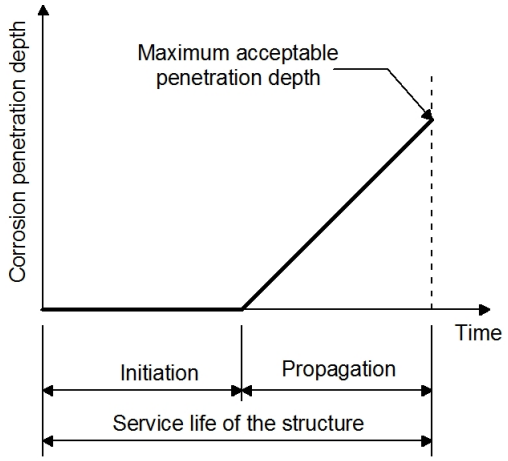

Figure 1.1: Initiation and propagation periods for corrosion in a reinforced-concrete structure (Tuutti 1982).

- *Initiation phase:* During this phase, aggressive substances (chloride ions) can depassivate the steel by penetrating from the surface into the concrete bulk. If their concentration at the surface of the rebar reaches a threshold value, the protective layer may be locally destroyed and corrosion starts.

The duration of the initiation phase depends on the cover depth, the penetration rate of aggressive argents as well as on the threshold concentration necessary to depassivate the steel. The influence of concrete cover is obvious and design codes define cover depths according to the expected environmental class (EN206). The rate of ingress of the aggressive agents depends on the quality of the concrete cover (porosity, permeability) and on the microclimatic conditions (temperature, wetting, drying, etc.) at the concrete surface. Additional protective measures can be used to prolong the initiation phase.

- *Propagation phase:* Breakdown of the protective layer is the necessary prerequisite for the initiation of corrosion. Once this layer is destroyed, corrosion occurs only if water and oxygen are present on the surface of the reinforcement. The corrosion rate determines the time necessary to reach the minimally acceptable structured conditions (Figure 1.1). This corrosion rate can vary considerably depending on surrounding temperature and humidity. Corrosion by chloride is generally localised (pitting corrosion), with penetrating attacks of

limited area (pits) surrounded by non-corroded areas. Only when very high levels of chlorides are present (or the pH decreases) the passive film may be destroyed over wide areas of the reinforcement and the corrosion will be of a general nature.

Taking into account concrete cracking, the propagation phase can be subdivided into two stages (Figure 1.2) (Bastidas-Arteaga 2010). Figure 1.2 shows that the effect of chloride induced deterioration during the service life of structures can be described by a coefficient called *reliability index* β. This parameter indicate the probability of interest events such as: corrosion initiation, concrete cracking or failure. It considers the uncertainties and deterioration processes that produce a decrease of the reliability index in time. In accordance with the deterioration phases described in Figure 1.1, we distinguish three deterioration stages:

- *Stage 1:* starting immediately after construction when the structural reliability has the maximum value β_{ini}, this stage finishes when the reinforcement bars start to be actively corroded corresponding to the *corrosion initiation time* (t_{ini}).
- *Stage 2:* it begins when corrosion appears. In this stage, corrosion products are created and they occupy more space than the original steel causing expansive stresses that initiate the concrete cracking process. This stage contains two sub-stages called: *time to crack initiation* (t_{cr}) and *time to severe cracking* (t_{sp}). The former is the time required to reach a hairline crack of 0.05mm width and the latter is the time required to reach a threshold crack size $\left(\text{e.g.}, c_{w\lim} = 0.5\text{mm}\right)$.
- *Stage 3:* after serve concrete cracking, the corrosion rate increases because more water and oxygen are available at the corrosion cell causing a significant decay in value of reliability. This stage ends when the reliability reaches a minimum value β_{min} corresponding with the cases where structural serviceability and/or safety are no longer satisfied.

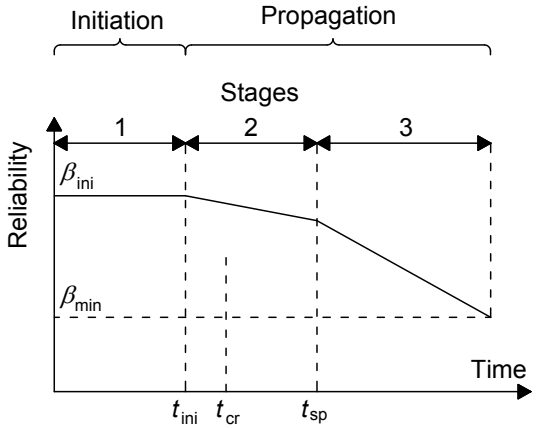

Figure 1.2: Reliability profile for RC structures subjected to corrosion (Bastidas-Arteaga 2010)

The consequences of corrosion of steel reinforcement do not involve only the serviceability or the external aspect of the structure, but may also affect its structure performance, and therefore its safety. The main structural consequences due to corrosion are summarised in Figure 1.3. Corrosion is often distinguished by rust spots that appear on the external surface of the concrete, or by damage to the concrete cover produced by expansion of the corrosion products. These products in fact occupy a much greater volume than the original steel bar producing tensile stresses that generate cracks in the concrete cover (Figure 1.4a), spalling in a localised area, or complete delamination (Figure 1.4b). Reduction of bond of the reinforcement to the concrete may also occur. In cases of localised corrosion, the cross section of the reinforcement can be significantly reduced (Figure 1.4c) and thus its loading capacity and its fatigue strength decrease. Finally, under very special conditions that lead to hydrogen embrittlement of high-strength steel, brittle failure of some types of prestressing steel can take place (Figure 1.4d).

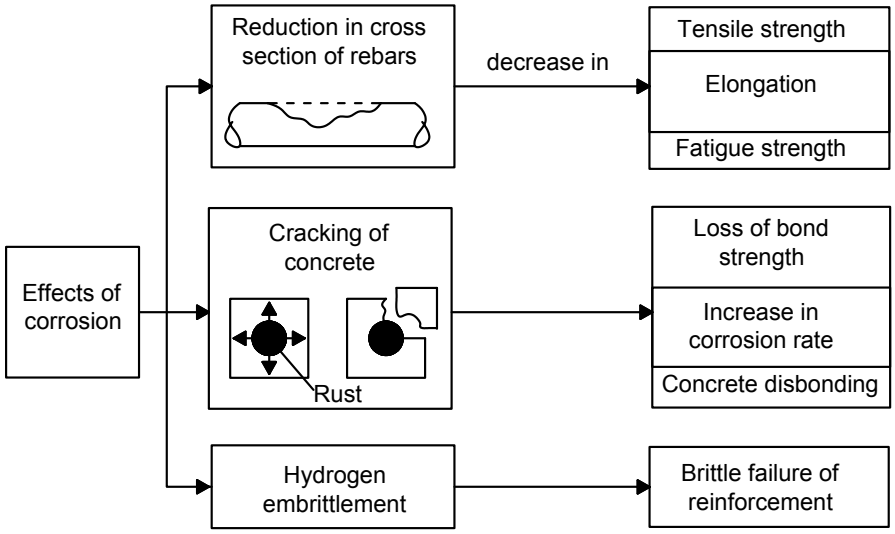

Figure 1.3: Structural consequences of corrosion in reinforced concrete structures (Bertolini et al. 2004)

In practice, structures could be maintained to avoid corrosion initiation which may lead to serious structural consequences. This preventive repair is performed by collecting measurements of chloride profiles and proposed appropriate repair techniques. In fact, according to Bastidas-Arteaga et al. (2009) the total corrosion-fatigue life (t_T) of structures can be divided into three stages: (1) corrosion initiation (t_{ini}), (2) pit-to-crack transition (t_{pt}) and (3) crack propagation (t_{cp}). Figure 1.5 compares the proportion of each stage in the total corrosion-fatigue life by the ratio of the time-spans. In two cases considered corresponding to two level aggressiveness of environment, the proportion of corrosion initiation stage is predominant, being larger than 60% of t_T. Therefore, it will be more efficient to spend maintenance efforts to control this stage of the process.

The maintenance strategies aim at ensuring optimal levels of serviceability and safety during the structural lifetime. This strategy often consists of two stages: inspection and repair in which inspection results are employed for the diagnosis: detecting corrosion at early stages, predicting its extent of damage and proposing appropriate repair actions. The preventive maintenance strategy considered in this study was previously proposed by Bastidas-Arteaga (2010) within the framework of the MAREO project. In this study, inspection is performed by determining the chloride content at the cover depth of concrete core. Then, based on inspection results, the repair technique consists of rebuilding the polluted concrete cover by several methods. The advantage of this approach is that repair is more preventive than corrective and thus, it will ensure an optimal level of safety and serviceability during structure's lifetime.

Figure 1.4: Examples of some consequences of corrosion of steel in concrete (a) cracking of column and cross beam; (b) spalling and delamination of concrete; (c) pitting corrosion causing cross section reduction; (d) brittle fracture of prestressing tendons due to hydrogen embrittlement (Bertolini et al. 2004)

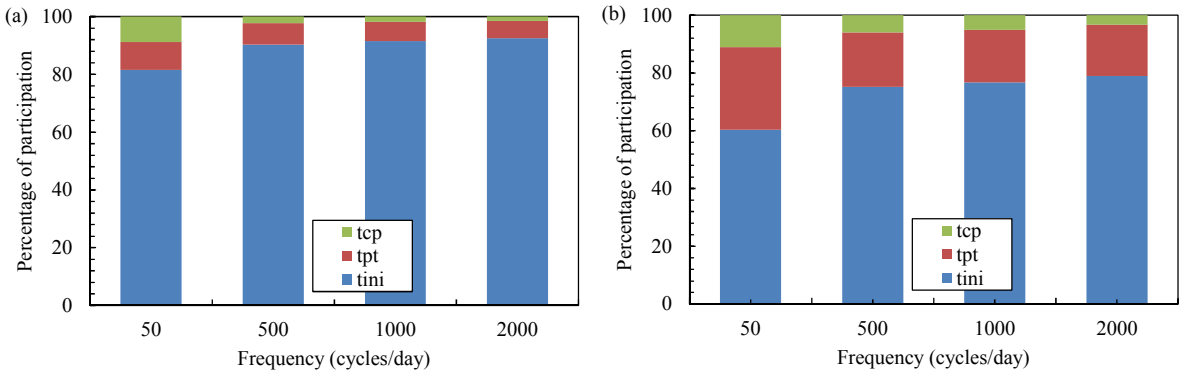

Figure 1.5: Participation of each phase in the total corrosion-fatigue life: (a) low aggressiveness and (b) extreme aggressiveness. (Bastidas-Arteaga et al. 2009).

1.3. Chloride ingress modelling

In general, the traditional steels used as reinforcing steel are very sensitivity to corrosion when they are exposed in the natural environment. However when they are combined with concrete to form reinforced concrete material, the chemical substances contained in hardened cement paste will create a passivating film forming on the surface of steel and protect it against corrosion. However, this characteristic will be weaken when structures are subjected to chloride attack, chemical solution will be altered by chloride contamination of the concrete cover. In most corrosions cases, the main causes often come from the improper use of material, inappropriate control in mixing and underestimate of concrete cover in design stage. The main consequences of chloride ingress in RC structures include a reduction in steel cross-sectional area, cracking, spalling and delamination of concrete cover as well as loss in bond between steel and concrete.

In recent years, a lot of model has been developed to predict chloride ingress into concrete (Khitab 2005). Most of these approaches are devoted to study corrosion in the initiation phase. As previously mentioned, this trend can be seen reasonable when this stage of corrosion process contributes major proportion in corrosion-fatigue life of structures. Therefore, it may lead to prevailing opinion that the occurrence of corrosion initiation defines the end of service life of structures, despite the fact that the propagation stage also makes significant proportion to service life (Figure 1.1).

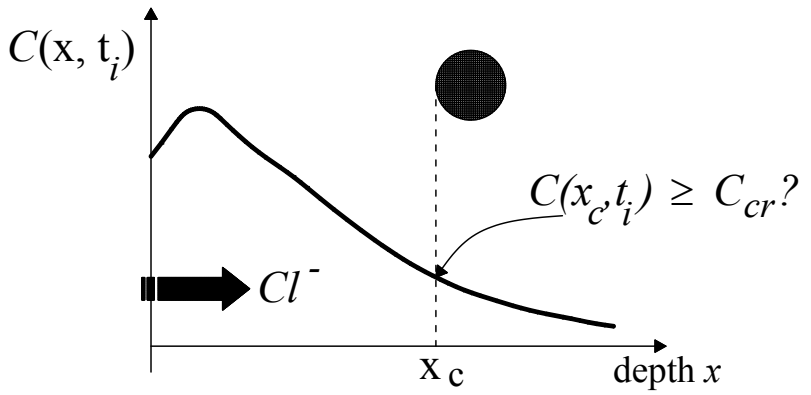

Figure 1.6: Comparison between the predicted chloride content at the depth of the reinforcement and the chloride threshold level for corrosion (Luping et al. 2012).

A model for predicting chloride ingress estimates chloride content $C(x,t)$ at depth x after a certain exposure time t. If the value of x is equal to the position of the steel bar, the results serve to evaluate the corrosion initiation risk by comparing the predict value with a chloride threshold level (Figure 1.6). Chloride ingress models have input parameters characterising material properties and exposure environment. The outputs then reflect or explain real data obtained from field inspections for a given environment and material.

1.3.1. Chloride penetration in saturated concrete

Chloride penetration from the environment produces a profile in the concrete characterised by a high chloride content near the external surface, that decreases at greater depths. In saturated concrete, the Fick's diffusion equation (Tuutti 1982) is usually used to predict the unidirectional diffusion (in x-direction):

$$\frac{\partial C_{f_c}}{\partial t} = D_c \frac{\partial^2 C_{f_c}}{\partial x^2} \tag{1.1}$$

where C_{fc} is the concentration of chloride dissolved in pore solution, t is the time and D_c is the effective chloride diffusion coefficient. Assuming that concrete is an homogeneous and isotropic material with the following initial conditions: (1) the concentration is zero at time $t = 0$ and (2) the chloride surface concentration is constant; the free chloride ion concentration $C(x,t)$ at depth x after time t for a semi-infinite medium could be expressed by an analytical solution to Fick's equation using the error function:

$$C(x,t) = C_s \left[1 - erf\left(\frac{x}{2\sqrt{D_c t}} \right) \right] \tag{1.2}$$

where C_s is chloride surface concentration and $erf(.)$ is the error function.

The equation above is used to calculate easily the chloride concentration at depth x and given time t. This relation theoretically describes the kinetics of a non-stationary diffusion process. However, the equation (1.2) is just valid when RC structures are saturated and subjected to constant concentration of chlorides on the exposed surface. These conditions are rarely present for real structures because concrete is a heterogeneous material that is frequently exposed to time-variant surface chloride concentrations. Only in concrete completely and permanently saturated with water can chloride ions penetrate by pure diffusion. In most situations, other transport mechanisms contribute to chloride penetration. For instance, when dry concrete comes into contact with salt water, initially capillary suction of the chloride solution occurs. In many cases, wetting and drying occur, at least in the outer zones of the concrete, so that evaporation of water leads to enrichment of chloride ions. Besides, this solution does not consider chloride binding capacity, concrete ageing and other environmental factor such as temperature and humidity (Saetta et al. 1993). Although, this model neglect some important phenomena and could not give a correct analysis for prediction of chloride ingress, this solution will be used in chapter 3 to illustrate the proposed methodology for the identification of random variables using BN because its complexity is sufficient to account for the non-linear effects in *x*-direction and in time.

In spite of oversimplified some assumptions, the error function models are widely used by practical applications due to their relative simple mathematical expressions. The simplest error function model represented by equation (1.2), which treats the chloride diffusion coefficient as constant in time and space, has been proved to be conservative due to the lack of consideration of the retarding effect on the diffusion process resulting from chloride binding and the refinement of the pore structure over time. Consequently, to take into consideration the time-dependency of chloride diffusion coefficient, a so-called age factor with exponential relationship is added.

The European Union project, Duracrete (2000), proposed an extension of equation (1.2) which considers the influence of material properties, environment, concrete ageing and curing on the chloride diffusion coefficient:

$$C(x,t) = C_s\left[1 - erf\left(\frac{x}{2\sqrt{k_e k_t k_c D_0 \left(\frac{t_0}{t}\right)^{n_D} t}}\right)\right] \tag{1.3}$$

where k_e is an environmental factor, k_t is a factor which considers the influence of the test method to measure the diffusion coefficient D_0, k_c is an influence factor for concrete curing, D_0 is the chloride migration coefficient measured at defined compaction, curing and environmental condition, t_0

is the reference period to measure D_0 and n_D is the age factor. This model can in theory provide a better service life assessment than one provided by equation (1.2). However, according to Bastidas-Arteaga (2010) it does not take into consideration: (1) chloride flow in unsaturated conditions, (2) time-variant nature and the influence of surface chloride concentration, environment humidity and temperature; (3) chloride binding capacity; and (4) the flow of chloride in two-dimensions. Since corrosion rates are higher in unsaturated conditions where the availability of both oxygen and water are large, a comprehensive model should include these phenomena.

Luping and Gulikers (2007) demonstrated that the simplified models such as equation (1.3) can be used for long-term prediction without significant mathematics errors if the age factor n_D is small $\left(n_D < 0.3\right)$, but it may underestimate the service life if high value of *n* is used. However, due to the fact that there is still a lack of information about the long-term effect of time-dependent chloride diffusion coefficient, this underestimation could be tolerated for long-term prediction. For short-term exposure, this solution should not be used because the model will overestimate significantly the chloride diffusion coefficient.

Nilsson and Carcasses (2004) proposed an improved analytical equation for modelling chloride ingress into concrete. This solution could describe the time-dependent diffusion in a more realistic way and give a relatively better prediction:

$$C\left(x,t\right) = C_s\left[1 - erf\left(\frac{x}{2\sqrt{\frac{D_0}{1-n_D}\left[\left(1+\frac{t_{ex}^{'}}{t}\right)^{1-n_D} - \left(\frac{t_{ex}^{'}}{t}\right)^{1-n_D}\right]\left(\frac{t_0^{'}}{t}\right)^{n_D} t}}\right)\right] \tag{1.4}$$

where D_0 is the chloride diffusion coefficient measured at time $t_0^{'}$, $t_{ex}^{'}$ is the age of concrete at the start of exposure, n_D is the age factor. This equation is valid only under these assumptions: (1) concrete is a homogeneous material, (2) chloride binding is time-independent and linearly proportional to the free chloride concentration, (3) the effect of co-existing ions is constant, and (4) the diffusion is one dimensional into semi-infinite space. This model is used to illustrate the time-dependency of the chloride ingress process in chapter 3.

1.3.2. Chloride penetration in unsaturated conditions

In unsaturated conditions, Saetta et al. (1993) proposed a numerical model for studying chloride penetration into concrete that accounts for material parameters and its variability with time, different environmental conditions, and the interaction between the diffusion chloride ions and the concrete material. This approach is based on a system of partial differential equations describing the

relationships between the chloride ingress coupled of other phenomena (environmental humidity and temperature, cement hydration degree, heat diffusion, chloride binding, etc.).

Based on this work, Martín-Pérez et al. (2001) proposed a solution to address a coupled boundary-value problem which is created from chloride transport, moisture and heat transfer. The study of Martín-Pérez et al. (2001) deals with the variations in time (t) by using a finite element formulation with a time-step integration procedure finite different schemes. This research also develops a two-dimensional (2D) finite element formulation to describe chloride ingress at a corner of a RC member (Figure 1.7). Results indicated that chloride content along the concrete cover is significant higher in the 2D model. The flattening part of chloride content curve near the surface is due to the "corner" effect. It is also worth noticing that the oxygen-transport to the reinforcement is added to the system of partial differential equations to account for its influence after corrosion initiation.

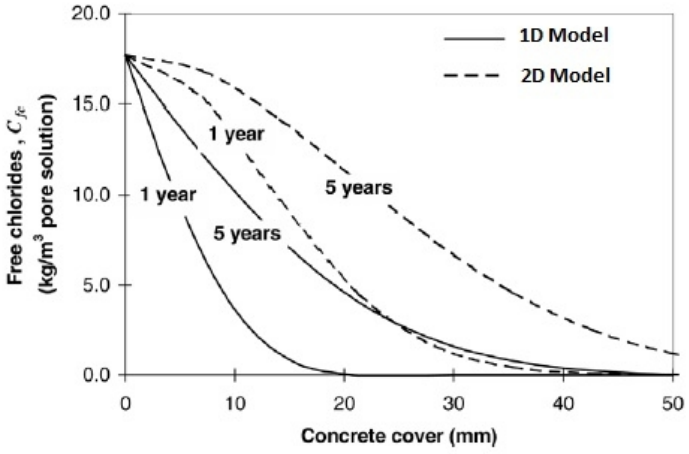

Figure 1.7: Free chloride profiles after one year and five years of exposure for one and 2D flows (Martín-Pérez et al. 2001).

Ababneh et al. (2003) developed a comprehensive model for chloride diffusion in non-saturated concrete by establishing a system of PDEs describing the penetration of chloride ion. In these equations, the material parameters considered the influences of the aggregate, the cement paste, the water cement ratio and curing time of concrete.

Under different exposure conditions, the saturation levels influence the chloride ingress process. Nielsen and Geiker (2003) proposed an approach to show the dependency of the chloride diffusion coefficient on several degrees of saturation by applying a combination of composite theory and Power's model (Table 1.1). Results from prediction in Figure 1.8 allow estimating the dependency of the diffusion coefficient on the degree of saturation. However, this study just deals with three saturated conditions (at 65% Relative Humidity (RH), 85% RH and Vacuum Saturated), thus the prediction from curve fitting can be inaccurate. Moreover, in nature conditions, the level of saturation is highly variant and more complex.

Table 1.1: Apparent Diffusion coefficient in different unsaturated conditions

Conditioning	Exposure	D_{app} $\left(m^2/s\right)\times10^{-12}$	$D_{simulated}$ $\left(m^2/s\right)\times10^{-12}$
65% RH	26.4% NaCl for 2h followed by drying and 65% RH	2.4	5.5
85% RH	26.4% NaCl for 2h followed by drying and 85% RH	3.8	7.9
Vacuum saturation	Immersed in 3% NaCl	12.9	20.2

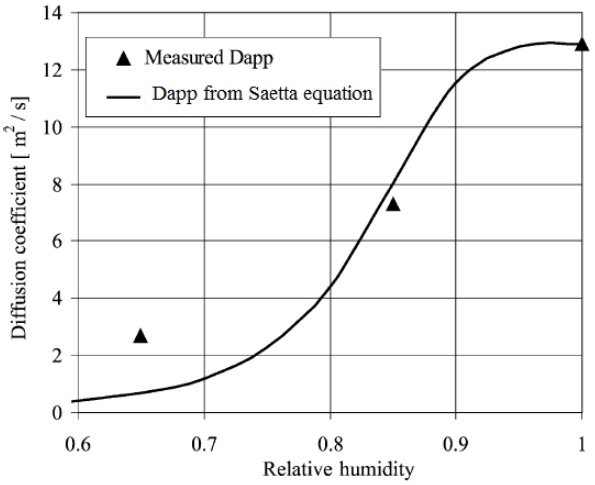

Figure 1.8: Apparent diffusion coefficient in several saturated levels (Nielsen and Geiker 2003).

Bastidas-Arteaga et al. (2011) introduced the model proposed by Martín-Pérez et al. (2001) into a stochastic framework, the proposed approach considers the phenomena of chloride ingress, moisture transport and heat transfer. This study proved that the mean of corrosion initiation time decreases when chloride binding is taken into account (Figure 1.9a) and when the randomness and seasonal variations of humidity, temperature and convection are considered (Figure 1.9b). It also revealed that high probabilities of corrosion initiation correspond to the 2-D exposure as compared to that in 1-D exposure. This research suggested that some implementations should be considered to improve the probabilistic model of chloride penetration such as: the interactions between concrete cracking and chloride penetration, the influence of time variation of temperature and humidity, the correlation of material properties and climatic condition from experimental data, the spatial variability and the model error.

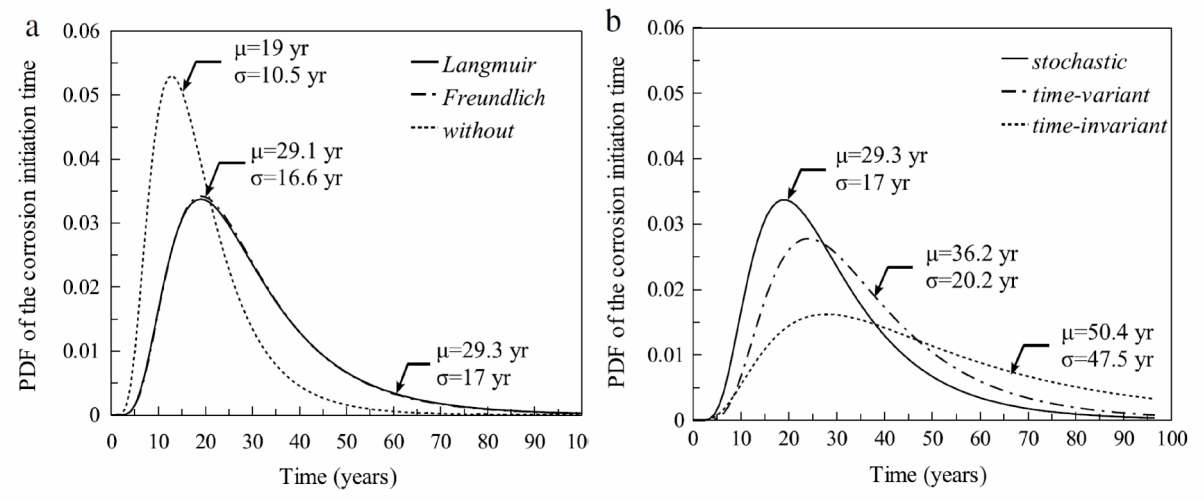

Figure 1.9: Effect of (a) binding and (b) weather model (Bastidas-Arteaga et al. 2011)

1.4. Parameter estimation methods

Parameter identification is a traditional modelling task. Generally, a model contains input variables, parameters, and output variables. It also describes, in a mathematical form for our purposes, how the output is related to the input and the parameters. A model can be viewed as a template of the modelled system. The parameter specification makes the template applicable to a particular experiment.

Experimental databases have certainly similar characteristics. First, measurement noise (error) is present. Second, the measurements are made at discrete times. These are the limitations of virtually all data sources and must be considered by all parameter identification methods. The task of the parameter identification is to recover "true" parameter values from these imperfect measurements. Often, the true values are not measured by other (more direct) means or represented by a theoretical concept without a physical counterpart. In any case, the presence of the measurement error always means that the exact parameter values cannot be determined with absolute confidence. These can be determined only within a certain confidence and the parameter estimation problem includes the subproblem of assessing the accuracy and precision of parameter estimates. The accuracy and precision are crucial for the results.

In chloride-induced corrosion, experimental data obtained after each inspection campaign is often chloride content in concrete. The data collected at different depths from the concrete surface is called "chloride profile". This data is used to determine chloride ingress model parameters which will further serve in assessment the lifetime of RC structure or planning inspection campaigns. This section describes different methods often used in parameter estimation of chloride-induced corrosion including: Least Squares (LS), Maximum Likelihood (ML) and Bayesian estimators.

1.4.1. Least Square Estimation (LSE)

The LSE method is a standard method for estimating model parameters. It aims at minimising the square differences between measurements and model prediction.

Let $q_i = f(x_i, \theta)$ denote the predicted model response at variable x_i, where θ is a vector denoting the uncertain parameter. The relation between the measured value y_i and the corresponding value calculated by the model can be written:

$$y_i = q_i + \varepsilon_i = f(x_i, \theta) + \varepsilon_i \tag{1.5}$$

where ε_i refers to model residual error at variable x_i, assumed to be $\varepsilon_i \sim N(0, \sigma_i^2)$

The parameters are chosen to minimise the sum of squared errors (SSE) between simulated and measured values:

$$SSE = \sum_{i=1}^{n} [y_i - f(x_i, \theta)]^2 \tag{1.6}$$

where n is the number of observation. The equation above can be rewriten with an explicit equation for LS parameters:

$$\hat{\theta}_{LSE} = \arg\min_{\theta} \left\{ \sum_{i=1}^{n} [y_i - f(x_i, \theta)]^2 \right\} \tag{1.7}$$

Equation (1.7) implies that the LS parameters are the arguments of the model that minimise the sum of squared errors.

1.4.2. Maximum Likelihood Estimation (MLE)

The LSE minimises a sum of squares of residuals. The functional form to be minimised might be somewhat arbitrary. Other functional forms, such as absolute values of residuals, could also be considered. In most cases, different functional forms define several performance planes with different positions of local and global minima and thus give different parameter estimates.

MLE formulates the parameter estimation problem within a probabilistic framework. This greatly clarifies the interpretation of parameter estimates provided by both methods. Let consider a given set of parameters that is employed to make model predictions. For this set, the residuals are defined as the differences between predictions and measurements. We may now be interested in the probability of the occurrence of these residuals, which means that we can evaluate the conditional probability of residuals given the parameter vector. This probability is called likelihood. Then the MLE method aims at finding the set of parameters that maximise the likelihood. The likelihood function can be written as:

$$L = \prod_{i=1}^{n} \frac{1}{\sigma_i \sqrt{2\pi}} \exp\left[-\frac{1}{2} \left(\frac{y_i - f(x_i, \theta)}{\sigma_i} \right)^2 \right] \tag{1.8}$$

Equation (1.8) assumes that the measurement errors (residuals) are uncorrelated and normally distributed with zero mean and variances σ_i^2. Maximising L is equivalent to minimise a negative logarithm of L. After removing some constant terms, we can write the function need to minimise:

$$-\ln L = \sum_{i=1}^{n} \left(\frac{y_i - f(x_i, \theta)}{\sigma_i} \right)^2 + 2\sum_{i=1}^{n} \ln(\sigma_i) \tag{1.9}$$

In the other way, the MLE method is to find a value of $\hat{\theta}_{MLE}$ that is given by:

$$\hat{\theta}_{MLE} = \arg\min \left\{ \sum_{i=1}^{n} \left(\frac{y_i - f(x_i, \theta)}{\sigma_i} \right)^2 + 2\sum_{i=1}^{n} \ln(\sigma_i) \right\} \tag{1.10}$$

Assuming that the residual errors are all independent and normally distributed with the same variance: $\varepsilon_i \sim N(0, \sigma^2)$, equation (1.10) becomes identical to equation (1.7).

1.4.3. Bayesian Estimation

The MLE is justified on the basis of a certain probabilistic concept. It considers the likelihood function, which is the conditional probability of a given set of parameters, and it aims at maximising it. The Bayesian estimation expands this concept. It considers not only the likelihood function, but also the a priori probability of the parameters. The a priori probability represents a priori beliefs expressed in the form of a probability distribution and normally reflects the knowledge of, for instance, the population mean and variation of the parameters. It is also possible to specify a non-informative a priori, for example, a uniform ("flat") distribution for a mean value, expressing a lack of a priori knowledge.

The Bayesian estimation updates the a priori probability of parameters using measured data. The updated probability is called a posteriori probability:

$$\pi(\boldsymbol{\theta}) = P(\boldsymbol{\theta} \mid \mathbf{y}) = \frac{P(\mathbf{y} \mid \boldsymbol{\theta}).P(\boldsymbol{\theta})}{P(\mathbf{y})} \tag{1.11}$$

where $\mathbf{y} = y_1 ... y_n$ is a vector containing measurement data, $P(\boldsymbol{\theta})$ is the a priori probability of parameters and $P(\mathbf{y} \mid \boldsymbol{\theta})$ is the conditional probability of measurements given data (similar to the likelihood given by equation (1.8)).

The term $P(\mathbf{y})$ is called "normalisation constant" and is independent of the parameters, therefore, the equation can be rewritten as:

$$\pi(\boldsymbol{\theta}) \propto P(\mathbf{y}\,|\,\boldsymbol{\theta}).P(\boldsymbol{\theta}) \tag{1.12}$$

This term determines the height of the probability density at each point and makes the integral of the probability equal to 1. However, in most cases we cannot compute directly its value and without it, we cannot compute values for the probability density function. Consequently, approximate solutions will be applied to estimate the a posteriori distribution. The most popular among these is the family of Markov Chain Monte Carlo (MCMC) methods that generates samples by using various sampling procedures: Metropolis, Metropolis-Hastings, and Gibbs.

1.4.4. Discussion

In chloride ingress modelling, LSE has been a popular choice of model fitting for parameter estimation. Due to its uncomplicated procedures and properties which does not require minimal distributional assumptions like MLE, LSE becomes a useful tool for parameter identification. For example, LSE has been used for finding parameters such as: C_s and D in equation (1.2) from chloride profiles (Bioubakhsh 2011; Khitab 2005; Li 2004). MLE, on the other hand is a method of parameter estimation preferred in statistics and is a necessary tool for many statistical modelling techniques. According to Myung (2003), this method exposes many optimal properties that cannot be found in LSE method such as: providing complete information about estimated parameters or resulting in lowest-possible variance of parameter estimates archived asymptotically, etc. In chloride ingress modelling, MLE has been used by Li (2004) and O'Connor and Kenshel (2013) to estimate the values of the scale of fluctuation of the parameters C_s and D from experimental data. O'Connor and Kenshel (2013) also pointed out that MLE could be inconsistent and did not yield a unique value for the investigated parameter. This disadvantage is also mentioned by Al (2014) as there is no guarantee to always have a unique MLE estimate. Although revealing some cons, in the view of most statisticians MLE is still considered as a general method for parameter estimation. The Bayesian estimation is an expanded method based on the concept of MLE. In chloride-induced corrosion, Bayesian estimation has been used as an effective statistical tool for parameter estimation. For example, the Duracrete project (Duracrete 2000a) suggested values for parameters in chloride ingress model obtained from experimental data based on this method. The benefits of the Bayesian estimation are that the parameters to estimate can be summarised in a statistically coherent way (a posteriori probabilities). This characteristic becomes very useful when most parameters in stochastic models represent stochastic quantiles. For continuous variables, recent advances in MCMC techniques could facilitate the difficult computational aspects of Bayesian estimation. On the other hand, for discrete-state models, the development of Bayesian networks brings an efficient and comprehensive tool for parameter estimation.

1.5. Reliability assessment for chloride ingress models

The most important roles of engineering are (1) to design reliable structures that perform a given function over a certain period of time and (2) to monitor their ageing processes to predict the evolution in time of their safety level to avoid unexpected damages. In all civil engineering problems, risk is always present due to inherent uncertainties and to the inability to determine the involved parameters. The existence of uncertainty is inevitable and it should be taken into consideration in structural modelling. The classical design method (deterministic approach) takes into account the variability by introducing safety factors for each parameter. The integration of such factors increases the reliability of design since they underestimate its structural stability. However, this approach always lead to results in non-economic designs and failure still occur because safety factors might be occasionally insufficient. The more appropriate solution is using probabilistic approach (stochastic approach). This methodology takes into account the uncertainty by modelling the uncertain parameters as random variables or stochastic processes and studies the propagation of the uncertainties in system response that becomes itself a random entity. The aim of the probabilistic approach is to characterise the random response with a mean value, a variance or even a probability density function through a reliability analysis.

The probabilistic approach was first developed as a reliability analysis tool. The objective of reliability assessment is to evaluate the probability of failure of a system taking into account the uncertainty the randomness of model parameters. In this approach the governing parameters of the problem are modelled as random variables. They are stored in a random vector $\mathbf{X}$ which joint PDF of $\mathbf{X}$ is equal to $f_{\mathbf{X}}(\mathbf{x})$. For reliability analysis, the domain of the problem D is divided into the failure domain and the safe domain (Figure 1.10). The failure domain D_f is defined by:

$$D_f = \left\{ \mathbf{X} \mid g\left(M\left(\mathbf{X}\right)\right) \le 0 \right\} \tag{1.13}$$

where $M(\mathbf{X})$ represents the response of the system and $g\left(M\left(\mathbf{X}\right)\right)$ is the limit state function (or performance function) of the problem. In the simplest case, $M(\mathbf{X})$ is expressed as the subtraction between the resistance $R(\mathbf{X})$ and the demand on the system $S(\mathbf{X})$:

$$M\left(\mathbf{X}\right) = R\left(\mathbf{X}\right) - S\left(\mathbf{X}\right) \tag{1.14}$$

The safety domain, D_s, is defined by:

$$D_s = \left\{ \mathbf{X} \mid g\left(M\left(\mathbf{X}\right)\right) > 0 \right\} \tag{1.15}$$

The boundary between these two domains constitutes the limit state surface – i.e., $\left\{ g\left(\mathbf{X}, M\left(\mathbf{X}\right)\right) = 0 \right\}$. By accounting for these definitions, the failure probability, p_f, is determined by:

$$p_f = P\left[g\left(M\left(\mathbf{X}\right)\right) \le 0 \right] = \int_{g\left(M\left(\mathbf{X}\right)\right)\le 0} f_{\mathbf{X}}\left(\mathbf{x}\right) dx_1 ... dx_n \tag{1.16}$$

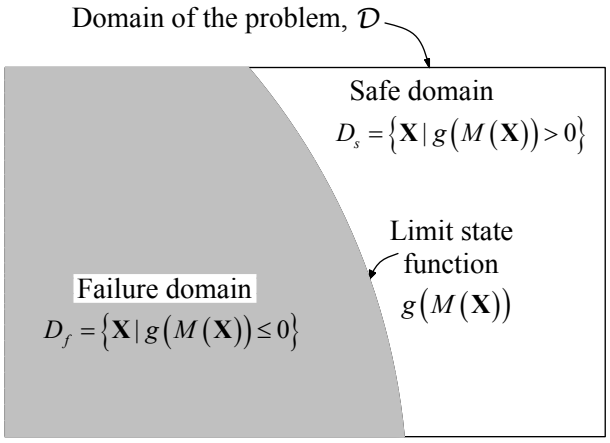

Figure 1.10: Domain of the problem for reliability analysis (Bastidas-Arteaga 2010).

The limit state functions are often used to describe the following structural conditions:

- Serviceability limit state: this state is defined when structural performances are still satisfied although a given deterioration is observed. In chloride ingress, the serviceability limit state is related to the probability of corrosion initiation.
- Ultimate limit state: this state reflects the conditions when the safety of structures is highly affected and may lead to total failure or collapse. When structures are subjected to chloride-induced corrosion, cross section of the reinforcement can be significantly reduced by corrosion and collapse occurs when the applied loading exceeds the remaining resistance. The ultimate limit state is related to the probability of failure.

In corrosion management, the probability of corrosion initiation and the probability of failure are important criteria for lifetime assessment or planning maintenance strategies for RC structures. In the literature, there are several studies using the probability of corrosion initiation for service life prediction (Nogueira and Leonel 2013; Samarakoon and Sælensminde 2015). In these studies, information about model parameters representing for material properties and exposure conditions are determined from experimental data before employing in reliability assessment. Since this study considers a preventive maintenance strategy, we focus on the identification of random variables for the evaluation of the probability of corrosion initiation. As mentioned above, since there are many sources of uncertainties related to chloride ingress, its modelling should account for a stochastic framework. However, numerical chloride ingress models are always complex and have non-linear forms. Hence, closed-form solutions for both the CDF of the time to corrosion initiation and the total chloride-induced corrosion life are difficult to obtain by traditional reliability methods. An appropriate method

to deal with this kind of issue is to use metamodels. To characterise the randomness of model parameters, the metamodels should also introduce a function for random parameter identification.

In section 1.6, different metamodels are presented and discussed to select an appropriate methodology for parameter identification and uncertainty modelling of the chloride ingress process.

1.6. Metamodels for parameter identification and uncertainty propagation

In this section, a brief introduction of reliability assessment by "metamodels" will be presented. Originally, in structural reliability assessment, metamodels are used to represent the response of a system (mechanical, social, biological, etc.) under stimuli influences. These stimuli are considered as input parameters that are often poorly known or uncertain. Therefore, metamodel is considered as approximate representations of structural behaviours. In structural reliability, it is usual to couple probabilistic algorithms with the model (assumed exact) to predict the system's responses and to plan future actions based on these results. In chloride ingress, the maintenance actions could be planed based on the evaluation of the probability of corrosion initiation with an expected target at approximate 10^{-2}. Random parameters used in reliability assessment of chloride ingress are often determined from experimental data which always contains significant uncertainty. Hence, the objective of this section is to deal with the stochastic meta-modelling of stochastic chloride ingress models and select an approach that gather the following requirements:

- deal with relative high target of probability of failure (about 10^{-2}),
- respect the transfer of distribution (stochastic characteristic of the meta-modelling), and
- introduce a function for variable identification.

1.6.1. Response Surface Method

In reliability calculation, the number of evaluations of outcomes of the performance function is a good indicator of the efficiency of the methods; as each outcome can result from a complex model associated with a complex numerical solution. Consequently, limiting the total number of outcomes is indispensable. Dealing with this problem, one of the possible methods is to construct a simple analytical representation. This representation is named 'response surface' (RS). The advantage of this method exposes in an explicit form in which the reliability calculation is largely simplified and at practically zero cost. However, it gives difficulties in justifying the approximation selected in a given domain. The flowchart of this method can be seen in (Figure 1.11) (Lemaire et al. 2010). In this approach, it is interesting that the mechanical model and reliability model are separated however the main disadvantage is that the reliability assessment is computed from an approximated mechanical model.

In structural reliability, the application of a RS is to represent the response of a system under the influence of stimuli. The response of the system, or response $\left(Y = M\left(\mathbf{X}\right)\right)$, is the result of a transfer function *M* that characterises the sensitivity of a system to input parameters (Baroth et al. 2011). Thus, this response varies corresponding to the variation of input parameters knows as stimuli. These parameters are modelled by random fields or random variables, denote X_i, $i=1,...,n$ and then characterised by a set of available statistical information, denoted θ_j, $j=1,...,p$. This process is described in (Figure 1.12). However, due to the lacking knowledge of a transfer function as an explicit form of basic random variables, an approximation called *response function*, *M* is used. This function can be written formally as (Figure 1.13). Consequently, in order to build a response surface, these information must be provided:

- $X = \left\{X_1,...,X_n\right\}$, a ranked set of representative random variables,
- $\theta = \left\{\theta_1,...,\theta_p\right\}$, a set of statistical information about *X* (independent or correlated probability density functions, normalised moments, etc.),
- $M\left(X/\theta\right)$, an approximation of the response *Y*, formulated as an explicit function of *X* knowing θ, and obtained by the fitting of the set of parameters χ, and
- |.| a metric in the probabilistic space of basic random variables and responses.

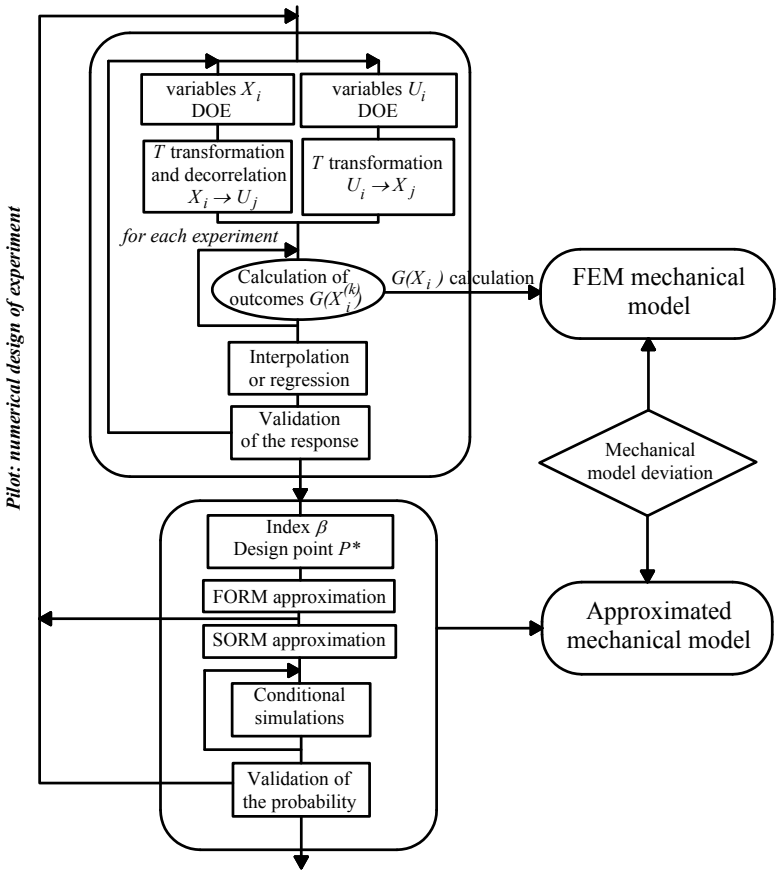

Figure 1.11: Principle of the response surface method (Lemaire 2010).

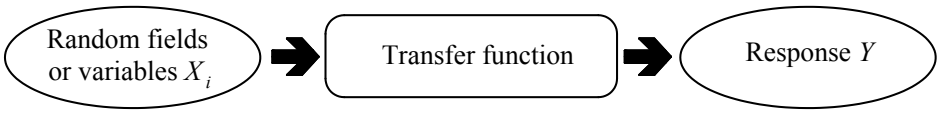

Figure 1.12: Response of a transfer function to stimuli, modelled by random fields or variables (Baroth et al. 2011).

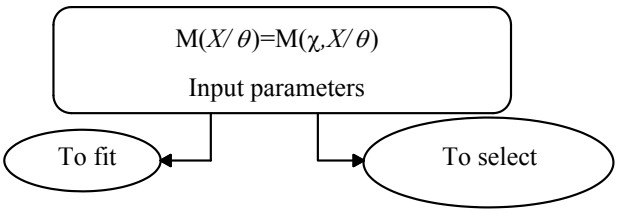

Figure 1.13: Formal writing of a response function (Baroth et al. 2011).

1.6.2. Polynomial Response Surfaces

As already mentioned, RS method is a well-established approach to deal with suitable approximations. Among the possible forms of response surface, polynomial response surface represents a classic way of building response surfaces that have been widely used.

If $X = \left\{ X_i, i = 1,...,M \right\}$ is the random variables vector, the quadratic response surface $\hat{g}(X)$ of the true limit state function $g(X)$ is expressed by:

$$\hat{g}(X) = a_0 + \sum_{i=1}^{M} a_i X_i + \sum_{i=1}^{M} a_{ii} X_i^2 + \sum_{i=1}^{M} \sum_{j=1 \neq i}^{M} a_{ij} X_i X_j \tag{1.17}$$

where $a = \left\{ a_0, a_i, a_{ii}, a_{jj} \right\}^T$ is the vector of unknown coefficients. These coefficients can be obtained by the least square method from the Numerical Experimental Design (NED) $\left\{ x^{(k)}, k = 1...,N \right\}$, where the number of sampling points is at least equal to the dimension of **a**:

$$\mathbf{a} = \arg\min_{a} \sum_{k=1}^{N} \left(y_k - \hat{g}\left(x^{(k)} \right) \right)^2 \tag{1.18}$$

where $y_k = g\left(x^{(k)} \right)$ is the true value of the true limit state function at point $x^{(k)}$. From $\hat{g}(X) = \left\{ 1, X_i, X_i^2, X_i X_j \right\} \left\{ a_0, a_i, a_{ii}, a_{jj} \right\}^T = \mathbf{B}(\mathbf{X})^T \mathbf{a}$, **a** is computed as: $\mathbf{a} = \left(\mathbf{C}^T \mathbf{C} \right)^{-1} \mathbf{C}^T \mathbf{y}$, where **C** is the matrix whose rows are the vectors $\mathbf{B}\left(x^{(k)} \right)^T$ and ***y*** the vector of components y_k. Its simplicity makes the identification of parameters easy and asymptotic properties (for distribution tails) could help to represent correctly the transfer of distribution tails. On the opposite, this simplicity is not compatible with complex transfer functions (Schoefs 2008).

1.6.3. Polynomial Chaos Expansions

The response of a structure $Y = M(\mathbf{X})$ can be considered as a random variable belonging to a specific space (such as the space of random variables with a finite variance), and can be represented in a suitable basis for this space. Therefore, the response can be modelled as a converging series called polynomial chaos (PC) expansion (Ghanem and Spanos 1991):

$$Y \approx \sum_{j=0}^{+\infty} a_j \Psi_j \tag{1.19}$$

where $\left\{ \Psi_j, j \in \mathbb{N} \right\}$ is a set of random variables that form the basis and $\left\{ a_j, j \in \mathbb{N} \right\}$ is the set of the "coordinates" of *Y* in this basis.

In practice, it is necessary to retain only a finite number of terms in the PC basis. By truncating in such a way that only those polynomial basis ψ_j with a total degree not greater than a given P are retained. Hence, the truncated series containing P terms is:

$$Y \approx M^{PC}(X) \equiv \sum_{j=0}^{P-1} a_j \psi_j(X) \tag{1.20}$$

By limiting to a specific number of terms, this method can address the problem due to high computational cost in stochastic analysis.

1.6.4. Neural Network

An alternative to the construction of a polynomial response surface is the construction of a neural network. A neural network consists of artificial neurons. Each neuron j receives an input datum $\mathbf{i}_j$ and transmits an output value $\mathbf{o}_j$ via an activation function $\phi_j : \mathbf{o}_j = \phi_j(\mathbf{i}_j)$. The neurons are organised in a network of which one of the simplest topologies is made up of several layers (Figure 1.14). For the reliability problem, the first layer contains as many neurons as there are design variables and the last layer contains a number equal to that of the performance functions G, only one in the case of the reliability component. Intermediate (hidden) layers are defined between the first and the last layers.

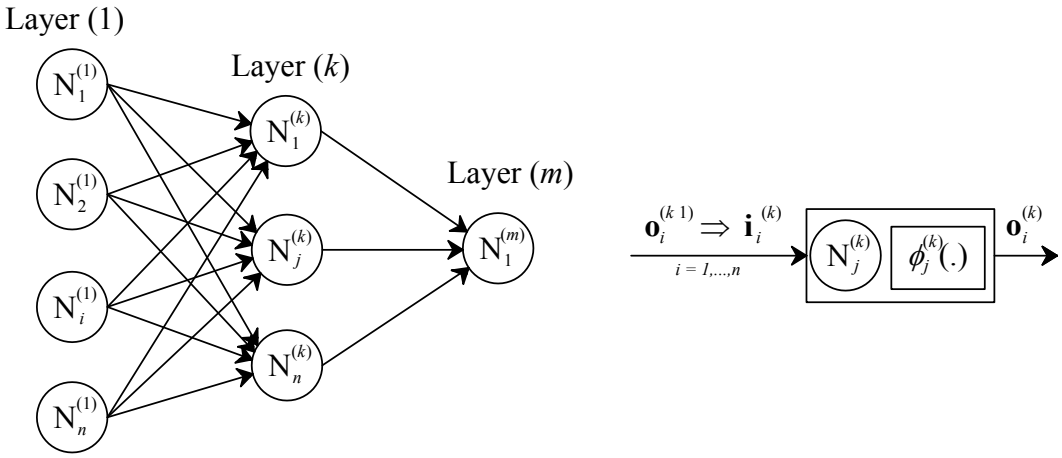

Figure 1.14: A simple neural network (Lemaire et al. 2010).

Constructing a neural network consists of five steps as follows:

1. Choose the architecture of the neural network, that is: the number of hidden layers and the number of neurons on each layer.
2. Choose the input data for each neuron:

The input data $\mathbf{i}_j^{(k)}$ for neuron j in the layer (k) is a weighted linear combination of i outputs $\mathbf{o}_i^{(k-1)} = \mathbf{i}_{ij}^{(k)}$ of the previous layers: $\mathbf{i}_j^{(k)} = \sum_i w_{ij}^{(k)}.\mathbf{i}_{ij}^{(k)} + b_j^{(k)}$. Where $w_{ij}^{(k)}$ are the weights of the i^{th} inputs of neuron $N_j^{(k)}$ and $b_j^{(k)}$ is a threshold termed bias.

3. Choose the activation function:

$$\phi_j^{(k)} = \begin{cases} F\left(\sum_i w_{ij}^{(k)}.\mathbf{i}_{ij}^{(k)} + b_j^{(k)}\right) if\ k > 1 \\ F\left(\mathbf{o}_i^{(0)}\right) if\ k = 1 \end{cases}$$

4. Determine the value of the weights and the bias that minimise the cost function: this is the learning procedure.
5. Validate the learning procedure.

The advantages of this method lies in the graphical representation of relationship between input variables and output parameters. This method also gives a more accurate and efficient results than polynomial-based response surface method (Hosni Elhewy et al. 2006).

1.6.5. Bayesian Network (BN)

Generally, a Bayesian Network is a specific type of graphical model that is represented as a Directed Acyclic Graph (DAG). Nodes in DAG are graphical representation of objects and events that exists in real world, and are usually termed "variables" or "states". Causal relations between nodes are represented drawing an arc (edge) between them. If there is a causal relationship between the variables (nodes), there will be a directional edge, leading from the cause variable to the effect variable. Each variable in the DAG has a probability distribution function (PDF), which dimension and definition depend on the edges leading into the variables.

A Bayesian Network is a probabilistic model that represent $P(\mathbf{X})$, the joint probability mass function (PMF) of a set of random variables $\mathbf{X}$, however, the BN allows an efficient modelling by factoring the joint probability distribution into conditional probability distribution for each variable. Figure 1.15 describes a simple BN. It consists of three nodes corresponding to three random variables X_1, X_2, X_3 in which X_2 and X_3 are children of the parent node X_1. Attached to the children node (X_2, X_3) is the conditional probability distribution of (X_2 or X_3) given X_1 which is defined conditional on its parents. However, attached to node X_1 is a marginal probability distribution because it has no parent.

A definition of the conditional probability gives that:

$$P(X_1, X_2) = P(X_1 \mid X_2)P(X_2) = P(X_2 \mid X_1)P(X_1) \tag{1.21}$$

where $P(X_1, X_2)$ is the probability of the joint event $(X_1 \wedge X_2)$

This formulation brings the Bayes' rule for computing a posteriori probability $P(X_1 \mid X_2)$, given the a priori one $P(X)$, and the likelihood $P(X_2 \mid X_1)$ that X_2 will be marginal if X_1 is true:

$$P(X_1 \mid X_2) = \frac{P(X_2 \mid X_1)P(X_1)}{P(X_2)} \tag{1.22}$$

The joint PMF of this network is given as a product of these conditional probabilities:

$$P(X_1, X_2, X_3) = P(X_1)P(X_2 \mid X_1)P(X_3 \mid X_1) \tag{1.23}$$

where: $P(X_i \mid X_j)$ is the conditional PMF of X_i given X_j

Generally, in case of any BN, the equation (1.23) can be written as:

$$P(\mathbf{X}) = P(X_1, ..., X_N) = \prod_{i=1}^{N} P(X_i \mid \mathbf{pa}_i) \tag{1.24}$$

where $\mathbf{pa}_i$ is the parent set of a node X_i.

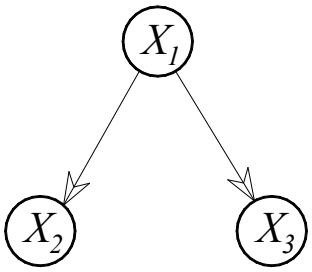

Figure 1.15: A simple Bayesian Network.

1.6.6. Discussion

All of the methods described above can be used for modelling stochastic processes including parameter identification. However, as mentioned above, because the most realistic chloride ingress models are based on finite elements, the responses should be defined in a specific finite space. Due to its flexibility, polynomial chaos expansion is used more popularly than the original form – the polynomial response surface. However, PC is exposed to be bulky when the number of terms to calculate grows significantly corresponding to the development of the size of the input random vector. Blatman and Sudret (2010) proposed an approach called "sparse polynomial chaos expansion" (SPCE) for retaining a small number of signification basis functions for minimising the number of model evaluations. However, SPCE cannot ensure a good convergence for the results. The difficulty in convergence of the Chaos expansion also mentioned by Soize (2010), results from the difficulties in

solving the inverse stochastic problem which can have a very large number of coefficients. Soize (2010) dealed with this problem by using inverse stochastic methods combined with Bayesian inference approach. The presentation of the Bayesian theorem in this method gives the possibility to update the a priori model for better representation of the experimental observations. This method can bring a good convergence for the results. However, the available experiment data was only used to obtain optimal a priori models, not for the updating. This method is also incompatible with data collected in different time. There are other studies in literature (Pence et al. 2011; Sepahvand and Marburg 2013) making a combination of Polynomial chaos expansion (PCE) and Bayesian theory to deal with the identification parameters from experimental data. These studies show that polynomial chaos theory can be used for parameter estimation, however it does not allow a state observer for updating and can present problems of computational time as well as convergence. To overcome these obstacles, RS methods must be combined with other methods such as Bayesian approach and this will give considerable complexity in the computational process.

Artificial neural networks and Bayesian networks, on the other hand, can be used as an effective tool for the identification of parameters. Yadaiah et al. (2000) proposed an algorithm based on Neural network namely “fast gradient decent technique” for dealing with the parameter identification. This method can bring a fast convergence independently of the choice of initial conditions. Huber and Tsakmakis (2001) pointed out that neural networks can be used for determining the material parameters from experimental data. Bastidas-Arteaga et al. (2012) and Richard et al. (2012) proposed an approach based on the use of Bayesian networks. These methodologies allowed the parameter identification from real data and showed an agreement between numerical prediction and experimental measurements. However, there are also some different points between the usage of BN and ANN that we have to take into consideration. ANN can be seen as an efficient tool for solving the identification problem (Huber and Tsakmakis 2001), however, there is no convergence property for the estimation of response or identification of parameters in the case of values not included in the original training database. ANN has limited ability to identify possible causal relationship (Tu 1996). Whereas in parameter identification of chloride ingress, causal relationship is important to study the influence of experimental data on parameter identification. In contrast, Bastidas-Arteaga et al. (2012) demonstrated that BN can be used in case all the main input data is considered as random. Rui and Bivens (2007) made a comparison in the usage of BN and ANN. This study pointed out that BN can be more effective in accuracy, domain knowledge incorporation, model interpretability and multi-way model evaluation. Heckerman (1997) mentioned that BN is an robust method with some characteristics which meet the demand of chloride ingress models data:

- BN can readily handle incomplete data set,
- allow one to learn about causal relationships,

- BN in conjunction with Bayesian statistical techniques facilitate the combination of domain knowledge data,
- Bayesian methods in conjunction with BN and other types of model offer an efficient and principled approach for avoiding the over fitting data.

Moreover, the objective of reliability analysis in chloride ingress is to predict the probability of corrosion initiation whose target value is approximate 10^{-2}. For such a target level, the use of a discrete approach for PDF approximation will be more consistent. Hence, the BN is an appropriate tool since it works with discrete representation of the PDF

From discussion above between the usage, the advantages and disadvantages of each method, Bayesian network has been chosen as a basic model for uncertainty modelling of chloride ingress in this study.

1.7. Conclusions

1. The first part of this chapter explained chloride-induced corrosion mechanism into RC structures. It is a complex process with three stages. The first stage can be considered as an incubation period where chloride ions from external environment penetrate into concrete and accumulate inside RC before reaching a threshold level to start active corrosion. The second stage is the progressive and accelerative period where cracks appear, propagate and cross-sectional area of steel is reduced. The consequence of this stage is the reduction of structural reliability. The third stage consists of deterioration after important cracks in concrete appear where corrosion rate of steel bar is accelerated and decreases significantly the bearing capacity of structures.
2. Modelling chloride ingress into concrete is a difficult task due to the complexity of this phenomenon. Several models describing this process can be found in the literature. The most common approach is based on the analytical solution to Fick's law. However, this model is just valid with some assumptions that are difficult to appear under real exposure conditions. The Duracrete model can improve the lifetime assessment by accounting for: the influences of material properties, environmental exposure, ageing and concrete curing. However, this model could underestimate the service life if high values of age factor are used. The model proposed by Nilsson and Carcasses (2004) can provide a better prediction despite the use of high age factor values.

   On the other hand, advances in modelling chloride ingress in unsaturated condition allows describing this phenomenon in a more realistic assessment. However, the solution can only be obtained numerically and requires a larger number of parameters.
3. To perform reliability assessment, it is necessary to select an appropriate approach for stochastic modelling. This approach should also be capable of integrating new information

from experimental data to identify model parameters and/or update the assessments. Thus, different approaches for uncertainty modelling as well as parameter identification have been presented. Each method exposes pros and cons that should be taken into consideration. By comparing different characteristics among these methods, BN was chosen as a basic model for uncertainty modelling and parameter identification of chloride ingress in this study. This method allows to represent causal relationship among model parameters in a graphical manner. The uncertainty of model parameters is taken into account by considering each node in BN as a random variable. By updating with experimental information, BN allows to identify model parameters

Chapter 2
BN configuration and numerical implementation for improving random variables identification

2.1. Introduction

Nowadays, in many civil engineering applications, it is of interest to update a probabilistic model if observations are available. Bayesian approach is recognised as an efficient and rational framework for such purposes. This approach has been applied to problems related to chloride ingress into RC structures in some previous studies (De-León-Escobedo et al. 2013; Engelund and Sorensen 1998; Keßler et al. 2013; Ma et al. 2013; Suo and Stewart 2009; Wang and Liu 2010). This approach provides a comprehensive and rational framework to update the estimations based on incorporating new information from inspection data for service-life prediction of RC structures (Keßler et al. 2013; Ma et al. 2013; Wang and Liu 2010) or parameter estimations (Engelund and Sorensen 1998; Enright et al. 1999; Suo and Stewart 2009). When applying to multi events and inverse analysis, the entire model can be converted in the form of Bayesian network (BN) and becomes a powerful approach which has a wide range of applications. Recent studies in corrosion of RC structures due to chloride attack (Bastidas-Arteaga et al. 2012; Deby et al. 2008, 2012; Hackl 2013; Ma et al. 2014), BN was used as a surrogate to original models to integrate experimental data in the updating process for reliability assessment. However, the complexity and the uncertainties of the deterioration process due to chloride attack requires improvements in BN modelling. The performances of BN should be optimised and easily modified and thus, Bayesian network toolbox (BNT) in Matlab could be a suitable tool.

The main purpose of this chapter is to discuss numerical issues for building and modelling chloride ingress by using BNT. The specific objectives of this chapter are:

1. to illustrate how chloride ingress could be modelled and updated by using BN.

2. to explain step-by-step implementation of the BNT for parameter identification in chloride ingress models. Algorithms and sample codes are provided and validated with a commercial software (NETICA).
3. to introduce some numerical aspects considered in this study that play an important role in the performance of BN and its outcomes.

BN theory and its application to chloride ingress is presented in section 2.2. Section 2.3 details procedures to build BN in BNT with a simple example. The results are validated with NETICA. Some strategies to improve the identification are discussed in section 2.4.

2.2. Theory of BN and its application to chloride ingress

2.2.1. Introduction to BN

Bayesian networks represent probabilistic models consisting of nodes that represent random variables and they are connected by links to illustrate probabilistic dependencies. Thus, BN could be seen as an efficient probabilistic tool to facilitate the representation of the dependence among random variables by graphical structures as a Directed Acyclic Graph (DAG). During the past 25 years, BN has been developed mostly in artificial intelligence, representing probabilistic information and reasoning (Russell and Norvig 2010). Its applications can be found in many fields such as statistical modelling, language processing, image recognition, machine learning, risk analysis, etc.

In BN, causal relations between nodes are represented by drawing an arc (edge) between them. If there is a causal relationship between the variables (nodes), there will be a directional edge, leading from the cause variable to the effect variable. Each variable in the DAG has a Probability Density Function (PDF), which dimension and definition depend on the edges leading into the variable. Consider the simple BN in Figure 2.1 that consists of three nodes corresponding to three random variables X_1, X_2 and X_3 in which X_2 and X_3 are children of the parent node X_1. The children nodes have conditional probability distributions that depend on their parent node. The parent node has a marginal probability distribution. The probability distribution of each node can in principle be continuous or discrete depending on the type of node itself. For a set of m random variables $\mathbf{X} = [X_1, X_2, \dots, X_m]$, a BN represents $P(X)$ which is the joint Probability Mass Function (PMF) in the case of discrete nodes or the joint PDF for continuous variables. The BN allows an efficient probabilistic modelling of the problem by factoring the joint probability distribution into conditional probability distribution for each variable.

Many applications of BN require modelling random variables as discrete and/or continuous forms. When there is no limitation for inference BN with all discrete nodes with many exact inference algorithms have been developed (Murphy 2001); continuous variables put severe limitations on available exact algorithms and software packages (Hofmann and Tresp 1996; Murphy 2001; Pearl

1991; Straub and Der Kiureghian 2010) except for linear Gaussian models. As an alternative, approximate inference algorithms using simulation techniques have been developed to facilitate the calculation with continuous variables. Among of them, Markov Chain Monte Carlo (MCMC) methods (Gilks et al. 1996) have become popular. However, these techniques still have some algorithmic difficulties that provide some limitations in the rate of convergence (Straub 2009). In this study, only exact inference in BNs with discrete random variables is investigated. That allows to update random variables and propagates the uncertainty with a good precision for significant probability of failure as those related to Service Limit State. The approximation errors due to the discretisation of continuous random variables are beyond the scope of this study.

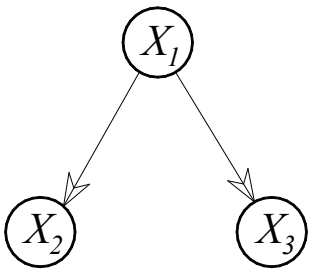

Figure 2.1: A Simple Bayesian Network

The PMF of each node in BN is defined conditional on its parents and the joint PMF of this network is described as a product of these conditional probabilities:

$$P(X_1, X_2, X_3) = P(X_1)P(X_2 \mid X_1)P(X_3 \mid X_1) \tag{2.1}$$

where $P(X_i \mid X_j)$ denote the conditional probability of X_i given X_j

BN allows introducing new information (evidences) from the observed nodes to update the probabilities in the network. For example, if we have some evidences to node $X_2 = o$, this information can propagate through the network and the joint PMF of the two other nodes can be recalculated as:

$$P(X_1, X_3 \mid o) = \frac{P(X_1, o, X_3)}{P(o)} = \frac{P(X_1)P(o \mid X_1)P(X_3 \mid X_1)}{\sum_{X_1} P(X_1)P(o \mid X_1)} \tag{2.2}$$

Therefore, the a posteriori probabilities of X_1 and X_3 are updated and equations (2.1) and (2.2) are the key of parameter identification from inspection data.

2.2.2. BN configuration for modelling chloride ingress

Chloride ingress could be modelled by the BN described in Figure 2.2 where C_s and D are the two parent nodes (random variables to identify). There are n child nodes $C\left(x_i, t_j\right)$ representing the discrete chloride concentration measurement in time and space *i.e.* at depth x_i and at inspection time t_j labelled number from 3 to k . The number of child nodes is computed as:

$$n = n_x n_t \tag{2.3}$$

where n_x is the total number of points in depth and n_t is the total number of inspection times. In numerical simulations, a BN with high value of n requires more computational time to perform inferences. However, in real practice, a high value of n corresponds to a large amount of experiment data. In fact, in recent years, inspection techniques have been developed to facilitate the assessment of corrosion consequences in RC structures. However, these techniques are still expensive and time consuming, especially, when n is larger. Consequently, it is necessary to find an optimal configuration of BN that provides optimal inspection schemes in real practice. The optimisation of inspection schemes will be detailed in chapter 3.

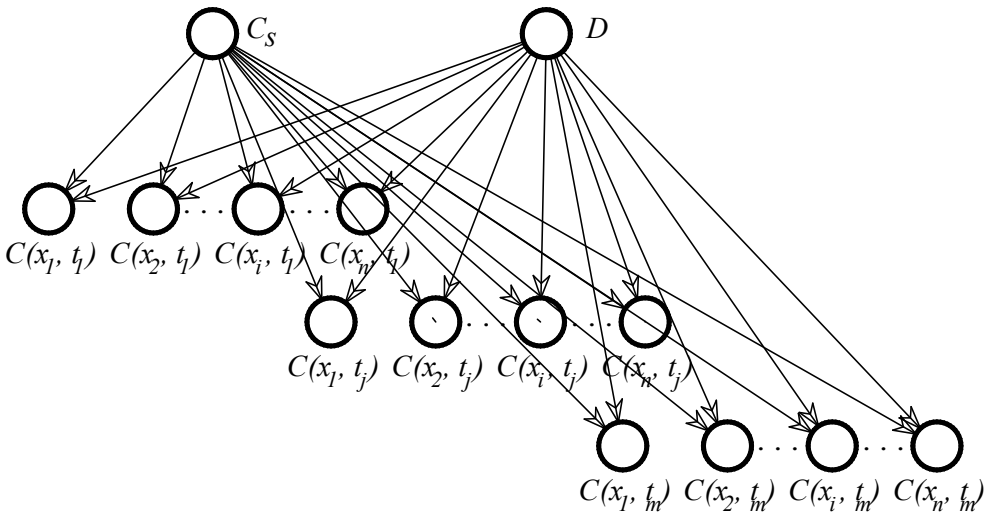

Figure 2.2: General BN configuration for modelling chloride ingress

Chloride content $C\left(x_i, t_j\right)$ at depth x_i and time t_j can be described as a general function of related parameters (Eq (2.4)). The number of involved parameters in Eq (2.4) depends on the model selected to describe the chloride ingress. For example, this section using model proposed by (Tuutti 1982) which is represented by Eq (1.2); thus, only two related parameters are considered (C_s and D).

$$C\left(x_i,t_j\right)=f\left(C_s,D,n_D,...\right) \tag{2.4}$$

Assuming that C_s and D are two independent random variables, there will be no arrow connection between these two nodes in BN. The values of $C\left(x_i,t_j\right)$ could be easily estimated from the chloride ingress models (e.g., Eq (1.2)). In this BN, the probability of chloride concentration $P\left(C\left(x_i,t_j\right)\right)$ can be calculated as follows (Bastidas-Arteaga et al. 2012; Nguyen 2007):

$$P\left(C\left(x_i,t_j\right)\right)=\sum_{D,C_s}P\left(C\left(x_i,t_j\right)|D,C_s\right)P\left(D,C_s\right) \text{ with } P\left(D,C_s\right)=P\left(D\right)P\left(C_s\right) \tag{2.5}$$

To estimate $P\left(C\left(x_i,t_j\right)\right)$, the conditional probability $P\left(C\left(x_i,t_j\right)|D,C_s\right)$ must be already known in Eq. (2.5). This conditional probability accounts for the dependence between the chloride content $C\left(x_i,t_j\right)$ with the two model parameters (D and C_s) and it can be derived from the Conditional Probability Table (CPT) of the BN. 48,000 Monte Carlo simulations are required to obtain an convergence in calculating the CPTs. The BN serves also for inverse analysis by entering evidences and then updating the probabilities in the network. In this study, evidences correspond to measures of chloride concentration at certain points and times (chloride profiles). Then, the term $P\left(C\left(x_i,t_j\right)|o\right)$ represents the probability distribution of $C\left(x_i,t_j\right)$ given evidence *o* and a posteriori distribution can be computed by applying the Bayes' theorem:

$$P\left(D|o\right)=P\left(D|C\left(x_i,t_j\right)\right)P\left(C\left(x_i,t_j\right)|o\right) \text{ with } P\left(D|C\left(x_i,t_j\right)\right)=\frac{P\left(C\left(x_i,t_j\right)|D\right)P\left(D\right)}{P\left(C\left(x_i,t_j\right)\right)} \tag{2.6}$$

and:

$$P\left(C_s|o\right)=P\left(C_s|C\left(x_i,t_j\right)\right)P\left(C\left(x_i,t_j\right)|o\right) \text{ with } P\left(C_s|C\left(x_i,t_j\right)\right)=\frac{P\left(C\left(x_i,t_j\right)|C_s\right)P\left(C_s\right)}{P\left(C\left(x_i,t_j\right)\right)} \tag{2.7}$$

The a posteriori distributions of parent nodes provide useful statistic information: mean, standard deviation, distribution shape. It is then expected that these statistic values provide information close to the real values.

2.2.3. Illustrating example

In this section we consider an example where Bayesian Network is used for modelling chloride ingress. The objective of this example is to illustrate the application of Bayesian algorithms in chloride ingress modelling for parameter updating.

2.2.3.1. Parameters of the illustrative example

Assume that Eq (1.2) describes chloride ingress into concrete. Generally, each parameter in chloride ingress model is considered as random variable. However, in this section, for illustrative purposes and to reduce the complexity of calculations, we consider chloride diffusion coefficient as constant (D =3×10^{-12} (m/s²)). We suppose to have some evidences obtained from inspection data after 10 years at two depth points x=1cm and x =4cm. They are denoted Cxt_1cm and Cxt_4cm . Consequently, with known values for *D, x,* and *t*, chloride content at depth x=1cm and x=4cm can be expressed as a function of C_s. Therefore, we can write:

$$Cxt\_1cm = f(C_s, D, x, t) = f(C_s) \quad \text{and} \quad Cxt\_4cm = f(C_s, D, x, t) = f(C_s) \tag{2.8}$$

2.2.3.2. BN configuration

The BN configuration could be modelled with 1 parent node represented for C_s and two child nodes represented for Cxt_1cm and Cxt_4cm . (Figure 2.3). The next chapters consider more complex BN configurations.

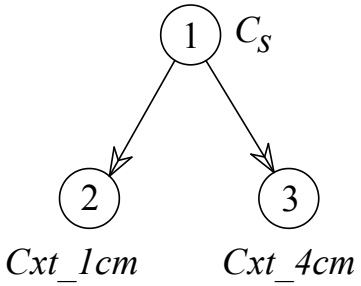

Figure 2.3: BN configuration for example case

Each node should be discretised into finite states to avoid using approximate algorithm in BN inference. The discretisation for each node is shown in Table 2.1 where node C_s is discretised into nC_s =8 states of same width in the range $[lb\_C_s, ub\_C_s]$=[1; 9] [kg/m^3] and two nodes Cxt_1cm and Cxt_4cm have 5 states of same width in the range $[lb\_Cxt, ub\_Cxt]$ = [0; 9] [kg/m^3]. In fact, the discretisation of parameters plays an important role in the accuracy of results. When a high number of states is chosen, it is expected to obtain better accurate results, however, more computational time is required in the other hand. The effects due to the discretisation of parameters in chloride ingress will be described in detail in section 2.4.3. Each parameter corresponds to a given possible range which is pre-defined from experience or expert knowledge. These ranges should cover all possible values of the parameters.

Table 2.1: Discretisation and ranges for parameters

Node	Number of states	Range
C_s [kg/m^3]	nC_s =8	$[lb\_C_s, ub\_C_s]$=[1; 9]
Cxt_1cm [kg/m^3]	$nCxt$ =5	$[lb\_Cxt, ub\_Cxt]$ = [0; 9]
Cxt_4cm [kg/m^3]	$nCxt$ =5	$[lb\_Cxt, ub\_Cxt]$ = [0; 9]

2.2.3.2. The CPT tables and evidences

The CPTs for each child node describing the relationship with their parents are computed by applying Monte Carlo simulation in equation (1.2). The algorithm for building CPTs with one or several parent nodes is described in section 2.3 and 2.4. From Monte Carlo simulations, the CPTs for two child nodes Cxt_1cm and Cxt_4cm are shown in Table 2.2 and Table 2.3 respectively. Each CPT table is a two-dimension matrix with $nCxt$ columns representing for number of the child node's states and nC_s rows corresponding to mutually exclusive collectively exhaustive states from its parent nodes. For example, in Table 2.2, when C_s falls in 2th state defined by interval [2; 3] [kg/m^3], the probability of Cxt_1cm falls into two first states [0; 1.8] [kg/m^3] and [1.8; 3.6] [kg/m^3] with 17.9% and 82.1% respectively. In this example, child nodes with one parent node are considered. However, in a more general cases when child nodes have several parent nodes, the number of rows in CPT tables is calculated by multiply the number of states of parent nodes (see section 2.4.1 for more details).

Table 2.2: CPT table for node *Cxt_1cm*

CPT	*Cxt_1cm* [kg/m^3]				
C_s [kg/m^3]	0-1.8	1.8-3.6	3.6-5.4	5.4-7.2	7.2-9
1-2	100	0	0	0	0
2-3	17.9	82.1	0	0	0
3-4	0	100	0	0	0
4-5	0	39.8	60.2	0	0
5-6	0	0	100	0	0
6-7	0	0	60	40	0
7-8	0	0	0	100	0
8-9	0	0	0	78.9	21.1

Table 2.3: CPT table for node *Cxt_4cm*

CPT	*Cxt_4cm* [kg/m^3]				
C_s [kg/m^3]	0-1.8	1.8-3.6	3.6-5.4	5.4-7.2	7.2-9
1-2	100	0	0	0	0
2-3	100	0	0	0	0
3-4	100	0	0	0	0
4-5	100	0	0	0	0
5-6	3.1	96.9	0	0	0
6-7	0	100	0	0	0
7-8	0	100	0	0	0
8-9	0	100	0	0	0

Simulated evidences for node Cxt_1cm and Cxt_4cm are generated from theoretical values in Table 2.4. These results are given in terms of probability of belonging to each state (Table 2.5). The algorithm for generating simulated evidences is described in section 2.4.2.

Table 2.4: Theoretical values for generating evidences

Parameter	Mean	Std	Distribution
C_s (kg/m^3)	5	1	Lognormal

Table 2.5: Simulated evidences for node Cxt_1cm and Cxt_4cm

State	*P(Cxt_1cm)*	*P(Cxt_4cm)*
0-1.8	0.002	0.5183
1.8-3.6	0.2714	0.4817
3.6-5.4	0.6666	0
5.4-7.2	0.06	0
7.2-9	0	0

2.2.3.3. Results and discussion

When no evidences are introduced, the marginal distribution of child nodes can be calculated as:

$$P\left(C\left(x_i,t_j\right)\right)=\sum_{C_s}P\left(C\left(x_i,t_j\right)|C_s\right)P\left(C_s\right) \tag{2.9}$$

where $P\left(C_s\right)=1/nC_s=1/8=0.125$ (assuming that C_s follows an a priori uniform distribution)

For example, the computation for state i^{th} of node Cxt_1cm denoted by Cxt_1cm^i $(i=1,\ldots,5)$ is expressed as:

$$P\left(Cxt\_1cm^i\right)=\sum_{j=1}^{8}P\left(Cxt\_1cm^i \mid C_s^{\,j}\right)P\left(C_s^{\,j}\right)$$

where the conditional probability $P\left(Cxt\_1cm^i \mid C_s^{\,j}\right)$ is taken from Table 2.2 and $P\left(C_s^j\right)(j=1,...,8)$ denotes the j^{th} state of a priori distribution of C_s $\left(P\left(C_s^j\right)=0.125\right)$.

Therefore:

$$P\left(Cxt\_1cm^1\right)=\sum_{j=1}^{8}P\left(Cxt\_1cm^1 \mid C_s^{\,j}\right)P\left(C_s^{\,j}\right)=100*0.125+17.9*0.125=14.74$$

$$P\left(Cxt\_1cm^2\right)=\sum_{j=1}^{8}P\left(Cxt\_1cm^2 \mid C_s^{\,j}\right)P\left(C_s^{\,j}\right)=82.1*0.125+100*0.125+39.8*0.125=27.74$$

$$P\left(Cxt\_1cm^3\right)=\sum_{j=1}^{8}P\left(Cxt\_1cm^3 \mid C_s^{\,j}\right)P\left(C_s^{\,j}\right)=60.2*0.125+100*0.125+60*0.125=27.53$$

$$P\left(Cxt\_1cm^4\right)=\sum_{j=1}^{8}P\left(Cxt\_1cm^4 \mid C_s^{\,j}\right)P\left(C_s^{\,j}\right)=40*0.125+100*0.125+78.9*0.125=27.36$$

$$P\left(Cxt\_1cm^5\right)=\sum_{j=1}^{8}P\left(Cxt\_1cm^5 \mid C_s^{\,j}\right)P\left(C_s^{\,j}\right)=0$$

Similarly, the marginal probability for Cxt_4cm with no evidences can be computed and results are shown in Table 2.6.

Table 2.6: A posteriori distributions of nodes Cxt_1cm and Cxt_4cm with no evidences

State	*P*(*Cxt_1cm*)	*P*(*Cxt_4cm*)
0-1.8	14.74	50.39
1.8-3.6	27.74	49.61
3.6-5.4	27.53	0
5.4-7.2	27.36	0
7.2-9	0	0

Introducing evidences (e_1) for node Cxt_1cm (Table 2.5), the probabilities of node C_s after updating with e_1 can be updated based on equation (2.7):

$$P\left(C_s \mid e_1\right)=P\left(C_s \mid Cxt\_1cm\right)P\left(Cxt\_1cm \mid e_1\right) \text{ with } P\left(C_s \mid Cxt\_1cm\right)=\frac{P\left(Cxt\_1cm \mid C_s\right)P\left(C_s\right)}{P\left(Cxt\_1cm\right)}$$

$$\rightarrow \quad P\left(C_s \mid e_1\right)=\frac{P\left(Cxt\_1cm \mid C_s\right)P\left(C_s\right)}{P\left(Cxt\_1cm\right)}\times P\left(Cxt\_1cm \mid e_1\right)$$

The $j^{th}\ (j=1,...,8)$ state of a posteriori distribution $P\left(C_s^j \mid e_1\right)$ can be calculated as:

$$P\left(C^j{}_s \mid e_1\right) = \sum_i^5 \frac{P\left(Cxt\_1cm^i \mid C^j{}_s\right) P\left(C^j{}_s\right)}{P\left(Cxt\_1cm^i\right)} \times P\left(Cxt\_1cm^i \mid e_1\right)$$

where $Cxt\_1cm^i\ (i=1,...,5)$ represents the i^{th} state of node Cxt_1cm . The probabilities $P\left(Cxt\_1cm^i\right)$ and $P\left(Cxt\_1cm^i \mid e_1\right)$ are taken from Table 2.6 and Table 2.5 respectively.

Therefore:

- $P\left(C^1{}_s \mid e_1\right) = \sum_i^5 \frac{P\left(Cxt\_1cm^i \mid C^1{}_s\right) P\left(C^1{}_s\right)}{P\left(Cxt\_1cm^i\right)} \times P\left(Cxt\_1cm^i \mid e_1\right) = \frac{100*0.125*0.002}{14.74} = 0.0017$

- $P\left(C^2{}_s \mid e_1\right) = \sum_i^5 \frac{P\left(Cxt\_1cm^i \mid C^2{}_s\right) P\left(C^2{}_s\right)}{P\left(Cxt\_1cm^i\right)} \times P\left(Cxt\_1cm^i \mid e_1\right)$

  $P\left(C^2{}_s \mid e_1\right) = \frac{17.9*0.125*0.002}{14.74} + \frac{82.1*0.125*0.2714}{27.74} = 0.1007$

- $P\left(C^3{}_s \mid e_1\right) = \sum_i^5 \frac{P\left(Cxt\_1cm^i \mid C^3{}_s\right) P\left(C^3{}_s\right)}{P\left(Cxt\_1cm^i\right)} \times P\left(Cxt\_1cm^i \mid e_1\right) = \frac{100*0.125*0.2714}{27.74} = 0.1223$

- $P\left(C^4{}_s \mid e_1\right) = \sum_i^5 \frac{P\left(Cxt\_1cm^i \mid C^4{}_s\right) P\left(C^4{}_s\right)}{P\left(Cxt\_1cm^i\right)} \times P\left(Cxt\_1cm^i \mid e_1\right)$

  $P\left(C^4{}_s \mid e_1\right) = \frac{39.8*0.125*0.2714}{27.74} + \frac{60.2*0.125*0.6666}{27.53} = 0.2309$

- $P\left(C^5{}_s \mid e_1\right) = \sum_i^5 \frac{P\left(Cxt\_1cm^i \mid C^5{}_s\right) P\left(C^5{}_s\right)}{P\left(Cxt\_1cm^i\right)} \times P\left(Cxt\_1cm^i \mid e_1\right) = \frac{100*0.125*0.6666}{27.53} = 0.3027$

- $P\left(C^6{}_s \mid e_1\right) = \sum_i^5 \frac{P\left(Cxt\_1cm^i \mid C^6{}_s\right) P\left(C^6{}_s\right)}{P\left(Cxt\_1cm^i\right)} \times P\left(Cxt\_1cm^i \mid e_1\right)$

  $P\left(C^6{}_s \mid e_1\right) = \frac{60*0.125*0.6666}{27.53} + \frac{40*0.125*0.06}{27.36} = 0.1926$

- $P\left(C^7{}_s \mid e_1\right) = \sum_i^5 \frac{P\left(Cxt\_1cm^i \mid C^7{}_s\right) P\left(C^7{}_s\right)}{P\left(Cxt\_1cm^i\right)} \times P\left(Cxt\_1cm^i \mid e_1\right) = \frac{100*0.125*0.06}{27.36} = 0.0274$

- $$P\left(C^8{}_s \mid e_1\right) = \sum_i^5 \frac{P\left(Cxt\_1cm^i \mid C^8{}_s\right) P\left(C^8{}_s\right)}{P\left(Cxt\_1cm^i\right)} \times P\left(Cxt\_1cm^i \mid e_1\right) = \frac{78.9 * 0.125 * 0.06}{27.36} = 0.0216$$

Introducing evidences (e_2) of *Cxt_4cm* into BN, the a posteriori probabilities of C_s can be calculated similarly and the results are shown in Table 2.7. By comparing a posteriori distributions with a priori and theoretical distributions (Figure 2.4), it can be seen that after updating with evidences, a posteriori distribution approaches the theoretical ones. Thus, statistical values (mean and standard deviation) of the identified parameter (C_s) can be computed from the a posteriori histogram.

Table 2.7: A posteriori distribution of C_s

State	$P(C_s)$ after updating with evidence *Cxt_1cm*	$P(C_s)$ after updating with evidence *Cxt_4cm*
1-2	0.0017	0.0009
2-3	0.1007	0.1052
3-4	0.1223	0.1280
4-5	0.2309	0.2402
5-6	0.3027	0.2928
6-7	0.1926	0.1858
7-8	0.0274	0.0263
8-9	0.0216	0.0207

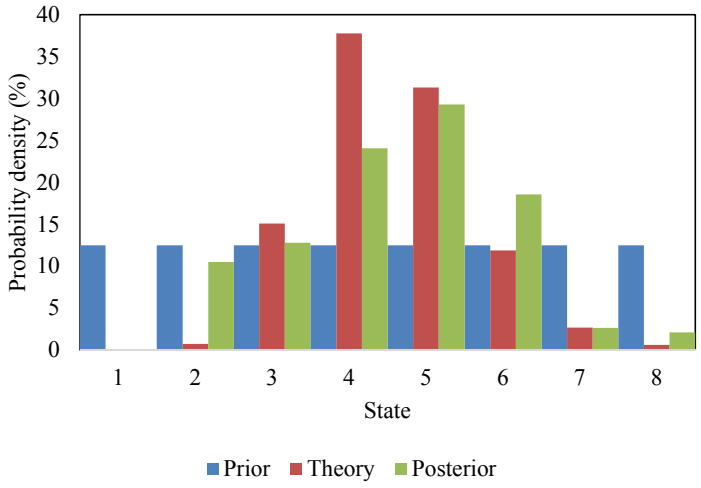

Figure 2.4: Comparing distributions

For further inferences in this study, the determination of these conditional probabilities are carried out by the BN Tool Box which is built on the Matlab® Software. Note that we assume that the

measurements are not affected by errors. Measurement errors can be modelled by adding additional nodes to represent their PDFs and their dependence on the magnitude of the measured values (Schoefs et al. 2012).

2.3. Parameter identification using BN built on BN toolbox on Matlab

2.3.1. Introduction to Bayesian Network Toolbox (BNT) on Matlab

The BN configurations were implemented in the Bayesian Network Toolbox (BNT) that is an open-source Matlab package for directed graphical models. This can be seen as a robust characteristic of BNT as compared with other softwares because users can add, modify or make complements of functions in order to fit with the different using purposes. BNT supports many types of conditional probability distributions (nodes), many inference algorithms (exact and approximate) for both static BNs and dynamic BNs parameters and structure learning (Murphy 2001). Murphy (2001) conducted a comparison of existing software package supporting BN inference which indicates that BN toolbox could be adapted for the most complicated issues.

However, BNT is a non-graphical interface environment. All manipulations of constructing BN are performed on Matlab windows. Therefore, in order to have a clear view of building a BN, we can follow the stages described in Figure 2.5. In fact, this toolbox package just supports the construction and inference of the BN. Thus, some numerical issues such as generating CPTs, generating simulated evidences should be defined by users.

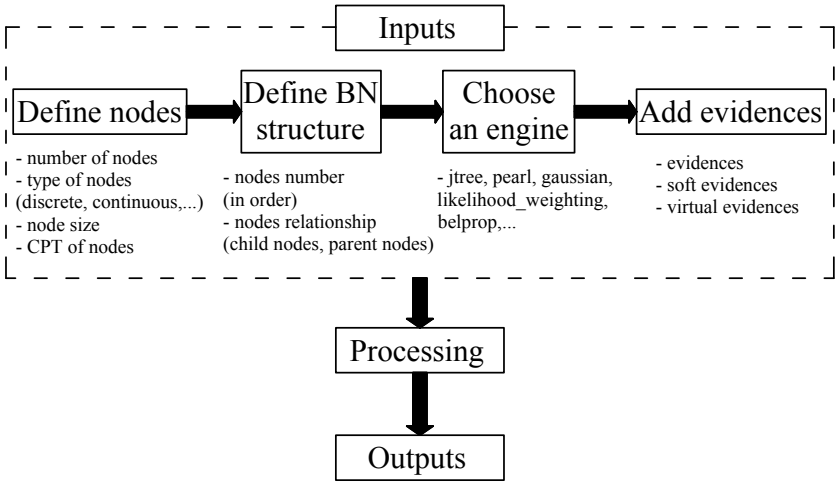

Figure 2.5: Flowchart of building BN on BNT

2.3.2. Example and comparison with Netica

This section illustrates step-by-step the use of BNT on Matlab to perform BN updating of the same BN configuration described in section 2.2.3 (Figure 2.3).

2.3.2.1. Step 1: Creation of BN nodes and generation of CPTs

The first step of constructing BNs involves the following steps: define total number of nodes, the type of nodes (continuous or discrete), the states for each node (if nodes are discrete) and the boundaries for each node, the deterministic values for constant parameters and compute CPT for random parameters.

Figure 2.6 illustrates an example of code for defining nodes in BNT. This example considers a BN configuration modelling chloride ingress with 3 discrete nodes (Figure 2.3). The node C_s has 8 discrete states in the range [1; 9] and nodes Cxt_1cm and Cxt_4cm have 5 states with the boundaries are $\{0;\ 9\}$. The deterministic values are inspection time $(t = 10\text{years})$ and chloride diffusion coefficient $\left(D = 3\times10^{-12}\,\text{m}^2/\text{s}\right)$. The surface chloride concentration (C_s) is considered as random variable to identify with theoretical values are $\left(\mu_{C_s} = 5;\sigma = 1\right)\left(kg/m^3\right)$. A priori, C_s is assumed follow uniform distribution and from Latin Hyper cube methods, 48000 simulations are generated with function *lhsu*. The CPT tables for nodes Cxt_1cm and Cxt_4cm are computed using function *CPT_child_node_trial*.

```
N=3; % Number of total nodes in Bayesian Networks
discrete_nodes=1:N; % Define discrete nodes
%% Define node sizes
nCs=8;% Node size of Cs
nCxt=5; % Node size of Cxt_1cm and Cxt_4cm
%% Define boundary for each node
lb_Cs=1; ub_Cs=9; %Boundary for Cs
lb_Cxt=0; ub_Cxt=9; %Boundary for Cxt_1cm and Cxt_4cm
%% Define theoretical values for creating evidences
t=10; %Time t = 10 years
mean_Cs=5; std_Cs=1; % mean and std of Cs
D=3e-12; %Define D as constant
%% Generating  random values for parent nodes
Nsim=48000;% Define number of simulations
Cs=lhsu(lb_Cs,ub_Cs,Nsim); %Latin hypercube simulations
%% Calculate CPT for parent node
CPT_Cs=(1/nCs)*ones(1,nCs); % A Priori Cs is uniform
%% Caculate CPT for child node
CPT_Cxt_1cm=CPT_child_node_trial(Nsim,nCs,nCxt,Cs,1,lb_Cs,lb_Cxt,ub_Cs,ub_Cxt,D,t);
CPT_Cxt_4cm=CPT_child_node_trial(Nsim,nCs,nCxt,Cs,4,lb_Cs,lb_Cxt,ub_Cs,ub_Cxt,D,t);
```

Figure 2.6: Matlab example code for defining nodes in BNT

The algorithms to generate the CPT tables of child nodes Cxt_1cm and Cxt_4cm are described in Figure 2.7. By using Latin Hypercube method, $Nsim$ values of C_s were drawn from a priori uniform distribution. Each simulated value of C_s was employed in equation (1.2) to compute the corresponding values for Cxt_1cm and Cxt_4cm. The CPT is a table with $nCxt$ columns and nC_s rows which represent all the states of child node and the total of combination states from the parent nodes respectively. At $i^{th}\left(i=1,...,Nsim\right)$ simulation, a set values of $C_s\left(i\right)$ and $Cxt\_1cm(i)$ belongs to an element at row $X_{C_s(i)}$ and column $X_{Cxt\_1cm(i)}$ in the CPT table of node Cxt_1cm with $X_{C_s(i)}$ and $X_{Cxt\_1cm(i)}$ are the belonging states of value $C_s\left(i\right)$ and $Cxt\_1cm(i)$, respectively. The CPT table of Cxt_1cm is determined by normalising itself after collecting all set values for each table element from $Nsim$. The CPT table for node Cxt_4cm can be computed in a similar way and results are presented previously in Table 2.2 and Table 2.3. Figure 2.8 presents the Matlab codes of the function *CPT_child_node_trial* which are used to compute the CPT tables for child nodes Cxt_1cm and Cxt_4cm. This code illustrates the algorithms presented in Figure 2.7.

Initialisation:

CPT_Cxt_1cm=zeros(nC_s, $nCxt$);

CPT_Cxt_4cm=zeros(nC_s, $nCxt$);

For i = 1,…,$Nsim$ (number of simulations used to generate the CPT)

- Generate $C_s\ (i)$ ~ uniform [1; 9] % Using Latin Hypercube method
- Calculate $Cxt\_1cm\ (i)$ using equation (1.2)
- Calculate $Cxt\_4cm\ (i)$ using equation (1.2)
- Find:
  - $X_{Cs(i)}$ = state of $C_s(i)$ in nCs states
  - $X_{Cxt\_1cm\ (i)}$ = state of $Cxt\_1cm(i)$ in $nCxt$ states
  - $X_{Cxt\_4cm\ (i)}$ = state of $Cxt\_4cm(i)$ in $nCxt$ states
- $CPT\_Cxt\_1cm\ (X_{Cs(i)}, X_{Cxt\_1cm\ (i)})$= $CPT\_Cxt\_1cm\ (X_{Cs(i)}, X_{Cxt\_1cm\ (i)})$+1;
- $CPT\_Cxt\_4cm\ (X_{Cs(i)}, X_{Cxt\_4cm\ (i)})$= $CPT\_Cxt\_4cm\ (X_{Cs(i)}, X_{Cxt\_4cm\ (i)})$+1;

End

Determine normalised CPT_Cxt_1cm and CPT_Cxt_4cm

Figure 2.7: Algorithm for generating CPTs for child node with one parent node

```
Function[CPT_Cxt]=CPT_child_node_trial(Nsim,nCs,nCxt,Cs,x,lb_Cs,lb_Cxt,ub_Cs,ub_Cxt,D,t)
   Cxt=zeros(1,Nsim); %Initial vector of Cxt
   %% Calculate
   for i=1:Nsim
      Cxt(i)=Cs(i)*(1-erf((x/100)/(2*sqrt(D*t*365*24*3600)))); % Compute Cxt at ith simulation
   end
   %% Define CPT table
   CPT_Cxt=zeros(nCs,nCxt); %Define size of CPT
   for i=1:Nsim
      X_Cxt=return_position(Cxt(i),nCxt,lb_Cxt,ub_Cxt); % Determine belonging state of Cxt(i)
      X_Cs=return_position(Cs(i),nCs,lb_Cs,ub_Cs); % Determine belonging state of Cs(i)
      CPT_Cxt(X_Cs,X_Cxt)=CPT_Cxt(X_Cs,X_Cxt)+1; % Determine belonging element of a set value of Cs(i) and Cxt(i)
   end
   %% Normalise CPT table
   temp_CPT=zeros(nCs,nCxt);
   for i=1:nCs
      if (sum(CPT_Cxt(i,:))>0)
         for j=1:nCxt
            temp_CPT(i,j)=CPT_Cxt(i,j)*100/sum(CPT_Cxt(i,:));
         end
      end
   end
   CPT_Cxt=temp_CPT;
end
```

Figure 2.8: Example codes for function computing CPTs

2.3.2.2. Step2: Definition of BN structure

This step consists of: labelling node number in topological order (e.g, ancestors before descendants), defining the node sizes (number of states) and assigning a priori distribution for each node. The Matlab code in Figure 2.9 illustrates the 2nd step for the present example. Node C_s is parent of nodes Cxt_1cm and Cxt_4cm therefore, they are numbered as follows: $C_s = 1$; $Cxt\_1cm = 2$ and $Cxt\_4cm = 3$. A logical array is used to present relation among nodes by the mean that if two nodes have relationship then the corresponding element for this pair nodes is set to 1. Then the BN is made simply from function *mk_bnet* with all nodes are discrete. Each node in BN is assigned with CPT to define the probability of a node knowing its parents. If a node has no parents, its CPT is a column vector representing its a priori distribution (e.g., node C_s).

```
dag=zeros(N,N);
Cs=1;% Label number for each node
Cxt_1cm=2;Cxt_4cm=3; %Label number for each node
dag(Cs,[Cxt_1cm Cxt_4cm])=1; %Present relation between each pair nodes
node_sizes=[nCs nCxt nCxt]; % input the node size for each node
bnet=mk_bnet(dag,node_sizes,'discrete',discrete_nodes); % Building Bayesian network
bnet.CPD{Cs}=tabular_CPD(bnet,Cs,CPT_Cs);
bnet.CPD{Cxt_1cm}=tabular_CPD(bnet,Cxt_1cm,'CPT',CPT_Cxt_1cm);
bnet.CPD{Cxt_4cm}=tabular_CPD(bnet,Cxt_4cm,'CPT',CPT_Cxt_4cm);
```

Figure 2.9: Example of code for defining BN structure in BNT

2.3.2.3. Step 3: Selection of an inference engine and introducing evidences

There are many algorithms for doing inference in BN with different tradeoffs between speed, complexity, generality, and accuracy. BNT therefore can provide a variety of inference engines for such a purpose (see (Murphy 2001) for more details). Among these engines, the "junction tree engine" is selected because it could be used for all exact inference algorithms (Bensi et al. 2011a). Toward this aims, each node in the BN is discretised into a number of states greater than 2; thus, these nodes are not binary nodes. The evidences introduced to each node must be in the type of "soft evidence". The term "soft" indicates that a node is not directly observed but we can provide information about the distribution over its possible states. Figure 2.10 presents Matlab code illustrating the definition of engine in the present example. A cell array was used to contain evidences from nodes in the BN. Each cell presents evidences of corresponding node in the BN.

```
engine=jtree_inf_engine(bnet); % Choose junction tree engine
evidence=cell(1,N); % Define vector of evidences
soft_evidence=cell(1,N); % Define soft evidences
```

Figure 2.10: Choosing engine and define evidences

When no evidences are introduced, marginal distributions can be computed by using the code in Figure 2.11.These distributions provide a priori information of each node in the BN (Table 2.8); for example, node C_s follows a priori uniform distribution.

```
[engine,loglik]=enter_evidence(engine,evidence,'soft',soft_evidence);
m1=marginal_nodes(engine,Cs); % Compute marginal distribution for Cs
m2=marginal_nodes(engine,Cxt_1cm); % Compute marginal distribution for Cxt_1cm
m3=marginal_nodes(engine,Cxt_4cm); % Compute marginal distribution for Cxt_4cm
```

Figure 2.11: Introducing evidences and computing marginal distributions

Table 2.8: Marginal distribution with no evidences introduced

Cs	*Cxt_1cm*	*Cxt_4cm*
0.125	0.1474	0.5039
0.125	0.2774	0.4961
0.125	0.2753	0.0000
0.125	0.2736	0.0000
0.125	0.0264	0.0000
0.125		
0.125		
0.125		

Assuming that we have some evidences at node *Cxt_1cm* and *Cxt_4cm* (Table 2.9), these evidences are provided in a vector representing the probability distribution over possible states of node. By assigning the evidences to the corresponding cell of node in the evidence array, we can set the evidence for one node (Figure 2.12). After introducing evidences into BN, the marginal distributions can be computed and the results are presented in Table 2.10. These probabilities are a posteriori distributions of parameters after updating the BN. Statistic information such as the mean and the standard deviation of the identified parameters can be computed directly from these a posteriori distributions.

Table 2.9: Evidences for nodes Cxt_1cm and Cxt_4cm

e_Cxt_1cm	*e_Cxt_4cm*
0.0020	0.5183
0.2714	0.4817
0.6666	0.0000
0.0600	0.0000
0.0000	0.0000

```
soft_evidence{Cxt_1cm}=e_Cxt_1cm;%Setting evidences for Cxt_1cm
soft_evidence{Cxt_4cm}=e_Cxt_4cm;%Setting evidences for Cxt_1cm
[engine,loglik]=enter_evidence(engine,evidence,'soft',soft_evidence);
m1=marginal_nodes(engine,Cs); % Compute marginal distribution for Cs
m2=marginal_nodes(engine,Cxt_1cm); % Compute marginal distribution for Cxt_1cm
m3=marginal_nodes(engine,Cxt_4cm); % Compute marginal distribution for Cxt_4cm
```

Figure 2.12: Introducing evidences and computing a posteriori distribution

Table 2.10: A posteriori distribution after updating BN

Cs	*Cxt_1cm*	*Cxt_4cm*
0.0009	0.0011	0.4841
0.1052	0.2840	0.5159
0.1280	0.6573	0.0000
0.2402	0.0576	0.0000
0.2928	0.0000	0.0000
0.1858		
0.0263		
0.0207		

2.3.2.4. Step 4: Validation with Netica

The performance of the Matlab BNT will be validated with the Netica commercial software which is a powerful and easy-to-use tool for working with belief networks and influence diagrams. The limit is that the free version has a limited number of nodes. By comparing results before and after updating

with evidences between Netica (Figure 2.13 and Figure 2.14) and BNT (Table 2.8 and Table 2.10), it is clear that with the same a priori information, the BN built on BNT could provides the same results for a posteriori distributions as the one built in commercial software (NETICA) and the algorithms used to create the CPTs are also validated. The objectives of this study are using BN as a sophisticated tool which is easy to modify, to extend with different BN configurations. In BN commercial software, these characteristics are difficult to fulfil and also require a lot of time for handling; however in Matlab BNT, it could be easy to perform by codes if the algorithms are already available and validated. Therefore, the BNT is used as a basic environment for analysis in this study.

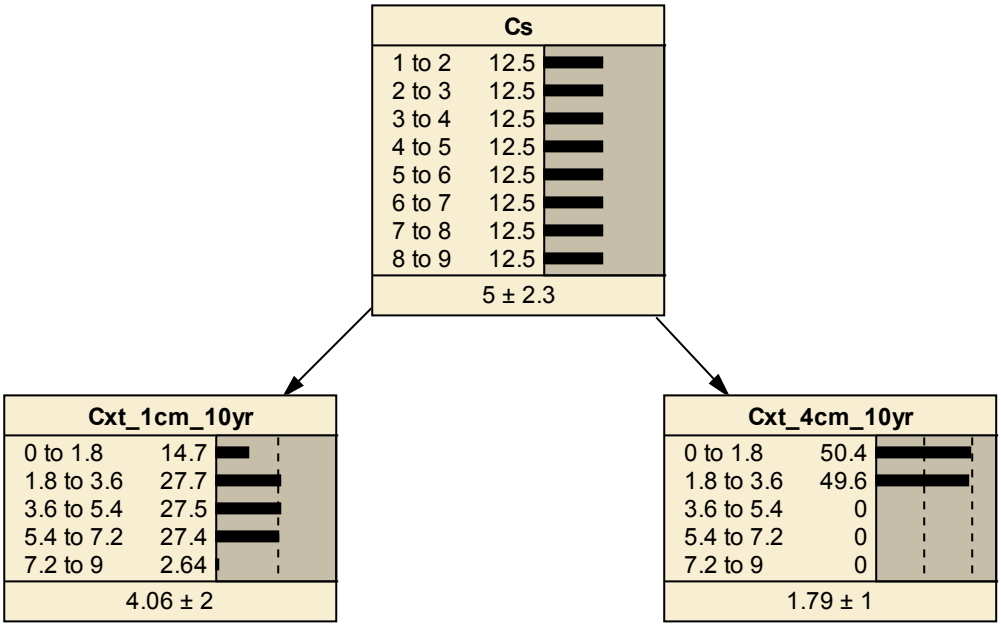

Figure 2.13: Probabilities with no evidences

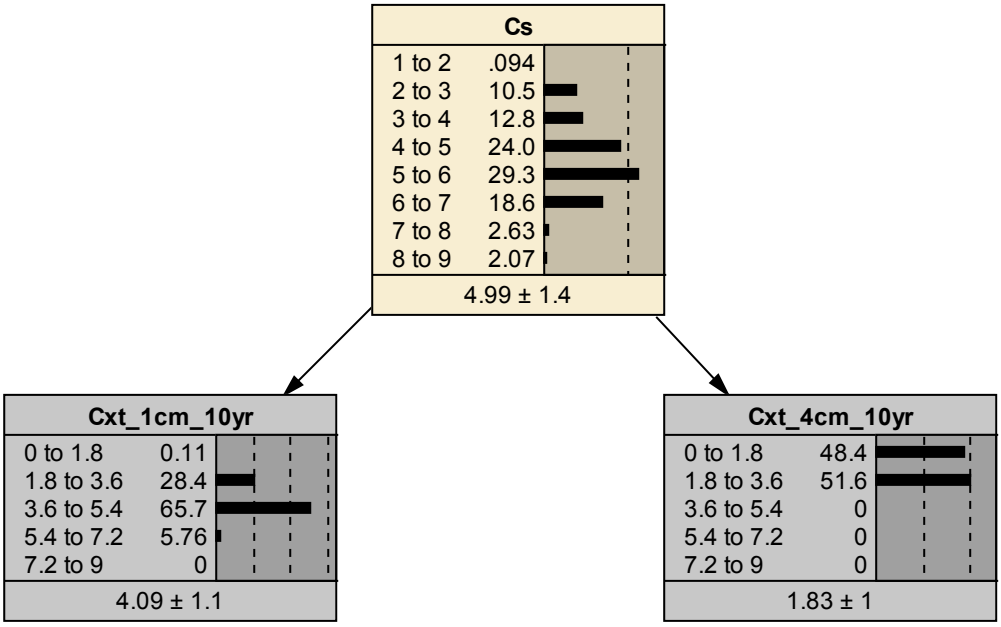

Figure 2.14: Probabilities after updating with evidences

2.4. Strategies for numerical implementation

2.4.1. Generating CPTs

2.4.1.1. Latin Hypercube and Monte Carlo Simulation

Monte Carlo (MC) simulations can be used to generate a random sample of N points for each uncertain input variable of a model. It selects each point independently from the probability distribution function of the input random variable. It generates a sample of N values or scenarios for each result that is after used to estimate statistical measures such as mean, standard deviation, fractiles (quantiles) and probability curves. Because MC relies on pure randomness, it can be inefficient when the number of simulation is limited. It might end up with some points clustered closely, while other states within the space get no samples. Latin Hypercube sampling (LHS) aims to spread the sample point more evenly across all possible values. It partitions each input distribution into N states of equal probability, and selects one sample from each state.

For example, for generating 5000 random variables of C_s with uniform distribution in the range [1; 9]. Both LHS and MC are performed and the histograms obtained from the results between the two methods are compared in Figure 2.15. It is clear that with LHS, histogram from sampling variables could be smoother. In BN inference, the CPTs define the relationship between each pair nodes. The CPTs of child nodes are calculated from random values of parent nodes that are generated from their a priori distributions. Consequently, the accuracy of sampling methods plays an important role in the accuracy and the BN's outputs. Based on the comparison between the two sampling methods above, LHS is used for generating random variables for calculating the CPTs.

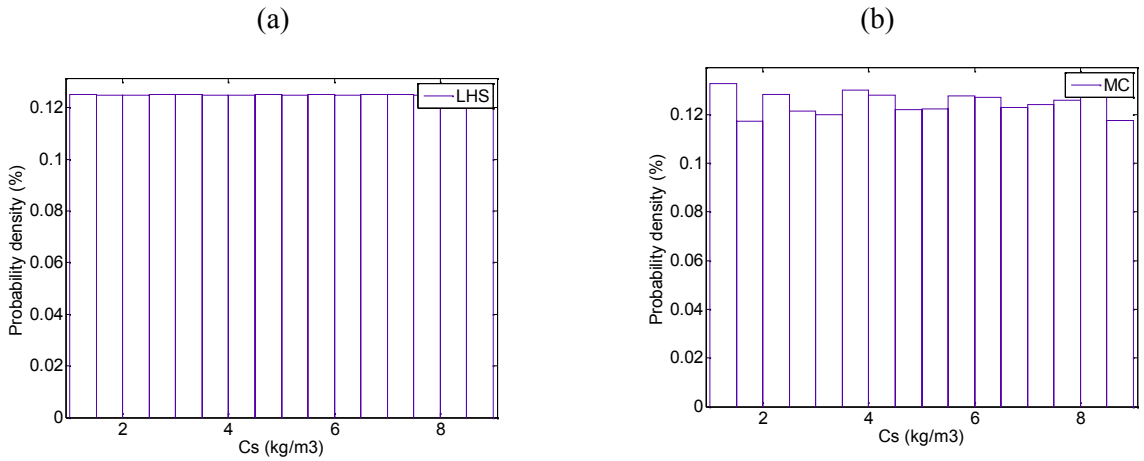

Figure 2.15: Histograms of data obtained from (a) LHS sampling - (b) MC simulation

2.4.1.2. Generating CPTs for BN with more than 2 parent nodes

Section 2.3.2 presented a simple algorithm for generating CPT in case of child nodes with only one parent node. Figure 2.17 illustrates the algorithms for calculating CPT table when child nodes have more than one parent node (e.g., Figure 2.16). The conditional distribution of each child node

must be defined for each combination of the $nC_s * nD$ states of its parents (C_s and D). Let's denote Cxt as a child node representing the chloride content at a certain depth and time. Each child node Cxt has $nCxt$ states. Assuming that $Nsim$ variables have been generated from Monte Carlo simulations for each parent nodes C_s and D, each value of $Cxt(i)$ is computed by the combination of $C_s(i)$ and $D(i)$ in Equation (1.2), $i = 1,...,Nsim$. The CPT for child node Cxt is then 2-dimensions array with $nC_s * nD$ rows and $nCxt$ columns. Let's denote now $X_{Cs(i)}$, $X_{D(i)}$, $X_{Cxt(i)}$ as states of a set values of $C_s(i)$, $D(i)$ and $Cxt(i)$. Each state of node represents a specific interval from its discretisation. The CPT table is built by counting the mean of all values of $Cxt(i)$ that belongs to the corresponding element in the CPT table. For example, at i^{th} simulation, $Cxt(i)$ will belong to an element at row $\left(\left(X_{D(i)} - 1\right) * nC_s + X_{Cs(i)}\right)$ and column $X_{Cxt(i)}$. The CPT table is then determined by normalising itself after collecting all belonging values for each element from $Nsim$ simulations.

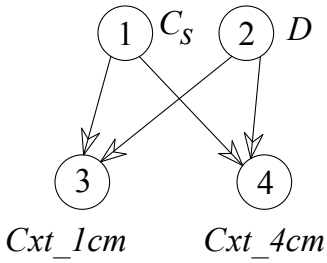

Figure 2.16: BN with more than 2 parent nodes

Initialisation:

$Cxt\_1cm = f(C_s, D, x, t) = f(C_s)$

For i = 1,…,*Nsim* (number of simulations used to generate the CPT)

- Generate $C_s(i)$ ~ uniform [lb_C_s; lb_C_s] % Using Latin Hypercube method
- Generate $D(i)$ ~ uniform [lb_D; lb_D] %Using Latin Hypercube method
- Calculate $Cxt(i)$ using equation (1.2)
- Find:
  - $X_{Cs(i)}$ = state of $C_s(i)$ in nCs states
  - $X_{D(i)}$ = state of $D(i)$ in nD states
  - $X_{Cxt(i)}$ = state of $Cxt(i)$ in $nCxt$ states
- $CPT\_Cxt\left(\left(X_{D(i)} - 1\right) * nC_s + X_{Cs(i)}, X_{Cxt(i)}\right) = CPT\_Cxt\left(\left(X_{D(i)} - 1\right) * nC_s + X_{Cs(i)}, X_{Cxt(i)}\right) + 1$

End

Determine normalised CPT_Cxt

Figure 2.17: Algorithm for generating CPTs of BN with two parent nodes

Bensi et al. (2011b) proposed an algorithm for creating CPT tables. This algorithm generates uniform variables within the states associated with each combination of the parent node states (Figure 2.18). By this means, all mutually exclusive collectively exhaustive states of parent nodes can have a good combination with the same number of simulations. It is a powerful characteristic of this algorithm. However, loops in algorithm will increase exponentially as the number of parent node's states increase. Therefore, more time is required for the computational process, especially when nodes have high number of states. This can be seen as a disadvantage of the algorithm of Bensi et al. (2011b) regarding to parameter identification in chloride ingress, because a high value of states is necessary to obtain a good estimated value. The algorithm proposed in this study (Figure 2.17) could not provide a good combination as the above approach, because it generates simulations in the pre-defined ranges for each parameter regardless the equality for each state. This disadvantage point could be solved considering larger number of simulations. However when there are more parent nodes in BN, mutual combinations in generating CPT could be inadequate. In fact, BN configurations for chloride ingress models in this study has a limited number of parent nodes. Consequently, the proposed algorithm given in Figure 2.17 is used for generating CPTs in this study. For other BN with more parent nodes, the approach proposed by Bensi et al. (2011b) should be considered.

Initialisation:

$CPT\_Cxt = zeros\left(nC_s * nD, nCxt\right)$;

For i = *1,..,nCs; j = 1,…,nD*

For n_i = 1,…,nsim (number of simulations per state to generate the CPT)

- Generate $C_s\,(n_i)$~ uniform $\left[lb\_C_s^i, ub\_C_s^i\right]$ %Generate uniform values in state i^{th}
- Generate $D\,(n_i)$~ uniform $\left[lb\_D^j, ub\_D^j\right]$ %Generate uniform values in state j^{th}
- Calculate $Cxt\,(n_i)$ using equation (1.2)
- Find:
  - $X_{Cxt\,(ni)}$ = state of $Cxt(n_i)$ in $nCxt$ states
- $CPT\_Cxt\left(\left(j-1\right)*nC_s + i, X_{Cxt(ni)}\right) = CPT\_Cxt\left(\left(j-1\right)*nC_s + i, X_{Cxt(ni)}\right) + 1$

End

Determine normalised CPT_Cxt

Figure 2.18: Algorithm from Bensi et al. (2011b) for generating CPTs of BN

2.4.2. Generating numerical evidences

Periodic inspection of RC structures subjected to corrosion is an important task for assessment of corrosion consequences, structure serviceability and safety levels. Bastidas-Arteaga & Schoefs (2012)

proposed that RC structures should be inspected every $\Delta t = 8-13\text{years}$ to ensure an optimal level of safety and to minimise maintenance cost. This means that inspection campaigns may take decades and data from inspection is rarely sufficient. Therefore, in this study, real evidences from inspection data are replaced by simulated evidences using Eq. (1.2) to provide general improved BN configurations.

Table 2.11: Theoretical values for generating evidences

Parameter	Mean	Std	Distribution
C_s (kg/m^3)	5	1	Lognormal
D (m²/s)	3×10^{-12}	0.3×10^{-12}	Lognormal

The theoretical values provided in Table 2.11 are used to generate 3000 random variables for C_s and D from Monte Carlo simulations. Then, each set of values is used to compute numerical profiles (evidences) at different depths and times. These results will serve afterwards to calculate the probability that $C(x,t)$ belongs to a given state for different depths. For instance, Table 2.12 presents the numerical evidences estimated for $x = 1\text{cm}$ and $x = 4\text{cm}$ at an inspection time $t = 10\text{years}$. It is assumed herein that inspections are perfect. These results are given in terms of probability of belonging to each state. It is observed that with inspection points far from the concrete surface, larger probabilities are focused on states with lower chloride content.

Table 2.12: Numerical evidence at t =10 years

State	*P(Cxt_1cm)*	*P(Cxt_4cm)*
0-1.8	0.002	0.5183
1.8-3.6	0.2714	0.4817
3.6-5.4	0.6666	0
5.4-7.2	0.06	0
7.2-9	0	0

2.4.3. Convergence of BN with the number of states

As previously mentioned in section 2.2, continuous variables need to be discretised into several states. The number of states could be adjusted to obtain a balance between accuracy of results and computational time. When a more accurate result is expected, a high number of states is often chosen. Figure 2.19 describes the assessment of mean and standard deviation values of D with several discretisation. The illustrated BN configuration has 2 parent nodes representing C_s and D, and 41 child nodes which comes from a discretisation of inspection length $L = 12\text{cm}$ by interval length $\Delta x = 0.3\text{cm}$

(minimum length required for measurement). Results reveal that the identification approaches converged to values when high values of states are used. This numerical implementation could be very useful when dealing with low chloride content at deeper inspection points. A discretisation with high value number of states can take advantage of poor information from low chloride content. The disadvantage of this solution is the increase of the CPT's size when the number of states increases which may lead to larger computational time.

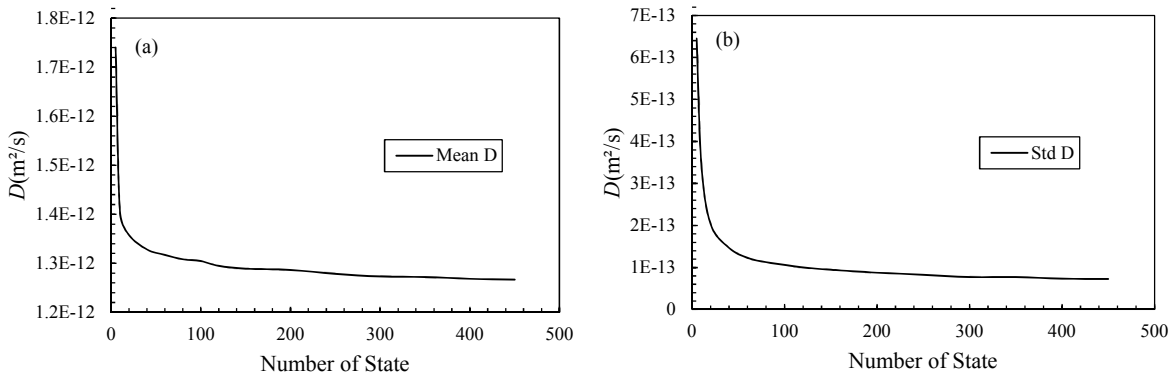

Figure 2.19: Identification of the mean and standard deviation values of D for child nodes discretised with several states

2.4.4. Using different boundaries for child nodes

Figure 2.20 describes a chloride profile simulated from equation (1.2) where chloride content follows a decreasing trend as the depth increases. In BN configuration with several child nodes representing chloride content at different depths, using the same boundary for all child nodes will be an inefficient approach to handle the evidences. Due to low chloride contents in deeper parts, most of these informations will fall in one or few states. For example, Figure 2.21a shows the evidence at depth $x = 6\text{cm}$, $t_{ins} = 10\text{years}$ and a discretisation with 15 states. It is noted in such a case that all the information of the evidences is concentrated in one state, and then, the evidence at these nodes will not provide valuable information for updating the BN. Increasing the number of states could solve this problem. Figure 2.21b indicates that 200 states are more convenient to represent the variability of the chloride concentration at this depth. Nevertheless, this solution increases the size of the CPTs and, therefore, the computational time.

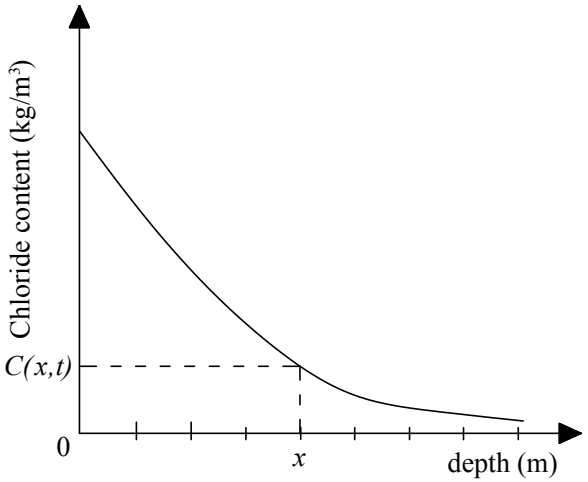

Figure 2.20: Simulated chloride profile

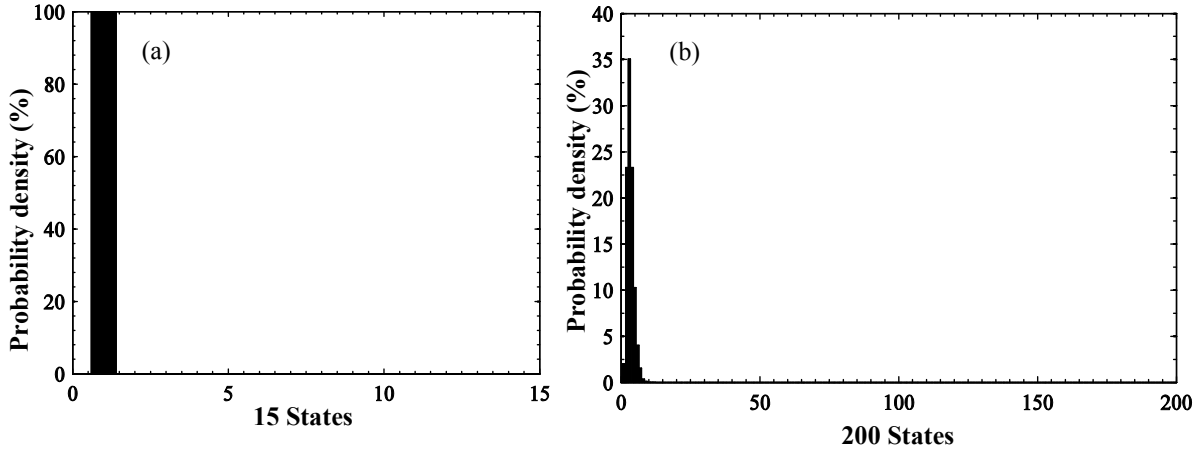

Figure 2.21: Evidence at *x*=6cm with different discretisation of child nodes: (a) 15 states – (b) 200 states

Consequently, it is proposed a procedure to improve the discretisation of child nodes. The number of states in the discretisation remains constant but we use different boundaries for the discretisation of all child nodes $C\left(x_i,t_j\right)$. These boundaries correspond to a specific range which is defined by the minimum and maximum values of the chloride concentration at depth x obtained from the a priori data used to create the CPTs (Figure 2.22a). By considering these boundaries, we take advantage of the information of deep points in the updating process. Figure 2.22b shows the evidence at depth $x = 6\text{cm}$ with 15 states. It is clear that the evidence at depth $x = 6\text{cm}$ could provide now more valuable information for updating the BN. This numerical implementation will be employed for all BNs in this study and can be seen as suboptimal issue.

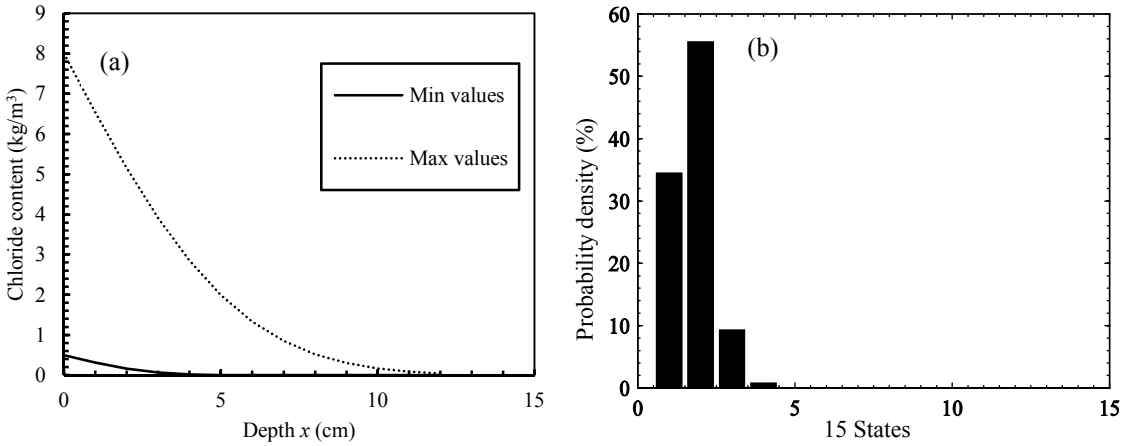

Figure 2.22: (a) Ranges for each child node at depth x – (b) Evidence at x=6cm with 15 states for each child node and different ranges.

2.5. Conclusion

This chapter described in details the procedure to construct a comprehensive Bayesian network methodology for parameter identification using BNT. Based on the Matlab environment, the BNT allows users to modify the BN structures, implement numerical issues as well as perform simulations very quickly and easily. Therefore, it will be an appropriate tool for updating information in chloride ingress model which is considered as a complex problem. The main conclusions in this chapter are summarised as follows:

1. The first part of this chapter summarised BN theory and discussed how this approach could be used to model chloride ingress and identification. The procedures (BN construction, introducing evidences, propagating evidences through BN, and updating to provide a posteriori distributions) were detailed by discussing numerical algorithms and illustrated with examples. Results from updating BN with evidences indicated that a posteriori distribution approaches the theoretical ones; therefore, this methods could be used as an efficient tool for parameter identification.
2. BN toolbox is an open-source Matlab package for graphical models which combines between probability and graph theories. Each module in constructing and performing the BN requires specific algorithms which are supported from available functions in Matlab. Therefore, the users can modify and implement easily for complex demanding. Examples of codes are provided.
3. BNT is designed as a general tool, therefore, in order to adapt it to a practical problem, some numerical issues must be discussed. Due to the lack of statistical and experimental data of chloride ingress, CPTs and evidences are created from simulations. The BN configuration in

this study only treat discrete random variables thus, continuous variables need to be discretised into states. The number of states should be optimised to ensure the convergence in the results and low computational cost. When the BN has several child nodes representing chloride content at different depth points, it will be more efficient to use different boundaries to take advantage of small chloride measured at deeper points

Chapter 3
Parameter identification of chloride ingress using BN

3.1. Introduction

Chloride ingress into concrete has been recognised as one of the main causes leading to the degradation of RC structures. Important damages due to chloride-attack are reported after 10-20 years (Kumar Mehta 2004; Poupard et al. 2006) and thus, structures should be inspected periodically to ensure optimal levels of serviceability and safety. Modelling chloride ingress into concrete, therefore, becomes an important task to plan and quantify maintenance operations of structures. Relevant material and environmental parameters required for modelling could be determined from inspection data obtained after each campaign. However, under natural exposure conditions, chloride ingress involves important uncertainties related mainly to material properties and exposure conditions. The level of uncertainty is even increased by effects of temporal and spatial variability in deterioration processes and their characterisation requires larger amount of inspection data. Nevertheless, these data is limited by expensive and time-consuming of inspection techniques that aim at determining chloride concentration levels. Therefore, this is a crucial challenge for optimising the use of these information.

The main objective of this chapter is to propose an approach to determine optimal BN configurations that minimise identification errors for each chloride ingress model parameter from data coming from normal and accelerated test. The specific objectives of this chapter are:

1. To test several BN configurations and to propose optimal BN configurations to identify each model parameter from natural tests and constant parameters of chloride ingress model.
2. To study the influences of combining various inspection times on parameter identification for constant and time-dependent parameters of chloride ingress models.
3. To propose a BN methodology for identifying an equivalent exposure time combining data from normal an accelerated tests.

4. To evaluate the sensitivity of identifying an age factor for the chloride diffusion coefficient and to propose a procedure to identify this age factor.

A general framework of parameter identification using BN is described in section 3.2. In this section, different BN configurations are generated to select the appropriate ones to identify each parameter. The efficiency of combining evidences from different inspection times is investigated in section 3.3 where two chloride ingress models are employed to (1) consider the time-dependency of chloride diffusion coefficient or (2) not consider this effect. Section 3.4 presents the normal and accelerated chloride ingress tests in the laboratory conditions. Based on general framework given in section 3.2, Section 3.4 develops a two-steps approach to identify a scale factor for accelerated tests. Section 3.5 studies the sensitivity of the age factor on parameter identification and proposes a procedure to estimate it from experimental data.

3.2. Parameter identification using data from normal tests

In this section, chloride ingress is modelled by the simplest chloride ingress model that only depends on two parameters: C_s and D (Eq. (1.2)). Despite some important physical phenomena are neglected, this solution is employed herein to illustrate the proposed methodology for the identification of random variables using BN because its complexity is sufficient to account for non-linear effects in x-direction and time. The methodology can be after extended to more realistic chloride ingress models but the computational time required for building the BN model will be increased by larger number of variables involved.

After presenting the methodology for evaluating the performance of BN configurations (section 3.2.1), this subsection studies the following configurations:

1. only one child node corresponding to one inspection point in depth and one inspection time (section 3.2.2),
2. various child nodes corresponding to several inspection points in depth and one inspection time (section 3.2.3), and
3. many child nodes corresponding to several inspection points in depth and varying the inspection times (section 3.2.4).

3.2.1. Generation of numerical evidences and BN discretisation

This study aims at determining an improved configuration of a BN for the identification of parameters of chloride ingress models. It this case, BN is used to update probabilistic models for the parameters to identify. The evaluation of the effectiveness of a given configuration should be based on a given criterion. Preferably, it should include a larger amount of experimental data (chloride profiles) that can be used to estimate ‘real’ probabilistic models of model parameters and consequently to test and compare various BN configurations. However, such a database is in practice very hard to obtain.

This data is obtained from semi-destructive tests that are expensive and time-consuming. Therefore, in order to provide general improved BN configurations, we consider sufficient numerical evidences generated from Monte Carlo simulations where the theoretical probabilistic models of the random variables to identify are known. Table 3.1 presents the considered probabilistic models for C_s and D. The mean values for each parameter were taken from (Bastidas-Arteaga et al. 2009). C_s corresponds to a structure placed in an atmospheric zone, close to the seashore but without direct contact with seawater. D is a typical diffusion coefficient for ordinary Portland concrete. The COV for each parameter were reduced to 20% and 15% for C_s and D, respectively. This is due to the fact that within one type of concrete, the variation is narrowed. The assumption that C_s and D follow lognormal distributions is also in agreement with other studies (Duracrete 2000b; Tang and Nilsson 1993; Vu and Stewart 2000).

Table 3.1 – Theoretical values of parameters to identify

Parameters	Distribution	Mean	COV
C_s	Lognormal	2.95 kg/m^3	0.20
D	Lognormal	1.33×10^{-12} m^2/s	0.15

The theoretical probabilistic models presented in Table 3.1 are used to generate 9,000 random values for C_s and D. Afterwards, each set values of C_s and D is used to compute the 9,000 independent chloride profiles from Eq. (1.2). The evidences to be introduced into the BN are then computed from these chloride profiles. In fact, to obtain simulated chloride profiles close to those in real conditions, it is necessary to employ a more advanced chloride ingress model. The same simulated values are used for all configurations to ensure that we update the BN with the same information.

Different BN configurations corresponding to various inspection schemes are analysed for selecting the configurations that provide the best identification of parameters. The performance of each configuration is evaluated in terms of the error of the identified parameter $Z_{identified}$ with respect to the theoretical value Z_{theory} as:

$$Error(Z) = \frac{\left| Z_{identified} - Z_{theory} \right|}{Z_{theory}} \times 100\% \tag{3.1}$$

where Z represents the mean or the standard deviation of the parameter to identify – e.g. mean or standard deviation of C_s and D, $Z_{identified}$ is the value identified from a posteriori histograms of parent nodes, and Z_{theory} is the mean and standard deviation values used to generate numerical evidences (Table 3.1).

Parameters should be discretised from continuous into discrete states. The discretised details and a priori information of variables are summarised in Table 3.2. Note that when different boundaries are applied to BN with several child nodes, the range for each node $C(x_i,t_j)$ varies with depth and is determined as previously described in section 2.4.4.

Table 3.2 – Discretisation of nodes and a priori distributions

Parameters	Number of states per node	A priori distribution	Range
C_s (kg/m^3)	variable	Uniform	[10^{-3}; 12]
D (m^2/s)	variable	Uniform	[6×10^{-13}; 20×10^{-12}]
$C(x_i,t_j)$ (kg/m^3)	variable	-	variable

3.2.2. Identification using a single inspection point

In this section, the identification of the random variables C_s and D is carried out from the most simple case where evidences are obtained at only one depth point (Figure 3.1). This study case could be useful for the identification from the resistivity based probe (Wenner probe) or resistivity based sensors (Du Plooy et al. 2013). The BN now consists of three nodes (Figure 3.1): two parent nodes are C_s and D, and one child node $C\left(x_i,t_j\right)$ representing the chloride concentration at depth x_i. The inspection time is $t_{ins} = t_1 = 10$ years (which is compatible with actual practices) and the total inspection depth is 12cm. Consequently, for a discretisation length with $\Delta x = 1\text{cm}$ we have 13 different BNs corresponding to 13 points in depth varying from 0cm to 12cm.

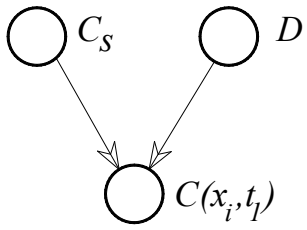

Figure 3.1: BN configuration using one inspection point in depth

Figure 3.2 shows the errors in the identification of the mean and standard deviation of C_s and D. For C_s, the evolution of the identification error of both mean and standard deviation increases with depth. These estimations are related to the evolution of the chloride profiles presented in Figure 3.3 where chloride content is lower when depth increases. This means that, data from chloride profiles

near to the surface provides more useful information for the identification of C_s, whereas information from deeper parts increases the error. When the chloride content is close to zero, these errors increase and they can even reach 40% for the mean. On the contrary, with the evidences near to the surface $(x \approx 0)$, we can obtain the best estimation for the mean and standard deviation of C_s, with errors of 1% and 3%, respectively. This is due to the fact that in equation (1.2), when we set $x \approx 0$, $C(x_i, t_j) \approx C_s$. Consequently, the chloride concentration at the surface is most valuable in the identification of C_s.

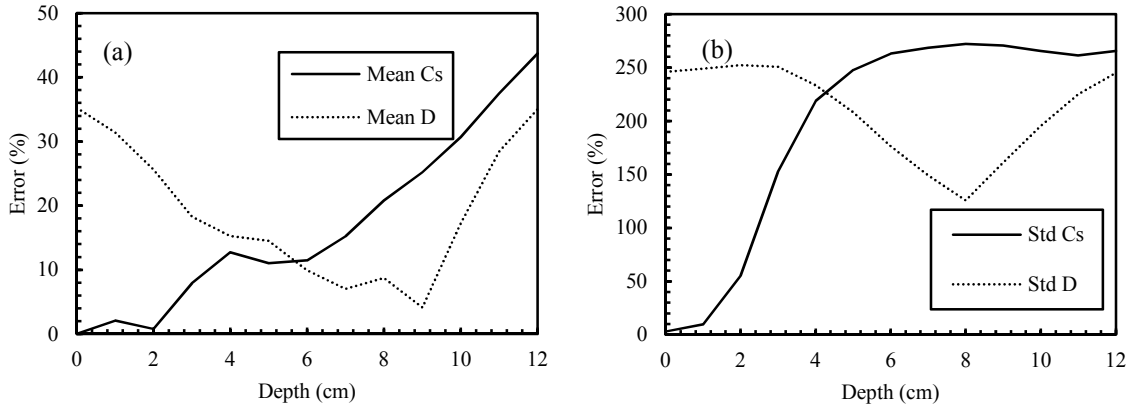

Figure 3.2: Identification error using one depth point: (a) Mean – (b) Standard deviation

It is also observed in Figure 3.2a that the error in the identification of D decreases until a depth $x < 9$ cm and it increases after this point. This behaviour corresponds to the fact that chloride content at deeper parts is more useful for predicting the diffusion coefficient. However, at deeper points where the chloride contents are close to zero for $t_{ins} = 10$ years, the error increases. The errors in the identification of the standard deviation of D followed a similar trend, however their values are very far from the theoretical values with important errors (more than 200%). Therefore, it can be concluded that it is very difficult to perform a good identification of D using evidences obtained from only one point in depth.

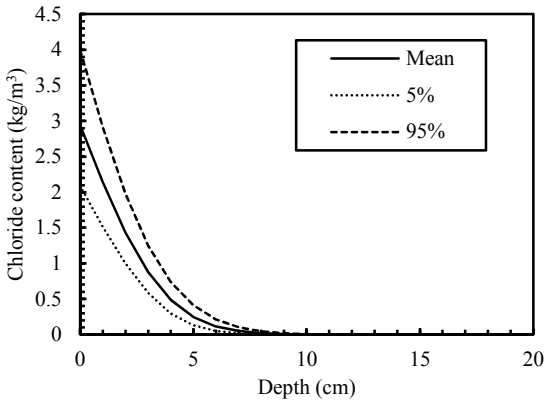

Figure 3.3: Mean chloride profile and confidence intervals at t=10 years

3.2.3. Identification using several inspection points

In this section, we keep the same inspection time for $t_{ins} = 10$ years to focus our analysis on other factors. This time considers both the actual practice for the first inspection time and a sufficient long time to obtain a sufficient chloride inside concrete. The identification in BN will use now data from total inspection depth. The total inspection depth (12cm) is selected to cover all the potential chloride presence after 10 years for the selected concrete characteristics according to the profiles obtained from theoretical data (Figure 3.3). The total inspection depth is divided into small concrete slides with grinding depth d_g=0.3cm. The grinding depth should not be smaller than 0.3cm due to the accuracy of the semi-destructive equipment (grinding) for determining chloride profiles.The average chloride content within a grinding depth can be assumed to represent the chloride content at the average depth of the corresponding concrete slide. By this means, it is possible to select several inspection points with the discretisation length Δx for updating the BNs. The BNs will now have a number of child nodes equal to the number of measurements in depth, n_x. For example, if $\Delta x = 2\text{cm}$, the BN configuration consists of 2 parent nodes and 7 child nodes as described in Figure 3.4. Table 3.3 presents the different cases considered in this section: 5 cases are studied whose number of points vary between 5 and 41.

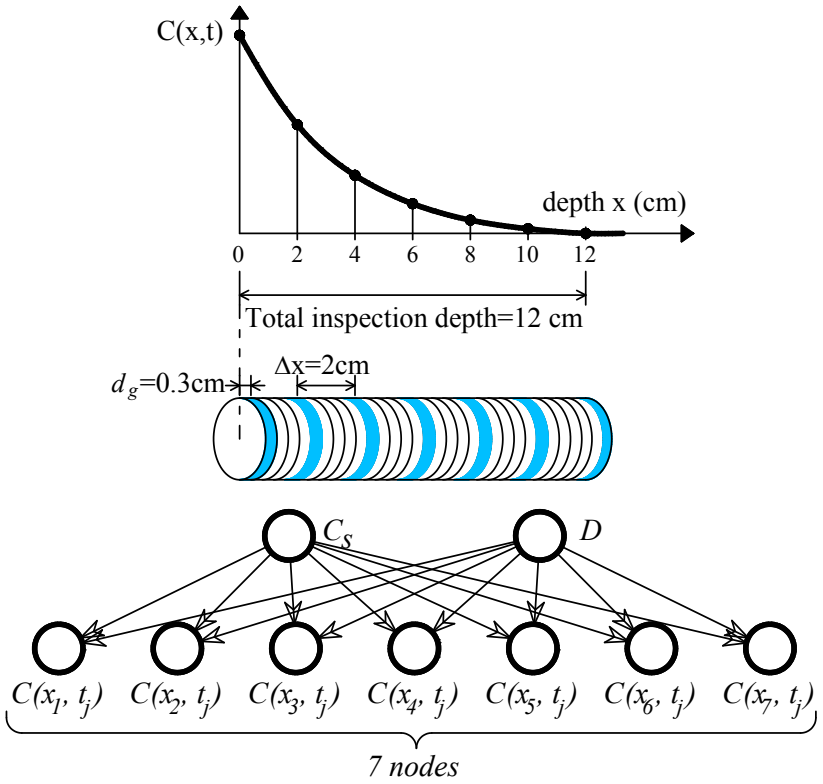

Figure 3.4: BN configuration with Δx=2 cm

Table 3.3: Discretisation cases and inspection points in depth

Δx (cm)	Discretisation (cm)	Inspection points in depth (n_x)
0.3	0:0.3:12	41
0.5	0:0.5:12	25
1	0:1:12	13
2	0:2:12	7
3	0:3:12	5

3.2.3.1. Using the same boundaries for all child nodes

Figure 3.5 presents the error in the identification using full inspection depth and the same boundaries for the child nodes. These results were obtained by discretising the child nodes into 15 states. For all BN configurations, it is noted that there is no remarkable change in the identification of the mean of C_s (Figure 3.5a) because the errors in all cases are close to 5%. Meanwhile, it seems that increasing the number inspection points might produce more errors for the standard deviation of C_s (Figure 3.5b). Interestingly, the gap between identified and theoretical values for D is reduced significantly when the size of the discretisation length Δx is smaller. The errors in the estimation of

the mean of D are less than 5% when $\Delta x < 0.5\text{cm}$. The standard deviation of D also reveals a better evolution when Δx decreases: the error was reduced from more than 200% with $\Delta x = 3\text{cm}$ to about 20% with $\Delta x = 0.3\text{cm}$. This behaviour is expected because when the inspection depth is divided into small Δx, we could obtain information describing the level of chloride ingress that is more useful for characterising the diffusion coefficient. Hence, we can conclude that data from full inspection depth is more valuable in the identification of D.

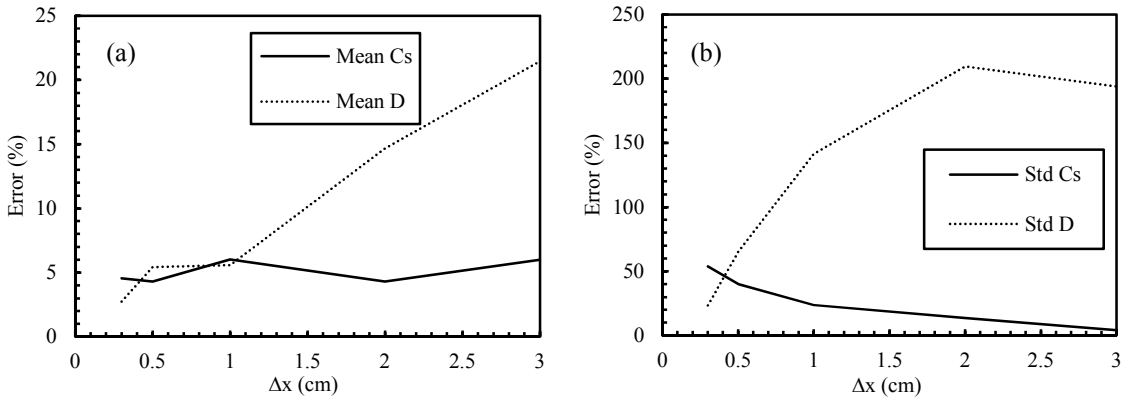

Figure 3.5: Identification error using full inspection depth: (a) Mean – (b) Standard deviation

3.2.3.2. Using different boundaries for all child nodes

As previously mentioned in section 2.4.4, when BN configurations have many child nodes representing for several inspection depth points, it is useful to use different boundaries for each child node to take advantage of information from deeper points where chloride content is low. The above section pointed out that using several inspection points could not improve the estimation of C_s, therefore, using different boundaries is just useful for the estimation of D. Figure 3.6 compares the error in the identification of the mean and standard deviation of D before and after improvement (rebuild case) of the discretisation of child nodes. It is clear that the consideration of large number of states and/or different boundaries reduces drastically the errors even when the inspection length was divided into large intervals ($\Delta x \in$ [2 cm, 3 cm]). This proposed approach could be very useful in practice when the number of measured points is limited or when the level of chloride content inside concrete is low.

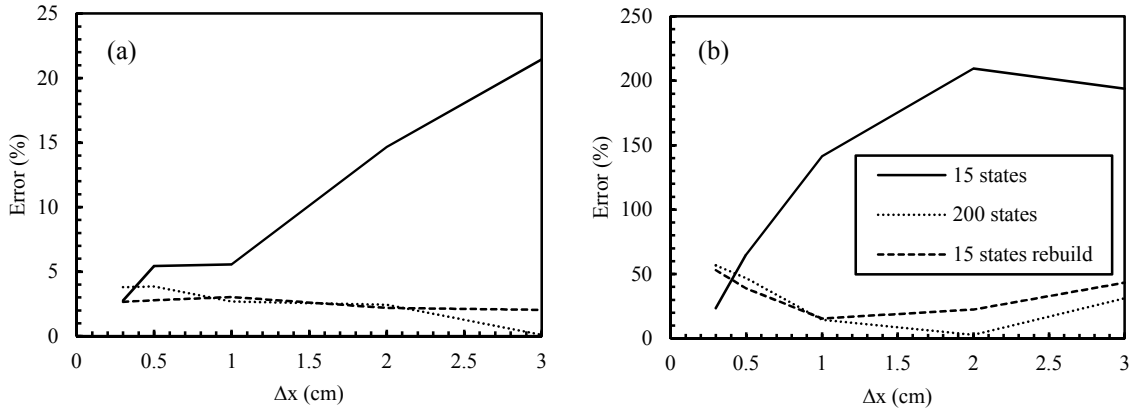

Figure 3.6: Identification error of D for three discretisation of child nodes: (a) Mean – (b) Standard deviation

Moreover, it is worth noticing that there are optimal discretisation lengths Δx_{opt}: for the standard deviation (Figure 3.6b), with 200 states it is obtained for $\Delta x_{opt} \approx 2\text{cm}$ and with 15 states rebuild for $\Delta x_{opt} \approx 1\text{cm}$. This means that the common idea that increasing the number of inspection points over the total inspection depth is better is not always true for Bayesian updating. In fact, by doing so, the large error obtained by considering some inspection depths can affect the updating: that is the case for low chloride content (around $x = 10\text{cm}$). Moreover, the difference between chloride content in adjacent inspection points is very close when the discretisation length is small ($\Delta x = 0.3\text{cm}$ for instance). Therefore, the probability densities of the evidences used for updating in BN are very similar for two neighbouring inspection points. Figure 3.7a illustrates this point by showing the almost identical probabilities at $x = 0\text{cm}$ and $x = 0.3\text{cm}$. That increase the identification errors when using close points. In contrast, when Δx increase $\left(\Delta x = 2\text{cm}\right)$, the probability densities of the evidences differ by reducing the identification errors (Figure 3.7b). That is why, even for the mean value (Figure 3.6a), the protocol with $\Delta x = 3\text{cm}$ is better. On the opposite, when Δx is larger than the optimal value, the errors for both mean and standard deviation increase because the information becomes poor for describing the chloride ingress process.

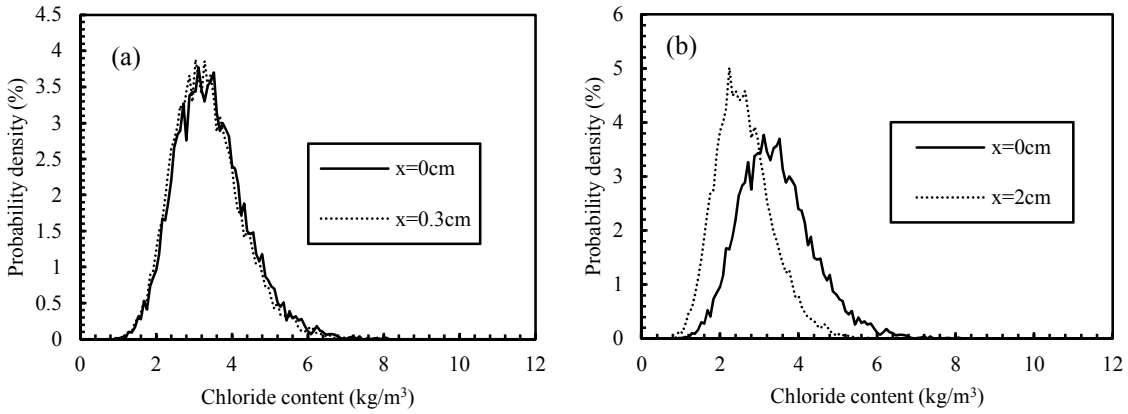

Figure 3.7: Effect of discretisation length Δx on the distribution of chloride content at: (a) $\Delta x = 0.3\text{cm}$ – (b) $\Delta x = 2\text{cm}$

3.2.4. Inspection optimisation with time and space

In this section, evidences obtained from various inspection times will be introduced in the BN for the identification process. According to previous section, different boundaries were used for each child node in the BN with a sufficient number of states to minimise the fluctuation effects/errors in the results.

3.2.4.1. Influence of the inspection time on the identification error

From Figure 3.8, it can be seen that the inspection time t_{ins} influences the estimation of both the mean and standard deviation of D. The identification is improved when t_{ins} increases until arriving at an optimal inspection value $t_{ins,opt}$ that varies between 40 and 50 years for the identification of the mean and standard deviation. This phenomenon can be explained by the fact that when $t_{ins} \approx 45\text{years}$ the chloride concentration in the total inspection length is sufficient for describing the chloride ingress process – i.e. there is sufficient chloride content at each point in the space to improve the identification. When $t_{ins} > 50\text{years}$, the chloride content at $x = 12\text{cm}$ is larger than zero and therefore the identification errors increase because the inspection length is not large enough to describe the problem.

It is also worth noticing that there is an optimal value of Δx for each inspection time that minimises the error. The optimum value decreases when t_{ins} increases. This is related to the fact that for larger t_{ins} the chloride content inside the total inspection length is larger. Consequently, it is necessary to add more information to improve the representation of the chloride profile. It is also noted that the error is larger for smaller values of Δx in comparison with the Δx_{opt}. There is no remarkable change in the estimation the mean value of D when Δx varies from 0.3 cm to the optimal

value. However, the variation is more important for the identification of the standard deviation of D. This is mainly related to the discretisation effect already described in the previous section.

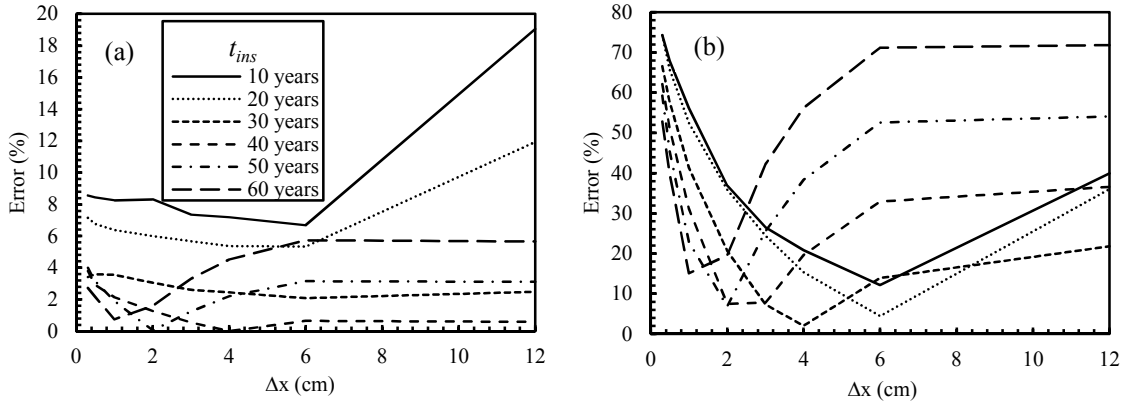

Figure 3.8 – Identification error for D with evidences from different inspection times: (a) Mean – (b) Standard deviation.

For C_s, the results presented in Figure 3.9 reveal that it is better to use the evidences at early inspection times to obtain a good estimation of C_s. This is because for a given discretisation, the chloride content at the surface $(x = 0\text{cm})$ is the same for all inspection times. However, at deeper points the chloride content rises when inspection times increase and such an increment disperses the information at the surface leading to the inaccuracy in the assessment. The results also show that the consideration of more points in depth increases significantly the errors in the assessment of the standard deviation as previously discussed in section 3.2.3.

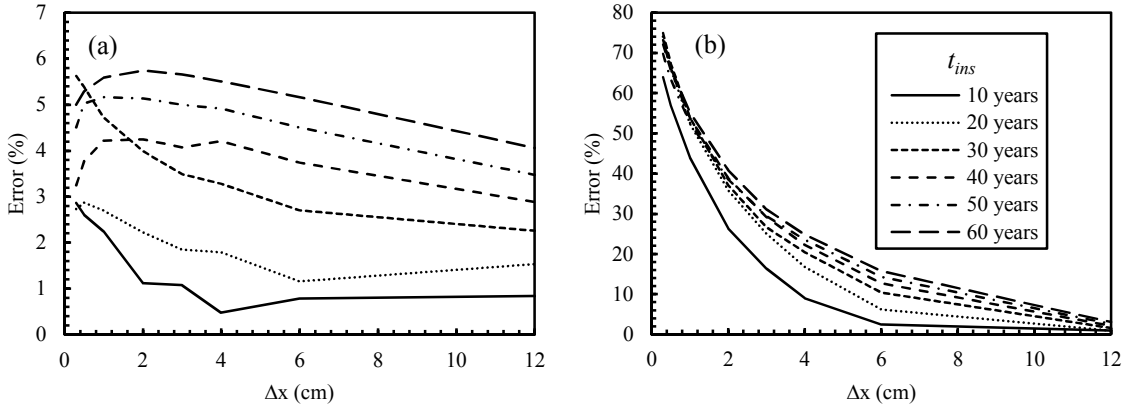

Figure 3.9 – Identification error for C_s with evidences from different inspection times: (a) Mean – (b) Standard deviation.

3.3. Efficiency of combining evidences from different inspection times in parameter identification

Inspection campaigns on RC structures can be carried out at different times. These data gives a significant information about chloride content inside concrete and thus on their history and it is also useful for prediction from updating time-variant models. In this section, the BN is used to evaluate the efficiency of combining simultaneously evidences obtained from different inspection times in parameter identification. The time-dependency of chloride diffusion coefficient in parameter identification is investigated by making comparisons between two models embedded in BN:

- the model proposed by Tuutti (1982), equation (1.2), and
- the model suggested by Nilsson and Carcasses (2004), equation (1.4).

As previously discussed in section 1.3.1, the major difference between the two models is the consideration of the age factor. Nilsson and Carcasses (2004) treated chloride diffusion coefficient as a time-dependent parameter, whereas Tuutti (1982) considered it as constant by omitting the age factor.

For comparative purposes, we consider the same number of chloride profiles for different schemes of inspection, thus all configurations have the same quantity of information. The evidences from each scheme may come from one inspection time or from the combination of several inspection times. The efficiency of each inspection campaign is evaluated based on the estimation of identification errors for the parameters according to Eq. (3.1).

3.3.1. Time-independent chloride diffusion coefficient

In this section, the model of Tuutti (1982) is used to describe chloride ingress into concrete with the same configuration as in section 3.2.3 (Figure 3.4). Input information such as: a priori information, discretisation and theoretical values of parameters are the same as in section 3.2.1 (Table 3.1 and Table 3.2). We consider 5 inspection schemes summarised in Table 3.4. Schemes 1, 2, and 3 use data from one inspection time, meanwhile scheme 4 and scheme 5 combining evidences from 2 or 3 inspection times for updating the BN, respectively. Note that the total number of chloride profiles for all schemes are the same (9,000 profiles).

Figure 3.10 depicts the identification errors for C_s with evidences from different inspection schemes. As previously analysed in section 3.2.4, since the deterioration model considers that the chloride surface concentration does not depend on time, it is better to use the evidences obtained at early inspection times. Indeed, the identification of C_s from inspection data at 10 years is more accurate than those at 20 years or 30 years. The results in Figure 3.10 have pointed out that combining data from different t_{ins} could not improve the identification. For example, in the inspection scheme 4

(10+20 years), the identification errors are larger than inspection scheme 1 which uses data from t_{ins}=10 years. This is because, for the inspection scheme 4, the 4,500 chloride profiles obtained at 20 years induce errors in the identification process.

Table 3.4: Schemes for combining evidences for different inspection times

Inspection scheme	Inspection times (t_{ins})	Number of chloride profiles
1	10 years	9,000
2	20 years	9,000
3	30 years	9,000
4	10 years + 20 years	4500 + 4500
5	10 years + 20 years + 30 years	3000+ 3000 + 3000

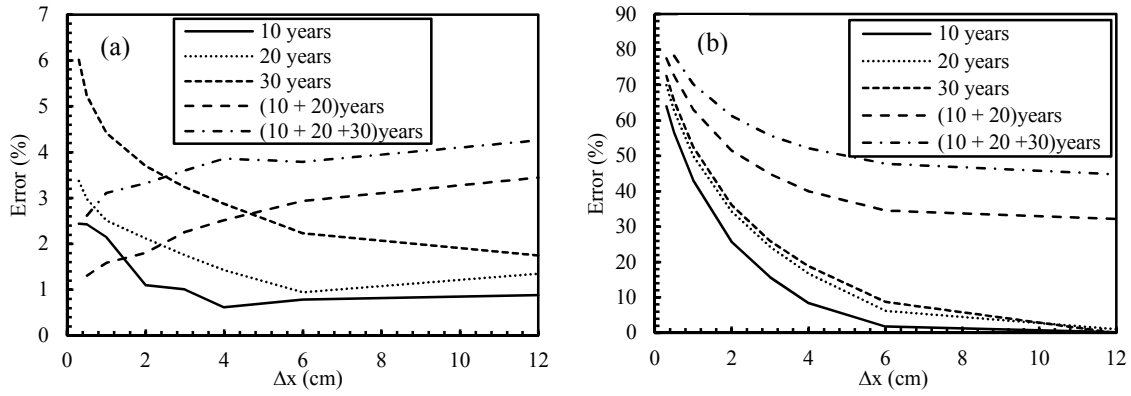

Figure 3.10: Identification error for C_s with evidences from different schemes of inspection: (a) mean - (b) standard deviation

Figure 3.11 presents the identification errors for D with evidences for different inspection schemes. As previously mentioned in section 3.2.4 evidences at t_{ins} = 30 years provide smaller identification errors than those at 10 or 20 years. Results in Figure 3.11 show that from inspection scheme 3 with 9,000 chloride profiles at t_{ins} = 30 years, the estimation of D is more close to the theoretical values than other inspection schemes that use data from early inspection times or combine the evidences from different t_{ins}. It can be concluded that there are optimal inspection years for minimising identification errors for each parameter. In this case, the consideration of several inspection times introduced errors in the identification process. However, inspection schemes that consider several inspection times could be more appropriated to identify time-dependent parameters. This issue will be investigated in the next section where a coefficient called age factor is introduced to account for a time-variant chloride diffusion coefficient.

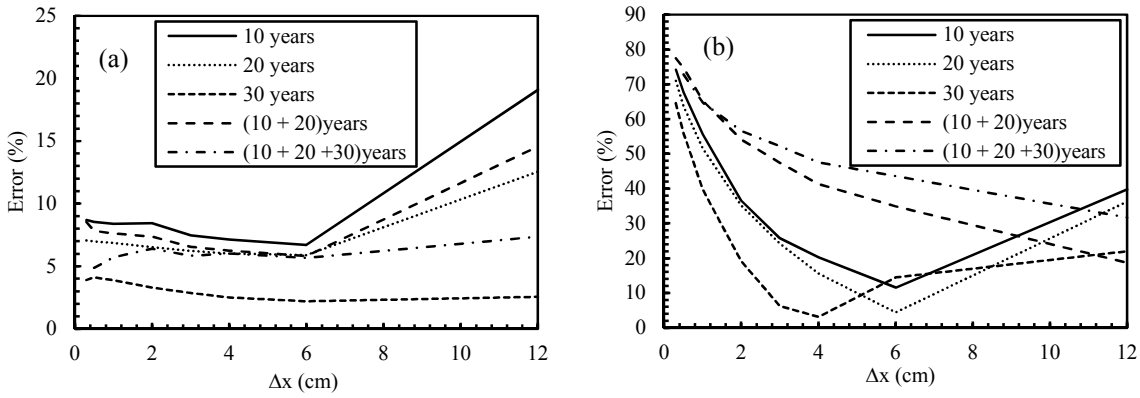

Figure 3.11: Identification error for *D* with evidences from different schemes of inspection: (a) mean - (b) standard deviation

3.3.2. Chloride ingress consider time-dependent of chloride diffusion coefficient

In this section, chloride ingress is modelled by equation (1.4) where chloride diffusion coefficient (D_0) is considered as time-variant by introducing an age factor (n_D). This factor takes into account the improvement of the resistance against chloride penetration and have a great influence on the estimated rate of chloride penetration (Gulikers 2003). It also accounts for changes in the properties of young concrete during its early age through the hydration degree increase.

The evolution with time of chloride diffusion coefficient ($D(t)$) can be illustrated from the following relationship:

$$D\left(t^{'}\right) = D_0\left(\frac{t^{'}}{t_0^{'}}\right)^{-n_D} \tag{3.2}$$

where D_0 is the chloride diffusion coefficient measured at time $t_0^{'}$. Figure 3.12 plots the evolution of D with time for age factors varying from 0.3 to 0.7, $t_0^{'}$ = 30 days and $D_0 = 1.33\times10^{-12}$ m^2/s. It is observed that for all values of n_D there is a significant decrease of chloride diffusivity at early ages and the values become almost constant at the mid- and long terms.

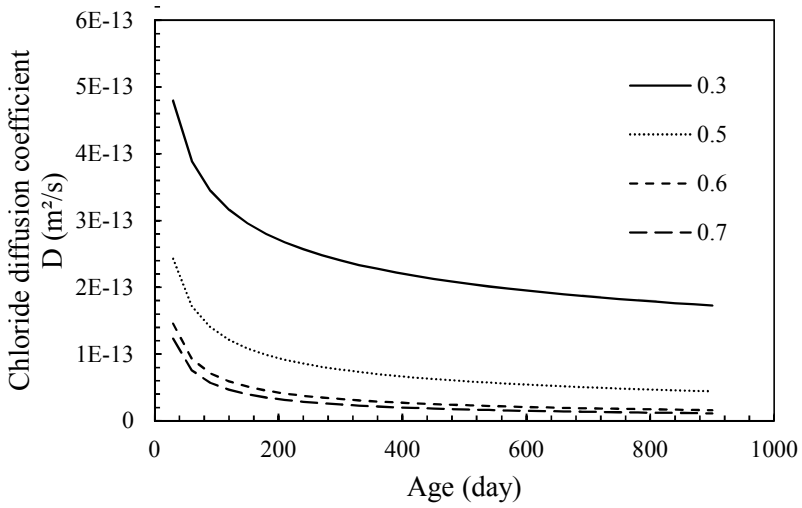

Figure 3.12 – Influence of age factor on time-variant of chloride diffusion coefficient

Data from section 3.2 is also used for a priori information, discretisation and theoretical values of parameters which are detailed previously in Table 3.1 and Table 3.2. We assume that $t_0^{'} = t_{ex}^{'} = 30$ days and the age factor $n_D = 0.5$. Different inspection schemes are considered with earlier inspection times as compared with Table 3.4. This is because as illustrated in Figure 3.12 information coming from lately times will provide less useful information to characterise the variation in time of D.

Table 3.5 –Inspection schemes and number of chloride profiles

Inspection scheme	Inspection time	Number of chloride profiles
1	300 days	9,000
2	600 days	9,000
3	900 days	9,000
4	300+600 days	4,500 + 4,500
5	300+600+900 days	3,000+3,000+3,000

BN configurations are built in a similar way as described in section 3.2.3 (Figure 3.4). With inspection times smaller than 900 days, chloride content at depth $x > 20\text{mm}$ is almost null. Consequently, the total inspection depth is 20mm. Various configurations of BN corresponding to several numbers of inspection points dividing the inspection length into equal interval lengths (Δx) are analysed to evaluate the identification errors.

Similar results are obtained for the estimation of C_s where the identification errors presented in Figure 3.13a and Figure 3.13b show that evidences obtained near the surface ($x \approx 0$) with early inspection time (t_{ins} = 300 days) could minimise the errors for the mean and standard deviation of C_s.

Using more inspection points in depth (smaller Δx) could not improve the identification for this parameter. These behaviours are previously analysed and explained in section 3.2.3. However, for D_0, combining evidences from different inspection times could improve the identification. This trend can be observed clearly in Figure 3.13d where the errors of standard deviation in cases combining data from inspection times (300+600) days or (300+600+900) days are reduced significantly. This is because the deterioration model herein takes into consideration the time-dependency of the chloride diffusion coefficient. This finding could be very useful when inspection data is limited because by combining these data, we can take advantage of the information after each inspection time. Figure 3.13c and Figure 3.13d also reveal that using more inspection points (smaller Δx) could reduce the gap between identified and theoretical values for D_0.

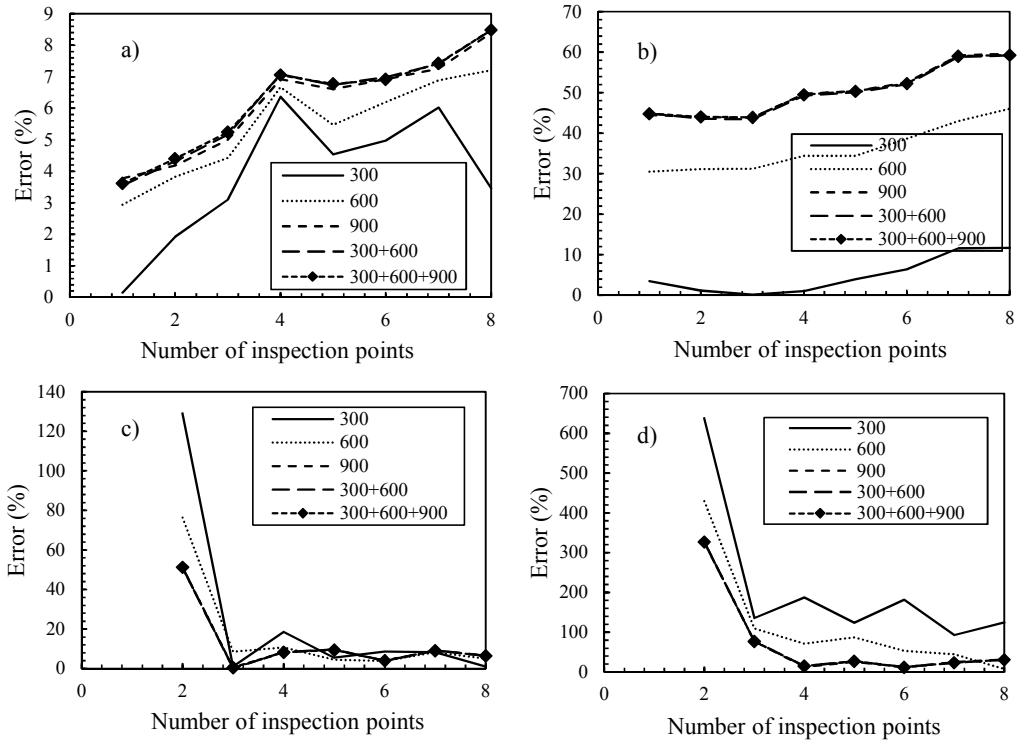

Figure 3.13: Identification errors: (a) Mean of C_s,(b) Standard deviation of C_s, (c) Mean of D_0, (d) Standard deviation of D_0.

3.4. Parameter identification using data from accelerated tests

3.4.1. Description of the experimental chloride ingress tests

The ageing tests on chloride-induced corrosion was carried out within the framework of the MAREO project (MAintenance and REpair of concrete coastal structure: risk based Optimisation-

2008-2012) (Bastidas-Arteaga and Schoefs 2015).It aimed at characterising the durability performance of new materials to repair RC components located in tidal zones by performing both normal and accelerated tests. For normal and accelerated tests, concrete slabs are placed in a tank with salted water. The exposure of the slabs ensures chloride ingress in one dimension. Tidal cycles (high and low) are simulated varying the level of water. For the accelerated tests, ventilators are used to dry the samples during the low tide cycle. The drying accelerates chloride ingress due to an increase of the capillarity sorption of concrete (Hong 1998). Normal tests are subjected to the same tidal cycles without drying by fans. The test is automatically controlled via a Labview® program. The tanks are placed inside a building and its environmental conditions (room temperature, water salinity and relative humidity) are recorded. Appendix A details the experimental set up for normal and accelerated tests. Additional tests for material characterisation were carried out within the framework of the study (Appendix B). This data was initially obtained for parameter identification of numerical chloride ingress models. However, the few obtained data cannot be used for identification purposes.

3.4.2. Identification procedure

For normal tests, the exposure time in laboratory (t_{exp}) could represent the exposure time in real conditions. However, in accelerated tests the chloride contents are larger than in natural conditions with the same time of exposure. Consequently, the exposure time in lab (t_{exp}) must correspond to an equivalent time (t_{eq}) under normal exposure conditions ($t_{exp} > t_{exp}$).

Chloride profiles obtained from normal tests could provide information about chloride content at depth x at real exposure time t_{exp}. However, those in accelerated tests just can provide information about chloride content at depth x. Section 2.2 presented approach for modelling chloride ingress into concrete in normal tests by the BN shown in Figure 2.2 where C_s and D_0 are two parent nodes and $C\left(x_i,t_j\right)$ are n child nodes, representing the discrete chloride concentration measurement in time and space i.e. at depth x_i and inspection time t_j. In accelerated tests, chloride ingress is modelled by the BN described in Figure 3.14 that has three parent nodes C_s, D_0 and t_{eq}. Child nodes in Figure 3.14 represent the chloride content at depth x_i

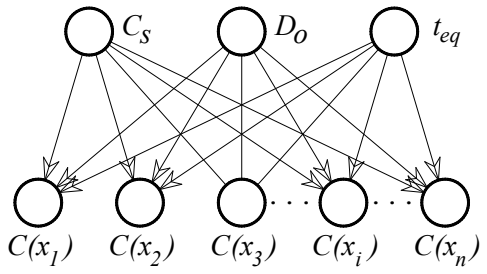

Figure 3.14: BN configuration for accelerated test.

The proposed approach for identifying t_{eq} is described in Figure 3.15. If a priori information about parameters C_s, D_0 and t_{eq} is not available, uniform distribution is often chosen (Bastidas-Arteaga et al. 2012; Hackl 2013; Robinson and Hartemink 2010). However, normal and accelerated tests are performed on the same material subjected to the same environmental chloride concentration. Therefore, data from normal tests could be used herein to provide some a priori information that reduces the level of uncertainty in the BN by improving the identification process.

The first step of the methodology consists of using the BN and data from normal tests to identify the two parameters C_s and D_0 respectively related to chloride exposure and concrete diffusivity. This step aims at characterising these two parameters under natural conditions by using optimised configuration for each parameter. Then, a posteriori histograms of the parameters C_s and D_0 are used in the second step as a priori information for the BN presented in Figure 3.14. The equivalent exposure time for accelerated test could be then identified by updating the BN with evidences obtained from accelerated test results. In fact, a fully BN consisting both normal test and accelerated test could be applied here for the identification. However, by applying a 2-steps procedure described in Figure 3.15, we can take advantage of optimised configurations for C_s which cannot be treated with a full BN that integrates all results coming from normal and accelerated tests. Indeed, Figure 3.16 compares the a posteriori histograms of C_s obtained from full and optimised BN after the identification process. It is clear that the optimised configuration could provide an estimation close to the theoretical histogram.

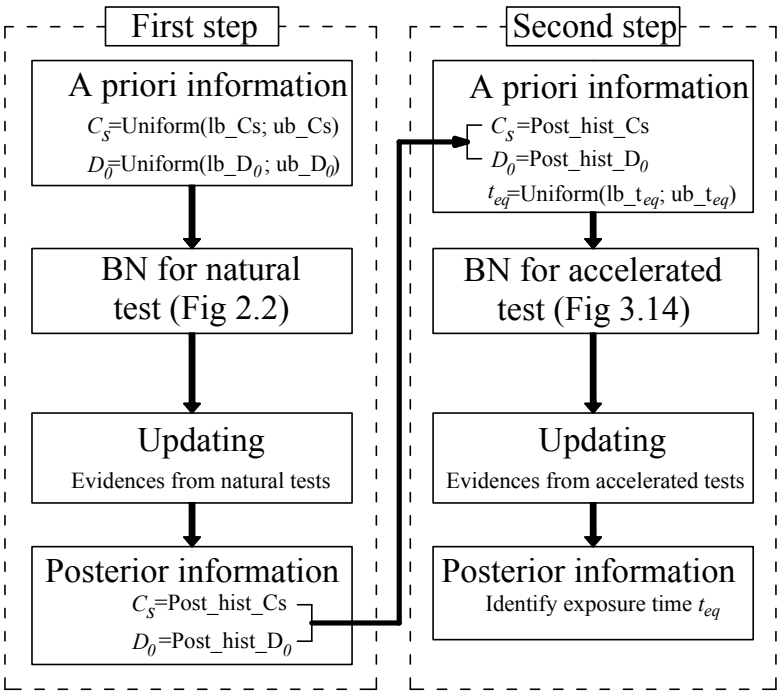

Figure 3.15: Flowchart of the proposed approach

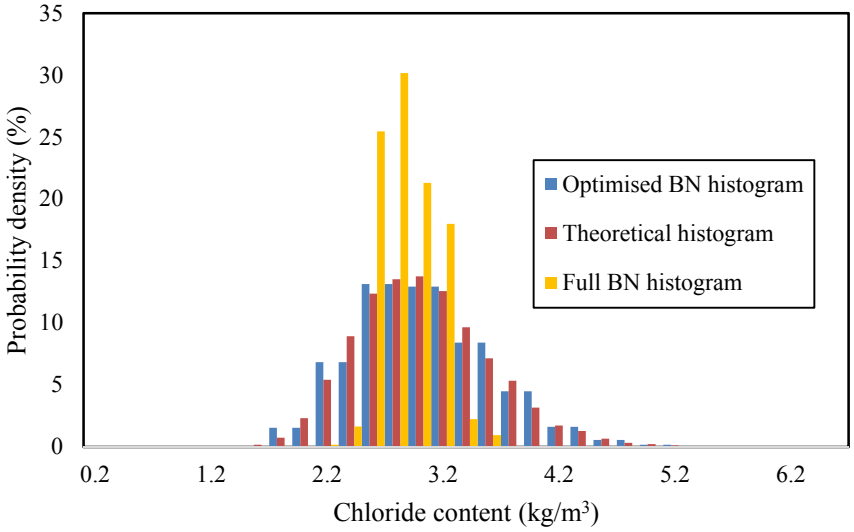

Figure 3.16: Comparison of a posteriori histograms of C_s from full BN, optimised BN and theoretical histogram.

3.4.3. Analysis of results from simulated data

In this section, data from simulations is used to evaluate the performance of the proposed approach to determine the equivalent time t_{eq} for accelerated tests. The model proposed by Nilsson and Carcasses (2004) (Eq. (1.4)) is embedded in BN for identification process.

The a priori information and the discretisation of the parameters are described in Table 3.6. We assume that $t_{ex}^{'} = t_0^{'} = 30$ days and $n_D = 0.5$.

Table 3.6: A priori information and discretisation of parameters in BN modelling for normal test

Parameter	A priori information	States per node
C_s [kg/m^3]	Uniform (10^{-3} – 12)	60
D_0 [10^{-12}m^2/s]	Uniform (0.6 – 20)	60
$C\left(x_i, t_j\right)$ [kg/m^3]	-	30

Numerical evidences are generated from equation (1.4) by using Monte Carlo simulations with the theoretical parameters given in Table 3.7. It is assumed that there are 3,000 chloride profiles for each inspection time: 300 days, 600 days and 900 days. Section 3.3.2 indicated that combining evidences from 3 inspection times provides a better estimation for parameter D_0 than spending the total number of profiles (9,000 profiles) in one inspection time. Therefore, inspection scheme (300 days + 600 days

+ 900 days) with a small interval length in depth Δx =3 mm is applied for the identification of D_0. With a total inspection depth of 20 mm, the BN configuration therefore has 8 child nodes. For C_s, the BN configuration with one child node representing for chloride content at surface ($x \approx 0$) and early inspection time t_{ins} = 300 days is used to reduce the identification errors. Figure 3.17 and Figure 3.18 indicates that a posteriori histograms obtained from optimised configurations for C_s and D_0 are close to those generated from theoretical values. By considering these histograms as a priori distribution instead of uniform distributions, the level of uncertainty in BN will be reduced in the identification of t_{eq}.

Table 3.7: Theoretical values of parameters to identify (Bastidas-Arteaga et al. 2009; Duprat 2007)

Parameters	Distribution	Mean	COV
C_s	Lognormal	2.95 kg/m^3	0.20
D_0	Lognormal	1×10^{-12} m^2/s	0.15

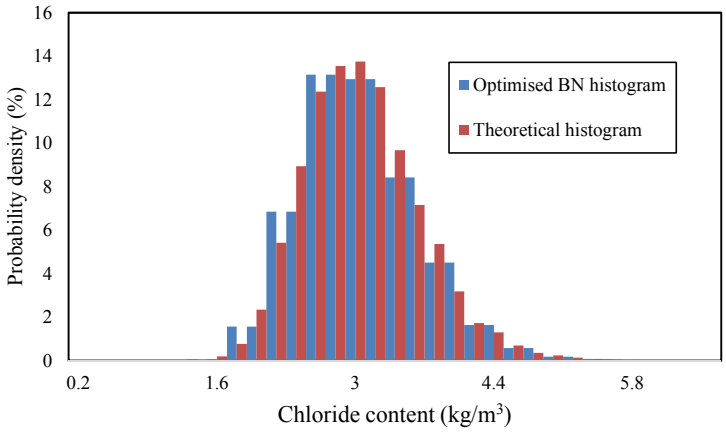

Figure 3.17: A posteriori histograms of C_s.

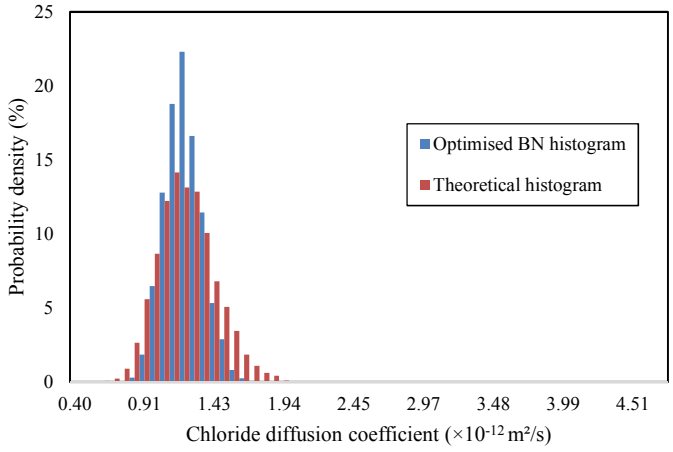

Figure 3.18: A posteriori histograms of D_0.

Both normal and accelerated tests are carried out for the same concrete subjected to the same in-lab environmental conditions. Consequently, chloride concentration at surface (C_s) and chloride diffusion coefficient (D_0) in normal and accelerated tests could be considered approximately to be the same. To avoid any assumption about distribution shapes, a posteriori histograms of C_s and D_0 obtained after updating the BN of normal tests are then used directly as a priori distribution in the BN modelling of accelerated tests (Figure 3.15). According to Figure 3.14, the equivalent exposure time t_{eq} is the variable to identify. It is then modelled as a parent node with the a priori distribution and discretisation shown in Table 3.8.

Table 3.8: A priori information and discretisation of parameter in BN modelling for accelerated test

Parameter	A priori information	States
$C_s\left[kg/m^3\right]$	Histogram from normal test (10^{-3} – 12)	60
$D_0 \times 10^{-12}\left[m^2/s\right]$	Histogram from normal test (0.4 – 20)	60
$t_{eq}\left[day\right]$	Uniform (0 – 3600)	100
$C(x)\left[kg/m^3\right]$	–	30

Numerical evidences in the BN for accelerated tests are generated from the theoretical values presented in Table 3.7 at different inspection times varying from 300 days to 3,000 days. 9,000 chloride profiles are generated for each inspection time. These inspection times reflect the equivalent times t_{eq} that are unknown in real practice and represent then the parameter to be identified. The total inspection depth is fixed at 30mm with Δx = 3mm, being sufficient to describe the penetration of chloride at 3,000 days of exposure.

The error on the identification of the equivalent exposure times (t_{eq}) from accelerated tests is shown in Figure 3.19. The errors for all cases are smaller than 20%. Especially, errors at 300 days, 600 days, and 900 days are smaller than other cases. This is because a priori information of C_s and D_0 was obtained from normal tests at these exposure times leading to a reduction of identification errors. When dealing with real data, the identified values of equivalent exposure times could be used to calculate a scale factor relating normal and accelerated exposure.

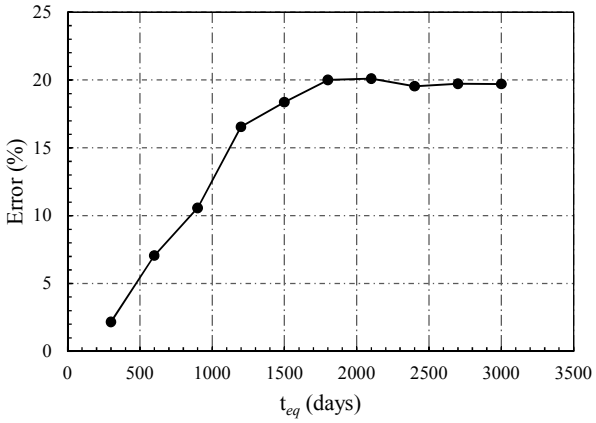

Figure 3.19: Identification error for the mean of t_{eq}.

3.4.4. Determination of scale factor from real data

Concrete cylinders (chloride profiles) from both normal tests and accelerated tests are used to determine chloride content at different exposure times (Table 3.9 and Table 3.10). Each chloride profile is discretised (grinded) into slices of Δx = 3mm. An approximated chloride profile (Figure 3.20) which is 42mm in length (14 points) could be derived from each measured profile by using curve fitting and Equation (1.2). The approximate chloride profiles are employed afterwards to build evidences for BN identification. In this study, the effects of convection zone are not considered.

Table 3.9 – Number of chloride profiles in normal tests

Normal test	T1	T2	T3
$t_{\exp}$ (days)	65	207	320
Number of profiles	3	3	3

Table 3.10 – Number of chloride profiles in accelerated tests

Accelerated test	T4	T5	T6
$t_{\exp}$ (days)	65	212	436
Number of profiles	6	6	6

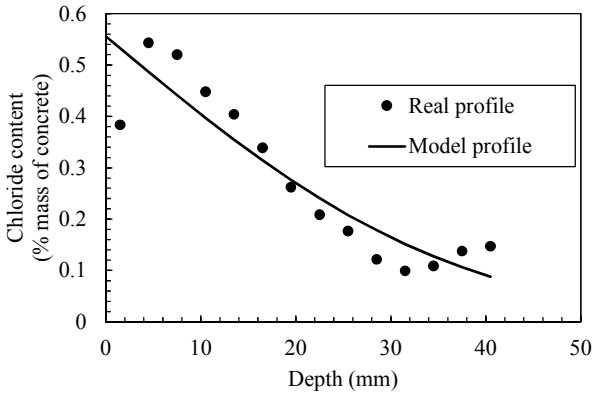

Figure 3.20: Approximated chloride profiles.

After identification, a scale factor for accelerated tests can be defined as a ratio between the exposure time in the experiment (t_{exp}) and the identified equivalent exposure time (t_{eq}):

$$k = \frac{t_{eq}}{t_{exp}} \tag{3.3}$$

The experimental exposure times in accelerated tests (t_{exp}) are given in Table 3.10. The equivalent exposure times (t_{eq}) are determined by the procedure given in Figure 3.15. Improved BN configurations defined according to the findings of section 3.3 are used to take advantage of limited data and minimise the identification errors in normal tests. Therefore, data at the surface $(x \approx 0)$ from chloride profiles obtained at inspection time T1 are introduced in BN updating to obtain the a posteriori histogram of C_s. Data combining three inspection times (T1 + T2 + T3) with 14 inspection points in depth are used to obtain a posteriori histogram of D_0 in the first step. These a posteriori histograms are then used as a priori information in BN modelling of accelerated tests. Equivalent exposure times are determined by updating the BN with evidences from accelerated tests and scale factors are then computed from Equation. (3.3).

The results for equivalent exposure times are given in Table 3.11. Identified values of t_{eq} show an expected trend where a longer exposure time (t_{exp}) in the laboratory will be equivalent to a larger value of t_{eq}. By approximating the scale factors evolution with the experimental times with a spline (Figure 3.21), it is noted that the scale factor is not constant. At early inspection times, this factor is high and then it decreases with time. This trend is expected due to the fact that the chloride diffusion coefficient is time-dependent and follow a similar trend (Tang and Nilsson 1996). The values of scale factors could be more accurate if more experimental data is available.

Table 3.11: Real exposure and equivalent times

Accelerated test	T1	T2	T3
$t_{\exp}\,[\text{day}]$	65	212	436
$t_{eq}\,[\text{day}]$	725.2	935.9	1050.3

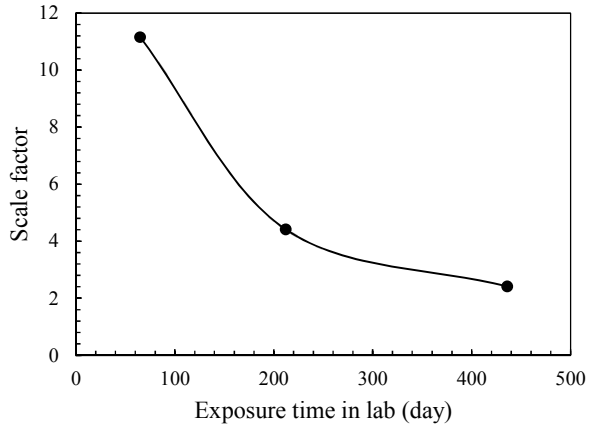

Figure 3.21: Scale factor for accelerated tests.

3.5. Approach for characterisation the age factor

As previously presented in section 3.3, when time-dependent effects of chloride diffusion coefficient are considered, the identification of parameters can be improved from the combination of data from different inspection times. Including these time-dependent effects has great impact on evaluating the structural condition from identified parameters. The time-dependency of chloride diffusion coefficient is considered by introducing a so-called age factor. This factor has larger influence on the prediction of chloride penetration. Its values can be determined from real chloride profiles at different exposure times. However, according to Gulikers (2003) there are three main difficulties concerning the assessment of the age factor: (1) the numerical approach to determine it is not clear, (2) the experimental data is limited, and (3) the exposure time considered is short.

Based on this context, this section aims at (1) performing sensitivity analysis to study the influence of the age factor on parameter identification and (2) proposing an approach to characterise the age factor from accelerated data.

3.5.1. Sensitivity analysis for age factor identification

To perform the sensitivity analysis, the model proposed by Nilsson and Carcasses (2004) (Eq. (1.4)) is embedded in the BN. However, in comparison with previous sections, the age factor is now considered as a random variable and modelled as a parent node in the BN configuration. Child nodes representing for chloride content at 3 inspection times (T1=300 days, T2=600 days and T3=900 days)

are introduced to combine evidences from different exposure times. Therefore, the BN configurations in this section have the general form as described in Figure 3.22.

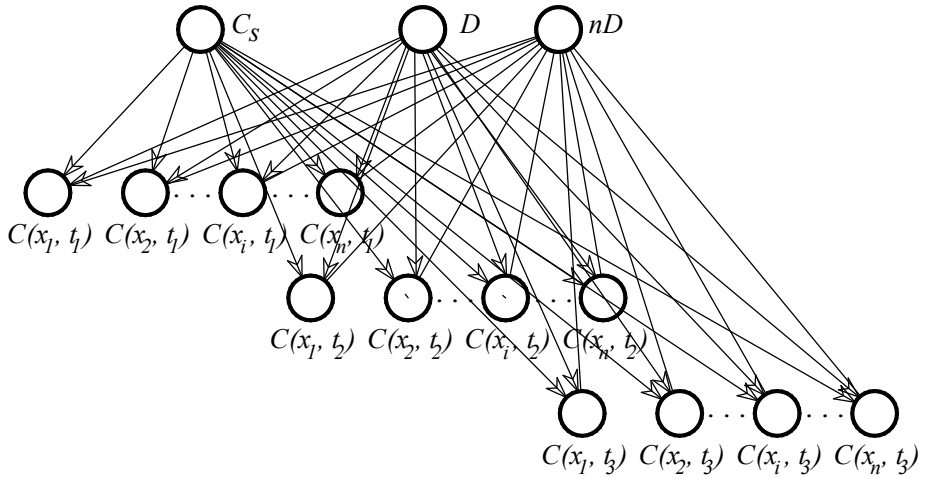

Figure 3.22: General BN configurations to perform sensitivity analysis

The sensitivity analysis is carried out by studying the identification errors of the chloride diffusion coefficient D_0 for 5 inspection schemes that combine evidences from one and/or several inspection times (Table 3.12). The discretisation and the a priori information for model parameters are defined in Table 3.13. The theoretical values to generate 3,000 simulated chloride profiles each exposure time are presented in Table 3.14. The theoretical values for the age factor correspond to an ordinary Portland cement (OPC) in a submerged environment. Note that, in sensitivity analysis, the inspection times (T1, T2 and T3), the theoretical values of n_D $\left(\mu_{n_D}, \sigma_{n_D}\right)$, and the a priori information of n_D can be varied to generate different studied cases. The total inspection length is 21mm and Δx = 3 mm.

Table 3.12: Description of the inspection schemes

Scheme 1	Scheme 2	Scheme 3	Scheme 4	Scheme 5
T1	T2	T3	T1+ T2	T1 + T2 + T3

Table 3.13: Discretisation and a priori information of model parameters

Parameter	A priori information	States per node
$C_s\left[\text{kg/m}^3\right]$	Uniform [10^{-3} – 12]	50
$D_0 \times 10^{-12}\left[\text{m}^2/\text{s}\right]$	Uniform [0.4 – 20]	50
n_D	Uniform [0 – 1]	30
$C(x,t)\left[\text{kg/m}^3\right]$	-	30

Table 3.14: Theoretical values for generating simulated chloride profiles

Parameter	Distribution	Mean	COV	Reference
$C_s\left[\mathrm{kg/m^3}\right]$	Lognormal	2.95	0.2	(Bastidas-Arteaga et al. 2009)
$D_0 \times 10^{-12}\left[\mathrm{m^2/s}\right]$	Lognormal	7	0.15	(Duprat 2007)
n_D	Beta [0 – 1]	0.3	0.167	(Duracrete 2000a)

3.5.1.1. Effect of different theoretical values of age factor on parameter identification

In this section, we study two analysis cases (Table 3.15) with two theoretical values of the age factor representing for OPC concretes in atmospheric and submerged environments, respectively (Duracrete 2000a).

Table 3.15: Considered theoretical values of n_D (Duracrete 2000a)

n_D	μ_{n_D}	σ_{n_D}
Case 1	0.65	0.07
Case 2	0.3	0.05

The identification errors of D_0 (Figure 3.23) shows significant differences when the age factor receive different values. Indeed, in case 2, the errors for all schemes are higher than 40% for the mean and higher than 250% for the standard deviation. In contrast, those for case 1 show lower values, under 10% and under 160% for the mean and standard deviation, respectively. These differences are due to the time-variant nature of the chloride diffusion coefficient illustrated in Figure 3.24. In case 1, evidences obtained at early times (T1 or T2) are sufficient to perform a good identification because after 300 days the evolution with time of $D(t)$ with $n_D = 0.65$ remains almost constant. However, it is noted that the combination of results adds error to the assessment of the mean of D. Larger errors observed for case 2 are related to the decreasing trend of $D(t)$. Contrarily to case 1, the combination of inspection data provides more information about this decreasing trend of $D(t)$ diminishing errors in case 2.

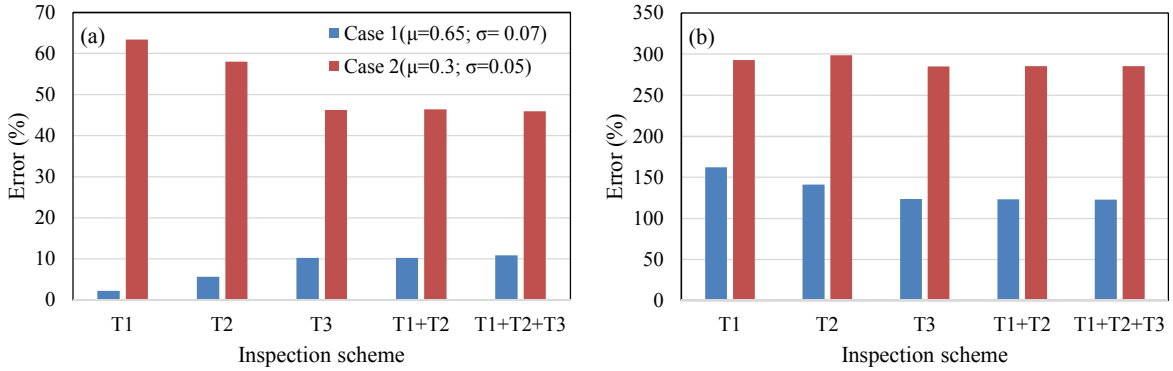

Figure 3.23: Identification errors of D_0 for: (a) mean - (b) standard deviation

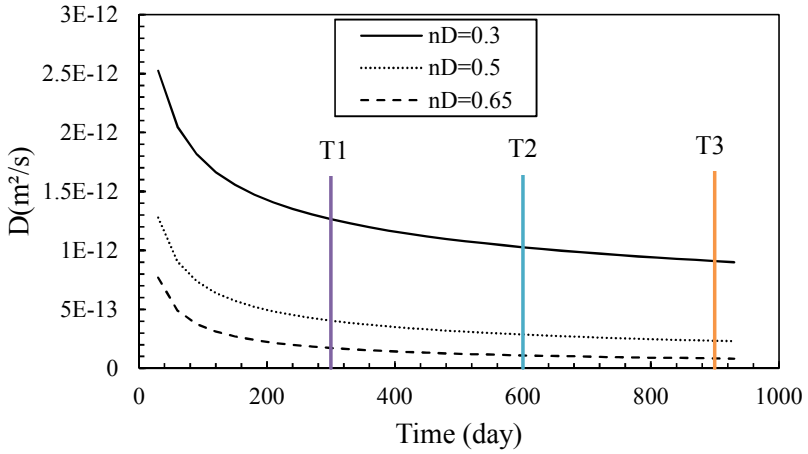

Figure 3.24: The time-variant of chloride diffusion coefficient with different values of age factor

The histograms plotted in Figure 3.25 reveal that the a posteriori distribution of D_0 obtained from case 1 is closer to the theoretical one in comparison with case 2. This means that the selected times are not capturing adequately the time-dependency of chloride diffusion coefficient in case 2 and introduce identification errors. In the next section, other values of inspection times (T1, T2 and T3) will be selected to illustrate this aspect for case 2.

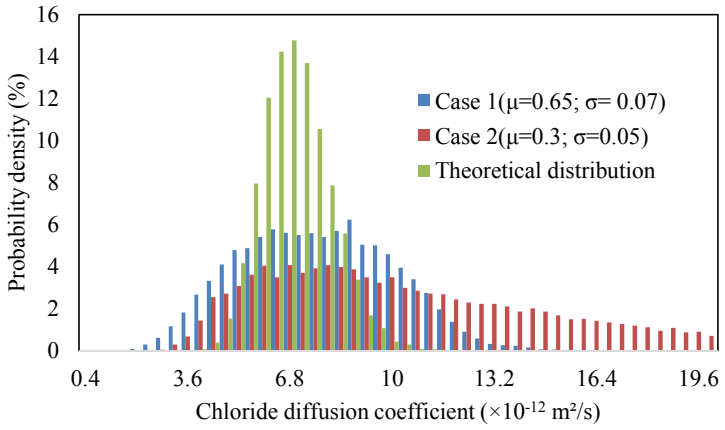

Figure 3.25: A posteriori distribution of D_0 in different cases

3.5.1.2. Effect of planning inspection schemes on parameter identification

As previously discussed in section 3.5.1.1, for a given material characterised by an age factor n_D the identification errors depend on the inspection times. When there is a decreasing trend of $D(t)$ (small values of n_D), identification could be more efficient if inspection times are selected to show as much differences as possible for the evolution with time of $D(t)$. This section compares two cases considering two different sets values of T1, T2 and T3 as presented in Table 3.16. According to Figure 3.24, the variation of chloride diffusion coefficient with inspection times in the case 2a (100, 300 and 600 days) is much higher than case 2b (300, 600 and 900 days). Especially, case 2a considered the first inspection at early exposure time (T1=100 days) in which the chloride diffusion coefficient is very high. By introducing this early time, the time-dependency of chloride diffusion coefficient can be described adequately. Consequently, the identification of D_0 in case 2a reveals smaller errors as compared with case 2b (Figure 3.26).

Table 3.16: Studied cases with different inspection times

Inspection times	T1 (day)	T2 (day)	T3 (day)
Case 2a	100	300	600
Case 2b	300	600	900

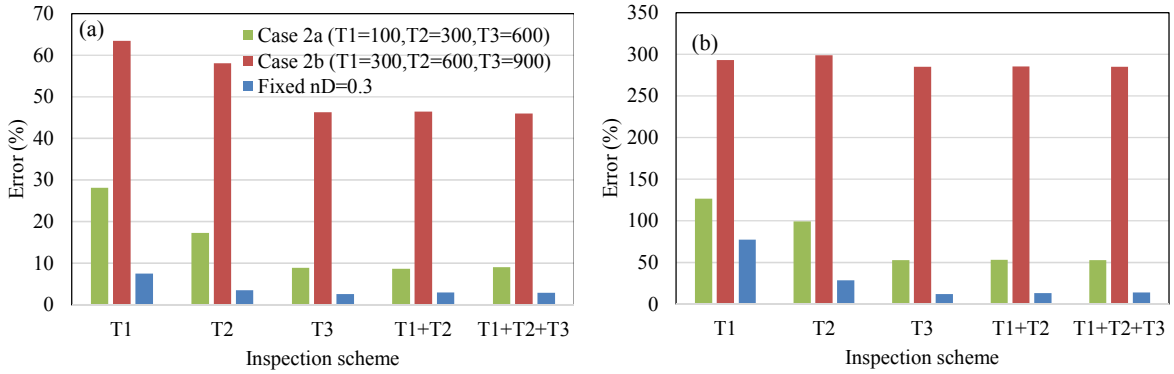

Figure 3.26: Identification errors of D_0 for: (a) the mean - (b) the standard deviation

The a posteriori histogram of case 2a also depicts a better shape closer to the theoretical ones; whereas that of case 2b shows a large variation (Figure 3.27). The combination of evidences in case 2a also diminishes significantly the identification errors. For example, the identification error for the mean of D_0 is reduced from 30% (T1) to under 10% (T1+T2+T3) (Figure 3.26a). Similar trends are also observed for case 2b, but at a lower reduction rate. These findings highlight the importance of early inspection on describing the time-dependency of chloride diffusion coefficient and on planning an efficient inspection campaign as well. Figure 3.26 also includes a case when the age factor is considered as a deterministic value (n_D=0.3). In such a case, there are observed smaller errors for the mean and standard deviation of D_0. This indicates that the identification errors increase significantly when the age factor is introduced as a random variable in the BN. To take advantage of this finding, section 3.5.2 proposes an approach to estimate a constant age factor in the BN configurations.

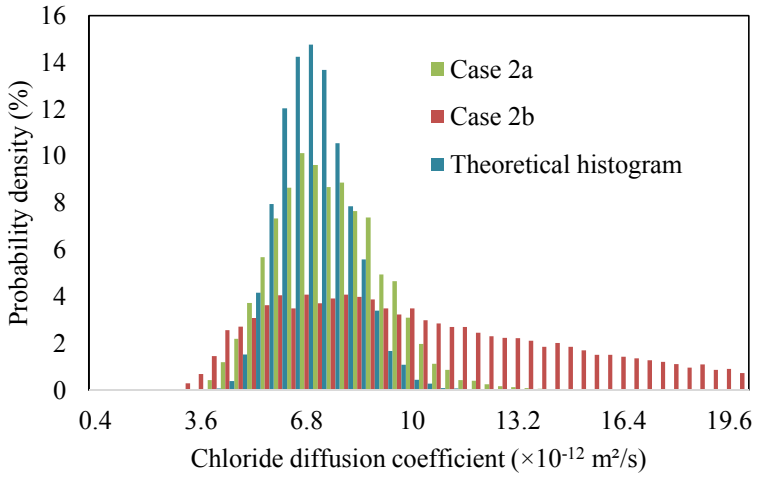

Figure 3.27: A posteriori distributions of D_0 for different inspection times.

3.5.1.3. Effect of different a priori information of n_D on parameter identification

On the BN framework for parameter identification, the accuracy of results depend significantly on the level of uncertainty. A priori information in the BN is often assumed from expert knowledge, existing database or similar study cases. Different assumptions about a priori information in BN therefore, may lead to results with different accuracy levels. Hence, it is important to select a priori information as close to the real information as possible to reduce the uncertainty level. This section considers different assumptions about a priori distribution of the age factor and studies their influences on parameter identification. Four cases are proposed in Table 3.17 in which case D is considered as a reference case where a priori information of n_D is identical to its theoretical values. Therefore, this case results in smallest identification errors of D_0 (Figure 3.28) and its a priori information can be considered as the 'ideal' assumption. For other cases, a priori information of n_D can be assumed following uniform (case A), triangular (case B) or beta (case C) distributions.

Table 3.17: Cases for studying the influence of a priori information of n_D.

Analysis case	Type of distribution	Parameters	Range
Case A	Uniform	-	[0, 1]
Case B	Triangular	(a=0;c=0.5;b=1)	[0, 1]
Case C	Beta	$\mu_{n_D} = 0.5; \sigma_{n_D} = 0.1$	[0, 1]
Case D (Reference)	Beta	$\mu_{n_D} = 0.3; \sigma_{n_D} = 0.05$	[0, 1]

Figure 3.28 shows that the error decreases if a priori triangular or beta distributions are considered. Despite there are no significant differences on the identification errors for the mean of D_0 among the 3 first cases, the error in case C is smaller than the two others (Figure 3.28a). For the standard deviation, the differences are much higher among cases A, B and C. They follow a similar trend for all inspection schemes where they are highest in case A following by case B and case C. Figure 3.29 compares a posteriori histograms of D_0 among the four cases. It is observed that the distribution shapes in cases C and D are closer to the theoretical values than case A or B. This behaviour is expected because with respect to the expected assumption, the level of uncertainty of a priori information in cases C and D (beta distribution) is lowest leading to more accurate results.

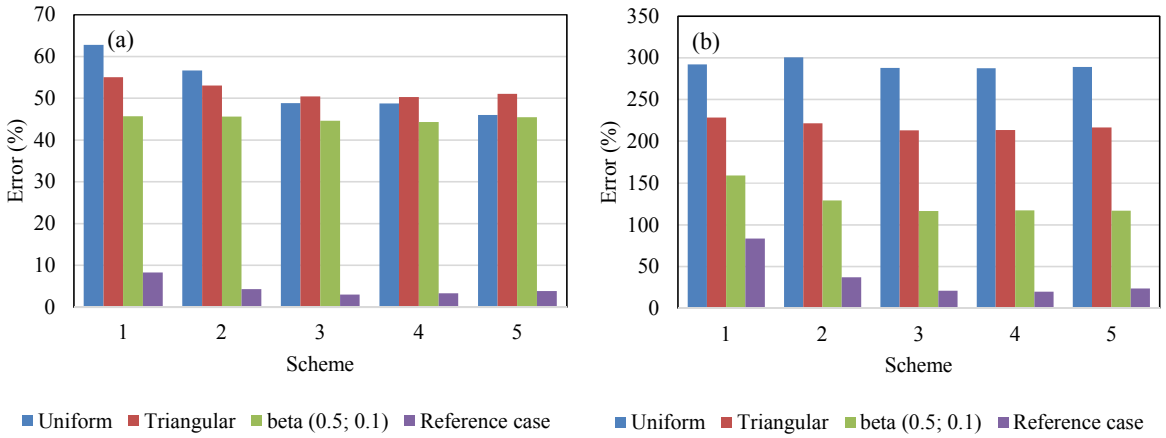

Figure 3.28: Identification errors of D_0 for: (a) the mean - (b) the standard deviation.

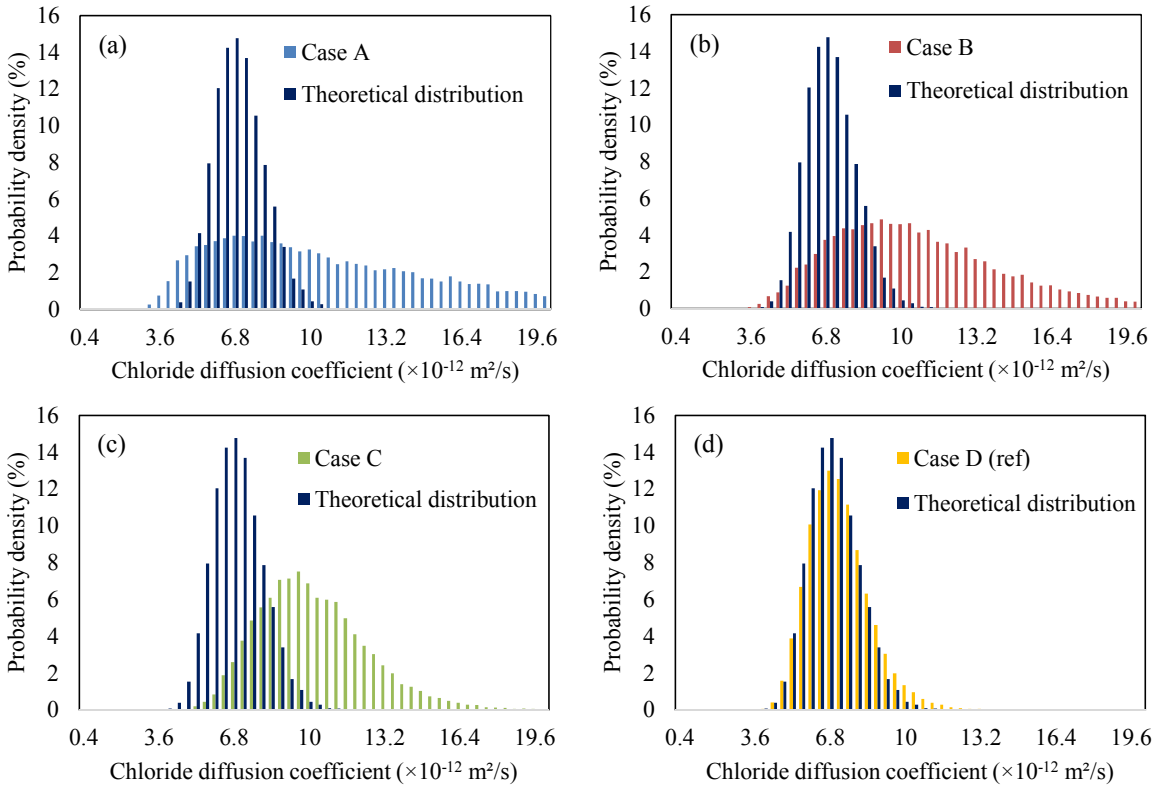

Figure 3.29: A posteriori distributions of D_0 for: (a) case A – (b) case B – (c) case C – (d) Reference case (case D).

3.5.2. Approach to characterise the age factor from accelerated data

3.5.2.1. Problem statement

Section 3.5.1.2 indicated that the identification error increases significantly when the age factor is considered as a random variable and introduced in the BN as a parent node. The level of uncertainty

and identification error can be reduced if the age factor can be determined and introduced as deterministic value in the BN. Data from inspection could be used for such a purpose. However the exposure time in normal ageing test is often short and it cannot provide information about mid- and long-term performance of concrete. Therefore, a combination of data from both normal and accelerated tests can lead to a better assessment of the ageing chloride process. In spite of that, this data is always limited and may lead to bad estimation of the age factor. As a consequence, the identification error in BN will increase. To illustrate this point, we consider a numerical example in which the BN configuration is used for modelling the combination of normal and accelerated data (Figure 3.30). It consists of 3 parent nodes representing for model parameters C_s, D_0 and the equivalent time (t_{eq}) for the accelerated test. The child nodes represent inspection points in chloride profiles obtained from normal and accelerated tests. In this section, we assume that normal data comes from 3 exposure times in the laboratory conditions (T1, T2 and T3). The chloride ingress model proposed by Nilsson and Carcasses (2004) (Eq. (1.4)) is employed herein to take into consideration time-dependent effects. By introducing the evidences from normal and accelerated data, this BN configuration allows to determine the equivalent time (t_{eq}) for accelerated tests.

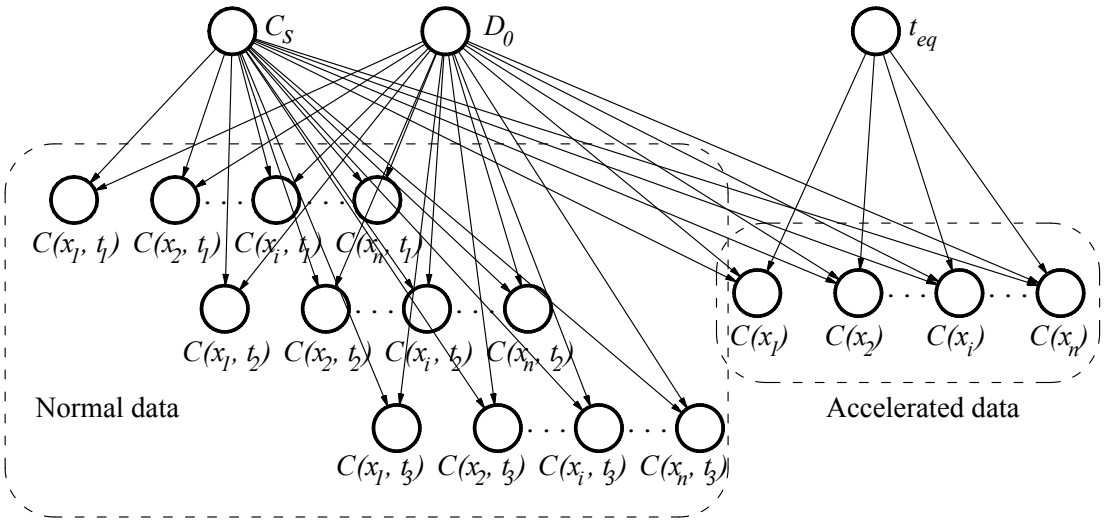

Figure 3.30: A fully BN configuration combining both normal and accelerated data.

A priori information and the discretisation of model parameters are described in Table 3.18 in which the three parent nodes are assumed to follow uniform distributions. We use the theoretical values given in Table 3.19 to generate simulated evidences for both normal and accelerated data with 9,000 simulations for each inspection time. Evidences from normal data are combined from 3 inspection times: T1=100 days, T2=300 days, and T3=600 days. Evidences from accelerated data are created from different equivalent times varying from 300 days to 3,000 days. The total inspection length is assumed at 30mm with a discretisation by $\Delta x = 3mm$. We also assume $t_{ex}^{'} = t_0^{'} = 30$ days.

In real practice, the 'theoretical' age factor for creating the evidences ($n_{D,theory}$) is unknown and it is an additional model parameter to identify. The BN configuration (Figure 3.30) considers that the age factor is deterministic with an assumed value $n_{D,assum}$. We study then different cases corresponding to various assumptions about the age factor (Table 3.20). Noted that in case I, the age factor is assumed as the same value as the theoretical one (reference case).

Table 3.18: A priori information and discretisation of model parameters.

Parameter	A priori information	States per node
$C_s\left[\mathrm{kg/m^3}\right]$	Uniform [10^{-3} – 12]	50
$D_0 \times 10^{-12}\left[\mathrm{m^2}/s\right]$	Uniform [0.4 – 35]	50
$t_{eq}\left[\mathrm{day}\right]$	Uniform [0 – 18000]	30
$C(x)\left[\mathrm{kg/m^3}\right]$	–	30
$C(x,t)\left[\mathrm{kg/m^3}\right]$	–	30

Table 3.19: Theoretical values for generating simulated evidences (Bastidas-Arteaga et al. 2009; Duprat 2007).

Parameter	Distribution	Mean	COV
$C_s\left[\mathrm{kg/m^3}\right]$	Lognormal	2.95	0.2
$D_0 \times 10^{-12}\left[\mathrm{m^2}/s\right]$	Lognormal	7	0.15
$n_{D,theory}$		0.5	

Figure 3.31 presents the identification errors for the mean of the equivalent time (t_{eq}) in accelerated tests. It is obvious that the errors are smaller when $n_{D,assum}$ is equal to the theoretical value. In both cases when this factor is under- ($n_{D,assum}$=0.3) or overestimated ($n_{D,assum}$=0.65;0.7) respect to $n_{D,theory}$, the identification errors are larger. Therefore, it is important to propose an approach for improving the characterisation of the age factor from experimental data.

Table 3.20: Considered values of $n_{D,assum}$.

Analysis case	$n_{D,assum}$
Case I	0.5
Case II	0.3
Case III	0.65
Case IV	0.7

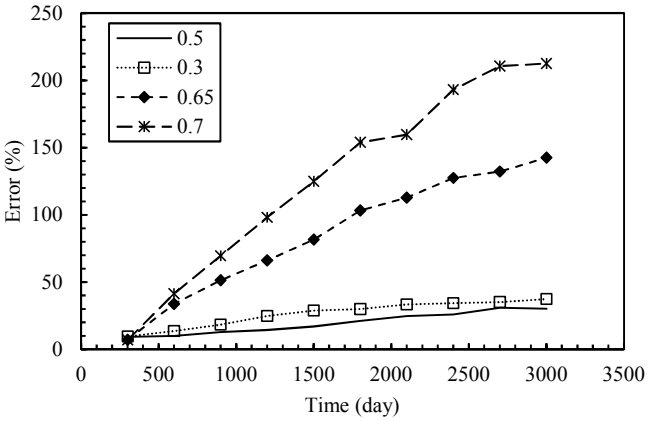

Figure 3.31: Identification errors for the mean of equivalent time (t_{eq}) with different $n_{D,assum}$.

3.5.2.2. Proposed approach.

This section proposes an approach to determine the age factor when the experimental data is limited. As previously mentioned, the combination of data from both normal and accelerated tests can lead to a more accurate assessment of the age factor; thus a full BN configuration is used to perform this combination (Figure 3.30). In this section, the real normal data comes from 3 exposure times in the laboratory conditions: 65 days (T1), 207 days (T2), and 320 days (T3). The accelerated data introduced in BN represents chloride content at a certain depth with unknown equivalent time of exposure. A priori information and the discretisation of model parameters are presented in Table 3.21. The age factor is considered as a deterministic value which is estimated from the experimental data. The total inspection length of chloride profiles is 42mm with a discretisation by $\Delta x = 3\text{mm}$. We also assume that $t_{ex}^{'} = t_0^{'} = 30$ days.

Table 3.21: A priori information and discretisation of model parameters.

Parameter	A priori information	States per node
$C_s\left[\text{kg/m}^3\right]$	Uniform [10^{-3} – 12]	50
$D_0 \times 10^{-12}\left[\text{m}^2/\text{s}\right]$	Uniform [0.4 – 35]	50
$t_{eq}\left[\text{day}\right]$	Uniform [0 – 3600]	100
$C(x)\left[\text{kg/m}^3\right]$	-	30
$C(x,t)\left[\text{kg/m}^3\right]$	-	30

The methodology to characterise the age factor can be described by the flowchart presented in Figure 3.32. Stage I of this procedure implements curve fitting to determine a set of values of C_s and D for each chloride profile from normal tests and its approximated chloride profiles. These approximated chloride profiles are used to calculate evidences that are afterwards used for updating the BN. The mean values of D at different times (Table 3.22) are used to estimate a preliminary age factor value by curve fitting from the equation (3.2). The results of curve fitting are presented in Figure 3.33 with the following results: $D_0 = 28.98 \times 10^{-12} \left(\mathrm{m}^2/\mathrm{s}\right)$ and $n_D = 0.5705$. This age factor is introduced in the BN to determine the equivalent times for accelerated test in the next stage.

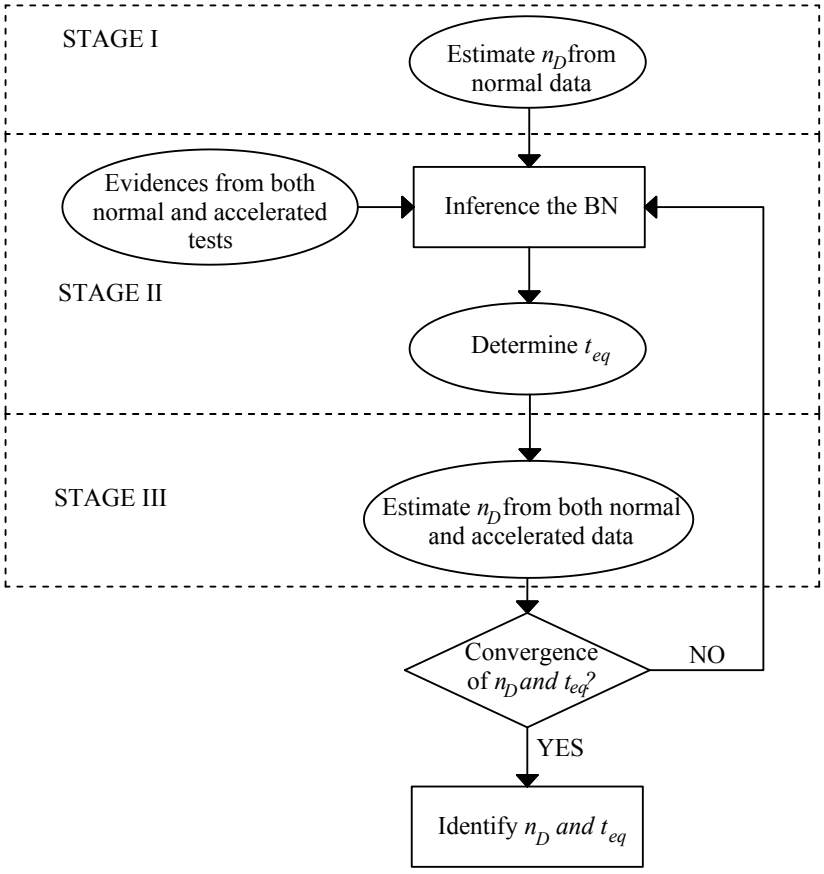

Figure 3.32: Flowchart to identify the age factor.

Table 3.22: Mean values of C_s and D at each exposure time in normal test.

Parameters	T1=65 days	T2=207 days	T3=320 days
$C_s \left[\mathrm{kg/m^3}\right]$	0.38	0.64	0.53
$D \times 10^{-12} \left[\mathrm{m^2/s}\right]$	18.82	8.34	8.70

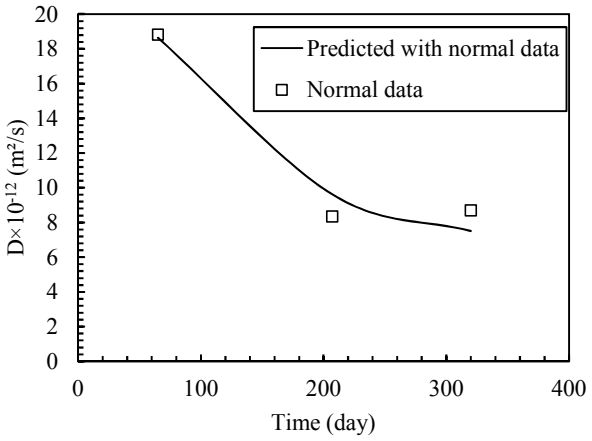

Figure 3.33: Estimation of age factor using curve fitting with normal data

Stage II of this procedure aims at determining the equivalent times from the BN with evidences from both normal and accelerated data. The accelerated data came from 3 different exposure times in the laboratory conditions. Let denote T4, T5 and T6 as the 3 equivalent times to identify. This stage ends when all equivalents times T4, T5 and T6 are determined.

The equivalent times identified in Stage II allow predicting chloride diffusion coefficients for accelerated data at these times by curve fitting in Stage III. For example, Table 3.23 presents the equivalent times determined from the BN and the mean values of D estimated by curve fitting at each time for the first iteration. This new information allows re-estimating the age factor by combining new values of D at times T4, T5 and T6 with those obtained from normal data at T1, T2 and T3. Results from applying the curve fitting method in equation (3.2) are shown in Figure 3.34. It can be seen that introducing data from accelerated tests gives a better assessment about long-term evolution with time of chloride diffusion coefficient that may be overestimated if using only data from normal test. A new value of the age factor is also obtained after fitting and it will be introduced to the BN for a new iteration until convergence by repeating Stages I and II.

Table 3.23: Mean values of D at the equivalent times in the first iteration.

Time (day)	T4=815	T5=939	T6=1069
$D \times 10^{-12}\left[\mathrm{m}^2/\mathrm{s}\right]$	1.0195	1.2881	1.4590

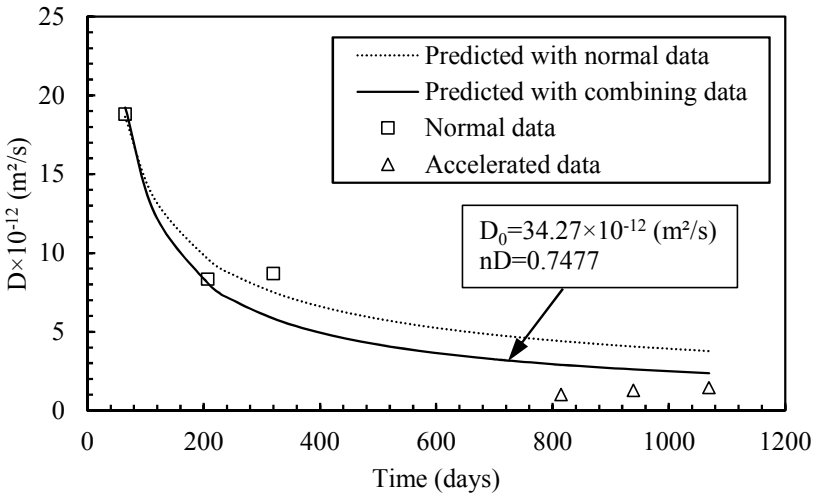

Figure 3.34: Re-estimation of age factor using curve fitting with normal and accelerated data at iteration 1.

With real data obtained from experimental tests, the procedure to identify the age factor in this study is stopped after 4 iterations when the value of n_D almost reaches a constant value – i.e. n_D = 0.7401 (Table 3.24). The equivalent times T4, T5 and T6 also follow a converging trend after 4 iterations (Table 3.24). After each iteration, information of parameters C_s and D_0 are updated and also converge (Table 3.24).

Table 3.24: Evolution of model parameters after the iterative procedure.

Parameter	Update with normal data	Iteration 1	Iteration 2	Iteration 3	Iteration 4
Mean C_s [kg/m^3]	0.6048	0.5912	0.5712	0.5719	0.5719
Std C_s [kg/m^3]	0.0999	0.0975	0.0920	0.0923	0.0923
Mean D [m²/s]	1.24E-11	1.21E-11	1.63E-11	1.62E-11	1.62E-11
Std D [m²/s]	4.91E-12	4.80E-12	5.09E-12	5.09E-12	5.10E-12
n_D	0.5700	0.5700	0.7477	0.7398	0.7401
T4 [days]	–	815	899	893	893
T5 [days]	–	939	1036	1035	1035
T6 [days]	–	1069	1253	1245	1245

Model parameters identified after each iterations (Table 3.24) are used in Monte Carlo simulation to compute 5% and 95% percentiles of chloride content at depth $x = 10.5$ mm at different times. By plotting these percentiles with real data from normal and accelerated tests, it can be seen in Figure 3.35 that the predicted 95% percentile at iterations 2 and 3 are closer to the accelerated data than those from BN updating with only normal data or iteration 1. There is no significant difference in the prediction of 5% percentiles among all cases. There are several data points that do not fall in the range 5% and 95% percentiles. This is, on the one hand, because the limitation of experimental data that leads to the poor quality of information used for BN identification. On the other hand, the inspection points at depth x=10.5 mm are quite close to the surface of structures (convection zone) where the selected model is in not able to account for convection effects (section 1.3.1). However, in practice, it is of interest to evaluate chloride content at deeper points near the rebar.

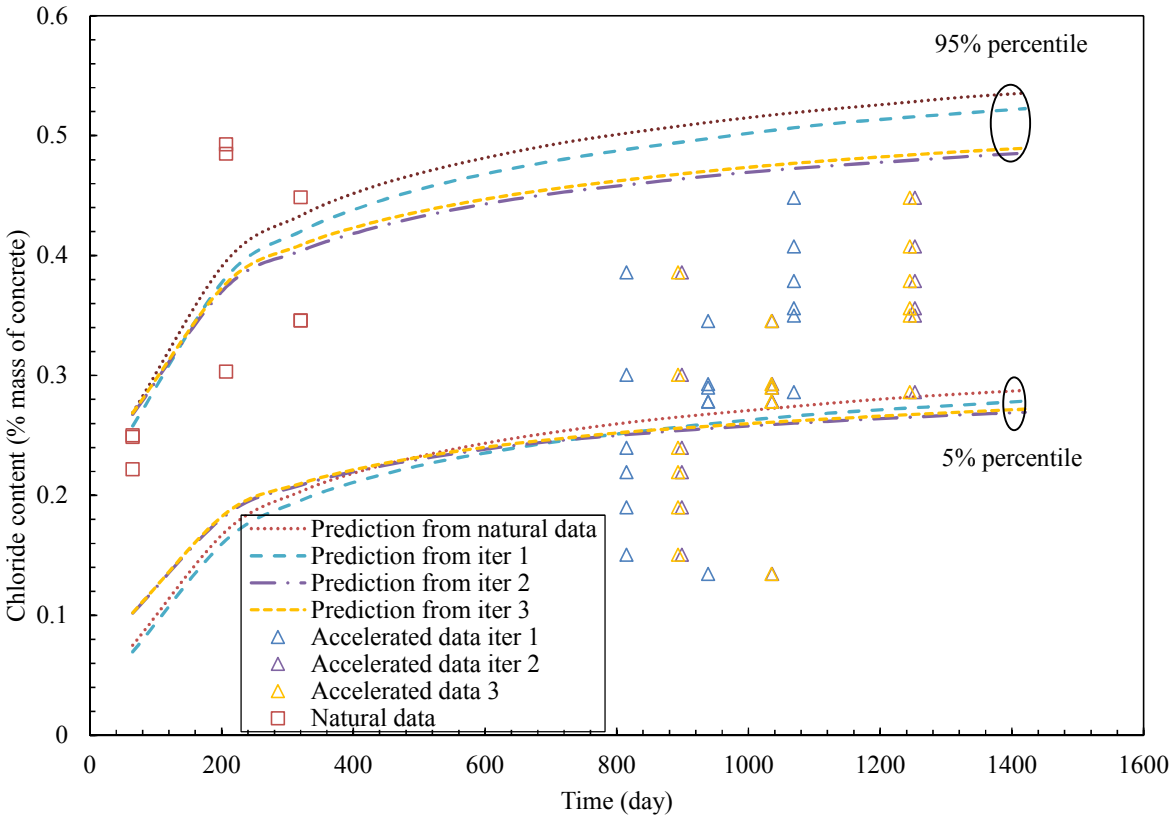

Figure 3.35: 5% and 95 percentiles of chloride content at depth x=10.5mm.

The exposure times considered in this study were not sufficient to allow significant chloride content to reach the cover depth. Therefore, we select a second depth (x=31.5 mm) to compare the 5% and 95% percentiles of chloride content and real data (Figure 3.36). Similar trend as x=10.5 mm is observed for x=31.5 mm when after iterations, predictions of 95% percentiles are closer to real data. It is also worth noticing that all of accelerated data is fall in the range of 5% and 95% percentage. This

behaviour can be explained by the fact that at depth x=31.5 mm, there is no more effect of convection zone due and the chloride ingress model is more appropriate to estimate chloride concentrations. Note that in both cases (x=10.5 mm and x=31.5 mm), the predicted 5% percentile remains almost the same after update. This is due to the effect of short distribution tails at 5% percentile where the updating process has no significant change (Figure 3.37). Therefore, it can be concluded that this approach is useful for identifying the age factor from real data. The identification will be improved if more experimental data is provided.

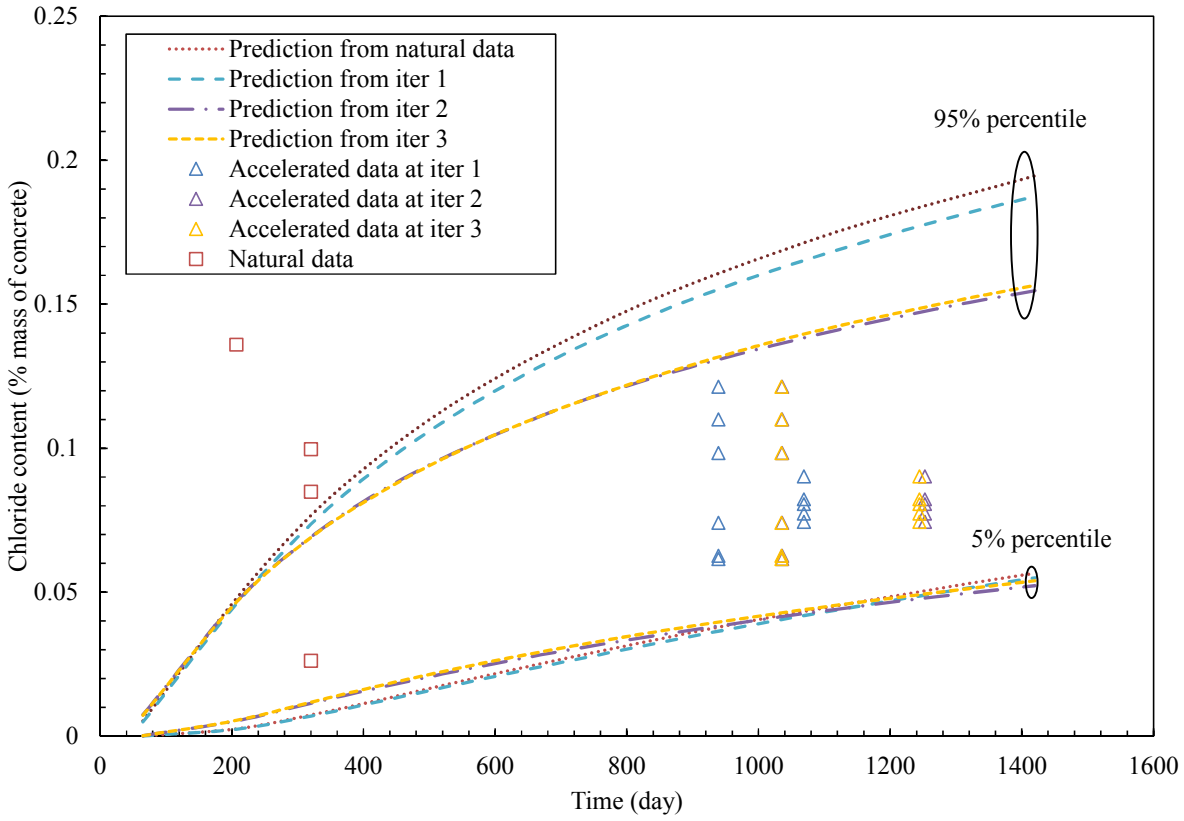

Figure 3.36: 5% and 95 percentiles of chloride content at depth x=31.5mm.

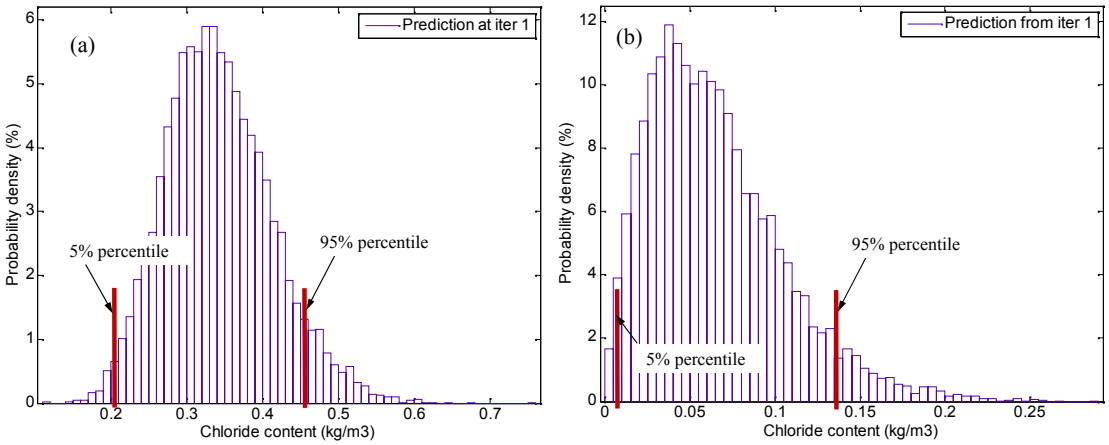

Figure 3.37: Distribution tails with 5% and 95% percentiles at: (a) x=10.5mm and (b) x=31.5mm.

3.6. Conclusions

Chloride ingress is one of the main causes inducing corrosion of RC structures. The identification of parameters in chloride ingress modelling is crucial for reliability and/or planning maintenance schedules. Inspection data used for the identification contains a high level of uncertainty related to material properties, environmental actions, measurements, and deterioration models. Therefore, it is necessary to use these data in comprehensive way to characterise these uncertainties. This chapter pointed out that BN could provide a possibility to identify random parameters from inspection data in an optimal manner. The main results from this chapter can be summarised as follows:

1. Parameter identification is a complex problem that requires improved BN configurations to reduce identification errors. Due to physical and model characteristics, it was found that there is an optimal configuration for the identification of each parameter. For C_s, it is the BN configuration with one child node close to the concrete surface. For D, it is necessary to use the information from total inspection length to provide a better characterisation of the kinetics of the chloride ingress process. For a certain total inspection depth, there exists an optimal inspection time in which chloride ingress could be described adequately and the identification errors of D is minimised. Especially, there is an optimal discretisation length Δx for each inspection time, which can be considered as a recommendation for planning inspection campaigns. The results also revealed that it is better to use the information at early inspection times for estimating parameter C_s; for D, the data at later inspection times is more useful.
2. BN reflects properties of the embedded models in their performances. In BN updating with model from Tuutti (1982), the estimation of D could not lead to a better result when combining evidences from several inspection times due to the time-independence of the

chloride diffusion coefficient considered by this model. For comprehensive modelling, the parameter D should be treated as time-dependent variable due to its natural characteristics. The BN configuration that considers the model proposed by Nilsson and Carcasses (2004) proved that the dependency of the chloride diffusion coefficient on exposure time is improved significantly by combining evidences from different inspection times. In both models, the parameter C_s is considered as time-independent. Therefore, combining data from inspection times could not reduce the estimation errors for C_s. Since the identification of these two parameters plays important roles in lifetime assessment and maintenance planning, appropriate deterioration models and combinations of inspection data should be considered to obtain a better assessment of model parameters.

3. The process of chloride ingress from external environment in RC structures until reaching a significant content requires decades. Inspection campaign therefore, also requires significant time to obtain a sufficient amount of data for condition assessment and reliability analysis. The accelerated ageing test described in this chapter is aimed at speeding up the penetration process of chloride ions into concrete. By performing BN updating from both simulated data and real data, the proposed framework gives a possibility to determine (1) an equivalent exposure time for accelerated tests, and (2) a scale factor reflecting the ratio between accelerated and normal test. Therefore, it brings a perspective for mid- and long-term chloride ingress characterisation from accelerated data, which is obtained faster than those in natural conditions.
4. More realistic chloride ingress models consider the time-dependency of the chloride diffusion coefficient by introducing an age factor. Results from a sensitivity analysis indicated that this factor has significant influence on parameter identification. Based on the BN identification framework, curve fitting, and an iterative process, this chapter used data from normal and accelerated tests to determine the age factor. Data from accelerated improves the characterisation of the mid- and long-term behaviour of concrete and leads to a better assessment of the age factor. After each iteration, the equivalent times in accelerated test and the age factor are re-estimated and this information will be introduced in the next iteration until reaching a converging trend. The predicted 5% and 95% percentiles of chloride content at larger depth are closer to real data after iterations. Consequently, it can be concluded that this approach is useful for characterising the age factor, despite experimental data is limited.

Chapter 4
Application of Bayesian identification in chloride ingress

4.1. Introduction

Under chloride-contaminated environments, the estimation of probability of corrosion initiation for RC structures is one of the outputs of probabilistic chloride ingress models. Its results are after used as crucial criteria to evaluate current reliability states of structures, to predict future extent of damage and to decide if the structure/component should be repaired. The owners of structures request for maintenance strategies that reduce the cost of possible repairs or replacement of existing components. Such strategies could be planed from deterioration models combined to relevant model parameters that are estimated from in-site measurements. However, chloride-induced deterioration damage is a very slow process and despite of many technological advances in chloride content measurements, inspection techniques are still difficult to implement. Consequently the inspection data become costly and limited. This creates an important challenge for owners when they plan optimal maintenance strategies from these limited data. Therefore, the main objective of this chapter is to propose strategies to improve the use of limited inspection data for the assessment of the probability of corrosion initiation.

The specific objectives of this chapter are:

1. To analyse different BN configurations corresponding to different levels of environmental aggressiveness and various material properties. For each case considered, an improved configuration is obtained representing for a discretisation that could minimise the identification errors.
2. To assess the probability of corrosion initiation when inspection data is limited and suggest a strategy to improve these estimations by proposing a two-step procedure. This strategy is also applied to various materials and exposure conditions.

Section 4.2 presents principles for assessment the probability of corrosion initiation with a numerical example. A procedure is proposed to improve the assessment of probability of corrosion initiation when inspection data is limited. Section 4.3 aims at determine an optimal BN configuration for parameter identification in chloride ingress models with different types of material and exposure environment. Based on these BN configurations, this section compares the prediction of probability of corrosion initiation in 2 cases: inspection data is (1) larger and (2) limited.

4.2. Strategies for assessment of probability of corrosion initiation when inspection data is limited

4.2.1. Probability of corrosion initiation

This section examines the influence of the probabilistic parameters identified from BN on the evaluation of the probability of corrosion initiation. Previous chapters have shown that there are different improved configurations for the identification of C_s and D . A multi-criteria analysis will not be efficient because the sensitivity of the response to these variables varies with time (Bastidas-Arteaga et al. 2011). Thus, this study is based on the effects of the quality of BN identification results on the probability of corrosion initiation. The time to corrosion initiation, t_{ini} , is defined as the time at which the chloride concentration at the steel reinforcement surface reaches a threshold value, C_{th} . This threshold concentration represents the chloride concentration for which the rust passive layer of steel is destroyed and the corrosion reaction begins. C_{th} depends on many parameters (Bastidas-Arteaga and Schoefs 2012): type and content of cement, exposure conditions, time and type of exposure, distance to the sea, oxygen availability at the bar depth, type of steel, electrical potential of the bar surface, presence of air voids, definition of corrosion initiation, methods and techniques for measuring C_{th} , etc. Then, the determination of an appropriate C_{th} becomes a major challenge for the owner/operator and it will be therefore assumed herein that C_{th} is a random variable.

The limit state function that defines corrosion initiation can be written as:

$$g(\mathbf{X},t) = C_{th}(\mathbf{X}) - C_{tc}(\mathbf{X},t) \tag{4.1}$$

where $C_{tc}(\mathbf{X},t)$ is the total concentration of chlorides at the concrete cover depth c at time t . The probability of corrosion initiation, p_{ini} is obtained by integrating the joint probability function over the failure domain – i.e., Eq.(4.1). p_{ini} is estimated herein by using Monte Carlo simulations.

4.2.2. Numerical example

4.2.2.1. Problem description

Let's consider a RC component placed in a chloride-contaminated environment. For illustrative purposes chloride ingress is be modelled by the simplest chloride ingress model (Eq. (1.2)). This model is governed by two parameters describing the exposure (C_s) and material properties (D). Table 4.1 provides the theoretical values for these parameters. The probability of corrosion initiation is computed by considering that the threshold of chloride concentration for initiation of corrosion follows a uniform distribution with following parameters: $C_{th} = U\left(\mu = 1kg/m^3; \sigma = 0.29kg/m^3\right)$ and a concrete cover depth of c = 6 cm. A priori information and discretisation of parameter are described in Table 4.2.

Table 4.1 – Theoretical values of parameters to identify

Parameters	Distribution	Mean	COV
C_s	Lognormal	2.95 kg/m^3	0.20
D	Lognormal	1.33×10^{-12} m^2/s	0.15

Table 4.2 – Discretisation of nodes and a priori distributions

Parameters	Number of states per node	A priori distribution	Range
$C_s\left(kg/m^3\right)$	50	Uniform	[10^{-3}; 12]
$D\left(m^2/s\right)$	50	Uniform	[6×10^{-13}; 20×10^{-12}]
$C\left(x_i, t_j\right)\left(kg/m^3\right)$	50	-	[0; 12]

We consider various inspection schemes considering one point or various points in depth for a single inspection time $t_{ins} = 10$ years (Figure 4.1b,c) and total inspection depth $L = 12$ cm (Figure 4.1a). When several points in depth are used in BN updating, different boundaries are applied for child nodes to take advantage of low chloride content (section 2.4.4). We also study the case in which the number of chloride profiles is limited and we propose a strategy to improve the assessment in such a case.

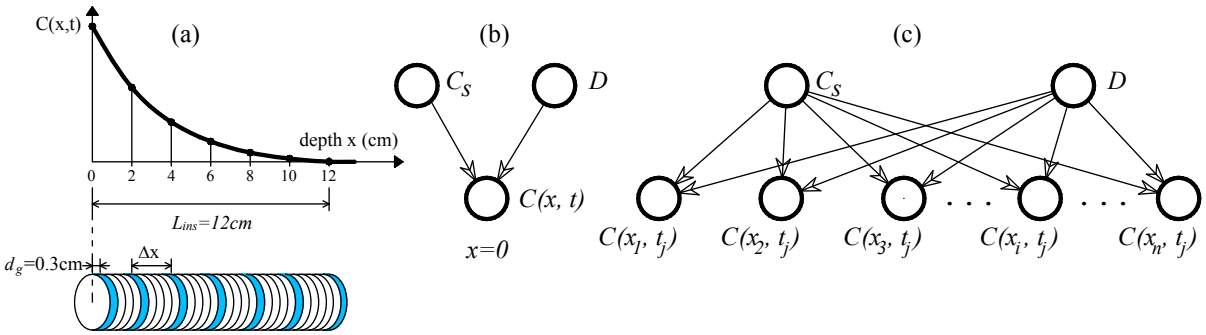

Figure 4.1: (a) Discretisation of inspection length – (b) BN with one inspection point – (c) BN with several inspection points

The histograms obtained after updating the BN for each parameter are used directly in Monte Carlo simulations to estimate the probability of corrosion initiation to avoid any assumption about analytical distribution laws.

4.2.2.2. Assessment of p_{ini} for larger inspection data

Figure 4.2a presents the probability of corrosion initiation with data obtained from a single point inspection depth. These results were obtained by identifying each parameter from 9,000 numerical chloride profiles. The results indicate that, data identified from one depth point does not provide an acceptable prediction of the probability of corrosion initiation in comparison with the theoretical assessment. Although the errors in the identification of C_s are low for this inspection strategy (section 3.2.2), the errors of the identification of D introduce larger differences in the assessment of p_{ini}. However, from Figure 4.2b, it is noted that the prediction of the probability of corrosion initiation is more close to the theoretical values when the parameters are identified from several inspection points. In this case, the consideration of more inspection points reduces identification errors by improving the assessment of p_{ini}. The error depends on the time of interest or target probability of corrosion initiation. This latter is more suitable because it is in link with actual recommendations schemes. By considering a target probability of corrosion lower than 0.5, larger values of Δx provide a better assessment. If a higher probability of corrosion is acceptable (between 0.6 and 0.9), the opposite trend is observed.

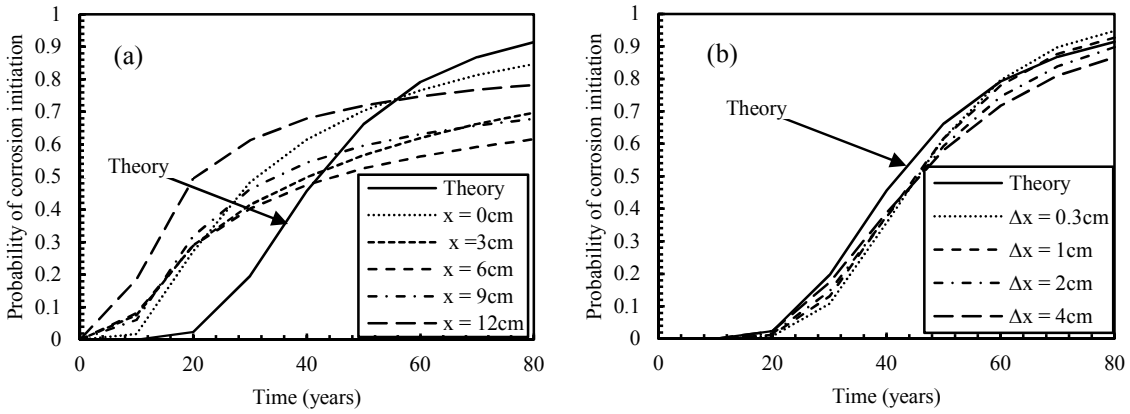

Figure 4.2: Probability of corrosion initiation with data obtained: (a) from a single point inspection depth - (b) from full inspection depth

4.2.2.3. Assessment of p_{ini} for limited data

The results presented above considered a large number of simulations for the generation of numerical evidences. However, in real practice, the number of profiles collected after an inspection campaign is very limited. Figure 4.3a presents the probability of corrosion initiation estimated with limited data obtained by considering the full inspection length. In this case, the numerical evidences were generated from 15 profiles of chloride content obtained from Monte Carlo simulations. It is noted that the assessment of the probability of corrosion initiation is far from the theoretical values. Consequently, it is necessary to improve the use of the information utilised for updating the BN. Towards this aim, it is proposed to combine results of BN configurations with one and several inspection points (Figure 4.4). We use therefore the results of the identification of C_s obtained with one depth point configuration (Step 1) as a priori data for the estimation of D by considering the full depth configuration (Step 2). By this mean, we can reduce the uncertainty level in the second step which can help improving results in estimation of D.

The assessments of probability of corrosion initiation that compare these two cases (before and after improvement) are shown in Figure 4.3. It is clear that this strategy improves the identification when data is limited. It could be concluded that this approach would be very useful for limited data. The assessment could be improved if we consider data of other inspection times as mentioned in section 3.2.4.

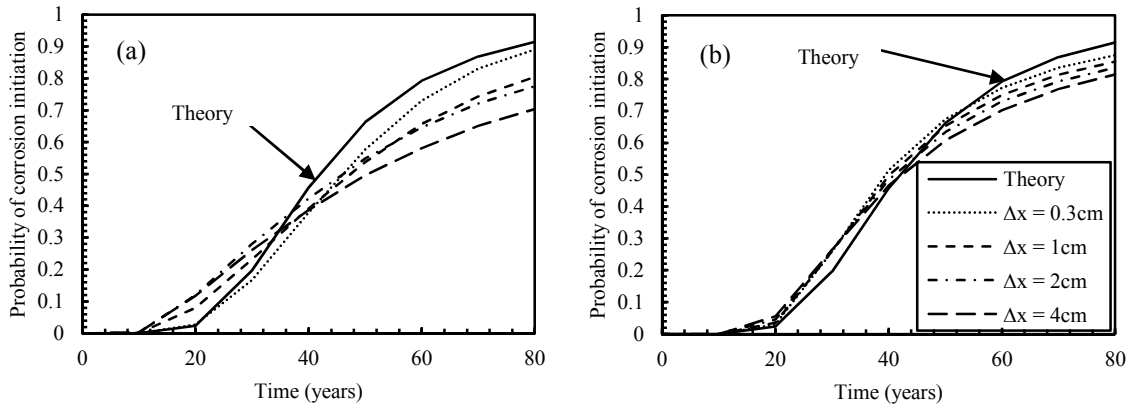

Figure 4.3: Probability of corrosion initiation with limited data: (a) before improvement - (b) after improvement

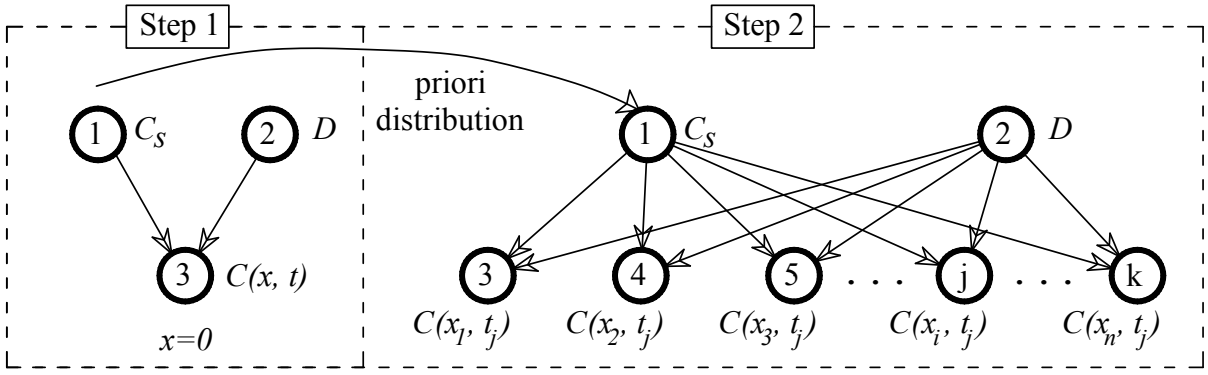

Figure 4.4 – Two-step procedure for improving identification with limited data

4.3. Strategies for inspection optimisation with different materials and exposure conditions

In management of corroding RC structures, it is necessary to draw a routine schedule for maintenance in which structures are inspected periodically every Δt years to ensure optimal levels of serviceability and safety during the structural life. Frequently maintenance strategies are divided into two stages: inspection and repair; in which inspection results are necessary for the diagnosis: detecting corrosion in early stages, evaluating its extent of damage as well as implementing repair measures. Nowadays, a large number of effective condition assessment techniques consisting of destructive and non-destructive methods has been developed to facilitate the assessment of corrosion consequences in RC structures. In order to obtain an accurate and reliable assessment of the state of corrosion damage, engineers and inspectors often have to gather information from different corrosion evaluation techniques. Among non-destructive methods, visual inspection is a techniques usually used as

preliminary survey to identify first indication of damage and give the basis for planning further surveys. However, its results are highly affected by environmental conditions and human errors reducing its accuracy. Semi-destructive inspection techniques (coring) on the other hand, could provide accurate inspection results, however they are more expensive and time-consuming. The main objective of this technique is to determine chloride content at selected points from a concrete core taken from existed structures. Frequently, each concrete core (chloride profile) is expected to be divided into as many intervals as possible. In fact, the time need to perform related actions in coring technique: crushing, filtration and titration increases significantly with number of points in a chloride profile meanwhile a discretisation with small interval lengths does not guaranty a good assessment of related model parameters. This section aims at determining an optimal configuration of a BN for the identification of parameters of chloride ingress models. BN will be used to update probabilistic models for the parameters to identify. These optimal configurations will correspond to discretisation schemes that minimise estimation errors and reduce experimental time.

4.3.1. Description of the studied cases and BN configurations

The ageing of RC structures placed in marine environment involves complex physical and chemical process. The complexity mainly comes from three sources:

1. The external environment and their interaction with the chloride ingress process are complex. In marine environments, the amount of chlorides in contact with concrete depends on whether the structure is fully submerged or in the tidal zones, or in contact only with marine moisture. Surrounding weather conditions (temperature, relative humidity, etc.) also influence the chloride ingress process.
2. Concrete is composed of different types of cement and binder, in different mix proportions, and thus is not a single material, being different in different structures.
3. The mechanisms of chloride penetration are not confined to one transport process (such as diffusion), and may be a combination of convection (absorption), chemical and physical binding (adsorption) and interaction with coexisting ions.

Lifetime assessment of RC structures subjected to corrosion should take into consideration these complexities. In this section, the complexities related to environment and material are described by different levels of aggressiveness and concrete qualities, respectively. The last source of complexity depends on the type of model used to predict chloride ingress. This section considers for illustrative purposes the model described by eq. (1.2). Although some important phenomena are neglected for this model, its non-linearity is useful to perform this analysis.

The effects of exposure conditions on parameter identification are considered by accounting for two levels of environmental aggressiveness (Table 4.3). Each level corresponds to one value of chloride surface concentration $\left(C_s\right)$ and one value for concrete cover depth $\left(c\right)$ (Table 4.4).

Table 4.3 – Description of two exposure conditions

Level of aggressiveness	Description
High	Structure situated to 0.1 km or less from the coast, but without direct contact with seawater. RC structures subject to de-icing salts can also be classified in this level
Extreme	Structure subject to wetting and drying cycles; the processes of surface chloride accumulation are wetting with seawater, evaporation and salt crystallisation

The complexity of concrete constituents could be represented by concrete quality. Three concrete qualities are proposed in this studied to characterise (1) chloride diffusion coefficient (D) and (2) threshold chloride concentration (C_{th}) (Table 4.4). Table 4.4 presents the considered probabilistic models for the random variables. The means of the chloride surface concentration (C_s) and cover depth (c) are taken from Bastidas-Arteaga et al. (2009). Meanwhile, those of chloride diffusion coefficient and threshold chloride concentration are referenced from Duprat (2007). The COV for C_s and D are reduced to 20% and 15%, respectively. This is due to the fact that within one type of concrete, the variation is narrowed. The assumption that C_s and D follow lognormal distributions is also in agreement with other studies (Duracrete 2000b; Vu and Stewart 2000).

Table 4.4: Probabilistic models of the random variables

Variables	Level of aggressiveness or concrete quality	Distribution	Mean	COV
C_s	High	Lognormal	2.95 kg/m^3	0.2
	Extreme	Lognormal	7.35 kg/m^3	0.2
c	High	Normal*	50 mm	0.25
	Extreme	Normal*	55 mm	0.25
C_{th}	Good	Uniform	2 kg/m^3	0.14
	Ordinary	Uniform	1.5 kg/m^3	0.19
	Poor	Uniform	1 kg/m^3	0.29
D	Good	Lognormal	1x10^{-12} m^2/s	0.15
	Ordinary	Lognormal	4x10^{-12} m^2/s	0.15
	Poor	Lognormal	7x10^{-12} m^2/s	0.15

*Truncated at 10mm (lower bound)

Six analysed cases are proposed by combining one level of environmental aggressiveness with one concrete quality (Table 4.5). The evaluation of the effectiveness of a given BN configuration should be based on a given criterion. Preferably, it should include a larger amount of experimental data (chloride profiles) that can be used to estimate 'real' probabilistic distribution of model parameters and consequently to test and compare various BN configurations. However, such a database is in practice very hard to obtain because it is obtained from semi-destructive tests that are expensive and time-consuming. Therefore, in order to provide general improved BN configurations, we generate sufficient numerical evidences from Monte Carlo simulations from theoretical probabilistic models. These theoretical values will be the target random variables to identify.

Table 4.5: Description of the studied cases

Case	Level of aggressiveness	Concrete quality
1	High	Good
2	High	Ordinary
3	High	Poor
4	Extreme	Good
5	Extreme	Ordinary
6	Extreme	Poor

The theoretical probabilistic models presented in Table 4.4 are used to generate 9,000 chloride profiles for each studied case. Different configurations of the BN corresponding to different discretisation of total inspection depth are investigated to select an optimal configuration by comparing the error of the identified parameter $\left(Z_{identified}\right)$ with respect to the theoretical value $\left(Z_{theory}\right)$:

$$Error\left(Z\right)=\frac{|Z_{identified}-Z_{theory}|}{Z_{theory}}100\% \tag{4.2}$$

where Z represents the mean or the standard deviation of the parameter to identify – e.g., μ_{C_S}, σ_{C_S}, etc.

Table 4.6 describes the discretisation of each parameter. A priori distributions of parent nodes (C_s and D) are used to generate a sufficient number of random chloride concentrations at depth x and time $t=10$ years by using Eq. (1.2) for each child node (Figure 4.1). This a priori data is used to compute the CPT for each child node in the BN.

Data from numerical simulations will be introduced to the BN as evidences. The BN is then updated to obtain a posteriori distributions which are after used to identify the parameter $\left(Z_{identified}\right)$ and afterwards, to evaluate the errors of the configuration by using Eq. (4.2).

Table 4.6: Discretisation of nodes and a priori distribution

Parameters	Number of states per node	A priori distribution	Range
$C_s\left(kg/m^3\right)$	50	Uniform	[0.5; 17]
$D\times10^{-12}\left(\mathrm{m}^2/\mathrm{s}\right)$	50	Uniform	[0,1; 20]
$C\left(x_i,t\right)\left(kg/m^3\right)$	50	-	-

As previously mentioned in section 3.2, the BN configuration using only one child node representing for chloride content at the surface is used for identifying C_s. However, for D, it is necessary to use the BN with several child nodes that accounts for several measurements in depth to obtain a better estimation. Therefore, this section focuses on finding an optimal number of inspection points in depth (optimal BN configuration) to identify D. The 2-step procedure described in section 4.2.2 is applied here to reduce identification errors. Various BNs with different number of inspection points (more or less information at depth *x*) are performed to compare the identification errors. The number of inspection points $\left(n_p\right)$ varies from 2 to $n_{p,\max}$, where $n_{p,\max}$ corresponds to the case that inspection lengths $\left(L\right)$ are divided with the minimum discretisation length $\Delta x = 0.3\mathrm{cm}$. The inspection length $\left(L\right)$ is determined from chloride profile (Figure 4.5) built for each case after $t = 10\mathrm{years}$ to cover all the potential chloride presence. The values of L and $n_{p,\max}$ for the 6 studied cases are shown in Table 4.7 .

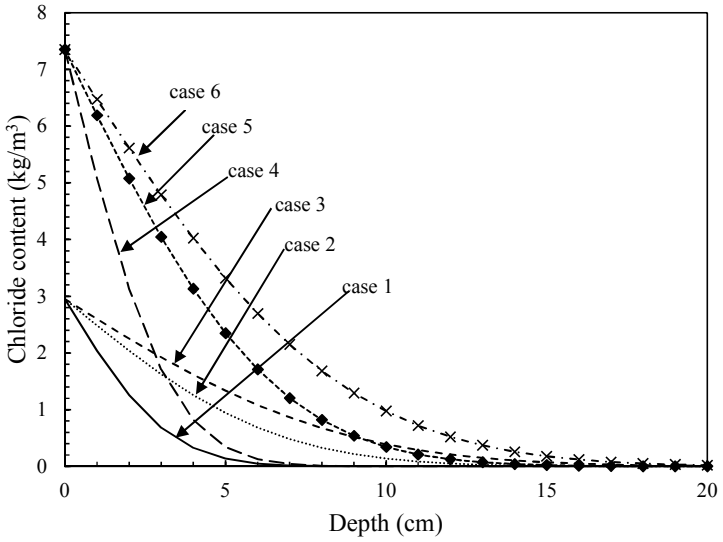

Figure 4.5: Mean chloride profiles for 6 analysed cases at t=10 years

Table 4.7: Inspection lengths and maximum inspection points for studied cases

Case	Inspection length $L(cm)$	$n_{p,\max}$
1	9	31
2	15	51
3	20	67
4	9	31
5	15	51
6	20	67

4.3.2. Optimised BN configuration for each analysis case

Figure 4.7 depicts the identification errors of the parameter D when the level of aggressiveness is high and moderate concrete quality (case 2). This is a case appearing frequently in practice. It can be seen that using a larger number of inspection points does not guarantee a better identification for the mean of D. The identification errors for the mean almost remains at about 2% with $n_p > 4$ (Figure 4.7a). However, using information from more inspection points could introduce additional errors for the estimation of the standard deviation. The evolution of errors given in Figure 4.7b shows an increasing trend with $n_p > 13$. Therefore, it is possible to determine value of n_p minimising the estimation errors of the standard deviation. This phenomenon was previously analysed in section 3.2.4. For other cases, similar behaviours are also observed in Figure 4.6, Figure 4.8, Figure 4.9, Figure 4.10 and Figure 4.11

In this study, we defined an optimal range of n_p where the identification errors for the mean are smaller than 10% and those for standard deviation are lower than 20%. In this range, the value of n_p that minimise the errors of standard deviation is defined as optimal value $\left(n_{p,opt}\right)$. For the case 2, the optimal range is (8 – 15) and the optimal number of inspection points is 8. The results for other cases are summarised in Table 4.8. It is worth noticing that under the same exposure condition, RC structures with better quality of concrete will require larger value of $n_{p,opt}$. For example, values of $n_{p,opt}$ for the cases 1, 2 and 3 (good, ordinary and poor concrete quality) are 19, 8 and 6 respectively, corresponding to the quality of concrete are good, ordinary and poor. This phenomenon is related to the chloride diffusion coefficient which determines directly the concrete quality. A chloride profile with a high diffusion coefficient will have small slope (e.g., case 3 in Figure 4.5). This means that the chloride content between two adjacent inspection points is less different. Therefore, including additional inspection points in case 3 will generate more identification errors. This issue was previously explained in section 3.2.3. Concerning the effect of exposure, it is notes that $n_{p,opt}$ decreases when the environmental chloride concentration is larger (case 4 to 6). In such cases, it is noted from Figure 4.5 that the slopes of chloride profiles are significant large and few inspection points could provide useful information for model parameter identification. However, more inspections points could be required if the structures are inspected lately because the larger chloride content inside concrete will reduce the slope of chloride profiles.

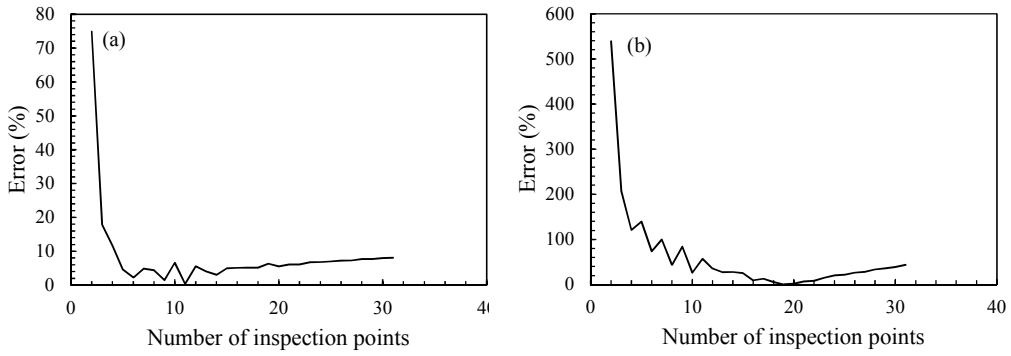

Figure 4.6 – Error in identification of D for case 1: (a) Mean-(b) Standard deviation

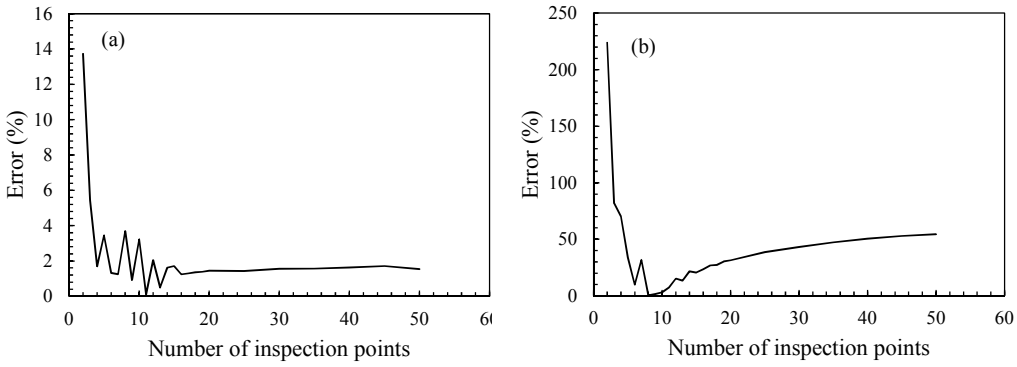

Figure 4.7 – Error in identification of D for case 2: (a) Mean-(b) Standard deviation

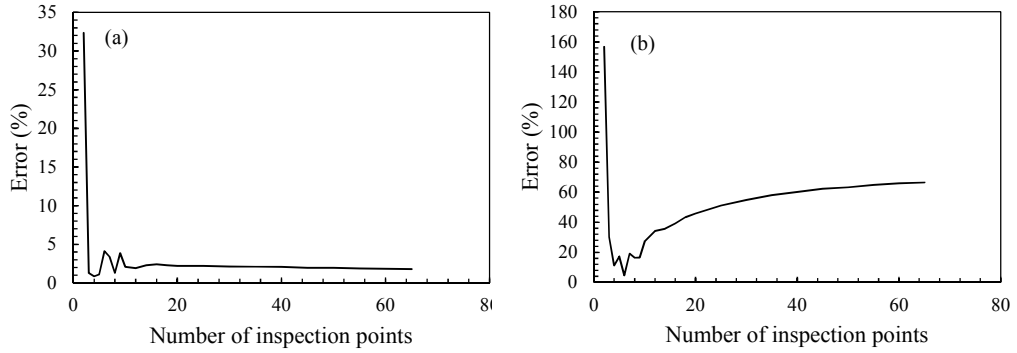

Figure 4.8 – Error in identification of D for case 3: (a) Mean-(b) Standard deviation

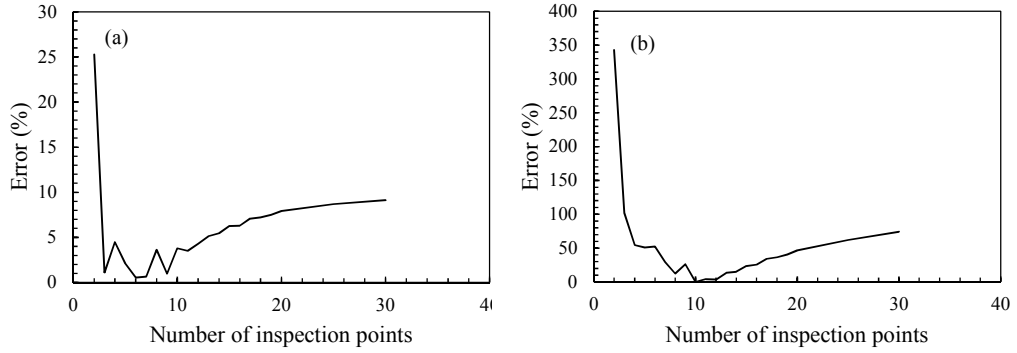

Figure 4.9 – Error in identification of D for case 4: (a) Mean-(b) Standard deviation

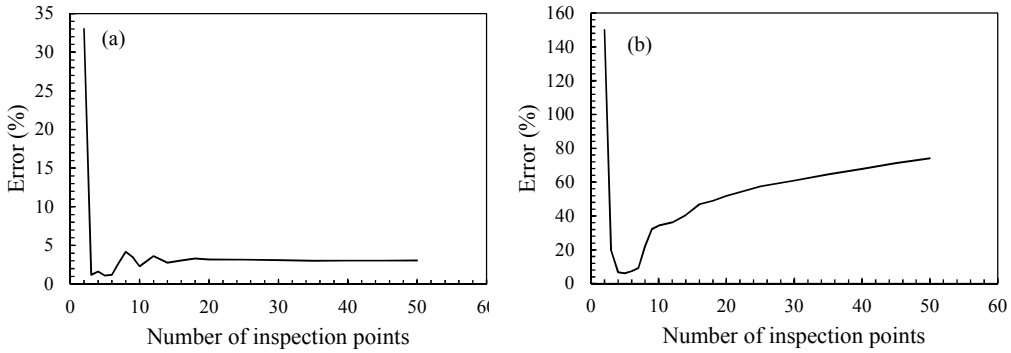

Figure 4.10 – Error in identification of D for case 5: (a) Mean-(b) Standard deviation

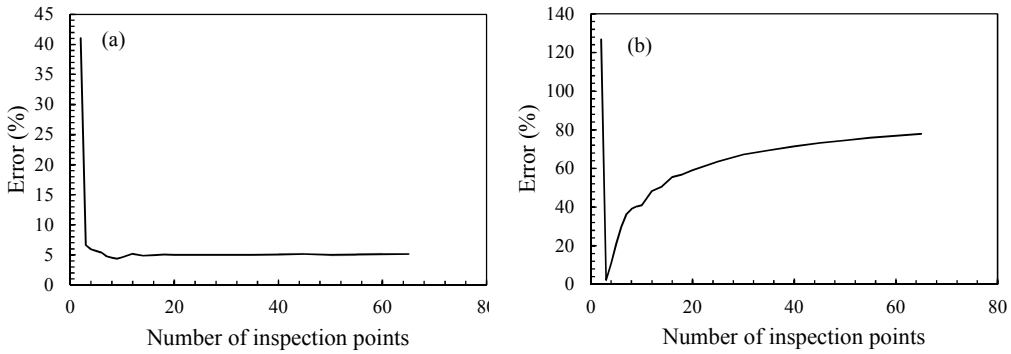

Figure 4.11 – Error in identification of D for case 6: (a) Mean-(b) Standard deviation

Table 4.8: Optimal values for 6 cases

Case	Optimal range	Optimal point $\left(n_{p,opt}\right)$
1	(16 - 24)	19
2	(8 - 15)	8
3	(4 - 9)	6
4	(10 - 14)	12
5	(3 - 7)	5
6	(3 - 5)	3

4.3.3. Assessment of p_{ini} for various materials and exposure conditions

We consider a RC component placed in a chloride-contaminated environment with high level of aggressiveness and ordinary quality concrete (case 2). Optimal configurations of BN proposed in section 4.3.2 with the 2-step procedure described in section 4.2.2 are used to identify both the mean

and standard deviation of the parameters C_s and D. These identified parameters are then used in Monte Carlo simulations to estimate the probability of corrosion initiation.

Figure 4.12 compares theoretical values with the predictions estimated from identified parameters when inspection data is larger (10,000 numerical profiles) and when inspection data is limited (15 numerical profiles). It is clear that by using the improved configurations presented in Table 4.8, the assessment of probability of corrosion initiation is close to the theoretical values even with 15 chloride profiles. The prediction errors of p_{ini} computed with respect to the theoretical values described in Figure 4.12b reveal small errors excepting for the prediction at $t_{ins} = 10\text{years}$. In fact, the probability of corrosion initiation at this time is relatively low $\left(p_{ini} \approx 0.1\right)$ and therefore, more information is required to improve the accuracy at earlier times. However, for long-term predictions, this approach provides an acceptable assessment of p_{ini}.

The errors on the assessment of the probability of corrosion initiation with 15 chloride profiles for other cases reveal similar trends (Figure 4.13). The larger values of error are related with earlier times where the probability of corrosion initiation is smaller. When $t > 40\text{years}$ the errors are lower than 6% for only 15 chloride profiles. This work considered data obtained from inspection time of 10 years for all study cases. However, as mentioned in section 3.2.4, for a specific study case the error could be also reduced if other inspection times are considered. Optimal inspection times could be defined for each exposure and concrete quality.

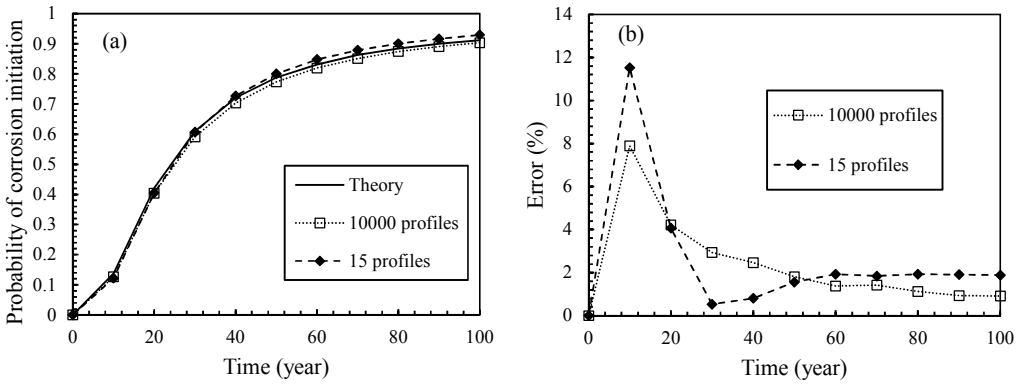

Figure 4.12: (a) Probability of corrosion initiation – (b) Prediction error for p_{ini}

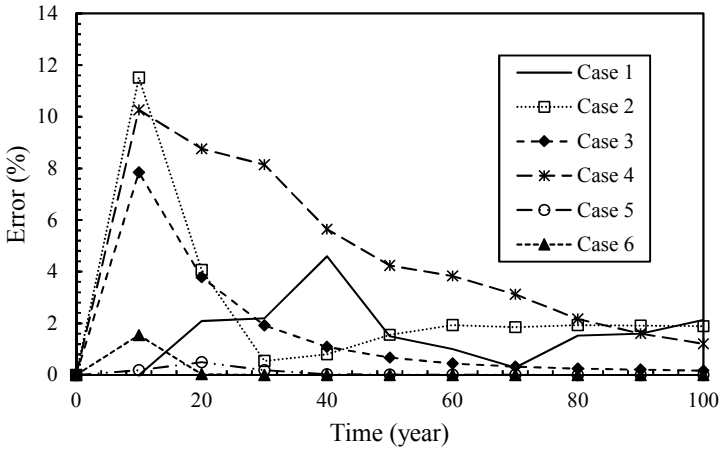

Figure 4.13: Errors on assessment of probability of corrosion initiation

4.4. Conclusions

1. The first part of this chapter described briefly the theory of probability of corrosion initiation assessment (p_{ini}) and its evaluation from BN identified parameters (C_s and D). It was found that, it is difficult to obtain a prediction of p_{ini} close to the theoretical value if parameters are identified from one inspection point. Identified parameters from BN with several points in depth could provide better estimation for p_{ini}. However when inspection data is limited, the differences between the prediction of p_{ini} and its theory becomes significant even if the chloride profiles are divided into small intervals. To deal with this problem, we proposed a 2-step procedure in which a posteriori information of C_s from one inspection point configuration is used as a priori information for BN configuration with several inspection points. This 2-step procedure could reduce the level of uncertainty and improve the identification of parameters. This improvement provided predictions of p_{ini} more close to the theoretical values even if information from inspection data is limited.
2. The discretisation of chloride profiles relates directly to the time and costs required in coring techniques and give important influences on parameter identification. Various exposure conditions and material qualities are mixed to create different studies cases. By comparing different BN configuration, we proposed an optimal discretisation minimising the identification errors of D for each case. It was found that under the same exposure condition, concrete with higher quality corresponds to larger values of optimal inspection points. Data from these optimal configurations was applied to the assessment of the probability of corrosion initiation. The results obtained from comparisons between: theory, larger data and

limited data indicated that for long-term prediction $\left(t_{ins} > 10\text{years}\right)$ improved configurations could provide results close to theoretical values.

Conclusions and perspectives

Conclusions

In accordance with the main objectives of this thesis, the following conclusions have been drawn:

1. Chloride ingress into concrete is a complex process but analytical solutions based on Fick's law are often used to describe this phenomenon. Models used to predict this process in unsaturated conditions could provide a more realistic assessment; however they require a larger number of parameters to model. Therefore, in this study, only analytical models valid in theory only for saturated conditions are used to illustrate the identification of parameters despite they neglect some important phenomena. Two models have been chosen to illustrate the effects of the time-dependency of chloride diffusion coefficient: (1) the model proposed by Tuutti, (1982) and (2) the model suggested by Nilsson and Carcasses (2004).

   In preventive maintenance, a reliability analysis of chloride ingress aims at evaluating the probability of corrosion initiation. Model parameters used for the reliability assessment of chloride ingress are often determined from experimental data that always integrate significant uncertainty. Therefore, the identification of random variables from real data becomes a main challenge for comprehensive probabilistic modelling. There are various methods for uncertainty modelling and parameter identification. Each method has some pros and cons that could be appropriate for particular problems. This study requires integrating experimental data in uncertainty modelling for parameter identification; thus BN could be useful than other tools for such purposes. The target of reliability assessment in chloride ingress leads to assess a probability of corrosion initiation at approximate 10^{-2}. BN provide then a discrete approach for

PDF approximation and therefore, it is well adapted to deal with such a level of reliability target. BN could be also integrated to numerical chloride ingress models.

The BNT has been chosen as a basic tool to build and analyse several BN configurations. This is an open-source Matlab package for directed graphical models. The procedures (construction, inference and updating of a BN in the BNT) are detailed with numerical algorithms and codes. The performance as well as the accuracy of BN configurations built on BNT are validated by comparing the results obtained from BNT with a commercial BN software (NETICA). The BNT can help to generate different BN configurations quickly as well as it is also well-adapted to more complex chloride ingress models (time-dependent models). In addition, to improve the identification, some numerical issues are also analysed:

- Latin hypercube sampling is used instead of crude Monte Carlo simulations to generate the uniform variables used for building the CPTs. This improvement reduces the number of simulations and increases the accuracy of BN modelling.
- The algorithms for creating the CPTs in this study generate simulations over pre-defined ranges for each parameter. This algorithm could provide a trade-off between efficiency and computational cost because the BN configurations used for modelling chloride ingress in this study limited the number of parent nodes (parameter to identify). In case the BN has more parent nodes, it is necessary to generate simulations in each state of parameters to ensure adequate mutual combinations between the child node and its parents.
- A discretisation with high value number of states is often used to obtain accurate results or to take advantage of poor information from deeper inspection points. However, this solution increases significantly the CPT size leading to larger computational time. By defining different boundaries for child nodes, the number of states decrease meanwhile BN can take advantage from information at deeper points.

However, there are also some short-comings in the use of BN for parameter identification that need to be implemented. BN can handle both discrete and continuous variables, however the approximation errors due to the discretisation of discrete variables or the use of approximate algorithms for continuous variables should be investigated. The uncertainty of BN will increases when more nodes are added into the networks. As a result, it will induces more identification errors. Therefore, it is necessary to construct an appropriate BN configurations to minimize identification errors.

2. Based on the general BN framework and numerical implementation proposed in chapter 2, chapter 3 analyses several BN configurations. It was found that BN configuration using one

inspection depth close to the concrete surface could minimise the identification errors for C_s. For D, it is necessary to use the information from total inspection length to provide a better characterisation of the kinematics of chloride ingress. At a given inspection time, there is an optimal discretisation length. This finding could be considered as recommendation for inspection techniques. Results also revealed that with inspection data obtained at early exposure time, the identification of C_s could be improved whereas those obtained at larger inspection times will reduce the identification errors of D.

The efficiency of combining evidences from different inspection times on parameter identification is analysed in two cases: using the chloride ingress models that (1) do not consider the time-dependence of chloride diffusion coefficient and (2) consider the time-dependence of this coefficient. In the latter case, we considered a more representative model that may lead to more accurate assessments. Results obtained from BN indicated that when the time-variant effect of chloride diffusion coefficient is considered, the identification error of D is reduced if inspection data is combined. In both cases, the estimation errors of C_s could not be reduced because both models do not consider the time-dependence of C_s.

To characterise the mid- and long-term durability performance of construction or repair material, this study developed in the laboratory normal and accelerated chloride ingress tests. These tests simulate daily tidal cycles (high and low). For the accelerated tests, samples are submerged in salted water during the high tidal cycle and during low tidal cycle ventilators are used to dry samples. For normal tests, samples are subjected to the same tidal cycles without additional drying during the low tidal cycle. An equivalent time in accelerated test is determined from BN by applying a proposed two-step identification procedure. The first step of this procedure uses evidences from normal data to update the distributions of two parameters: C_s and D. The a posteriori information is afterwards used in the second step as a priori information to determine the equivalent time by integrating evidences from accelerated data. A scale factor reflecting the ratio between normal test and accelerated tests can be computed. Consequently, the chloride profiles determined from accelerated test can be used now to characterise mid- or long-term behaviour of concrete that cannot be usually treated from short exposure times in normal data. This methodology can be extended to other long-term degradation mechanisms.

A sensitivity analysis is carried out to study the influence of the identification of the age factor accounting for the time-dependency of the chloride diffusion coefficient. The results reveal that depending on concrete characteristics and exposure (a given age factor), the inspection schemes should consider specific inspection times describing adequately the evolution of chloride diffusion coefficient with time. Combining information coming from these inspection times allows improving the identification of parameters. It is also worth

noticing that, the presence of the age factor in BN as a random variable will increase uncertainty and add more errors for the identification of the other model parameters. The uncertainty due to the age factor can be reduced if an appropriate assumption about its a priori information is applied. Results from a comparative study indicated that using a priori beta distribution might lead to more accurate results.

A procedure is proposed to characterise the age factor from limited experimental data from data coming from normal and accelerated tests. This factor is introduced in the chloride ingress model that accounts for the time-dependent effect of chloride diffusion coefficient. The procedure estimates priori information from normal tests and after, determines the equivalent times, integrates information from accelerated test to update the age factor and iterates to update the equivalent times and age factor. A convergence trend was obtained when both equivalent times and age factor lead to constant values. By combining data from normal and accelerated tests, it provides a better assessment of the time-dependent process of chloride diffusion coefficient which can be under- or overestimated if only normal data is used. By comparing the confidence intervals estimated from probabilistic modelling of chloride ingress and real data, it can be concluded that this approach is useful for characterising the age factor and that BN is a powerful tool for analysing such a time-dependent problem.

3. Chapter 4 presented a strategy to improve the assessment of probability of corrosion initiation (p_{ini}) when inspection data is limited. In this strategy, the model parameters used to estimate p_{ini} are identified from a 2-step procedure. In the first step, the distribution of C_s is updated from the BN configuration with one child node representing chloride content close to the surface. The distribution of C_s is then used in the second step as a priori information in the BN configuration with several inspection points to update the distribution of D. Results from the illustrative examples indicated that this strategy could improve the assessment of p_{ini} even if inspection data is limited.

   This study also proposed an optimal discretisation for several study cases corresponding to various exposure conditions and material qualities. Specific optimal discretisation schemes were found for each case. For example, under the same exposure condition, the optimal configuration for concrete with higher quality requires a higher number of inspection points in comparison to less quality concrete. BN configurations built from these optimal discretisations could minimise the identification errors of the parameter D and could be seen as recommendations for improving the protocols of coring techniques

Recommendations for future research

There are many areas in which further research is needed to improve the identification of model parameters and consequently to improve lifetime assessment and to optimise maintenance actions:

- Consideration of modelling error as new parameter to identify and to be determined from real data. The error of measurement in the BN could be updated from repetitive tests for existing or new techniques;
- Extension of the identification of random variables to the identification of random fields. Auto correlation function describes the relationship in a random field and implies link in BN between two variables. The challenge is the case the correlation matrix is fully populated that increases significantly the size of CPT.
- Extension of the proposed procedure for the identification of model parameters for other deterioration processes (carbonation, biodeterioration, etc.). The larger number of uncertainty and/or lack of real data may be possible challenges.
- Implementation of the methodology to numerical chloride ingress models. It was an initial objective of the work. Additional experiments on chloride ingress were carried out (Appendix B) to generate the simulated chloride profiles from comprehensive model of chloride ingress into concrete (Bastidas-Arteaga et al. 2011). Although data from these experiments could provide useful information to extend the present study, it was no sufficient for dealing with the initial identification purposes. A larger number of experimental tests are therefore required.
- Consideration of costs for recommending inspection procedures (inspection times, number of cores, number and positions of measures in each core, etc) that provide a balance between error and cost.

Appendix A
Description of normal and accelerated chloride ingress tests

A.1. Introduction

The MAREO project (MAintenance and REpair of concrete coastal structure: risk based Optimisation-2008-2012) is a collaborative innovation, research and development program that aims to compare the economical, reliable and sustainable performance of repair techniques on reinforced concrete of coastal structures (Bastidas-Arteaga and Schoefs 2015). Indeed, the French port infrastructures play an important role with 80% of commercial trading passing through the ports, touristic stakes and European defence issues. However, 60% of these structures have more than 50 years. This ageing brings us the major concerns: what is the real serviceability state of these structures? Should they be deconstructed or rehabilitated and what will be their behaviour after repair?

The MAREO project is born to answer these questions with three objectives:

- Identify performance indicators
- Develop experimental protocols
- Propose methods for calculating port structures

In the long-term, the MAREO project aims to open the market of rehabilitation and re-engineering of port infrastructure

A.1.1. Experimental set up

The ageing test used 3 concrete slabs with dimensions 45cm x 45cm x 12cm casted from the commercial concrete MAPEI BS08. This concrete is used for repairing a port in Saint Nazaire in the period between 10 and 25 of August 2009. All slabs are referenced, for example I1N09 indicating for: I (type of concrete: I-MAPEI)-1 (N° of slab sample)-N09 (Port of Nantes, 2009 sites: place and date of concrete placement). Two slabs with number 1 and 2 are used for accelerated ageing test, slab with number 3 is served for natural ageing test.

Preparation for the samples: The timber formworks and steel handles of slabs are removed. Each slabs is marked and applied on the edge sides the epoxy resin layer. These layers guaranty that the penetration of chloride ions is occurred unidirectionally. The submerged part of the slabs is the top because it is rough shotcrete (not smooth). When slabs are not tested, they are covered with polyane (plastic film) to maintain the existing moisture in the concrete.

Materials used to carry out the drawdown test are listed as follows:

1. 2-dimentional aluminium trays: 370cm x 68 cm and height = 41cm
2. 1 tank of salt water with capacity $1m^3$.
3. 2 valves for filling containers
4. 2 pumps for emptying containers
5. 6 fans to dry the slabs
6. 1 scale for weighting slabs (before, during and after the test)
7. 1 transmitter-sensor providing temperature and ambient relative humidity
8. 1 transmitter-sensor giving the salinity and temperature of the water
9. 2 double level sensors
10. Several industrial static relays
11. 2 acquisition unit NI(USB-6008 and cRIO-9472)
12. 1 computer with Labview® software.

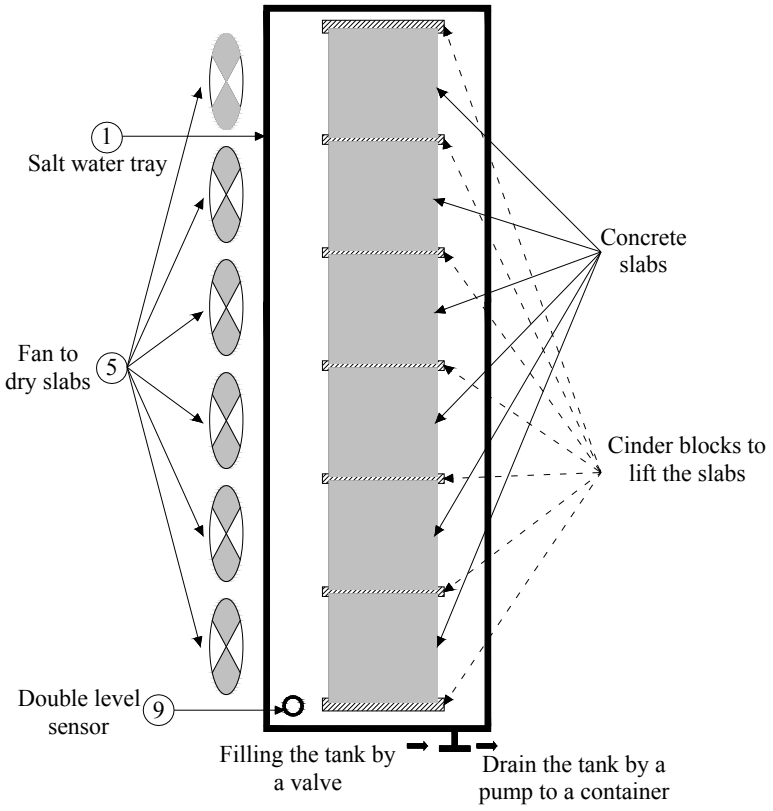

Figure A.1 – Installation of concrete slabs in a tank

The installation of concrete slabs in each tank is described in Figure A.1. Each tank is connected with a salt water container by a drainage pump system which can help adjusting the water level in each tank (Figure A.2). To create laboratory tidal conditions (up and down), we immerse concrete slabs in salt water (sea water) or non-submerged and dry (low tide) (Figure A.3). In order to accelerate the penetration of chloride ions:

- At high tide phase: we partially immerse concrete slabs (capillary action). The depth of immersion of concrete slabs is $2cm \pm 1cm$.
- At low tide phase (not submerged slabs), we dry the top face of the slabs by free air (natural ageing test) or by fans (accelerated ageing test).

To provide and ensure a stable environmental condition, during the test, sensors will provide measures taken for:

- Ambient temperature of the room (°C)
- Relative humidity of the room (%)
- Water temperature (°C)
- Water salinity (g/L)
- Weighting slabs (kg)
- Level of water (high level = 20cm; low level = 10cm)
- Date and time.

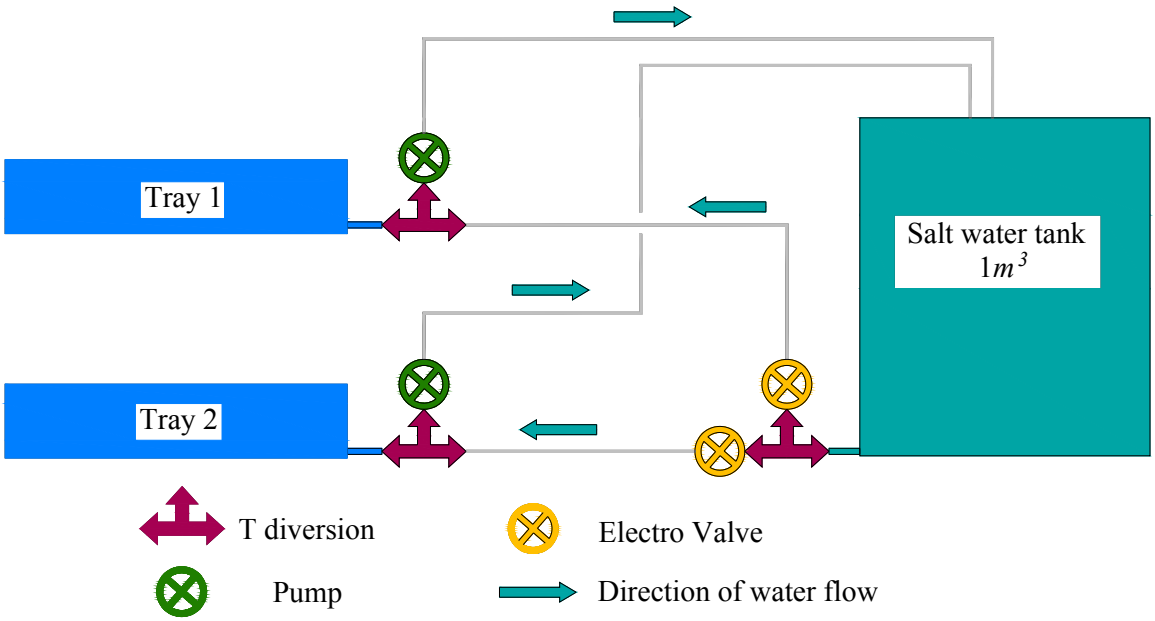

Figure A.2 – Drainage pump systems

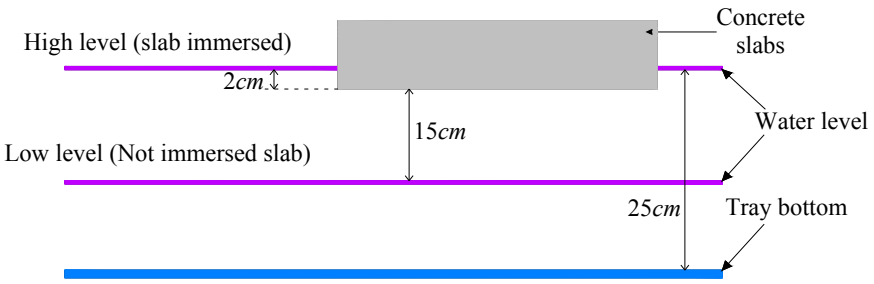

Figure A.3 – Creating tidal conditions in laboratory

Salinity of the solution plays an important role in this experiment. It guaranties a simulation of chloride ingress closing to natural conditions. Therefore, it is necessary to create solutions with salinity level closing to natural sea-water. The measuring salinity range of sea water that we want to create is : $30(g/L) \leq salinity\ solution\ (g/L) \leq 37(g/L)$. This range corresponds to the average salinity in the North Atlantic seawater. This salinity corresponds to an average of 30g/L chloride ions. The salinity level is automatically checked by the sensor and Labview program and adjusted if necessary by an operator. In this experiment, we used the proposed approach by Djerbi et al. (2008) to create in the laboratory the salinity of seawater. According to this study, 1 litter of seawater contains of:

- 30g of sodium chloride (NaCl)
- 4.65g of potassium hydroxide (KOH)
- 1g of sodium hydroxide (NaOH)

The above mixture is made with demineralised water created from a deionised laboratory filtration. During the test, the salinity of water is monitored continuously by a sensor and will be adjusted according to the ratio among ingredients. However, the solution pH is around 13, which is higher than that of seawater at 8.2. In fact, this high pH could avoid unwanted reaction between the solution and concrete slabs. Consequently, concrete slabs can be conserved in the solution without micro cracks resulting from pH excepting for the migration of chloride ions in concrete.

A.2 Experimental procedures

A.2.1. Accelerated ageing test

The accelerated ageing of concrete in the marine environment is carried out in non-stationary tidal conditions. A daily exposure with 24 hours of a concrete slab is divided by 6h immersed and 18h not immersed. The operation of this test is combined with the following activities:

1. Weight slab by the operators and recorded values automatically in an Excel file
2. Install slabs in the trays.
3. Start accelerated ageing test.
4. Fill the tray by electro valve until the solution reaches high level.

5. Keep concrete slabs in tidal condition for 6h. Concrete slabs are therefore immersed in salt water for 6h. The depth of immersion of the test is 2cm±1cm. Measures are taken automatically every hour (relative humidity, salinity, water level, date and time,…).
6. Empty the tray by pumps until the solution reaches low level.
7. Dry continuously slabs by fans during 18h. The slabs are in free air and are dried for 18h. Measures are taken automatically every hour (relative humidity, salinity, water level, date and time,…).
8. Stop drying. The final daily report is created and saved
9. Repeat steps from 4 to 8 until the end of the test period.

Note that, slabs weighting is performed once per month. This test allows accelerating ageing of concrete slabs in tidal condition by decreasing the immersion time of concrete (6h for immersion instead of 12h) and increasing the non-immersion time (18h instead of 12h at low level) associated to an accelerated drying by fans.

A.2.2. Natural ageing test

In order to study the natural ageing of the concrete, we recreate in the laboratory the natural conditions of high tide and low tide. We use the same procedure for accelerated ageing test excepting for:

- Concrete slabs are dried naturally by free air without the use of fans at low tide phase (not immersed slabs).
- The duration for each phase is 12h as natural tidal cycle.

A.2.2.1. Determination chloride profiles from normal test and accelerated test

At a certain exposure time in ageing tests, slabs are cored to archive the corrosion measurements. There are 9 concrete cores taken from each slabs at 3 different times (Figure A.4). Each concrete core is a cylinder concrete with 10.5cm of diameter and 12cm in height. Table A.1 details 3 different times in which concrete cores are drilled from slabs. Therefore, we have a total 18 cores for accelerated ageing test and 9 cores for normal test.

Table A.1 – Different times to take cores from slabs

Time (day)	Accelerated test		Natural
	Slab I1N09	Slab I2N09	Slab I3N09
T1	65	65	65
T2	212	212	207
T3	436	436	320

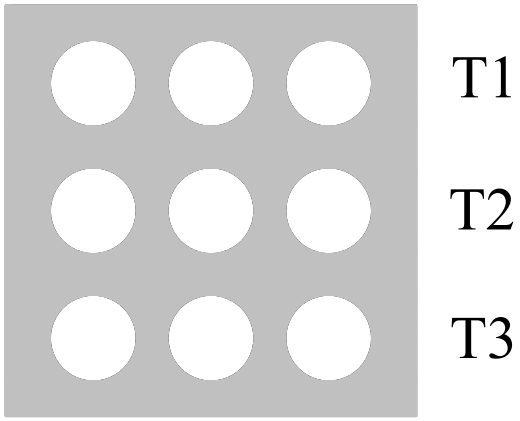

Figure A.4 – Taking cores from slabs

Each core is divided into small intervals for being crushed into concrete powder. The length for each interval should not be smaller than 3mm due to the accuracy of equipment. These powders are stored in plastic bags which are afterward served for filtration and titration tests to determine chloride content at each depth point corresponding to the average depth of each interval. The filtration and titration test follows the same procedures described in (BEN FRAJ 2009). Due to the short exposure time, the maximum length for each chloride profile is 42mm. For chloride profiles with lower chloride content, the total length of chloride profiles might be shorter.

Appendix B
Experimental characterisation of the repair material

B.1. Introduction and preparation of specimens

In this part, some experiments are carried out to build the database for the identification. Each experiment will determine parameters for modelling chloride ingress. The types of test and the corresponding parameters as well as the specific specimens used in each test are described in Table B.1. The specimens used for experiments are from MAREO project. They were extracted from the same slab which is casted for repairing dock at the port in Nantes by the company ETPO in the 25th August 2009. The concrete used to cast the slab is a product of MAPEI company, named *"mapegrout gunite BS"*. It is a one-component premixed cementitious mortar composed of hydraulic binders, silica fume, select aggregate and special additives. The total number of specimens extracted is 9 with position for each specimen showed in Figure B.1. Each specimen is cylinder concrete which is divided into two smaller concrete cylinder with 5cm in depth and 10,5cm in diameter. After being taken from structures, each specimen is applied an epoxy layer on the lateral faces and then dried in a desiccator at 60°C for 1,5 months. Samples 1; 2 and 9 are crushed for experiments involving in equilibrium properties: chloride binding, sorption/desorption. Samples numbered from 3 to 8 are used for experiment with transport properties.

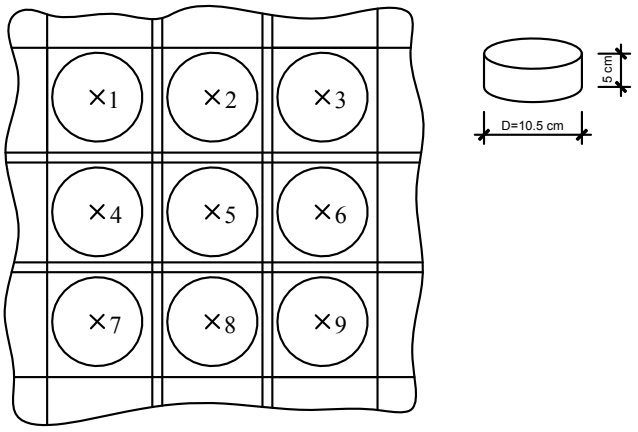

Figure B.1: Positions of samples in concrete slabs

Type of test	Measured parameter	Specimens	Date start	Date finish
Water porosity	*p (%)*	3.1; 3.2; 5.1; 5.2; 6.1; 6.2; 7.1; 7.2; 8.1; 8.2	24/01/2013	01/03/2013
Intrinsic gas permeability	$k_v(m^2/s)$	3.1; 3.2; 4.1; 4.2; 5.1; 5.2; 6.1; 6.2; 7.1; 7.2; 8.1; 8.2	10/2012	Unknow
Stationary migration at 20°C	$D_{eff}\ (m^2/s)$	5.1; 6.1; 6.2	14/03/2013	15/04/2013
Chloride binding isotherm	$c_b\ (g)$	Crushed concrete from samples 1 ;2 and 9	16/04/2013	29/07/2013
Sorption isotherm (with/without chloride)	*W=f(HR)*	Crushed concrete from samples 1 ;2 and 9	20/06/2013	05/03/2014
Activation energy	$E_a(J/mol)$	3.1; 3.2; 4.2; 5.1; 5.2; 6.1; 6.2; 7.2	14/03/2013	15/07/2013

Table B.1: Types of tests, parameters to identify, specimens used and experimental time

B.2. Water porosity

The test is performed on concrete discs of 10,5cm in diameter and 5cm in depth. To identify the porosity, the samples must be completely water saturated. Two procedures for saturation were used: AFPC-AFREM and AFPC-AFREM modified. As shown in Figure B.2, the principle consists of placing a sample in a watertight desiccators and using a spacer for elevating samples in order to optimise the contact surface.

When the desiccator is closed, vacuum is created by means of a vacuum pump until a constant pressure of 25mbar is reached, the vacuum is maintained for at least 4 hours. The basic solution (NaOH/KOH) is then pumped in this desiccators. The immersion time for each saturate procedure are detailed in Figure B.3. In this experiment, we used AFPC-AFREM modified procedure as the saturate

procedure because some physical results (porosity and water mass volume) from AFPC-AFREM procedure is “underestimated”. This is due to the short duration of saturation does not fulfil all the pores of concrete samples, which indicate a lower estimate of porosity (BEN FRAJ 2009).

Figure B.2: Saturate equipment

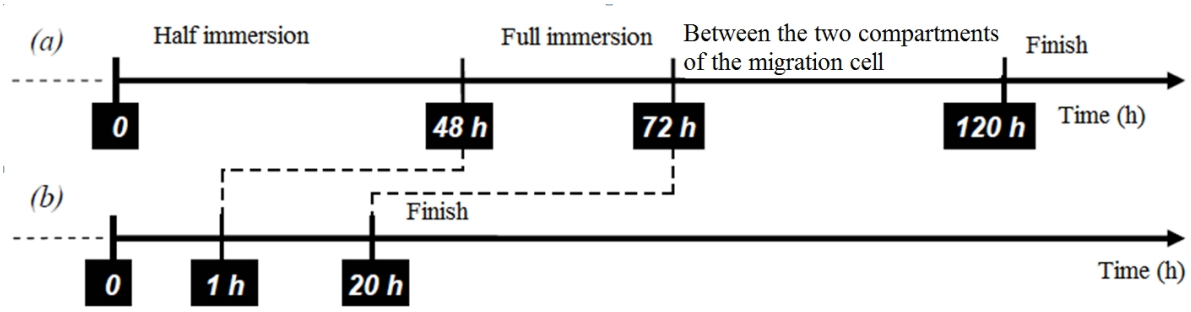

Figure B.3: (a) Procedure AFPC-AFREM modified and (b) procedure AFPC-AFREM

The water porosity, p, was evaluated using the following equation:

$$p = \frac{M_{air} - M_{dry}}{M_{air} - M_{water}} \times 100 \qquad \text{(B.1)}$$

where: M_{air}(g), M_{dry} (g), M_{water} (g): are respectively the mass of saturated sample weighed in air, the mass of the dry sample, and hydrostatic mass.

This test also allows us to determine the mass volumetric using the following equation:

$$\rho = \frac{M_{dry}}{M_{air} - M_{water}} \qquad \text{(B.2)}$$

The results are showed in Table B.2 and Figure B.4.

Samples	Dry mass(g)	Saturate mass(g)	Hydrostatic mass(g)	Porosity (%)
3.1	861,9	917	502,5	13,29
3.2	886,4	945,1	518,6	13,76
5.1	892,4	947,4	519,1	12,84
5.2	857,7	913,1	497,8	13,34
6.1	923,1	977,1	536,8	12,26
6.2	854,2	911	499,1	13,79
7.1	892,2	962,3	533,6	16,35
7.2	881,7	944,8	528,5	15,16
8.1	895,4	965,5	536	16,32
8.2	878,6	943,1	525,8	15,46

Table B.2: Results on water porosity

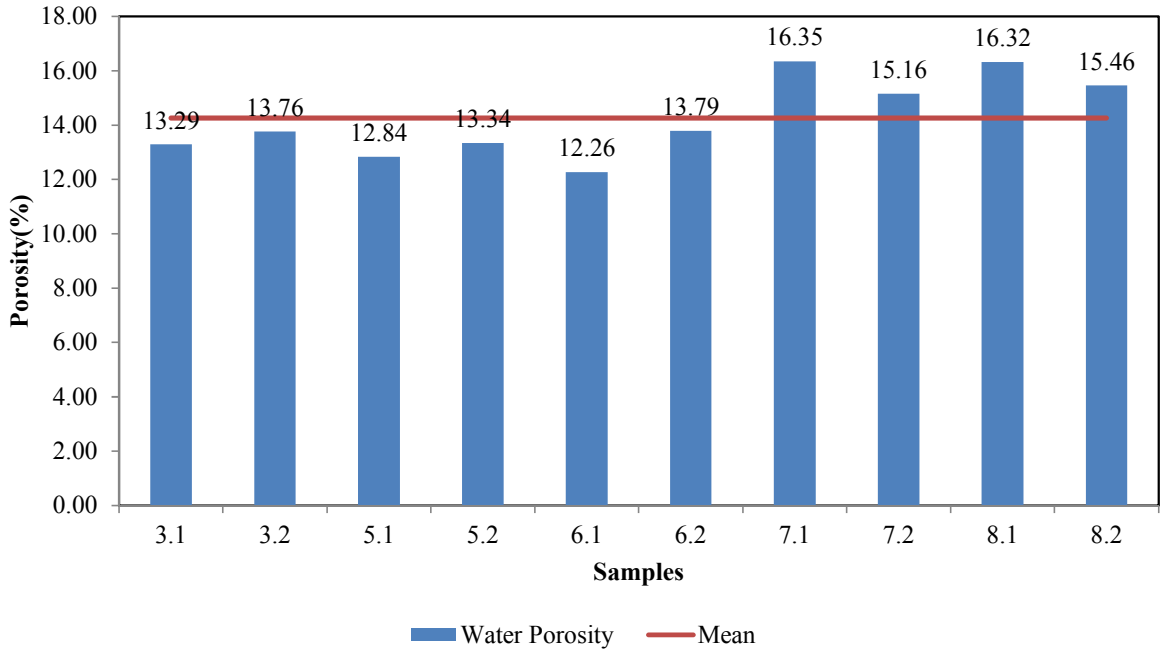

Figure B.4: Water porosity value and mean value

B.3. Intrinsic gas permeability

B.3.1. Gas permeability of the concrete

Permeability defines the ability of a material to be traversed by a fluid pressure gradient. The permeability of a porous medium is dependent not only on porosity, but also on the connectivity and tortuosity of the porous network constrictivity related to the pore size

B.3.2. Determination of the intrinsic permeability

This parameter can be determined in two ways, depending on whether the flow is laminar or turbulent. In this section, the determination of intrinsic permeability in case of laminar flow is investigated.

The intrinsic permeability k_v is evaluated by Klinkenberg approach. It is calculated from measurements of apparent permeability k_A for different injection pressures and is expressed by the following relationship:

$$k_A = k_v\left(1+\frac{\beta_k}{P_m}\right) \tag{B.3}$$

where P_m and β_k are respectively the mean pressure ($P_m=(P_1+P_2)/2$) and the coefficient β_k is the function depending on the porosity of the medium and infiltrated gas. It increases with the permeability of the medium.

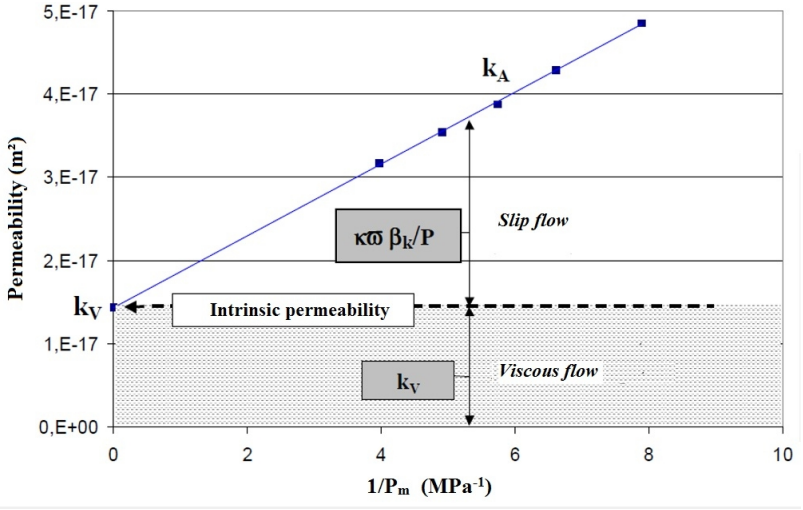

Figure B.5: Example and interpretation a graph $k_A=f(1/P_m)$ obtained from measurements experimental

Therefore, the intrinsic permeability of concrete subjected to a laminar flow of a gas can be determined by extrapolation (linear regression) shown in Figure B.5. The intrinsic permeability k_v is the limit value of the apparent k_A when gas permeability tends to a liquid phase.

B.3.3. Experimental equipment

The gas permeability was measured using the permeameter constant load type Cembureau. A diagram of the permeameter used is given Figure B.6. This device was used by Picandet (Picandet et al. 2001) determined that the flow rate by measuring with a stopwatch and visually the speed of an air bubble at the outlet of the cell permeability. To improve the flow measurement system was placed two mass flowmeter (EL flow) at the inlet and outlet of the cell permeability. They convert a mass flow in standard volumetric flow rate, in particular the pressure of 1013.25 bar and temperature of 0°C. The acquisition of flow measurement is automatically insured, continuously and in real time, thanks to a data logger. This allowed us to control the stabilisation of the flow and to minimise measurement errors.

The method for measuring gas permeability is to apply a pressure gradient to the sample until the stabilisation of the gas flow through the material (steady state). Permeability measurements were conducted in air-conditioned room at 20°C and 50% RH, with nitrogen gas as percolating. After being dried and coated with two layers of epoxy resin, the sample is placed in a suitable cell. The two flat sides rest on a corrugated plate to a uniform pressure distribution. Laterally, the sample is surrounded by a sleeve waterproof neoprene plated pressure air chamber.

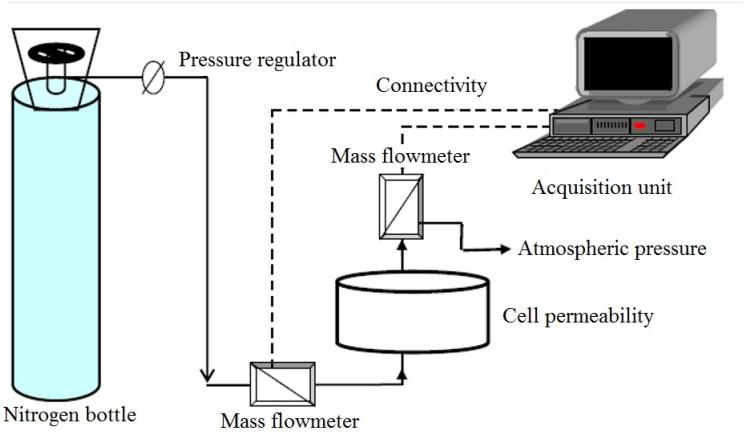

Figure B.6: Schematic of the experimental setup of the permeameter constant load

B.3.4. Measuring protocol

Once the drying is completed, the sample is removed from the oven and then placed in a desiccator at 20°C for 24 h, before being placed in the cell permeability. Each test includes permeability flow measurements on five differential pressures (P_i-P_{atm}) injection, which is generally around 0.1, 0.15, 0.2, 0.3 and 0.4 MPa. These pressures are adjusted each time according to the output rate of damage depending on the sample rate. The stability of the system is continuously monitored by following the evolution of the flow with time

B.3.5. Results

The intrinsic permeability is measured using the procedure described above. Different values of intrinsic permeability for different samples of concrete, determined by linear regression, are summarised in the Figure B.7 below:

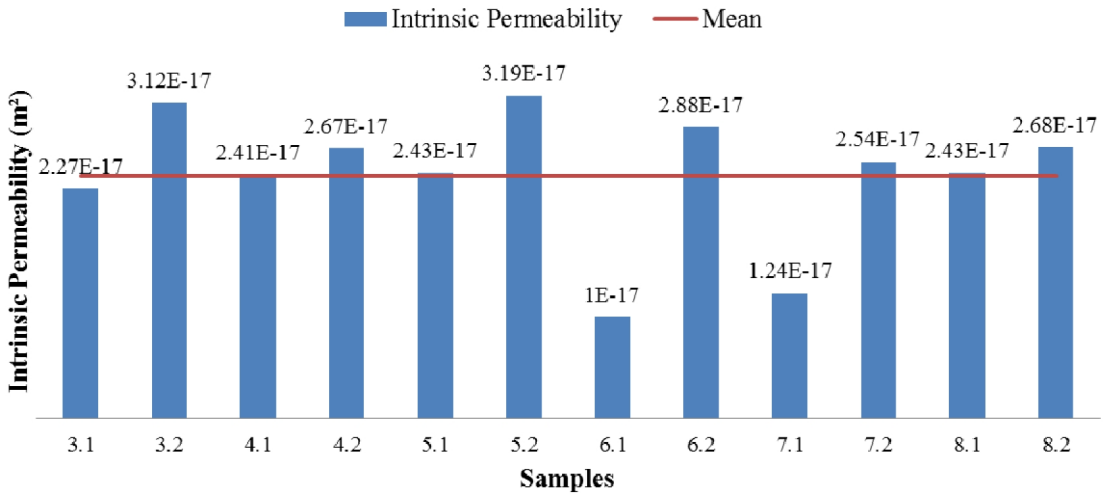

Figure B.7: Intrinsic permeability

B.4. Migration stationary of chloride ions in concrete

The objective of this experiment is to determine the effective chloride diffusion coefficient $D_{ediff.}$

B.4.1. Preparation of the experimental samples

There are three samples used in this all experiments, numbered 5.1; 6.1; 6.2, each sample are concrete discs with 10,5cm in diameter and 5cm in depth. Before starting the migration test, samples must be completely saturated. In this experiment, we used AFPC-AFREM modified procedure to saturate samples. This procedure is previously described in the porosity part.

B.4.2. Experimental equipment

The effective diffusion coefficient is determined in the stationary regime using a migration cell which has two electrodes supplying an applying electric field and therefore, accelerate the test (Figure B.8). In this experiment, the transportation of chloride ions is made by two driving forces: the difference in concentration of chloride through the concrete thickness and the applied electric.

After saturated in the desiccators, two compartments of the cell are fixed with the specimen on plate using the six threaded rods. During the first two days, the two compartments of the cell are filled with a base solution of 1g/l NaOH and 4,65g/l KOH to complete the saturation and also to check the system for leaks. Thereafter, the solution of upstream compartment is replaced by a basic charge solution of NaCl 30g/l in concentration which closes to that of seawater. For migration test (accelerated test), the electric field is applied via two electrodes: cathode (located in the upstream compartment) and anode (placed in the downstream compartment). These electrodes are connected to a DC voltage generator. The voltage passing through the sample will be measured using two reference electrodes connected to a voltmeter.

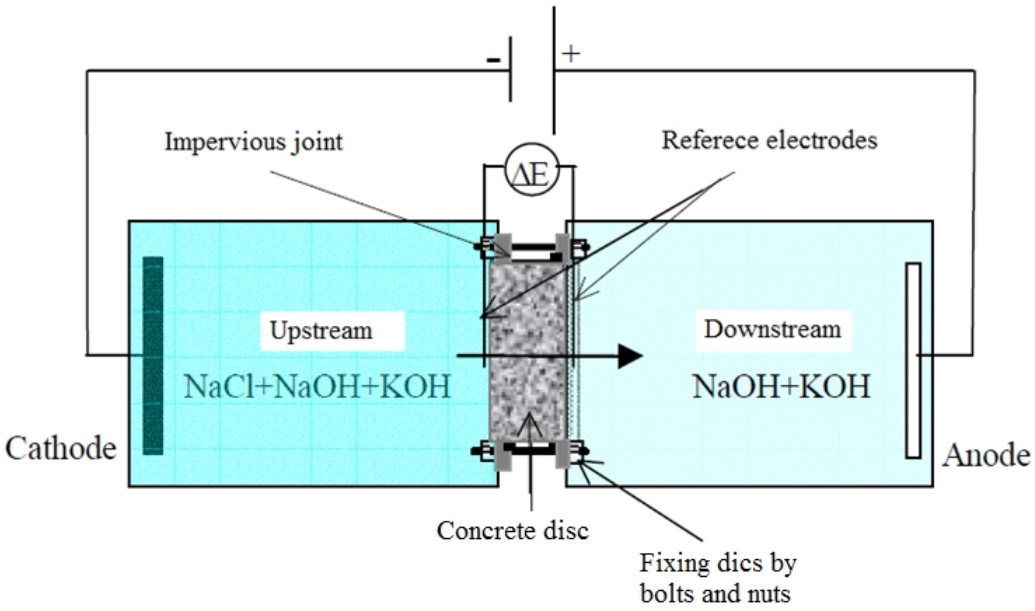

Figure B.8: Patterns of migration cell

B.4.3. Measuring protocol

All tests are carried out in a temperature controlled at 20±2°C and in 50% humidity room. The migration test begins after the upstream compartment filled with saline, the migration occurs when the electric fields is applied with a voltage of 12V is imposed and maintained during the test. These solutions are renewed once per day for the downstream compartment and once per week for the

upstream compartment and afterward being stored for analysing with titrator equipment. The test is stopped when the results shown a constant revolution of the cumulative chloride concentration versus time.

Two samples of 50ml downstream solution were assayed each times to determine the concentration of chloride. As shown in (Figure B.9) the analysis is carried out by potentiometer titration with AgNO3 0,05M using a titrator (Metrohm) equipped with an autosampler (13 samples) and an integrated software which records the measured results. The cumulative concentration of chloride ions versus time is then obtained with a curve. As described in Figure B.10, this curve usually has two parts:

- The non-stationary state where the evolution of the concentration versus time is not linear. This state can be defined as a period of time needs for chloride to pass through the specimen and saturate it.
- The steady state where the evolution of concentration is linear. In this state, the flux of chloride ions through the specimen becomes constant. The slope of this curve is used to determine the coefficient of diffusion.

Figure B.9: The potentiometer titrator

When a constant evolution of the figure is reached, the general equation describing transport process in solution is Nernst-Plank equation (ANDRADE 1993) which can be written as:

$$-J_i(x) = D_i \frac{\partial C_i}{\partial x} + \frac{z_i F}{RT} D_i C_i \frac{\partial E}{\partial x} + C_i V \qquad \text{(B.4)}$$

where:

J(x): unidirectional flux of ion i (mole/m²/s)

D_i: diffusion coefficient of ion i (m^2/s)

C_i: the concentration of ion i ($mole/m^3$)

z_i : the electrical charge of ion (with Cl^-, z=1).

F: the Faraday constant (96500 coulombs/mole)

R: the gas constant (8.31 Joule/mole/°K)

T: the absolute temperature (°K)

V: the velocity of solute (m/s)

In general, it can be seen that the unidirectional flux of ion *i* in downstream compartment is a function made of three components, that is:

Flux = diffusion + migration + convection

However, when chloride penetrates into specimen and saturates it, the concentration gradient decreases gradually to zeros and thus, the contribution of the first term in equation B.4 due to diffusion can be neglected. The third term of equation B.4 involving in convection could also be ignore if we just take into consideration what happens inside the specimen (ANDRADE 1993). Consequently, only the migration can be seen as an important factor affecting the flux. After consideration these assumptions, a new equation can be rewritten:

$$J_i(x) = -\frac{z_i F}{RT} D_i C_i \frac{\partial E}{\partial x} \tag{B.5}$$

In the steady state, it allows to make $\partial E/\partial x = \Delta E/L$, where L is the thickness of specimen. The effective chloride diffusion coefficient can be calculated as:

$$D_{eff} = \frac{RTJ}{zC_0 F\left(\frac{\Delta E}{L}\right)} \tag{B.6}$$

where:

$\Delta E/L$: the electrical field (V/m); where ΔE is the potential drop across the specimen.

C_0: the pore solution concentration (mol/m^3) at the surface; in this experiment, c_0 = 0.513 (mol/l)

J: the gradient of the linear part of the curve giving the constant flux at the steady state:

$$J = \frac{\Delta C}{\Delta t}\frac{V}{S}$$

where:

V: the volume of the downstream compartment of the cell (V = 1.82e-3 m^3)

S: the sample surface submitted to ionic transfer (m^2).

ΔC : the variation of the chloride concentration measured during a period of time Δt (Figure B.10)

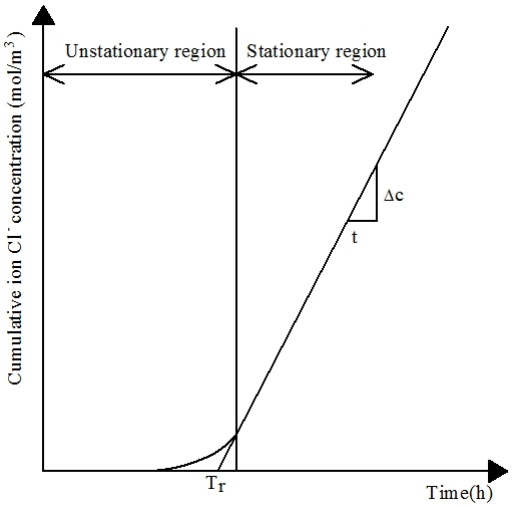

Figure B.10: Changing in cumulative chloride concentration versus time

B.4.4. Results

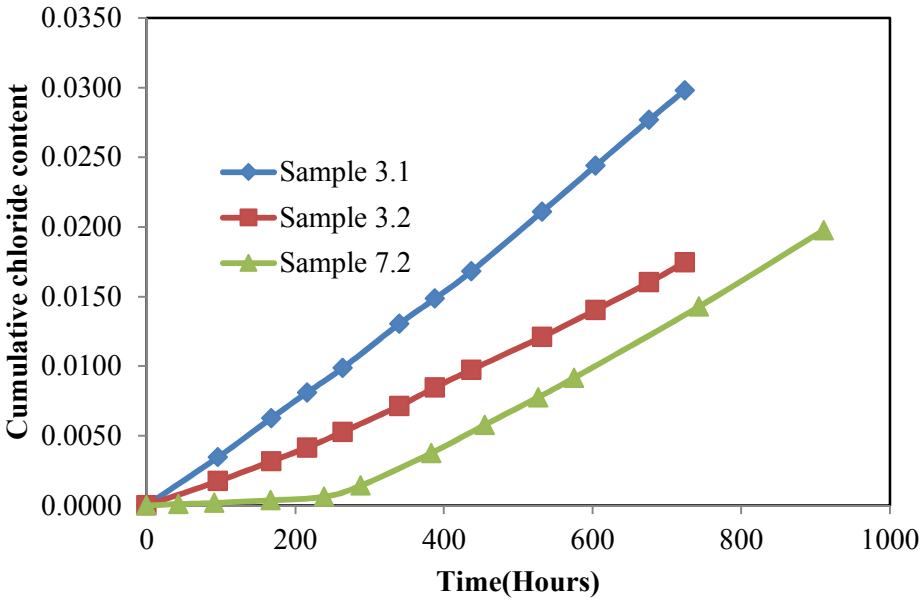

Figure B.11: The cumulative chloride content versus time at 5°C

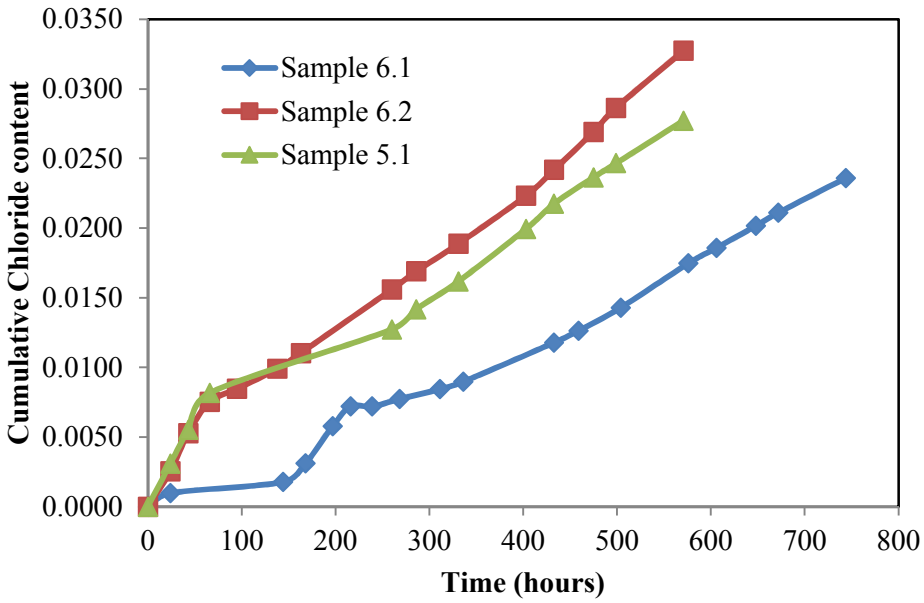

Figure B.12: Cumulative chloride content versus time at 20°C

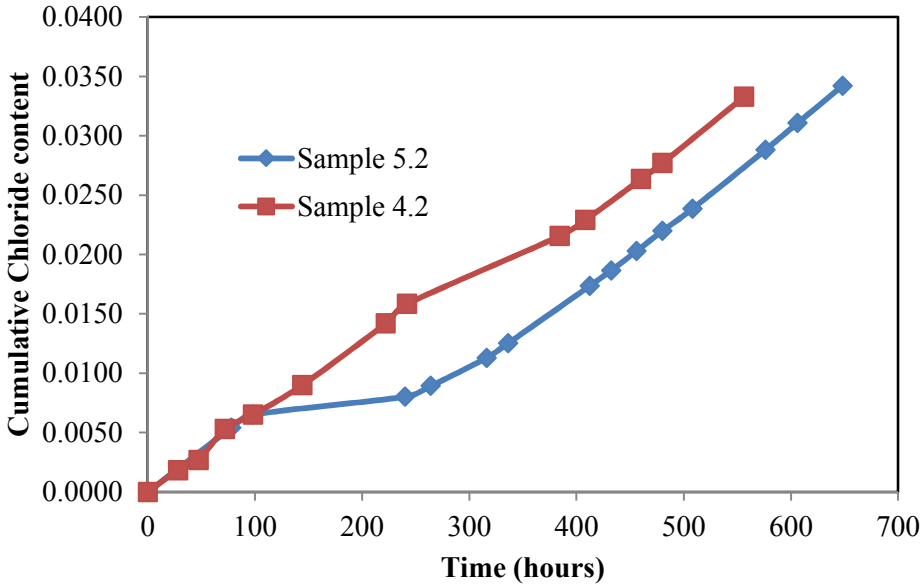

Figure B.13: The cumulative chloride content versus time at 40°C

Table B.3 presents values of effective diffusion coefficient determined at different temperatures (5°C, 20°C and 40°C). Choosing the effective diffusion coefficient at 5°C as an reference diffusion coefficient (D_{ref}=$D_{5°C}$), plotting the ratio D/D_{ref} versus temperature, we can obtain a curve (Figure B.14). The results are also compared with results in concrete from Samson and Marchand (2007b) and Yuan Q. Yuan (2009) and results in mortar from Nguyen et al. (2009). In both case for concrete and mortar, Figure B.14 describes an increasing trend in efficient diffusion coefficient with temperature. It

is worth noticing that while the experimental curve is close to the results found on concrete from Samson and Marchand (2007) and Yuan (2009) , there is a significant different in the slope of curve obtained from concrete and mortar with a higher slope is recorded for mortar from Nguyen et al. (2009). This can make a contribution to explain the differences in activation energy between concrete and mortar which is discussion more details in Appendix B.5.

Table B.3: Effective diffusion coefficients at different temperatures

T (°C)	Sample	D_{eff} .10^{-13}($m^2.s^{-1}$)	Mean .10^{-13}($m^2.s^{-1}$)
5	3,1	4,67	3,65
	3,2	2,83	
	7,2	3,44	
20	6,1	4,66	5,53
	6,2	5,86	
	5,1	6,06	
40	5,2	8,75	8,86
	4,2	8,96	

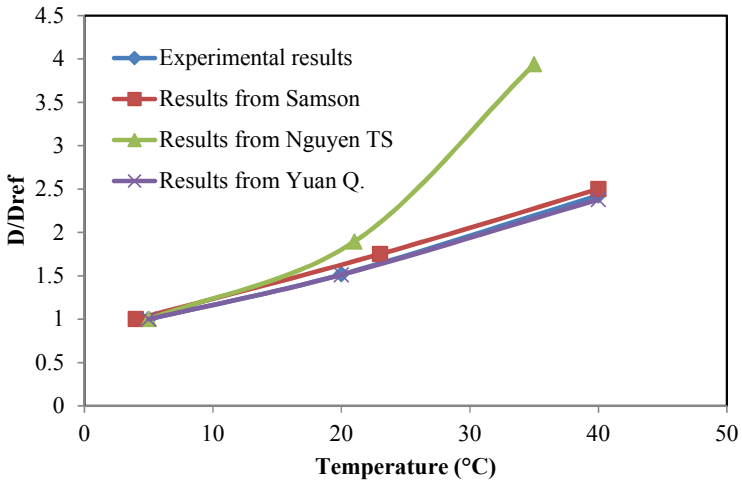

Figure B.14: The ratio D/D_{ref} at different temperature

B.5. Activation energy

The term “activation energy” was introduced by Svante Arrhenius in 1889 to define the minimum amount of energy required to start a chemical reaction. In chloride diffusion in concrete, the activation energy characterises the sensitivity of diffusion coefficient of concrete to temperature.

The determination of activation energy is mentioned previously by Nguyen et al. (2009); Page et al. (1981); and Samson and Marchand (2007). In our experiment, the activation energy will be

determined from stationary migration test at different temperatures: 5°C, 20°C and 40°C. The activation energy can be determined by plotting the log-variation of the chloride diffusion coefficient with the inversed of the temperature (Figure B.15). As can be seen from Figure B.15, the set of effective diffusion coefficient could be fitted with a straight line which can reveal that the dependence of diffusion coefficient on temperature T can be expressed by Arrhenius Equation B.7:

$$D(T) = D(T_0)\exp\left[\frac{E_a}{R}\left(\frac{1}{T_o} - \frac{1}{T}\right)\right] \tag{B.7}$$

where E_a is the energy of activation (J/mol), R is the gas constant (8.314 J/mol K), T is the temperature (K) and T_0 is the temperature of reference (K), $D(T)$ and $D(T_0)$ are diffusion coefficient at temperature T and T_0 respectively.

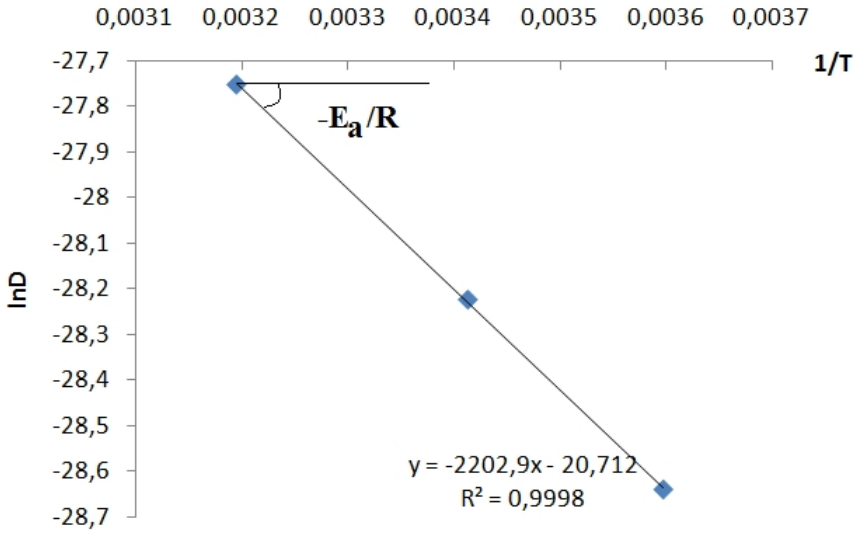

Figure B.15: Determining activation energy

From Figure B.15 and Equation B.7, a value of 18.3kJ/mole of activation energy E_a is determined. In literature, Page et al. (1981b) found that activation energy in OPC pastes were 41.8 kJ/mol, 44.6 kJ/mol and 32.0 kJ/mol corresponding to the water-to-cement ratio 0.4; 0.5 and 0.6 respectively. Collepardi et al. (1972) obtained a value of 35.6 kJ/mol for cement paste. Recently, Nguyen et al. (2009) carried out an accelerated test for the measurement of the chloride diffusion coefficient and the activation energy obtain obtained for material CEM-1 mortar and CEM-V mortar were 35.7 kJ/mol and 32.3 kJ/mol respectively. This means that the experimental result is considerable low as compared with these values. However, there results were archived from cement pastes or mortar, not from concrete. Chloride transport in concrete could be difference from that in cement paste or mortar due to the differences in porosity, mineral admixture and interface transition zone (ITZ) between these

materials. In contrast, the experimental value is agreement with results calculated from experimental data of Samson and Marchand (2007) (Table B.4) which indicates the activation energy in concrete ranging from 16.2 to 20.6 kJ/mol for concrete type T10 and from 13.3 to 26.8 for concrete type T50. A value of 18.3 kJ/mol of E_a is also concurrent with results archived on concrete by Yuan (2009) which indicates the activation energy of concrete ranges from 15.5 to 26.7 kJ/mol.

W/C	Hydration	Chloride diffusion coefficient (E-11 m²/s)						Activation energy	
		4°C		23°C		40°C		Ea (kJ/mole)	
	(days)	Type 10	Type 50	Type 10	Type 50	Type 10	Type 50	Type 10	Type 50
0,45	28	3,2	7,1	5,6	11,0	8,0	13,7	18,4	13,3
	91	3,0	4,5	5,2	7,5	6,7	11,3	16,2	18,4
	365	2,6	4,5	4,4	7,5	7,1	13,5	20,1	21,8
0,65	28	5,3	7,7	8,3	13,0	12,9	19,7	17,7	18,8
	91	5,3	7,3	8,0	11,4	14,5	19,7	19,9	19,7
	365	6,2	6,6	9,1	12,8	15,7	25,3	18,4	26,8
0,75	28	6,1	10,7	10,5	15,7	16,1	25,4	19,4	17,2
	91	6,7	9,4	11,5	15,0	18,8	23,1	20,6	17,9
	365	7,4	10,3	11,9	16,7	19,4	27,0	19,2	19,2

Table B.4: Activation energy calculated from Samson and Marchand (2007)

B.6. Chloride binding isotherms

B.6.1. Preparation of samples

The concrete discs numbered 1.1; 1.2; 2.1; 2.2; 9.1; 9.2 were dried at 60°C in the oven until the weight can reach constant value. Next, these discs were crushed and particles sized between 0.25-2.5mm were retained for further experiment. Afterwards, these particulate samples were stored in oven at 60°C.

B.6.2. Experimental procedures

6 small plastic boxes containing 6 solutions of NaOH and KOH with the different concentrations of NaCl: 0.05M, 0.25M, 0.5M, 1M, 1.5M, 2M were prepared (Table B.5). The volume solution in each box was 2 litres and about 150g of particulate sample was put into each box. These small boxes were sealed and stored in a room which temperature is maintained at 20°C for equilibrium. Every week, we take a volume of 2ml solution (for solution with concentration of NaCl: 0.05M, 0.25M, 0.5M) to determine the chloride concentration by potentionmetric titrarion using 0.05M $AgNO_3$. For solution with the concentration of NaCl is higher (solution 4, solution 5, solution 6), 2ml of each solution was taken to make a dilution with 100ml demineralise water. Thereafter, a volume of 10ml

solution after dilution was pippetted to determine the chloride concentration. When the equilibrium of solution is reached, the content of bound chlorides absorb to the solid phase could be calculated by the following equation:

$$C_b = \frac{M_{Cl}.V.\left(C_{ini} - C_{(t)}\right)}{w} \tag{B.8}$$

Where: C_b : the bound amount of chloride (*g/kg* of dry sample)

M_{Cl} : molar mass of chloride (M_{Cl} = 35.453 g/mol)

V : volume of solution (V=*2* littre)

C_{ini} : the initial concentration (mol/l)

$C_{(t)}$: the chloride concentration at time t .

w : weight of dry sample (w = 150g = 0.15kg)

Solution	NaCl	NaOH	KOH
	(mol/l)	(g/l)	(g/l)
Solution 1	0,05	1	4,65
Solution 2	0,25	1	4,65
Solution 3	0,5	1	4,65
Solution 4	1	1	4,65
Solution 5	1,5	1	4,65
Solution 6	2	1	4,65

Table B.5: 6 Solutions

Using non-linear Freundlich-type equations to fit the experimental data, the shape of the curve is similar to those obtained from BEN FRAJ (2009). The experimental points fit the curve with correlation coefficient R^2= 9.366 (Figure B.16).

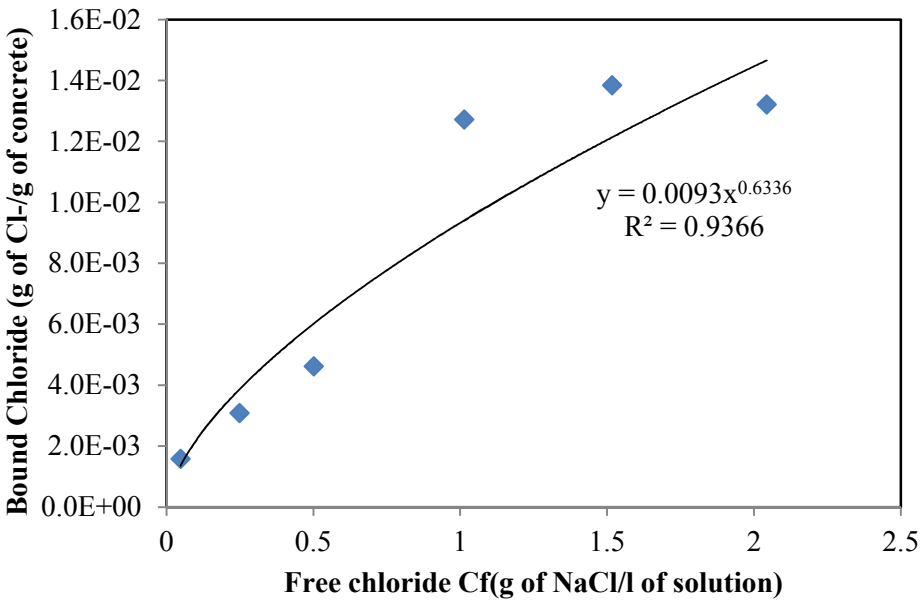

Figure B.16: Chloride binding isotherms

The isotherms equation obtained describes chloride binding isotherms is:

$$C_b = 0.0093 \times C_f^{0.6336}$$

B.7. Water vapour absorption

B.7.1. Water vapour absorption isotherms

The principle of this experiment is putting specimens in a sealed plastic box, where temperature and humidity are maintained at constant values. Every week, the specimens are weighted regularly and the test is finished when an equilibrium state can reach. As such gravimetric experiment could require long time to get the equilibrium (Poyet 2009), samples in small dimensions should be used. In this experiment, to reduce the experimental duration, the specimen is concrete crushed with size between 0.25mm-2.5mm.

Each samples is stored in a plastic cup to avoid corrosion problems. Six plastic boxes were used and in each box, a container filled with a volume of 2 liters solution is placed at the bottom, which can produce and maintain a constant relative humidity inside the box during the experiment. Table B.6 reveals the relative humidity produced by 6 chemical solutions in practice and in theory. The difference between measured values and theoretical values can be explained due to condensation.

The mass water content could be calculated as the mass variation of the samples for each relative humidity by following equation:

$$m_{water} = \left(\frac{\Delta m}{m}\right)(t) = \frac{m(t) - m_0}{m_0} \tag{B.9}$$

where: m_{water} is the mass water content (g/g), m_0 (g) and $m(t)$ (g) are initial samples mass and the mass at time t.

No	Product description	Fomulation	Humidity (%)	
			Theoretical value	Measured value
1	Potassium Sulfate Anhydre poudre	K_2SO_4	97	86
2	Sodium Chlorure PA	NaCl	76	73,5
3	Magnesium Nitrate Hexahydrate PA	$Mg(NO_3)_2.(H_2O)_6$	55	57
4	Potassium Chlorure PA	KCl	86	79,8
5	Ammonium Nitrate for Analysis 99	NH_4NO_3	65	65,4
6	Magnesium Chloride Anhydrous PUR	$MgCl_2$	33	46,8

Table B.6: Relative humdity measured comparing with theory

The change of mass water content for different relative humilities are described in Figure B.17.

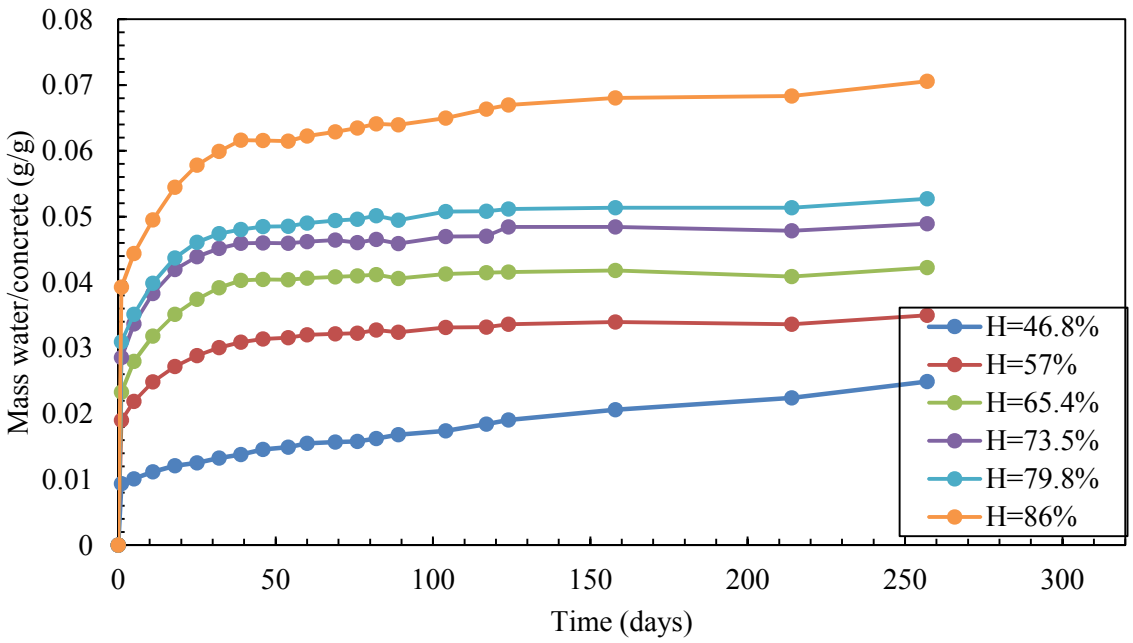

Figure B.17: Water absorption kinetic without chloride contaminated

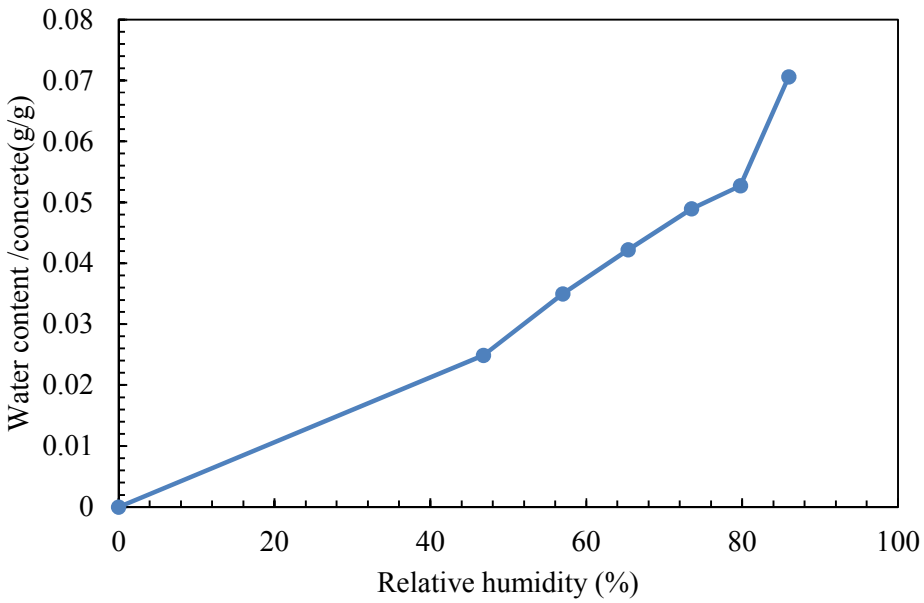

Figure B.18: Isotherm absorption for concrete without chloride contaminated

B.7.2. Effect of chloride contamination on water vapour absorption

In this section, concrete samples contaminated with chloride in different concentration from the chloride binding isotherm are used to evaluate the influence of chloride contamination (chloride/matrix interaction) on the equilibrium moisture properties. The water content at equilibrium is highest for relative humidity at 86%, especially for concrete samples contaminated with high chloride concentration (C=60 g/l, C=90 g/l, C=120 g/l).There is a clear trend for all cases that, the equilibrium water content increases with the chloride concentration. These characteristics are also observed by (Ben Fraj et al. 2012).

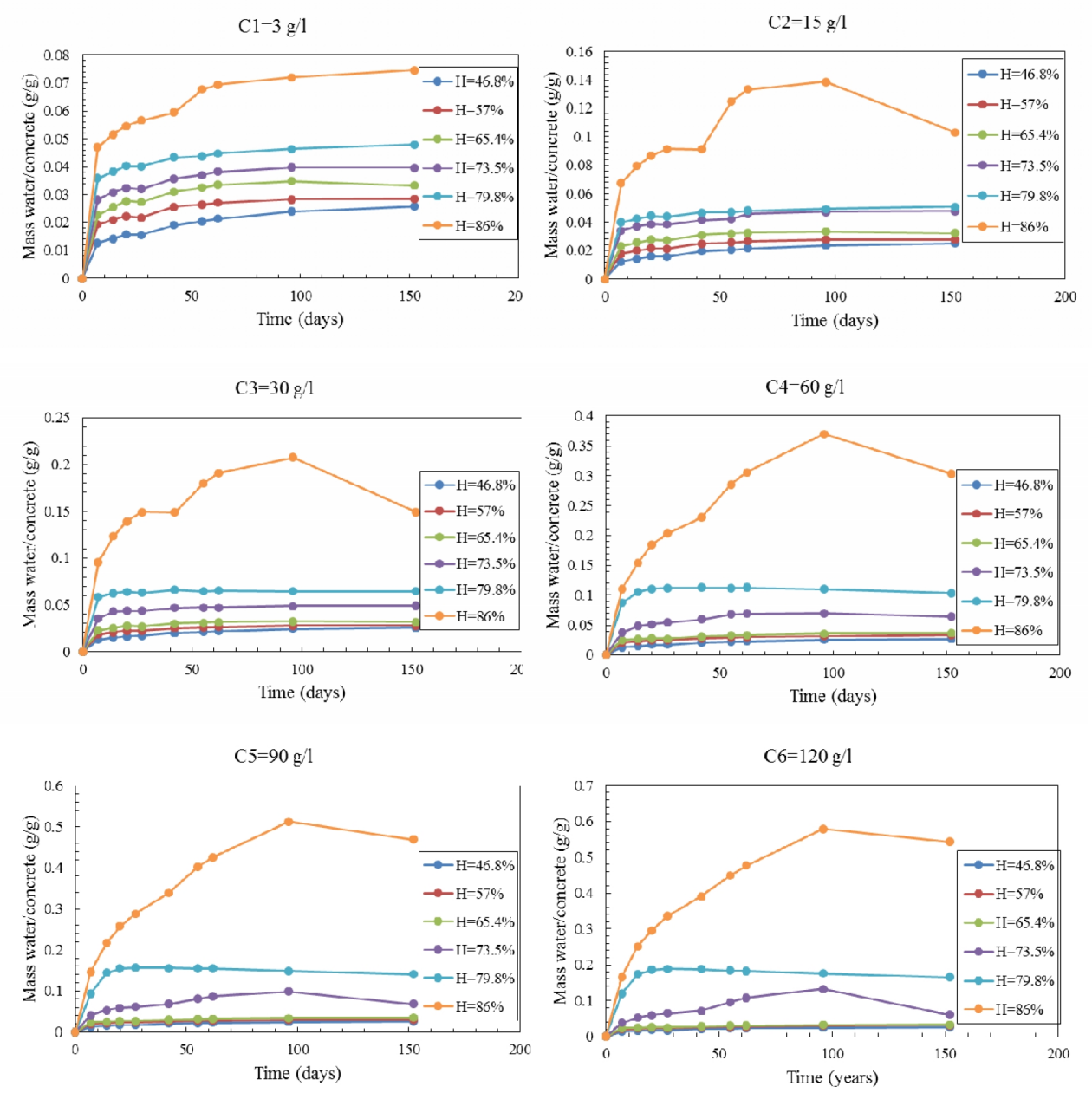

Figure B.19: Water absorption kinetic in concrete with chloride contaminated

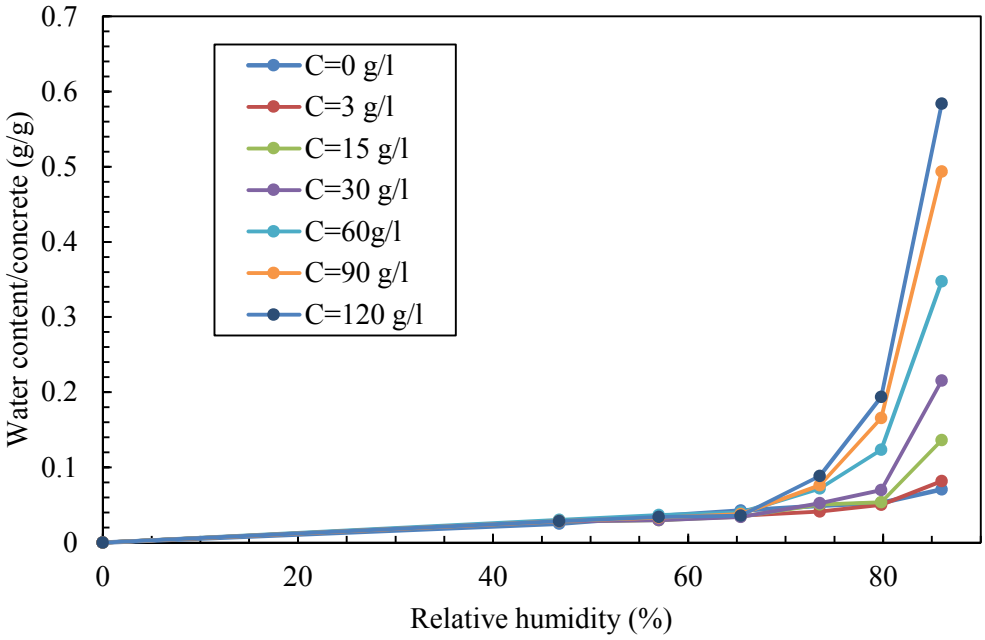

Figure 5: Isotherm absorption for concrete with chloride contaminated

Bibliography

Ababneh, A., Benboudjema, F., and Xi, Y. (2003). "Chloride Penetration in Nonsaturated Concrete." *Journal of Materials in Civil Engineering*, (15), 183–191.

Al, L. I. (2014). "Comparing between Maximum Likelihood and Least Square Estimators for Gompertz Software Reliability Model." *International Journal of Software Engineering & Application*, 5(4), 51–61.

ANDRADE, C. (1993). "Calculation of chloride diffusion coefficient in concrete from ionic migration measurements." *Cement and Concrete Research*, 23, 724–742.

Baroth, J., Schoefs, F., and Breysse, D. (2011). *Construction Reliability: Safety, Variability and Sustainability*.

Bastidas-Arteaga, E. (2010). "Contribution for sustainable management of reinforced concrete structures subjected to chloride penetration." PhD Thesis, University of Nantes.

Bastidas-Arteaga, E., Bressolette, P., Chateauneuf, A., and Sánchez-Silva, M. (2009). "Probabilistic lifetime assessment of RC structures under coupled corrosion–fatigue deterioration processes." *Structural Safety*, Elsevier Ltd, 31(1), 84–96.

Bastidas-Arteaga, E., Chateauneuf, A., Sánchez-Silva, M., Bressolette, P., and Schoefs, F. (2011). "A comprehensive probabilistic model of chloride ingress in unsaturated concrete." *Engineering Structures*, 33, 720–730.

Bastidas-Arteaga, E., and Schoefs, F. (2012). "Stochastic improvement of inspection and maintenance of corroding reinforced concrete structures placed in unsaturated environments." *Engineering Structures*, 41, 50–62.

Bastidas-Arteaga, E., and Schoefs, F. (2015). "Sustainable Maintenance and Repair of RC Coastal Structures." *Maritime Engineering*.

Bastidas-Arteaga, E., Schoefs, F., and Bonnet, S. (2012). "Bayesian identification of uncertainties in

chloride ingress modeling into reinforced concrete structures." *Third International Symposium on Life-Cycle Civil Engineering (IALCCE)*.

Bastidas-Arteaga, E., Schoefs, F., Chateauneuf, A., Breysse, D., Sheils, E., and O'Connor, A. (2010a). "Stochastic approach for the optimization of inspection intervals of RC structures subjected to chloride penetration." *MEDACHS10 International Congress*, La Rochelle.

Bastidas-Arteaga, E., Schoefs, F., Chateauneuf, A., Sánchez-Silva, M., and Capra, B. (2010b). "Probabilistic evaluation of the sustainability of maintenance strategies for RC structures exposed to chloride ingress." *International Journal of Engineering Under Uncertainty*, 2, 61–74.

Bensi, M., Der Kiureghian, A., and Straub, D. (2011a). "Bayesian network modeling of correlated random variables drawn from a Gaussian random field." *Structural Safety*, Elsevier Ltd, 33(6), 317–332.

Bensi, M. T., Der Kiureghian, A., and Straub, D. (2011b). *A Bayesian Network Methodology for Infrastructure Seismic Risk Assessment and Decision Support*. University of California,Berkeley.

Bertolini, L., Elsener, B., Pedeferri, P., and Polder, R. (2004). *Corrosion of Steel in Concrete*. *Corrosion*, (R. W. Revie, ed.), WILEY.

Bhide, S. (1999). *Material Usage and Condition of Existing Bridges in the U.S. Technical Report SR342, Portland Cement Association*, Skokie, Illinois, US.

Bioubakhsh, S. (2011). "The penetration of chloride in concrete subject to wetting and drying: measurement and modelling." University College London.

Blatman, G., and Sudret, B. (2010). "An adaptive algorithm to build up sparse polynomial chaos expansions for stochastic finite element analysis." *Probabilistic Engineering Mechanics*, Elsevier Ltd, 25(2), 183–197.

Broomfield, J. (2006). *Corrosion of Steel in Concrete*. Taylor and Francis.

Collepardi, M., Marciallis, A., and Turriziani, R. (1972). "Penetration of chloride ions in cement pastes and in concretes." *Journal of the American Ceramic Society*, 55(10), 534–535.

Daly, A. . (2000). "Bridge management in Europe (BRIME): Modeling of deteriorated structures." *Bridge Management 4-Inspection, maintenance, assessment and repair*.

Deby, F., Carcasses, M., and Sellier, A. (2008). "Toward a probabilistic design of reinforced concrete durability: application to a marine environment." *Materials and Structures*, 42(10), 1379–1391.

Deby, F., Carcasses, M., and Sellier, A. (2012). "Simplified models for the engineering of concrete formulations in a marine environment through a probabilistic method." *European Journal of Environmental and Civil Engineering*, 16(3-4), 37–41.

De-León-Escobedo, D., Delgado-Hernández, D.-J., Martinez-Martinez, L.-H., Rangel-Ramírez, J.-G.,

and Arteaga-Arcos, J.-C. (2013). “Corrosion initiation time updating by epistemic uncertainty as an alternative to schedule the first inspection time of pre-stressed concrete vehicular bridge beams.” *Structure and Infrastructure Engineering*, 10(8), 1–13.

Djerbi, a., Bonnet, S., Khelidj, a., and Baroghel-bouny, V. (2008). “Influence of traversing crack on chloride diffusion into concrete.” *Cement and Concrete Research*, 38(6), 877–883.

Duprat, F. (2007). “Reliability of RC beams under chloride-ingress.” *Construction and Building Materials*, 21, 1605–1616.

Duracrete. (2000a). *Statistical quantification of the variables in the limit state functions, DuraCrete - Probabilistic Performance based Durability Design of Concrete Structures, EU - Brite EuRam III, Contract BRPR-CT95-0132, Project BE95-1347/R9*.

Duracrete. (2000b). *Probabilistic performance based durability design of concrete structures.* The European Union-Brite EuRam III. Project BE95-1347.

Ebrahim Abbas, E.Weyers, R., William J.Wright, and Roberts-Wollmann, C. L. (2014). *Corrosion Assessment for the Failed Bridge Deck Closure Pour at Mile Marker 43 on I-81*. Virginia.

Engelund, S., and Sorensen, J. D. (1998). “A probabilistic model for chloride-ingress and initiation of corrosion in reinforced concrete structures.” *Structural Safety*, 20(1), 69–89.

Enright, M. P., Member, A., and Frangopol, D. M. (1999). “Condition prediction of deteriorating concrete bridges using Bayesian updating.” *Journal of Structural Engineering ASCE*, 125(10), 1118–1125.

BEN FRAJ, A. (2009). “Transfert dans les bétons non saturés : Influence des laitiers et de l ’ endommagement mécanique Introduction générale Contexte de l ’ étude et problématique.” PhD Thesis, University of Nantes.

Ben Fraj, A., Bonnet, S., and Khelidj, A. (2012). “New approach for coupled chloride/moisture transport in non-saturated concrete with and without slag.” *Construction and Building Materials*, Elsevier Ltd, 35, 761–771.

Geocisa, and the Torroja Institute. (2002). *Contecvet: A validated users manual for assessing the residual service life of concrete structures. Manual for assessing corrosion-affected concrete structures. Annex {C} Calculation of a representative corrosion rate*. British Cement Association, UK.

Ghanem, R. G., and Spanos, P. D. (1991). *Stochastic Finite Elements: A Spectral Approach*. Springer, New York, USA.

Gilks, W. R., Richardson, S., and Spiegelhalter, D. J. (1996). “Markov Chain Monte Carlo in Practice.” *Technometrics*, Chapman & Hall, London.

Gjorv, E. (2009). *Durability Design of Concrete Structures in Severe Environment*. Taylor and Francis.

Gulikers, J. (2003). "Practical Relevance of Service Life Modeling of Steel Reinforced Concrete Structures." *Proceedings: Joint JCSS, fib and LCC03 workshop on Life-Cycle Cost Analysis and Design of Civil Infrastructure Systems and Probabilistic Modeling of Deterioration Process in Concrete Structures*, EPFL, Lausanne, Switzerland, 312–318.

Hackl, J. (2013). "Generic Framework for Stochastic Modeling of Reinforced Concrete Deterioration Caused by Corrosion." Master Thesis, Norwegian University of Science and Technology.

El Hassan, J., Bressolette, P., Chateauneuf, A., and El Tawil, K. (2010). "Reliability-based assessment of the effect of climatic conditions on the corrosion of {RC} structures subject to chloride ingress." *Engineering Structures*, 32(10), 3279–3287.

Heckerman, D. (1997). *Bayesian Networks for Data Mining*. Springer.

Hofmann, R., and Tresp, V. (1996). "Discovering structure in continuous variables using Bayesian networks." *Advances in Neural Information Processing Systems*, (1988), 500–506.

Holland, D. . (1990). "Bridge Rehabilitation: Department of Transport's Fifteen-Year Strategy." *Bridge Management*, Springer US, 135–143.

Hong, K. (1998). "Cyclic wetting and drying and its effects on chloride ingress in concrete." MSc Thesis, University of Toronto.

Hosni Elhewy, A., Mesbahi, E., and Pu, Y. (2006). "Reliability analysis of structures using neural network method." *Probabilistic Engineering Mechanics*, 21(1), 44–53.

Huber, N., and Tsakmakis, C. (2001). "A neural network tool for identifying the material parameters of a ® nite deformation viscoplasticity model with static recovery." *Computer Methods in Applied Mechanics and Engineering*, 191, 353–384.

Keßler, S., Fischer, J., Straub, D., and Gehlen, C. (2013). "Updating of service - life prediction of reinforced concrete structures with potential mapping." *Cement and Concrete Composites*, 47, 47–52.

Khitab, A. (2005). "Modélisation des transferts ioniques dans les milieux poreux saturés: application à la pénétration des chlorures à travers les matériaux cimentaires." Institute National of Applied Science of Toulouse.

Koch, G. H., Brongers, M. P. H., Thompson, N. G., Virmani, Y. P., and Payer, J. . (2002). *Corrosion Costs and Preventive Strategies in the United States*. *Publication No. FHWA-RD-01-156*, Federal Highway Administration, Washington, D.C.

Kumar Mehta, P. (2004). "High-performance, high-volume fly ash concrete for sustainable

development." *International Workshop on Sustainable Development and Concrete Technology*, K. Wang, ed., Center for Transportation Research and Education, Iowa State University, USA, Beijing, China, 3–14.

Lee, D. (1990). "Comparative Maintenance Costs of Different Bridge Types." *Bridge Management*, Springer US, 145–153.

Lemaire, M., Chateauneuf, A., and Mitteau, J.-C. (2010). *Structural Reliability*.

Li, Y. (2004). "Effect of Spatial Variability on Maintenance and Repair Decisions for Concrete Structures." PhD Thesis, Delft University.

Lounis, D. Z., and Amleh, L. (2003). "Reliability-Based Prediction of Chloride Ingress and Reinforcement Corrosion of Aging Concrete Bridge Decks." *Proceeding of the 3rd International IABMAS Workshop on Life-Cycle Cost Analysis and Design of Civil Infrastructure Systems*, D. M. Frangopol, E. Bruhwiler, M. H. Faber, and B. Adey, eds., American Society of Civil Engineers, Lausanne, Switzerland, 139–147.

Luping, T., and Gulikers, J. (2007). "On the mathematics of time-dependent apparent chloride diffusion coefficient in concrete." *Cement and Concrete Research*, 37, 589–595.

Luping, T., Nilsson, L., and Basheer, P. a M. (2012). *Resistance of Chlorides to Chloride Ingress: Testing and Modelling*. Taylor and Francis.

Ma, Y., Wang, L., Zhang, J., Xiang, Y., and Liu, Y. (2014). "Bridge Remaining Strength Prediction Integrated with Bayesian Network and In Situ Load Testing." *Journal of Bridge Engineering ASCE*, 19(10), 1–11.

Ma, Y., Zhang, J., Wang, L., and Liu, Y. (2013). "Probabilistic prediction with Bayesian updating for strength degradation of RC bridge beams." *Structural Safety*, Elsevier Ltd, 44, 102–109.

Martín-Pérez, B., Pantazopoulou, S. J., and Thomas, M. D. A. (2001). "Numerical solution of mass transport equations in concrete structures." *Computers and Structures*, 79, 1251–1264.

McDonald, R. (2013). "Algo Centre Mall Collapse." *Failures Wiki*.

Moore, G., and Emerton, G. (2010). *A report on the impact of failure of infrastructure assets through corrosion as a result of current practices and skilling in the Australian mainland urban water and Naval defence sectors*.

Murphy, K. P. (2001). "The Bayes Net Toolbox for Matlab." *Computing Science and Statistics*.

Myung, I. J. (2003). "Tutorial on maximum likelihood estimation." *Journal of Mathematical Psychology*, 47(1), 90–100.

Nguyen, T. S., Lorente, S., and Carcasses, M. (2009). "Effect of the environment temperature on the chloride diffusion through CEM-I and CEM-V mortars: An experimental study." *Construction*

and Building Materials, Elsevier Ltd, 23(2), 795–803.

Nguyen, X. S. (2007). "Algorithmes probabilistes appliqués à la mécanique des ouvrages de génie civil." PhD Thesis, INSA de Toulouse.

Nielsen, E. P., and Geiker, M. R. (2003). "Chloride diffusion in partially saturated cementitious material." *Cement and Concrete Research*, 33(1), 133–138.

Nilsson, L.-O., and Carcasses, M. (2004). *Models for Chloride Ingress into Concrete - A Critical Analysis*. Report of Task 4.1 in EU-Project G6RD-CT2002-00855, ChlorTest.

Nogueira, C. G., and Leonel, E. D. (2013). "Probabilistic models applied to safety assessment of reinforced concrete structures subjected to chloride ingress." *Engineering Failure Analysis*, Elsevier Ltd, 31, 76–89.

O'Connor, A. J., and Kenshel, O. (2013). "Experimental Evaluation of the Scale of Fluctuation for Spatial Variability Modeling of Chloride-Induced Reinforced Concrete Corrosion." *Journal of Bridge Engineering*, (January), 3–14.

Page, C., Short, N., and Tarras, A. E. (1981). "Diffusion of chloride ions in hardened cement pastes." *Cement and Concrete Research*, 11(3), 395–406.

Pearl, J. (1991). "Probabilistic reasoning in intelligent systems: Networks of plausible inference." *International Journal of Bio-Medical Computing*, Morgan Kaufmann, San Francisco, California.

Pence, B. L., Fathy, H. K., and Stein, J. L. (2011). "Recursive maximum likelihood parameter estimation for state space systems using polynomial chaos theory." *Automatica*, Elsevier Ltd, 47(11), 2420–2424.

Picandet, V., Skoczylas, M. F., and Khelidj, M. A. (2001). "INFLUENCE D ' UN ENDOMMAGEMENT MÉCANIQUE SUR LA PERMÉABILITÉ ET SUR LA DIFFUSIVITÉ."

Du Plooy, R., Palma Lopes, S., Villain, G., and Derobert, X. (2013). "Development of a multi-ring resistivity cell and multi-electrode resistivity probe for investigation of cover concrete condition." *NDT&E International*, 54, 27–36.

Poupard, O., L'Hostis, V., Catinaud, S., and Petre-Lazar, I. (2006). "Corrosion damage diagnosis of a reinforced concrete beam after 40 years natural exposure in marine environment." *Cement and Concrete Research*, 36, 504–520.

Poyet, S. (2009). "Experimental investigation of the effect of temperature on the first desorption isotherm of concrete." *Cement and Concrete Research*, Elsevier Ltd, 39(11), 1052–1059.

Rasheeduzzafar, H. ., Dakhil, F. ., Bader, M. ., and Khan, M. . (1992). "Performance of corrosion resisting steel in chloride-bearing concrete." *ACI Materials Journal*, (89(5)), 439–448.

Richard, B., Adelaide, L., and Cremona, C. (2012). "A Bayesian approach to estimate material properties from global statistical data." *European Journal of Environmental and Civil Engineering*, (March 2013), 37–41.

Robinson, J. W., and Hartemink, A. J. (2010). "Learning Non-Stationary Dynamic Bayesian Networks." *The journal of Machine Learning Research*, 11, 3647–3680.

Rui, Z., and Bivens, A. (2007). "Comparing the Use of Bayesian Networks and Neural Networks in Response Time Modeling for Service-oriented." *Proceeding of the 2007 workshop on Service-oriented computing performance: aspects, issues, and approaches*, New York, USA, 67–74.

Russell, S., and Norvig, P. (2010). *Artificial Intelligent: A Modern Approach*. Prentice-Hall,Upper Saddle River, N.J.

Saassouh, B., and Lounis, Z. (2012). "Probabilistic modeling of chloride-induced corrosion in concrete structures using first- and second-order reliability methods." *Cement and Concrete Composites*, Elsevier Ltd, 34(9), 1082–1093.

Saetta, A., Scotta, R., and Vitaliani, R. (1993). "Analysis of chloride diffusion into partially saturated concrete." *ACI Materials Journal*, 90(5), 441–451.

Samarakoon, S. . S. M. ., and Sælensminde, J. (2015). "Condition assesSment of reinforced concrete structures subject to chloride ingress: A case study of UPdating the model prediction considering inspection data." *Cement and Concrete Composites*, Elsevier Ltd, 60, 92–98.

Samson, E., and Marchand, J. (2007). "Modeling the effect of temperature on ionic transport in cementitious materials." *Cement and Concrete Research*, 37(3), 455–468.

Schoefs, F. (2008). "Sensitivity approach for modelling the environmental loading of marine structures through a matrix response surface." *Reliability Engineering and Systems Safety*, 93, 1004–1017.

Schoefs, F., Boéro, J., Clément, A., and Capra, B. (2012). "The αδ method for modelling expert judgement and combination of non-destructive testing tools in risk-based inspection context: application to marine structures." *Structure and Infrastructure Engineering*, 8(6), 531–543.

Sepahvand, K., and Marburg, S. (2013). "On Construction of Uncertain Material Parameter using Generalized Polynomial Chaos Expansion from Experimental Data." *Procedia IUTAM*, 6, 4–17.

Soize, C. (2010). "Identification of high-dimension polynomial chaos expansions with random coefficients for non-Gaussian tensor-valued random fields using partial and limited experimental data." *Computer Methods in Applied Mechanics and Engineering*, Elsevier B.V., 199(33-36), 2150–2164.

Straub, D. (2009). "Stochastic Modeling of Deterioration Processes through Dynamic Bayesian Networks." *Journal of Engineering Mechanics*, 135(10), 1089–1099.

Straub, D., and Der Kiureghian, A. (2010). "Bayesian Network Enhanced with Structural Reliability Methods: Application." *Journal of Engineering Mechanics*, 136(10), 1259–1270.

Suo, Q., and Stewart, M. G. (2009). "Corrosion cracking prediction updating of deteriorating RC structures using inspection information." *Reliability Engineering & System Safety*, 94(8), 1340–1348.

Tang, L., and Nilsson, L. (1996). "A numerical method for prediction of chloride penetration into concrete structures." *NATO/RILEM Workshop on the modelling of Microstructure and its Potential for Studying Transport Properties and Durability*, Kluwer, Dordrecht, The Netherlands, 539–552.

Tang, L., and Nilsson, L. O. (1993). "Chloride binding capacity and binding isotherms of OPC pastes and mortars." *Cement and Concrete Research*, 23, 247–253.

Tu, J. V. (1996). "Advantages and disadvantages of using artificial neural networks versus logistic regression for predicting medical outcomes." *Journal of clinical epidemiology*, 49(11), 1225–1231.

Tuutti, K. (1982). *Corrosion of steel in concrete*. Swedish Cement and Concrete Institute.

Virmani, Y. P. (2002). *Corrosion cost and preventive strategies. Publication No . FHWA-RD-01-156*.

Vu, K. A. T., and Stewart, M. G. (2000). "Structural reliability of concrete bridges including improved chloride-induced corrosion." *Structural Safety*, 22, 313–333.

Wang, J., and Liu, X. (2010). "Evaluation and Bayesian dynamic prediction of deterioration of structural performance." *Structure and Infrastructure Engineering*, 6(6), 663–674.

Wikipedia. (2009). "Silver Bridge." *Wikipedia*, <http://en.wikipedia.org/wiki/Silver_Bridge>.

Wikipedia. (2012). "Mianus River Bridge." *Wikipedia*, <http://en.wikipedia.org/wiki/Mianus_River_Bridge>.

Yadaiah, N., Sivakumar, L., and Deekshatulu, B. L. (2000). "Parameter identification via neural networks with fast convergence." *Mathematics and Computers in Simulation*, 51(3-4), 157–167.

Yuan, Q. (2008). "Effect of temperature on transport of chloride ions in concrete." *2nd International Conference on Concrete Repair, Rehabilitation and Retrofitting, ICCRRR-2*, CRC Press, Cape Town, South Africa, 345–352.

l'université nantes angers le mans
PÔLE DE RECHERCHE ET D'ENSEIGNEMENT SUPÉRIEUR

UNIVERSITÉ DE NANTES

Thèse de Doctorat

Thanh Binh TRAN

Titre de thèse : Un cadre basé en réseaux bayésiens pour l'identification probabiliste des paramètres du modèle à partir d'essais normaux et accélérés: application à la pénétration des chlorures dans le béton

Title of thesis : A Bayesian Network framework for probabilistic identification of model parameters from normal and accelerated tests: application to chloride ingress into concrete

Résumé

La pénétration des chlorures dans le béton est l'une des causes principales de dégradation des ouvrages en béton armé. Sous l'attaque des chlorures des dégradations importantes auront lieu après 10 à 20 ans. Par conséquent, ces ouvrages devraient être périodiquement inspectés et réparés afin d'assurer des niveaux optimaux de capacité de service et de sécurité pendant leur durée de vie. Des paramètres matériels et environnementaux pertinents peuvent être déterminés à partir des données d'inspection. En raison de la cinétique longue des mécanismes de pénétration de chlorures et des difficultés pour mettre en place des techniques d'inspection, il est difficile d'obtenir des données d'inspection suffisantes pour caractériser le comportement à moyen et à long-terme de ce phénomène. L'objectif principal de cette thèse est de développer une méthodologie basée sur la mise à jour du réseau bayésien pour améliorer l'identification des incertitudes liées aux paramètres matériels et environnementaux des modèles en cas de quantité limitée de mesures. Le processus d'identification est appuyé sur des résultats provenant de tests normaux et accélérées effectués en laboratoire qui simulent les conditions de marée. Sur la base de ces données, plusieurs procédures sont proposées pour : (1) identifier des variables aléatoires d'entrée à partir de tests normaux ou naturels; (2) déterminer un temps équivalent d'exposition (et un facteur d'échelle) pour les tests accélérés; et (3) caractériser les paramètres en dépendants du temps. Les résultats indiquent que le cadre proposé peut être un outil utile pour identifier les paramètres du modèle, même à partir d'une base de données limitée

Mots clés
Pénétration des chlorures, identification des paramètres, réseaux bayésiens, incertitude, test accéléré, corrosion.

Abstract

Chloride ingress into concrete is one of the major causes leading to the degradation of reinforced concrete (RC) structures. Under chloride attack important damages are generated after 10 to 20 years. Consequently, they should be periodically inspected and repaired to ensure an optimal level of serviceability and safety during its lifecycle. Relevant material and environmental parameters for reliability analysis could be determined from inspection data. In natural conditions, chloride ingress involves a large number of uncertainties related to material properties and exposure conditions. However, due to the slow process of chloride ingress and the difficulties for implementing the inspection techniques, it is difficult to obtain sufficient inspection data to characterise the mid- and long-term behaviour of this phenomenon. The main objective of this thesis is to develop a framework based on Bayesian Network updating for improving the identification of uncertainties related to material and environmental model parameters in case of limited amount of measurements in time and space. The identification process is based on results coming from in-lab normal and accelerated tests that simulate tidal conditions. Based on these data, several procedures are proposed to: (1) identify input random variables from normal or natural tests; (2) determine an equivalent exposure time (and a scale factor) for accelerated tests; and (3) characterise time-dependent parameters combining information from normal and accelerated tests. The results indicate that the proposed framework could be a useful tool to identify model parameters even from limited

Key Words
Chloride ingress, parameter identification, Bayesian Network, uncertainty, accelerated test, corrosion.